Thermochemical Conversion of Lignocellulosic Biomass into Biofuels and Petrochemicals

Submitted in fulfilment of the requirements of the degree of Doctor of Engineering in the Faculty of Engineering and the Built Environment at the Durban University of Technology

Manqoba Shezi

2024

Supervisor: Prof. S.L. Kiambi

Co-Supervisor: Prof. Y Isa

DEDICATION

This thesis is dedicated to my family and friends, whose unwavering support and encouragement have strengthened me throughout this journey. To my supervisors, mentors, and lecturers, thank you for your guidance and inspiration.

RESEARCH OUTPUTS

Shezi, M., Kiambi, S. L., & Yusuf, I. M. (2024). Seasonal Harvesting Impact on Biomass Fuel Properties and Pyrolysis-Derived Bio-Oil Organic Phase Composition. https://doi.org/10.1111/gcbb.70011.

Shezi, M., Kiambi, S. L., & Yusuf, I. M. (2024). Seasonal Harvesting Impact on Biomass Fuel Properties and Pyrolysis-Derived Bio-oil Organic Phase Composition. Zenodo. [**dataset**]. https://doi.org/10.5281/zenodo.14055297.

Shezi, M. *, Kiambi, S. L. Isothermal Pyrolysis of Bamboo and Pinewood Biomass: Product Characterization and Comparative Study in a Fluidized Bed Reactor. bioengineering-3276410. (Bioengineering Accepted).

Shezi, M., Sakharmy, M., Adhikari, S., & Kiambi, S. L. Stabilization of Bio-oil Organic Phase via Solvent-assisted Hydrotreating: Investigating the Influence of Various Solvents. Elsevier (Materials Journal under review).

Shezi, M., Kiambi, S. L., & Yusuf, I. M. (2024). Catalytic and Non-Catalytic Fast Pyrolysis of Giant Reed Biomass in a Fixed Bed Reactor. Academia.edu Journals (Academia.edu under review).

Shezi, M., Sakharmy, M., Adhikari, S., & Kiambi, S. L. Thermochemical Conversion of Lignocellulosic Biomass and Valorization of Bio-oil Organic Phase to Fuel Range Hydrocarbons. Research Symposium. 26 March 2024. Auburn University Melton Student Center, USA.

Shezi, M., Kiambi, S. L., & Yusuf, I. M. (2022). Non-catalytic and Catalytic Pyrolysis of Giant Reed for Bio-oil Production. 2nd Sustainable Bioenergy and Processes Conference (SBP 2022). Cape Town, South Africa, 12 – 14 December 2022.

Shezi, M., Sakharmy, M., Adhikari, S., & Kiambi, S. L. Pyrolysis of Bamboo Biomass and Valorization of Bio-oil Organic Phase to Fuel Range Hydrocarbons. ASABE Annual International Meeting. Anaheim, California, USA, 28 – 31 July 2024.

DECLARATION

I, **Manqoba Shezi**, declare that

(i) The research reported in this thesis, except where otherwise indicated, is my original work.

(ii) This thesis has not been submitted for any degree or examination at any other university.

(iii) This thesis does not contain other persons' data, pictures, graphs, or other information, unless expressly acknowledged as being sourced from other persons.

(iv) This thesis does not contain other persons' writing, unless specifically acknowledged as being sourced from other researchers. Where other written sources have been quoted, then:

a) their words have been re-written but the general information attributed to them has been referenced;

b) where their exact words have been used, their writing has been placed inside quotation marks, and referenced.

(v) This thesis does not contain text, graphics or tables copied and pasted from the Internet, unless specifically acknowledged, and the source being detailed in the thesis and in the references sections.

Candidate: Mr M. Shezi

Signature: 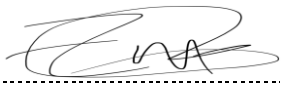 Date: 05/12/24

As supervisors of the aforementioned candidate, we do not have any objections to the submission of this dissertation.

Supervisor: Prof. S.L. Kiambi

Signature:…… Date:…….

Co-supervisor: Prof. Y. Isa

Signature:…… Date:…….

ACKNOWLEDGEMENTS

Gratefulness, honour and glory to God Almighty for the opportunity He has granted me in carrying out my work with appreciation and peace during my best and worst times.

I extend my deep gratitude to my project supervisors, Prof Y Isa and Prof SL Kiambi, for their guidance, support, and input in enhancing this work's quality. Moreover, I would like to thank Prof Y Isa for ensuring I can participate in renewable energy conferences. I would also like to thank Prof Sushil Adhikari and Mr Manish Sakharmy for hosting me at Auburn University to complete my research at the Biosystems Engineering (USA).

I also acknowledge the financial support from the Durban University of Technology (DUT, RSA), National Research Foundation (NRF, RSA), Fulbright Foreign Student Program (FFSP, USA) towards this research. The gratitude is also extended to the School of Chemical and Metallurgical Engineering at the University of Witwatersrand (WITS), the Department of Chemistry at the University of Cape Town (UCT, RSA), CALEB laboratories (RSA), and Auburn University (AU, USA) for providing sophisticated analyses and equipment for the current study.

I would also like to acknowledge my departmental staff members and fellow postgraduate students of the Department of Chemical Engineering and Biosystems Engineering for their support towards the completion of this research. I would also thank my family and friends for their exceptional support during this challenging journey. Last but not least, I am grateful to Mr Vishnu Kribagaran Moodley for endless support on the lab supplies and the design of the pyrolysis unit.

NOMENCLATURE

Symbol & Abbreviations	Description (Units)
BOP	Bio-oil organic phase yield (%)
BAP	Bio-oil aqueous phase yield (%)
ESP	Electrostatic precipitator
BC	Biochar product yield (%)
BG	Biogas product yield (%)
ADL	Acid detergent lignin (%)
ADF	Acid detergent fibre (%)
NDF	Neutral detergent fibre (%)
m_{bm}	Mass of biomass sample (mg)
X_p	Product yield (%)
UV_{abs}	Absorbance of hydrolysis liquor
DOD	Degree of deoxygenation (%)
MC_p	Moisture content of stabilized bio-oil (%)
ε	Absorptivity of biomass (L/g.cm)
DOD^h	Degree of dehydration (%)
$V_{filtrate}$	Volume of filtrate (mL)
AIL	Acid insoluble lignin (%)
AIR	Acid insoluble residue (%)
ASL	Acid soluble lignin (%)
AIF	Ash in filter (%)
MC_f	Moisture content of bio-oil feed (%)
ODW	Oven dry weight (g)

ABSTRACT

The depletion of conventional fossil fuel reserves, including oil, gas, and coal, has intensified concerns over environmental sustainability and energy security. Consequently, there has been a substantial shift towards exploring alternative energy technologies and developing sustainable products and processes. Biomass has gained significant traction as a renewable feedstock of interest in recent decades. Bio-oil derived from biomass holds promise for diverse energy production, chemical synthesis, and potential energy carrier applications. However, crude bio-oil exhibits inherent challenges stemming from its physical and chemical properties that preclude its direct integration into existing fuel infrastructures. Notably, the high acidity, low viscosity, high density, elevated oxygen content, substantial moisture levels, low heating value, complex molecular composition, and instability. These drawbacks can lead to issues such as corrosion, coking during upgrading, and difficulties in storage and transport. Addressing these challenges require advanced refining and treatment techniques to enhance the bio-oil's compatibility and usability within established industrial frameworks. Hence, studies that aimed to improve the properties of the bio-oil organic phase were conducted. Initially, the research embarked on catalytic and non-catalytic fast pyrolysis of Giant Reed using a zeolite as a catalyst. The results indicated that the presence of the HZSM-5 catalyst significantly improved the quality of the pyrolysis oil. Catalytic pyrolysis consistently yielded bio-oil with lower moisture content and higher carbon content than non-catalytic pyrolysis. At 550°C and 10 °C/min, the HHV of the catalytic pyrolysis product was 23.0 MJ/kg compared to 21.3 MJ/kg for non-catalytic pyrolysis. Applying the HZSM-5 catalyst at 650°C and 50 °C/min significantly enhanced the production of aromatic hydrocarbons and phenolic compounds while reducing the presence of undesirable oxygenates in the bio-oil organic phase. However, this observation was a trade-off to lower bio-oil yields and high energy consumption due to a high operating temperature. As a result, 550°C and 10 °C/min was considered as the operating condition for bio-oil organic phase production.

Another sub-study focused on investigating the effect of periodic variations on the fuel properties of Giant Reed and assessing its influence on pyrolysis product yield, quality, and distribution. This study was carried out after the incineration of giant reed along the river banks in Ladysmith, RSA, with the aim of minimizing artificial flooding occurrence as a result of stormwater drainage blockages. Four periodic variations, late spring (HS-4), late summer (HS-1), late autumn (HS-2), and late winter (HS-3), were considered to investigate the effect of harvest time on biomass fuel properties, pyrolysis product distribution, non-condensable gas

characterization, and bio-oil organic phase (BOP) fuel properties. The considered biomasses herein had average calorific values of 18.86 ± 0.05, 19.73 ± 0.05, 19.23 ± 0.04, and 18.44 ± 0.04 MJ/kg during HS-1, HS-2, HS-3, and HS-4, respectively. The biomass, bio-oil organic phase, biochar, and pyrolysis gas were characterized using thermogravimetric analysis (TGA), gas chromatography-mass spectroscopy (GCMS), Fourier transform infrared spectroscopy (FTIR), micro-GC, and scanning electron microscopy (SEM/EDS). The organic phase of bio-oil was isolated using a 125 ml separating funnel, allowing natural stratification of the immiscible phases. BOP yield increased from 5 to 11 wt% during HS-4 and HS-3, respectively. The increase in the BOP yield correlated with the lignification effect significantly, as shown by the R^2 value of 0.97. Higher heating values (HHV) of the BOP ranged from 19.4 ± 0.03 to 22.6 ± 0.02 MJ/kg in relation to the active growth stage and senescence-dormant phase. Physical and chemical properties (TAN, density, viscosity, water content, and CHNS) and chemical compound groups of organic phase bio-oil were analyzed. The produced BOP was rich in phenolics for all considered periods. The effect of harvest time showed that biomass and bio-oil organic phase fuel properties are improved during the senescence-dormant period. As a result, giant reed biomass should be harvested during autumn to avoid incineration that releases carbon dioxide into the atmosphere and will also reduce the occurrence of artificial flooding.

Fast pyrolysis of biomass is crucial for sustainable biofuel production, necessitating thorough characterization of feedstocks to optimize thermal conversion technologies. The third study investigated the isothermal pyrolysis of bamboo and pinewood biomass in a sand-fluidized bed reactor to assess biomass suitability for commercial bio-oil production. The pyrolysis products and biomass species were characterized through proximate and ultimate analyses, GCMS, FTIR, SEM/EDX, and structural analysis, to assess their chemical and physical properties. Results indicated that pine bio-oil possesses superior energy density, with a higher calorific value (20.38 MJ/kg) than bamboo (18.70 MJ/kg). Pine biomass yielded greater organic phase bio-oil (BOP) at 13 wt%, while bamboo produced 9 wt%. Energy yields were also notable, with pine exhibiting an energy yield of 15% for bio-oil organic phase (EBOP), compared to 11% for bamboo. The fibrous nature of bamboo biomass resulted in less reacted biomass at constant reaction time due to flow resistance during pyrolysis. Pine bio-oil organic phase (P-BOP) demonstrated a higher heating value (23.90 MJ/kg) than bamboo (B-BOP). The findings suggest that while both biomass types are viable renewable energy sources, pine biomass is more favourable for commercialization due to its superior energy properties and efficiency in pyrolysis.

Conventional mild hydrotreatment processes of bio-oil present significant challenges of high degree of polymerization, low oil yield, high coke formation, and poor catalyst recovery. To address these challenges, the fourth study looked into investigating and enhancing the properties of raw bio-oil organic phase samples via a solvent-assisted stabilization approach using methanol (METH), ethanol (ETHA), isopropyl alcohol (IPA), and ethyl ether (ETH). Solvents like methanol (METH) and ethanol (ETH), which are highly polar, yielded higher oil fractions (64% and 62% respectively) compared to less polar solvents like ethyl ether (DME) at 59%. Isopropyl alcohol (IPA), with intermediate polarity, achieved a balanced oil yield of 63%, indicating its ability to dissolve both polar and non-polar components. The moisture reduction in stabilized bio-oils followed the order: IPA > ETH > METH > DME, with IPA showing the highest reduction due to its structural characteristics facilitating dehydration. Viscosity reduction varied with IPA > ETH > DME > METH. Carbon recovery in stabilized bio-oils ranged from 65% to 75% for DME, ETH, and METH and was 71% for IPA. The heating values of stabilized bio-oils ranged from 28 to 29 MJ/kg, with IPA-stabilized bio-oil showing the highest value (29.05 ± 0.06 MJ/kg). METH demonstrated high efficiency (74.8%) in stabilizing bio-oil, attributed to its strong hydrogen-donating capability. ETH followed closely at 69.5%, indicating its comparable performance in bio-oil stabilization. With moderate efficiency (69.3%), IPA presented a balanced alternative considering its molecular structure and hydrogen solubility. In contrast, DME exhibited lower efficiency (63.6%) due to its weaker hydrogenation capability and propensity for undesired side reactions. The study suggested that subcritical conditions up to 200°C are adequate for METH, ETH, and IPA in bio-oil stabilization, comparable to results obtained under supercritical conditions.

TABLE OF CONTENTS

DEDICATION i
DECLARATION ii
ACKNOWLEDGEMENTS iii
NOMENCLATURE iv
ABSTRACT v
CHAPTER 1 1
1. INTRODUCTION 1
1.1 Background 1
1.2 Research Aim and Objectives 4
1.3 Significance of the Study 4
CHAPTER 2 5
2. LITERATURE REVIEW 5
2.1 Introduction 5
2.2 Lignocellulosic Biomass 6
2.3 Plants 8
2.3.1 Energy Crops 9
2.4 Bio – Oil 10
2.5 Pyrolysis Reaction Mechanisms 11
2.5.1 Biochar Formation 12
2.5.2 Depolymerisation 12
2.5.3 Fragmentation 13
2.5.4 Secondary Mechanisms 13
2.6 Pyrolysis Reactors 13
2.7 Types of pyrolysis 14
2.7.1 Slow Pyrolysis 15
2.7.2 Fast Pyrolysis 15
2.7.3 Intermediate Pyrolysis 16
2.7.4 Vacuum Pyrolysis 16
2.8 Effect of Operating Parameters on Product Yield of Pyrolysis Process 17
2.9 Catalytic Pyrolysis 20
2.9.1 Catalyst Configurations 20
2.9.2 Catalyst Mixing for in situ Pyrolysis 21
2.9.3 Catalyst to Biomass Ratio 22
2.9.4 Catalyst Selection 23

2.10 Summary of Relevant Literature....26
2.11 Upgrading of Bio-oil....27
2.12 Solvent-Assisted Biomass Conversion Processes....29
2.12.1 Solvent-Assisted Bio-oil Upgrading....29
2.12.2 Catalytic Solvent-Assisted Bio-oil Upgrading....31
CHAPTER 3....37
3. CATALYTIC AND NON-CATALYTIC FAST PYROLYSIS OF GIANT REED BIOMASS IN A FIXED BED REACTOR....37
Abstract....37
3.1 Introduction....38
3.2 Materials and Methods....40
3.2.1 Sample Harvesting and Preparation....40
3.2.2 Catalyst Preparation....40
3.2.2.1 Chemicals....40
3.2.2.2 Catalyst Synthesis....40
3.2.3 Catalyst Characterization....41
3.2.3.1. Py-IR....41
3.2.3.2. X-ray Diffraction (XRD)....42
3.2.3.3. Brunauer-Emmett-Teller (BET)....42
3.2.4 Analytical Methods....42
3.2.5 Semi-Batch Pyrolysis Setup and Procedure....43
3.3 Results and Discussion....45
3.3.1 Characterization of feedstock....45
3.3.2 Thermal Degradation of Feedstock....46
3.3.3 HZSM-5 Phase Structure....48
3.3.4 Specific Surface Area of HZSM-5 Catalyst....48
3.3.5 Acidity of HZSM-5 Catalyst....50
3.3.2 Effect of Temperature: Non-Catalytic vs Catalytic....52
3.3.3 Bio-oil Analyses: Proximate, Ultimate, and Properties....53
3.3.4 GCMS Analysis of Bio-oil....54
3.3.5. ^{13}C NMR Analysis of Bio-oil....57
3.3.6. Van Krevelen Plot....62
3.4 Conclusions....64
CHAPTER 4....66
4. SEASONAL HARVESTING IMPACT ON BIOMASS FUEL PROPERTIES AND PYROLYSIS-DERIVED BIO-OIL ORGANIC PHASE COMPOSITION....66
4.1 Abstract....66
4.2 Introduction....67

4.3 Materials and Methods....69
4.3.1 Sample Harvesting and Preparation....69
4.4 Estimation of Biomass Structural Composition....69
4.4.1 Acid Insoluble Lignin....69
4.4.2 Detergent Fibre Method....69
4.4.3 ADF Technique....69
4.4.4 ADL Technique....70
4.4.5 NDF Technique....70
4.5 Analytical Methods....71
4.6 Semi-Batch Pyrolysis Setup and Procedure....72
4.7 Results and Discussion....74
4.7.1 Composition of Biomass....74
4.7.2 Structural Components of Giant Reed at Different Seasons....78
4.7.3 FTIR of Giant Reed at Different Seasons....80
4.7.4 Thermal Degradation of Giant Reed at Different Seasons....81
4.7.5 Pyrolysis Product Distribution....83
4.7.6 Properties of Bio-oil Organic Phase....84
Figure 4. 7: Van Krevelen plot of giant reed biomass and bio-oil organic phase (BOP) compared to crude oil and gasoline....86
4.7.7 GCMS Analysis of Bio-oil Organic Phase....87
4.7.8 GCMS analysis on the distribution of "Others"....89
4.7.9 Energy Density of Bio-oil Organic Phase....90
4.7.10 Characterization of Biogas....91
4.8 Conclusions....92
CHAPTER 5....93
5. ISOTHERMAL PYROLYSIS OF BAMBOO AND PINEWOOD BIOMASS: PRODUCT CHARACTERIZATION AND COMPARATIVE STUDY IN A FLUIDIZED BED REACTOR....93
5.1 Abstract....93
5.2 Introduction....94
5.3 Materials and Methods....96
5.3.1 Sample Harvesting and Preparation....96
5.3.2 Biomass Characterization....96
5.3.3 Fast Pyrolysis with Fluidized Bed Reactor....97
5.3.4 Product Characterization....99
5.4 Results and Discussion....100
5.4.1 Biomass Characterization: Proximate and Ultimate Analysis....100
5.4.2 Biomass Structural Composition....101
5.4.3 Biomass FTIR....104

5.4.4 Fast Pyrolysis Product Distribution 105
5.4.5 BOP Characterization: Proximate, Ultimate, and Properties 106
5.4.6 Bio-oil Organic Phase GCMS 109
5.4.7 Bio-oil Organic Phase FTIR 111
5.4.8 Biochar Characterization 112
5.4.9 Van Krevelen Plot 113
5.4.10 SEM/EDX of Biochar 114
5.4.11 Energy Yield and Gas Analysis 115
5.5 Conclusions 117
CHAPTER 6 118
6. STABILIZATION OF BIO-OIL ORGANIC PHASE VIA SOLVENT-ASSISTED HYDROTREATING: INVESTIGATING THE INFLUENCE OF VARIOUS SOLVENTS 118
6.1 Abstract 118
6.2 Introduction 119
6.3 Materials and Methods 121
6.3.1 Materials 121
6.3.2 Fast Pyrolysis Procedure 122
6.3.3 BOP Stabilization Procedure 123
6.3.4 Product characterization 124
6.4 Results and Discussion 125
6.4.1 Product Yields 125
6.4.2 Physicochemical Properties of Raw, Blend and Stabilized BOP 127
6.4.3Energy Density and Moisture Content Reduction 128
6.4.4 Degree of Deoxygenation and Carbon Recovery 129
6.4.5 GCMS Analysis of Stabilized BOP 131
6.4.6 Van Krevelen Plot of Raw, Blend and Stabilized BOP 135
6.4.7 Turnover Frequency Thermogravimetric Analysis of Catalyst 136
6.5 Conclusions 137
CHAPTER 7 139
7. CONCLUSIONS AND RECOMMENDATIONS 139
7.1 Catalytic vs. Non-Catalytic Fast Pyrolysis of Giant Reed 139
7.2 Seasonal Variations in Giant Reed Biomass 140
7.3 Comparative Analysis of Wood-Based and Cane-Based Biomass 141
7.4 Stabilization of Raw Bio-Oil Using Solvent-Assisted Approach 141
8. REFERENCES 143
9. APPENDICES 161

9.1 Appendix A: Acid Hydrolysis Sample Calculation 161
9.2 Appendix B: Seasonal Effect GCMS Analysis Data 163
9.3 Appendix C: HPLC Sugar Curves and Calibration Curves 173

LIST OF FIGURES

Figure 1. 1: Floods in Ladysmith (Northern Natal News, 2021) 2

Figure 2. 1: Global energy-related CO_2 emissions, 1990-2021 ((IEA), 2021) 6
Figure 2. 2: Classification of biomass feedstocks (Patel and Kumar, 2016). 7
Figure 2. 3: Reaction pathways for pyrolysis of biomass (Jahirul et al., 2012) 12
Figure 2. 4: Relative product distribution during pyrolysis process of biomass at different temperature (Bioenergy, 2006). 17
Figure 2. 5: Schematic of biomass pyrolysis chemistry with acid catalysts (Yildiz et al., 2014) 25
Figure 2. 6: Evolution of bio-oil upgrading techniques/methods (Gollakota et al., 2016). 27
Figure 2. 7: Schematic presentation of bio-oil upgrading in stirred tank reactor (fixed volume). 32
Figure 2. 8: Solvent-assisted bio-oil stabilization approach of the current study. 36

Figure 3. 1: Schematic representation of semi-batch fast pyrolysis unit. 43
Figure 3. *2*: Thermal degradation behaviour of Giant Reed biomass. 46
Figure 3. 3: XRD pattern of synthesized HZSM-5 catalyst 48
Figure 3. 4: Py-IR spectra of HZSM-5 catalyst. 50
Figure 3. 5: Effect of temperature during catalytic (C) and non-catalytic (P) fast pyrolysis of Giant Reed biomass. 52
Figure 3. 6: GCMS analysis of bio-oil at different heating rates for 550 ^{0}C. 54
Figure 3. 7: GCMS analysis of bio-oil at different heating rates for 650 ^{0}C. 55
Figure 3. 8: ^{13}C NMR of bio-oil produced from non-catalytic fast pyrolysis of Giant reed biomass at 550 ^{0}C and 10 ^{0}C/min. 57
Figure 3. 9: ^{13}C NMR of bio-oil produced from non-catalytic fast pyrolysis of Giant reed biomass at 650 ^{0}C and 10 ^{0}C/min. 59
Figure 3. 10: ^{13}C NMR of bio-oil produced from catalytic fast pyrolysis of Giant reed biomass at 650 ^{0}C and 10 ^{0}C/min. 61
Figure 3. 11: ^{13}C NMR of bio-oil produced from catalytic fast pyrolysis of Giant reed biomass at 550 ^{0}C and 10 ^{0}C/min. 62
Figure 3. 12: Van Krevelen plot of catalytic and non-catalytic bio-oils versus conversional gasoline and crude oil. 62
Figure 3. 13: Zoom in of Van Krevelen plot of catalytic and non-catalytic bio-oils at different temperatures and heating rates. [Incr. = Increase, HR = Heating Rate, Temp. = Temperature]. 63

Figure 4. 1: Typical graphical Typical graphical abstract. 66
Figure 4. 2: Schematic representation of semi-batch fast pyrolysis unit. 72
Figure 4. 3: SEM/EDS of Giant Reed, A: external and B: internal. 76
Figure 4. 4: FTIR spectre of Giant Reed at different periodic variations. 80
Figure 4. 5: Thermogravimetric analysis of giant reed biomass at different seasons (a) TGA and (b) DTG. 81

Figure 4. 6: Thermochemical conversion products of Giant Reed biomass. 83
Figure 4. 7: Van Krevelen plot of giant reed biomass and bio-oil organic phase (BOP) compared to crude oil and gasoline. 86
Figure 4. 8: Functional groups of BOP as detected by the GCMS. 88
Figure 4. 9: Distribution of "Others" functional groups detected by the GCMS. 89
Figure 4. 10: Energy density and distribution of BOP.....90
Figure 4. 11: Biogas distribution during thermochemical conversion of Giant Reed. 91

Figure 5. 1: Schematic diagram for fast pyrolysis in a Fluidized Bed Reactor (FBR). 97
Figure 5. 2: Absorbance peaks of pine and bamboo biomass after acid hydrolysis. 103
Figure 5. 3: FTIR profiles of pine and bamboo biomass. 104
Figure 5. 4: Fast pyrolysis product yields. [BOP: bio-oil organic phase, BAP: bio-oil aqueous phase, BO: bio-oil, BC: biochar, and BG: pyrolysis gas]. 105
Figure 5. 5: Biomass balance for fast pyrolysis in a Fluidized Bed Reactor. 106
Figure 5. 6: GCMS analysis of bio-oil organic phase for pine (P-BOP) and bamboo (B-BOP). 109
Figure 5. 7: FTIR spectres of bio-oil organic phase for pine (P-BOP) and bamboo (B-BOP). 111
Figure 5. 8: Van Krevelen Plot of pine (P) and bamboo (B) for biomass (BM), biochar (BC), and bio-oil organic phase (BOP).....113
Figure 5. 9: SEM/EDX of bamboo biochar (Biochar-B) and pine biochar (Biochar-P). 114
Figure 5. 10: Pyrolysis gas analysis and energy yields for bio-oil organic phase (EBOP), pyrolysis gas (EBG), biochar (EBC), and losses. 116

Figure 6. 1: Typical rationale of the proposed solvent-assisted bio-oil organic phase stabilization. 121
Figure 6. 2: Schematic flow of solvent-assisted bio-oil organic phase stabilization. 123
Figure 6. 3: Product distribution of solvent-assisted bio-oil organic phase stabilization. 125
Figure 6. 4: Energy density and moisture content reduction of stabilized bio-oil organic phase. 128
Figure 6. 5:Degree of deoxygenation, carbon recovery and energy efficiency of stabilized bio-oil organic phase [Carbon (solvent) is available carbon in the feed solvent].....130
Figure 6. 6: GCMS analysis of raw and stabilized bio-oil organic phase using various solvents. [BOP-raw bio-oil organic phase]. 132
Figure 6. 7: " Others" GCMS analysis of raw and stabilized bio-oil organic phase using various solvents. [BOP-raw bio-oil organic phase]. 133
Figure 6. 8: Van Krevelen plot of raw, blend and stabilized bio-oil organic phase.[H/C_{eff} = H/C – 2(O/C), raw bio-oil (BOP), feed blends (-F), stabilized/effective bio-oils (-P/eff)] ..135
Figure 6. 9: Turnover frequency of catalyst during solvent-assisted bio-oil organic phase stabilization. 136
Figure 6. 10: Thermogravimetric analysis of clean and spent catalyst after solvent-assisted bio-oil organic phase stabilization. 137

Figure 9. 1: HPLC curve of pine biomass during determination of sugars. 173
Figure 9. 2: HPLC curve of bamboo biomass during determination of sugars. 173
Figure 9. 3: Calibration curve of glucose sugar content. 174
Figure 9. 4: Calibration curve of arabinose sugar content. 174
Figure 9. 5: Calibration curve of xylose sugar content. 175
Figure 9. 6: Calibration curve of glucose sugar content. 175
Figure 9. 7: Analysis of pine and bamboo biomass. 176

LIST OF TABLES

Table 2. 1: Proportions of components in biomass (Liang et al., 2021, Patel and Kumar, 2016) 8
Table 2. 2: Giant reed compound distribution (Patel and Kumar, 2016).....9
Table 2. 3: Different types of reactors used in literature (Patel et al., 2020).....14
Table 2.4: Relative outcomes of end products in different types of pyrolysis (Balat et al., 2009, Bridgwater, 2007). 15
Table 2. 5: Summary of fast pyrolysis studies for different biomass. 26
Table 2. 6: Upgrading techniques of bio-oil with their advantages and disadvantages (Xiu and Shahbazi 2012).....28
Table 2. 7: Frequently used solvents during bio-oil upgrading processes. 30
Table 2. 8: Summary of bio-oil upgrading results. 34

Table 3. 1: Characterization of Giant Reed biomass. 45
Table 3. 2: HZSM-5 surface properties. 48
Table 3. 3: Distribution of Lewis acid sites and Brønsted acid sites of HZSM-5 catalyst. 50
Table 3. 4: Characterization of bio-oil produced from catalytic and non-catalytic fast pyrolysis of Giant Reed biomass. 53

Table 4. 1: Ultimate analysis and higher heating values (HHV) of Giant Reed.....74
Table 4. 2: Proximate analysis of Giant Reed.....75
Table 4. 3: Internal and external surface elements of Giant Reed according to SEM/EDS spectrums. 77
Table 4. 4: Structural components and neutral fibres of Giant Reed.....79
Table 4. 5: Proximate, ultimate analysis and properties of BOP. 85

Table 5. 1: Proximate and ultimate analysis of lignocellulosic biomass. 100
Table 5. 2: Structural composition of pine and bamboo biomass.....102
Table 5. 3: Proximate, ultimate, and properties of bio-oil organic phase.....107
Table 5. 4: Proximate, ultimate and energy density of biochar. 112

Table 6. 1: Physicochemical properties of raw, blend and stabilized bio-oil organic phase. 127

Table 9. 1: GCMS analysis of BOP from Giant Reed biomass during HS-4 season. 163
Table 9. 2: GCMS analysis of BOP from Giant Reed biomass during HS-1 season. 164
Table 9. 3: GCMS analysis of BOP from Giant Reed biomass during HS-2 season. 165
Table 9. 4: GCMS analysis of BOP from Giant Reed biomass during HS-3 season. 166
Table 9. 5: GCMS Analysis of BOP from Pine biomass.....167
Table 9. 6: GCMS analysis of BOP from Bamboo biomass.....168
Table 9. 7: GCMS analysis of ethanol stabilized BOP.....169
Table 9. 8: GCMS analysis of methanol stabilized BOP.....170
Table 9. 9: GCMS analysis of ether stabilized BOP.....171
Table 9. 10: GCMS analysis of isopropyl alcohol stabilized BOP.....172
Table 9. 11: Isothermal pyrolysis of biomass. 176
Table 9. 12: Moisture content data of biomass for isothermal pyrolysis.....177
Table 9. 13:Fixed carbon and volatiles data of biomass for isothermal pyrolysis.....177
Table 9. 14: Ash content data of biomass for isothermal pyrolysis.....177

CHAPTER 1

1. INTRODUCTION

1.1 Background

The continued use of fossil fuels poses a severe challenge because of the world's limited supply, energy insecurity, and environmental concerns over global warming due to the production of greenhouse gases (Fernandez et al., 2021, Patel et al., 2020). Inevitably, the world will run out of oil that can be mined and burned in the long term. Sustainable energy transport and infrastructure are the endpoint. Dependence on fossil fuels is dangerous and poses a great threat to biodiversity, thus attaining sustainable energy transport and infrastructure is critical. Additionally, dependence on fossil fuels for energy has tampered with the natural carbon cycle. It is well known that the natural carbon cycle has existed for millions of years and there was no urgency around it. The problem started when extra carbon was added to the natural carbon cycle through human activities, and the net result is that the carbon in the atmosphere is increasing over time. It is much more than that can be absorbed by the ecosystem. As a result, it has become evident that energy should be renewable, cost-effective, convenient, safe, and sustainable. Nowadays, it is considered feasible and promising to convert biomass via thermochemical processes into petrochemicals and biofuels (Çağlar and Demirbaş, 2002). These processes use various biomasses that can be processed into a wide range of products, offering great productivity. In thermochemical conversion, the primary techniques include pyrolysis, liquefaction, gasification, and combustion (Awasthi et al., 2023). Among the aforementioned thermochemical techniques, pyrolysis is the most preferred approach that is cost-effective and easy to use for the production of biofuels and petrochemicals from biomass. This technique is categorized into slow, fast, and flash pyrolysis (Pawar et al., 2020). The choice of pyrolysis type to employ depends on the desired product distribution. Fast pyrolysis is known to be a good choice when high bio-oil yields are desired, while slow and flash are selective to higher yields of biochar and biogas, respectively. The bio-oil from fast pyrolysis is a potential source of a variety of valuable petrochemicals, however, due to undesired properties, it is incompatible with direct application as an engine fuel (Lohitharn and Shanks, 2009). Low heating value and high water content, acidity, and corrosiveness are well-known limitations of raw bio-oil. The aforementioned drawbacks of raw bio-oil are attributed to the presence of oxygenated compounds such as phenols, alcohols, furans, water, acids, ketones, and aldehydes (Auersvald et al., 2019, Oasmaa et al., 2012).

Energy crops such as bamboo and Giant Reed have gained enormous exploration for future energy production due to their high economic value, short rotation, high productivity, and improvement for sustainable management. Bamboo is considered invasive in other parts of the world, especially the running type bamboo; thus, its application in biofuel production is vital for the efficient use of marginal lands (Cappelli et al., 2021). Giant Reed species make it to the top 100 most invasive plant species globally, as stated by the International Union for the Conservation of Nature (Lowe et al., 2000).

Figure 1. 1: Floods in Ladysmith (Northern Natal News, 2021)

Giant Reed leads to artificial flooding by blocking stormwater drainage systems. During the flood the stems and rhizomes of Giant Reed deposit in the drainage systems and under bridges, resulting in the blocking of waterways, structural damage, and hazards to bridges and other structures (Ba et al., 2020). Figure 1.1 shows Ladysmith CBD during the floods. Artificial flooding was witnessed in Ladysmith (a semi-rural area in South Africa) in February 2021. It had a significant impact as it led to damage of property, loss of jobs, loss of shelter, and loss of cattle among other impacts. The concentration of Giant Reed is high in Ladysmith (in riverbanks and in-land). At present, there is no effective control measure for dealing with the extensive amount of invasive energy crops. Incinerating it directly is the adopted technique to dispose of it, however this results in the release of harmful gases which are, carbon monoxide, carbon dioxide, nitrogen oxides, and fine particulate matter (Corno et al., 2014). The attempts to apply biological and burning methodologies to control the invasiveness of the non-food energy crops add no value compared to utilizing the plants for bioenergy generation. Patel and Kumar (2016), investigated the pyrolysis of gigantic reed grass using TG-MS. The authors concluded that energy grass has a stronger thermochemical reactivity and a quicker devolatilization. Woody biomass, on the other hand, is known for its low ash content when compared to energy crops. Pinewood is among the most abundant biomass sources in the world and extensive work has been done in producing bio-oil and biochar via thermochemical conversion technologies. In forested areas, logs are often harvested for fuelwood or incinerated in open settings once dry, to clear space for alternative forest activities. Wood shavings and

residuals from sawmills are similarly combusted as a method of disposal (Azeez et al., 2010). The emissions resulting from combustion exacerbate environmental challenges related to climate change. Optimal utilization of biomass for bioenergy production holds considerable promise in addressing global energy demands and economic issues in developing countries.

The PhD research focused on four major sub-studies. Initially, the research embarks on catalytic and non-catalytic fast pyrolysis of Giant Reed using a zeolite as a catalyst. This sub-study looked into the effect of temperature and heating rate at constant catalyst loading. A well-known zeolite catalyst is HZSM-5 which has a high efficacy for decreasing biomass-derived oxygenates and promoting aromatic production (Garba et al., 2018, Liang et al., 2021, Charusiri and Vitidsant, 2017). During the first sub-study, a synthensized HZSM-5 catalyst was used during catalytic fast pyrolysis (CFP) of Giant Reed. Another sub-study focused on investigating the effect of periodic variations on the fuel properties of Giant Reed and assessing its influence on pyrolysis product yield, quality, and distribution. This study was performed to obtain an optimal harvest season for Giant Reed biomass, while considering the aim to minimize the possibility of artificial flooding occurrence. The third sub-study investigated bio-oil organic phase bulk production for wood-based biomass and cane-based biomass. The two biomass species were characterized and pyrolyzed in a sand-fluidized bed reactor to determine their suitability for commercial bio-oil production. Other pyrolysis products were also characterized to assess their potential as sources of bioenergy. The last sub-study looked into investigating and enhancing the properties of raw bio-oil organic phase samples via a solvent-assisted stabilization approach. It has been demonstrated in previous studies that supercritical fluids offer significant advantages in the upgrading of bio-oil. Therefore, methanol, ethanol, and isopropanol were utilized under subcritical conditions to facilitate the upgrading of the raw bio-oil whereas ethyl ether was applied under supercritical conditions. This approach was adopted to address drawbacks that still exist in conventional mild hydrotreatment processes. The major drawbacks include polymerization of bio-oil and the impossibility of recovering and reusing the catalyst. It is worth noting that during bio-oil stabilization, a noble catalyst such as Ru/C is used, thus it is prominent to recover, reactivate, and reuse the catalyst to save cost as these catalysts are expensive.

1.2 Research Aim and Objectives

The aim of this research is to develop a sustainable process for producing high-quality biofuels from invasive lignocellulosic biomass, thereby contributing to both renewable energy development and invasive species management. The aim is to be achieved using the following objectives:

1. Evaluate the effect of HZSM-5 catalyst on the yield and composition of Giant Reed bio-oil produced via fast pyrolysis, determining optimal operating parameters for maximizing bio-oil yield.
2. Conduct a comprehensive characterization of Giant Reed biomass, bio-oil, and biochar, including their physicochemical properties, chemical composition, and thermal decomposition behaviour using Thermogravimetric Analysis (TGA).
3. Investigate the effect of harvest time on the fuel properties of biomass and its influence on pyrolysis product distribution and quality.
4. Compare the bio-oil yield and properties obtained from cane-based and wood-based biomass using a sand-fluidized bed reactor.
5. Optimize a solvent-assisted stabilization process to improve the quality and stability of bio-oil produced from a fluidized bed reactor.

1.3 Significance of the Study

This study is motivated by the observation of the recurring floods in Ladysmith, KZN, which have devastating environmental and socioeconomic consequences. The direct beneficiaries of this research include:

- The local communities of Ladysmith and the uThukela District Municipality: They will benefit from the reduced flood risks achieved through the removal of invasive plants, which contribute to river blockages and exacerbate flooding.
- The South African biofuel industry: They will gain access to a viable method for producing biofuels from invasive species, potentially creating new economic opportunities and contributing to sustainable energy goals.
- Environmental agencies and conservation organizations: They will benefit from the research's contribution to invasive species management and the promotion of sustainable land use practices.

- Researchers and industries involved in bio-crude processing: They will gain valuable insights into solvent-assisted bio-oil stabilization techniques, which can improve the quality and applicability of bio-crude as a fuel source.

Furthermore, the study explores an upgrading technique for bio-crude, i.e., solvent-assisted bio-oil stabilization, which will directly benefit those seeking to enhance the properties of bio-crude for various applications.

CHAPTER 2

2. LITERATURE REVIEW

2.1 Introduction

The continued use of fossil fuels poses a severe challenge because of the world's limited supply, energy insecurity, and environmental concerns over global warming due to the production of greenhouse gases (Fernandez et al., 2021, Patel et al., 2020). As a result, it has become evident that energy should be renewable, cost-effective, convenient, safe, and sustainable. Demand of fuel in transportation is expected to rise from 134 billion litres in 2015 to 226 billion litres in 2026 (Patel et al., 2020). Despite the reduction in demand during the lockdown period of 2020, global CO_2 emissions from energy sources remained steady at 31.5 Gt. This led to CO_2 concentrations in the atmosphere reaching a record high of 412.5 parts per million, approximately 50% higher than pre-industrial levels. Looking ahead to 2023, energy-related CO_2 emissions are expected to rise by 4.8%, driven by the resurgence in demand for coal, oil, and gas as the global economy recovers. As a result, global emissions in 2023 are projected to be about 400 Mt CO_2, or 1.2%, lower than the peak observed in 2019, as illustrated in Figure 2.1 ((IEA), 2023).

84

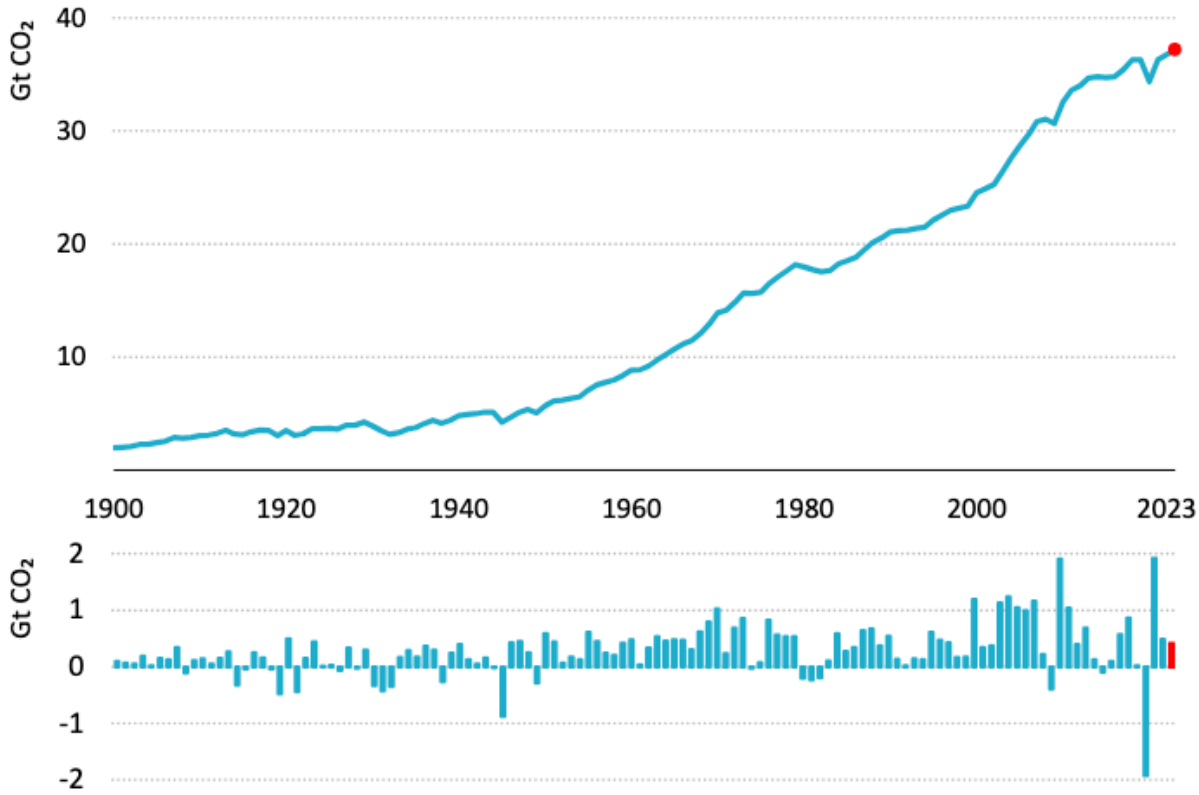

Figure 2. 1: Global energy-related CO_2 emissions, 1990-2023 ((IEA), 2023)

The increase in the carbon dioxide calls for an urgent sustainable intervention, the current study will look at employing fast pyrolysis technique (catalytic and non-catalytic) of Giant Reed to produce bio-oil which will be further upgraded through esterification in an attempt to meet the desirable fuel properties or blending requirements as per South African Bureau of Standards (SABS). The schematic diagram of biomass chemistry with acid catalyst is shown in Figure 2.5. Arundo donax is a typical C3 energy plant and its pyrolysis has and its pyrolysis characteristics are influenced by temperature, heating rate, sweeping gas flow rate, and particle size (Ba et al., 2020).

2.2 Lignocellulosic Biomass

Biomass is a word used to describe organic hydrocarbon materials that contain principally carbon, hydrogen, oxygen, nitrogen and sulphur, however sulphur and nitrogen are present in minor proportions (Patel and Kumar, 2016). Some inorganic contaminants, like as ash, are found in biomass, and their concentration varies by species. In agricultural residues, ash concentrations range from 5 to 10% by weight (Patel and Kumar, 2016, Patel et al., 2020). The classifications of biomass feedstocks are shown in Figure 2.2. Food and non-

food/lignocellulosic biomass feedstocks are split into two categories based on their final use (Patel and Kumar, 2016).

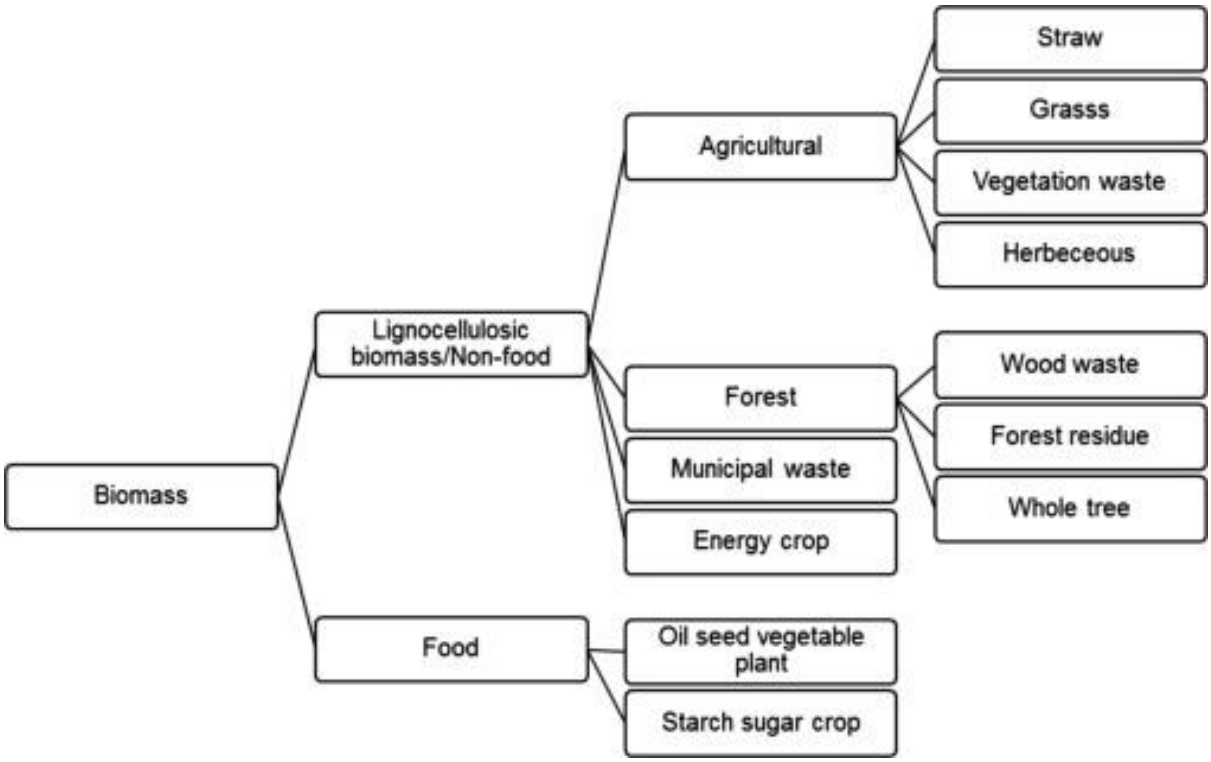

Figure 2. 2: Classification of biomass feedstocks (Patel and Kumar, 2016).

Starch sugar crops and oil seed vegetable plants are two different types of biomass food feedstocks. Rice, wheat, maize, root vegetables (potatoes and cassava), sugarcane, and barley are some of the most important starch sugar crops. This feedstock is mostly starch with a lot of glucose units in it (Patel and Kumar, 2016). Bioethanol and biodiesel are produced from starch sugar crops utilizing different catalysts for fermentation and transesterification (Bastos et al., 2020). Coconut, corn, cottonseed, olive, palm, rapeseed, sunflower, sesame seed, soybean, mustard, canola, camellia, jatropha, and pine are examples of oil seed vegetable plants, which belong to the other food category (Liang et al., 2021, Biswas et al., 2017). The solvent extraction method is used to obtain the vegetable oil. Depending on the temperature and soil conditions, feedstocks varies from place to country (Patel et al., 2020).

Non-food biomass, also known as lignocellulosic or second-generation biomass, is gaining traction as a biofuel feedstock that can replace refinery crude oil in transportation fuel production. Due to its advantages over other feedstocks, the focus of this study is on lignocellulosic biomass feedstock (Tsekos et al., 2021, Liang et al., 2021). Figure 2.2 depicts the four primary kinds of non-food biomass feedstock. Agricultural, forest, and municipal

waste feedstocks are the most common. Lignocellulosic biomass is the non-edible part of major food crops that is now underutilized but might be used to make biofuels (Patel and Kumar, 2016, Tsekos et al., 2021, Nanda et al., 2014). Figure 2.2 depicts the four types of agricultural feedstock. Bagasse, vegetable wastes, and residues from cereal production are all examples of straw and vegetative waste. Willow, poplar, and switchgrass are energy crops that are grown expressly for energy generation (Patel et al., 2020). They have a high yield per unit area when compared to traditional crops and trees and are widely employed for biofuel generation.

Agricultural residues have a moisture content of 10 to 20 wt%, which is advantageous for the quick pyrolysis process (Patel and Kumar, 2016). Whole trees, forest residue, and wood debris are all examples of forest biomass. Tree branches and tops make up forest residues, whereas saw mill trash and rotten and dead trees make up wood waste. For bio-oil production, several types of feedstock are constantly available and accessible.

The three most important organic components in biomass are cellulose, hemicelluloses, and lignin. Their weight percentages are roughly 30–50, 20–40, and 10–20, respectively (Collard and Blin, 2014). The proportion of cellulose and lignin in feedstock is used to classify it. Hardwood, for example, is made up of tightly bonded cellulose with little lignin content, whereas softwood is the opposite as seen in table 2.1 (Patel and Kumar, 2016).

Table 2. 1: Proportions of components in biomass (Liang et al., 2021, Patel and Kumar, 2016)

Biomass	Cellulose	Hemicellulose	Lignin	Extractives
Softwood	$42 \pm 2\%$	$27 \pm 2\%$	$28 \pm 3\%$	$3 \pm 2\%$
Hardwood	$45 \pm 2\%$	$30 \pm 2\%$	$20 \pm 4\%$	$5 \pm 3\%$
Sawdust	45.2%	20%	24.3%	9%

2.3 Plants

Plant-derived biomass has received a lot of interest since it is abundant and readily available, and it comes from natural photosynthesis. Herbaceous biomass, ligneous biomass, energy crops, and model compounds are the four types of biomass pyrolysis studies now being conducted from plant sources (Patel et al., 2020, Ba et al., 2020). Table 1 shows the approximate range of properties.

2.3.1 Energy Crops

Giant reed grass, an energy grass, has a higher calorific value and yield while requiring less area and emitting less sulphur dioxide (Ba et al., 2020, Corno et al., 2014). Patel and Kumar (2016), investigated the pyrolysis of gigantic reed grass using TG-MS. The authors concluded that, energy grass has a stronger thermochemical reactivity and a quicker devolatilization.

Table 2. 2: Giant reed compound distribution (Patel and Kumar, 2016)

Index	*Arundo donax*
C (wt.%)	46.73 ± 0.05
H (wt.%)	5.73 ± 0.03
O* (wt.%)	41.75 ± 0.11
N (wt.%)	0.54 ± 0.02
S (wt.%)	0.72 ± 0.01
V (wt.%)	79.12 ± 0.08
A (wt.%)	4.53 ± 0.11
M (wt.%)	7.05 ± 0.06
FC* (wt.%)	9.30 ± 0.13
HHV (MJ kg^{-1})	17.30 ± 0.15
LHV (MJ kg^{-1})	16.04 ± 0.11

Energy crops, in general, have high solar energy conversion efficiency, high water use efficiency, low nutritional requirements, robust breeding capacity, wide geographic dispersion, and excellent environmental adaptability (Patel and Kumar, 2016, Patel et al., 2020, Ba et al., 2020). These properties make energy crops suited for use in South Africa, where climates vary, agricultural area is restricted, and water supplies are scarce.

2.3.1.1 Cellulose

Cellulose, the predominant element in lignocellulosic biomass, typically constitutes between 40 and 50 wt.% of the total biomass, when measured on a dry weight basis, free from ash and extractive materials (Serrano-Ruiz and Dumesic, 2012). It is composed of a linear chain of glucose units, which are interconnected through beta-1,4-glycosidic bonds. Each polymer chain is made up of approximately 9,000 to 10,000 glucose molecules (Rowell et al., 2005). This structure results in the formation of interchain hydrogen bonds, contributing to cellulose's high degree of crystallinity and low surface area, which, in turn, enhances its resistance to chemical degradation and increases its overall stability (Serrano-Ruiz and Dumesic, 2012).

2.3.1.2 Hemicelluloses

Hemicelluloses are non-crystalline polysaccharides that form a matrix around cellulose fibers, typically representing 20–30 wt.% of the total biomass when measured on a dry, ash-free, and extractive-free basis (Serrano-Ruiz and Dumesic, 2012). These compounds have a diverse structure and are categorized based on the specific sugars they contain. In hardwoods, the predominant form of hemicellulose is xylan, whereas in softwoods, glucomannan is more common. Examples of these include glucuronoxylan and galactoglucomannan. Xylan-based hemicelluloses often feature acetyl groups; for instance, glucuronoxylan typically contains an average of seven acetyl groups for every ten xylose molecules. The acetyl content in hardwood hemicelluloses generally varies between 3.1 and 4.4 wt.%, while it is usually under 1.7 wt.% in softwoods (Rowell et al., 2005).

2.3.1.2 Lignin

Lignin plays a crucial role in providing structural support to wood by linking cellulose and hemicellulose fibers. It is composed of three-dimensional polymers made up of propyl-phenol units, which are joined together via carbon-carbon and ether linkages (Serrano-Ruiz and Dumesic, 2012).

2.4 Bio – Oil

To transform lignocellulosic biomass into more valuable products, a variety of thermal, mechanical, and biological techniques are used. Converting lignocellulosic biomass to a bio-oil intermediate is required for renewable diesel production from lignocellulosic biomass. Fast pyrolysis can be used to create bio-oil (Moreira et al., 2017). The type of feed, moisture level, temperature, residence period, and ash content all play a role in its formation. In this method, biomass is heated to 450–550 °C in a pyrolyzer in the absence of oxygen for 2 seconds at atmospheric pressure (Aysu et al., 2016). Because the residence period is so short, the liquid yield is high, and the product has a low ash level. According to a product study, liquid yield is roughly 75–80 wt%, with the rest being gaseous components and solid char. This method produces bio-oil, which has a higher heating value than raw biomass and can be used directly as an intermediate in the conversion of lignocellulosic biomass to transportation fuel (Dhanavath et al., 2017). Bio-oil is a thick, non-polar, dark-brown, free-flowing liquid in general. It's a complicated mixture of various organic chemicals formed when cellulose, hemicellulose, and lignin are thermally decomposed (Collard and Blin, 2014). Acids, alcohols,

aldehydes, esters, ketones, sugars, phenols, phenol derivatives, nitrogen compounds, and lignin-derived oligomers make up a considerable component (20–30 wt%) of bio-oil. Moreover, bio-oil is highly unstable because of the presence of unsaturated carbon, which is active during polymerization and condensation.

Bio-oil has a heating value of 16–20 MJ/kg which is higher than raw biomass but lower than crude oil, which has a value of roughly 35–40 MJ/kg (Patel et al., 2020). The inclusion of high molecular-weight oxygenated chemicals in bio-oil results in a lower heating value than crude oil (Rathore et al., 2020). The declining heating properties of bio-oil contribute to its very unstable nature. Polymerization and condensation between the oxygen compounds themselves cause this deterioration over time. On the fast pyrolysis process, the catalyst has a considerable impact. Bio-oil from a fast catalytic pyrolysis method in the presence of a mesoporous ZSM-5 zeolite catalyst was more stable than bio-oil from a non-catalytic pyrolysis technique, according to Liang et al. (2021). The oxygen percentage of non-catalytic bio-oil is typically approximately 40–50 wt%, but depending on the catalyst type and feed condition, the oxygen content in the catalytic pyrolysis process can be greatly reduced. The catalytic pyrolysis, according to Liang et al. (2021), can remove oxygen partially or completely. However, because to the high cost of catalysts, catalytic pyrolysis is uneconomical. Before shipping, bio-oil can be kept in a refinery. Oil can be kept in one of two ways. It can be kept in a stainless steel or olefin polymer tank that won't corrode from the bio-oil for short periods of time (Liang et al., 2021, Patel and Kumar, 2016, Moreira et al., 2017). The oil is combined with methanol (10% by weight) to prevent polymerization and condensation over lengthy periods of time (Patel et al., 2020).

2.5 Pyrolysis Reaction Mechanisms

Pyrolysis is a thermal decomposition process that occurs in the absence of oxygen, converting biomass into bio-oil, biochar, and pyro-gas. The key chemical processes involved include decarboxylation and the breakdown of hemicellulose, cellulose, and lignin. Decarboxylation starts at approximately 250 °C, releasing carbon dioxide and leaving behind either aliphatic or aromatic char. Hemicellulose is the first component to degrade, typically between 220 and 315 °C, followed by cellulose, which decomposes in the range of 315 to 400 °C. Lignin is the most heat-resistant and breaks down last, at temperatures ranging from 100 to 900 °C (Dhyani et al., 2017). Biomass pyrolysis is characterized by various chemical processes occurring in both parallel and sequential manners, including dehydration, depolymerization, decarboxylation,

isomerization, aromatization, and the formation of char. The process generally unfolds in three distinct phases: (i) the removal of free moisture, (ii) the primary breakdown phase, involving char formation, depolymerization, and fragmentation of the biomass, and (iii) the secondary phase, where vapor cracking and repolymerization occur. (Collard and Blin, 2014).

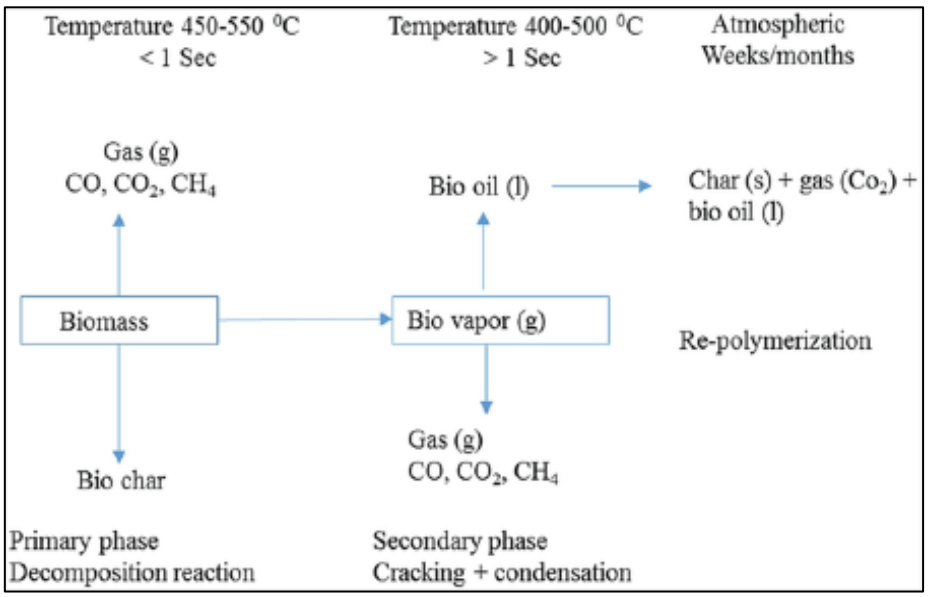

Figure 2. 3: Reaction pathways for pyrolysis of biomass (Jahirul et al., 2012).

2.5.1 Biochar Formation

Biochar consists of a polycyclic aromatic structure, which arises from the formation and fusion of benzene rings into larger, multi-ringed structures. The reactions responsible for char formation typically lead to the release of relatively simple compounds, such as water and/or gases that do not condense. (Moreira et al., 2017, Collard and Blin, 2014).

2.5.2 Depolymerisation

During the depolymerization process, the bonds that hold the polymer's monomer units together are broken. The newly created chain ends are likely to participate in additional reactions. As bond disruption continues, the polymer chains shorten until the resulting molecules become volatile. These volatile products, generated from the depolymerization of lignocellulose, are able to condense at ambient temperatures and are found in the liquid phase. (Collard and Blin, 2014).

2.5.3 Fragmentation

In the fragmentation process, a significant number of covalent bonds within the polymer are broken, resulting in the release of non-condensable gases and various low molecular weight organic compounds that can condense (Collard and Blin, 2014).

2.5.4 Secondary Mechanisms

When the volatile compounds released are unstable, they may undergo further reactions such as cracking or recombination before exiting the reactor. During cracking, the chemical bonds within these volatile substances are broken, resulting in the formation of lower molecular weight products. Given that similar bonds can also be cleaved within the polymer, fragmentation and cracking processes exhibit some common characteristics (Patel and Kumar, 2016). Recombination occurs when two volatile compounds combine to form a new compound with a higher molecular weight, which may no longer remain volatile at the reactor's operating temperature. Additionally, secondary char can be generated when these recombination reactions take place within the polymer matrix (Collard and Blin, 2014). Secondary reactions can also be catalyzed by the reactor surfaces, the char, or any introduced catalyst, leading to the formation of secondary char on the catalyst material's surface (Sun et al., 2020).

2.6 Pyrolysis Reactors

The most widely used types of pyrolysis reactors include batch, fluidized bed, and rotary kiln/auger reactors, all of which are typically cylindrical in shape.

To ensure an inert atmosphere before and sometimes during pyrolysis, a carrier gas, often nitrogen, is introduced into these reactors. This helps control the residence time of the volatiles within the reactor. However, in vacuum pyrolysis, no carrier gas is used, and instead, a vacuum pump is connected to the reactor's outlet to create the required conditions.

In batch reactors, the feed material is loaded into the reactor, heated to the desired temperature, and maintained at that temperature for a set period (Pütün, 2010; Stefanidis et al., 2011; Aysu, 2015). For auger and fluidized bed reactors, the feedstock is added through a hopper and pushed by mechanical means, such as a screw or piston, into a pre-heated reactor (Veses et al., 2014; Kim, Weaver, and Labbé, 2016; Funke et al., 2017).

In auger reactors, the feed moves into a horizontally rotating chamber, whereas in fluidized bed reactors, the feed is introduced into a bed of hot material, typically sand. The contact between the feed material and the hot sand in fluidized bed reactors results in very rapid heating rates (Bridgwater, 2003). Table 2.3 provides examples of different reactor types used in biomass pyrolysis. Generally, batch reactors are employed for slow pyrolysis, auger reactors for intermediate pyrolysis, and fluidized bed reactors for fast pyrolysis.

Table 2. 3: Different types of reactors used in literature (Patel et al., 2020)

Reactor Type	Heating Rate (°C/min) / Pyrolysis Type	Feed Throughput	Reference
Batch	10 / Slow	50 g	Ertaş and Hakki Alma (2010)
	10 – 50 / Slow	20 g	Aysu (2015)
	70 / Intermediate	5 g	Pütün (2010)
Rotary kiln / Auger	Intermediate	2 kg/hr	Veses et al. (2014)
	Intermediate	8 kg/hr	Kim, Weaver, and Labbé (2016)
	Intermediate	3 kg/hr	Funke et al. (2017)
Fluidised Bed	Fast	20 kg/hr	Oasmaa et al. (2003)
	Fast	0.3 – 0.43 kg/hr	Shen et al. (2009)
	Fast	100 g/hr	Funke et al. (2017)

Batch reactors are constrained in terms of output due to the need for loading and unloading the reactor between cycles. However, fluidized bed and auger reactors are designed for continuous feeding of the material, with a throughput capacity that can reach up to 3100 kg/hr (Dhyani and Bhaskar, 2018).

The conditions under which the pyrolysis processes occur have a significant impact on both the quality and yield of the products. A detailed discussion of how these parameters affect the outcomes can be found in Section 2.8.

2.7 Types of pyrolysis

Pyrolysis processes can be categorized into slow, fast, and flash pyrolysis, as per operating conditions applied in the process. Slow pyrolysis is also known as conventional pyrolysis. The major difference among all these types are in the temperature of the process, heating rate, solid

residence time, as well as biomass particle size (Patel et al., 2020). Table 2.4 indicates types of products that rely extensively on pyrolysis operating parameters and type of pyrolysis.

Table 2.4: Relative outcomes of end products in different types of pyrolysis (Balat et al., 2009, Bridgwater, 2007).

					Yield (%)		
Type of pyrolysis	Temp. range (K)	Rate of heating (K/s)	Residence time (s)	Particle size (mm)	Oil	Gas	Char
Slow	550–950	0.1–1	450–550	5–50	30	35	35
Fast	850–1250	10–200	0.5–10	<1	50	30	20
Flash	1050–1300	>1000	<0.5	<0.2	75	13	12

In the following section, the main attributes and operating conditions of the different pyrolysis processes will be discussed.

2.7.1 Slow Pyrolysis

In this pyrolysis method, low heating rates and extended residence times for volatiles in the reactor are characteristic. The biomass is heated at rates slower than 1 °C/s (60 °C/min) and reaches temperatures between 400 and 500 °C (Tripathi, Sahu, and Ganesan, 2016). The study also noted that the vapor residence time for slow pyrolysis typically falls between 300 and 550 seconds. These longer residence times enable the completion of secondary reactions. The primary product of slow pyrolysis is char, and larger biomass particles, ranging from 5 to 50 mm in size, are needed (Tripathi, Sahu, and Ganesan, 2016). Liquid yields from slow pyrolysis are typically around 30 wt.%, while char and permanent gases yield approximately 35 wt.% (Bridgwater, 2003).

2.7.2 Fast Pyrolysis

Fast pyrolysis is characterized by extremely rapid heating rates, typically between 10 and 200 °C/s, and very short volatile residence times (Tripathi, Sahu, and Ganesan, 2016). This process is primarily designed to convert biomass into volatiles before any char formation occurs. With a very brief vapor residence time, usually around 1 second, the risk of secondary reactions that could transform some condensable products into permanent gases is minimized (Bridgwater, 2012). Consequently, fast pyrolysis is most employed to produce pyrolysis oil, as the liquid product yield surpasses both the solid and gaseous yields. Typical product yields in fast pyrolysis include: 60–75 wt.% liquid, 15–25 wt.% char, and 10–20 wt.% non-condensable gas. For efficient fast pyrolysis, biomass particles are generally required to be smaller than 1 mm (Tripathi, Sahu, and Ganesan, 2016). The optimal reaction temperature for maximizing liquid

yields in biomass fast pyrolysis is usually around 500 °C (Neves et al., 2011; Bridgwater, 2012).

2.7.3 Intermediate Pyrolysis

Intermediate pyrolysis refers to processes that operate between the conditions of fast and slow pyrolysis. These processes typically employ heating rates from 1 to 10 °C/s and reach final temperatures between 500 and 650 °C. For intermediate pyrolysis, biomass particle sizes usually range from 1 to 5 mm (Tripathi, Sahu, and Ganesan, 2016), and the vapor residence time is generally under 30 seconds (Bridgwater, 2012).

According to Hornung, Apfelbacher, and Sagi (2011), the typical product distribution for intermediate pyrolysis consists of 40–60 wt.% liquid, 15–25 wt.% char, and 20–30 wt.% permanent gases. Although the liquid yield in intermediate pyrolysis is lower than that of fast pyrolysis, this process is gaining popularity due to its simpler design. Furthermore, it does not require the very fine biomass particles necessary for fast pyrolysis, which demand rapid heating rates (Hornung, Apfelbacher, and Sagi, 2011). The reduction of particle size, however, can decrease energy efficiency, as substantial energy is consumed during the milling process.

2.7.4 Vacuum Pyrolysis

Vacuum pyrolysis is often viewed as a variant of intermediate pyrolysis, taking place at low pressure, typically below 15 kPa (absolute) (Roy et al., 1998; García-Pérez et al., 2007; Carrier et al., 2011). The heating rates in vacuum pyrolysis are generally similar to those used in intermediate or slow pyrolysis, with temperatures reaching between 350 and 600°C (Tripathi, Sahu, and Ganesan, 2016). The low or vacuum pressure applied during the process helps to efficiently remove pyrolysis vapors, leading to a reduced residence time for these vapors. This minimizes the occurrence of secondary reactions, resulting in a higher yield of liquid products and a bio-oil that contains more primary compounds compared to the products of slow pyrolysis (Benallal et al., 1995). Under conditions of slow heating rates combined with vacuum, liquid yields have been reported to range from 35% to 50% by weight (Bridgwater, 2003).

2.8 Effect of Operating Parameters on Product Yield of Pyrolysis Process

Several factors influence both the rate of pyrolysis and the resulting product distribution and quality. Key elements include the biomass type, the operating conditions (like temperature, heating rate, biomass particle size, and gas flow rate), as well as the biomass's physical and chemical properties (Jahirul et al., 2012).

2.8.1 Temperature

Temperature plays a crucial and pivotal role in the pyrolysis process. According to existing literature, bio-oil yield rises as the pyrolysis temperature increases, reaching its peak between 500 and 550°C, before declining at higher temperatures. Bio-char yield is highest at approximately 350°C, and it decreases as the temperature rises above this point. In contrast, the yield of gaseous products consistently increases with temperature, reaching its maximum at the highest temperatures (Varma and Mondal, 2017). Figure 2.4 illustrates the distribution of products from fast pyrolysis of biomass at different temperatures.

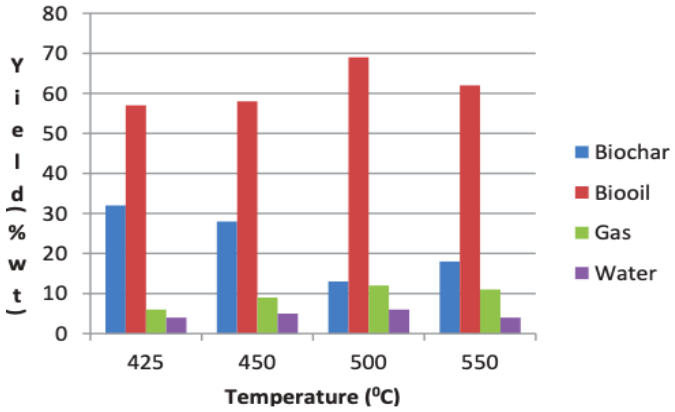

Figure 2. 4: Relative product distribution during pyrolysis process of biomass at different temperature (Bioenergy, 2006).

2.8.2 Heating Rate

To reduce the likelihood of secondary reactions that can decrease both the liquid yield, and its quality, rapid heating and cooling of the primary vapours are necessary. In contrast, slower heating promotes a higher yield of char (Varma et al., 2018). When the heating rate is high, the biomass undergoes rapid endothermic decomposition, generating more volatiles. This rapid process minimizes the time available for secondary reactions (like tar cracking or repolymerization). As a result, high molecular weight char and volatiles are removed more quickly, leading to a reduced amount of char remaining.

2.8.3 Biomass Particle Size

Smaller biomass particles have a greater surface area, which enhances heat transfer. As a result, using smaller particles in a pyrolyzer leads to more efficient heat transfer compared to larger ones. This increased heat transfer facilitates the production of more vapours during pyrolysis, resulting in a higher yield of gaseous products and a lower yield of char. In contrast, larger particles reduce heat transfer efficiency, slowing down the vaporization rate, which leads to greater char production and less gas formation. Additionally, larger biomass particles create higher temperature gradients within the particles, meaning not all parts of the particle reach the same temperature, unlike smaller particles, which experience more uniform heating (Varma et al., 2018).

2.8.4 Sweeping Gas Flow rate

In the pyrolysis process, biomass initially generates volatile vapours, which are carried out of the reactor by an inert gas such as nitrogen (N_2) and subsequently condensed to produce bio-oil. The vapours that do not condense, along with the carrier gas, contribute to the formation of gaseous products. At lower N_2 flow rates, the volatiles spend more time in the heated reactor zone, which reduces the overall vapor production and leads to increased char formation. On the other hand, when the N_2 flow rate is increased, the residence time of the vapours in the hot reactor zone decreases, resulting in more vapor generation, and thus a higher gas yield and lower char formation (Saikia et al., 2015).

2.8.5 Volatile Residence Time

Volatile residence time refers to the duration that the volatiles stay in the heated section of the reactor, where secondary reactions are more likely to occur. As such, extending the vapor residence time tends to promote more secondary reactions. Factors such as reactor pressure (as seen in vacuum pyrolysis) and the flow rate of the sweeping gas can be adjusted to regulate the volatile residence time. Generally, reducing the flow rate of the sweeping or carrier gas increases the volatile residence time, leading to lower liquid yields, while enhancing the yields of char and gas (Pütün, 2010; Auta, Ern, and Hameed, 2014; Aysu, 2015).

In slow pyrolysis, long volatile residence times (ranging from 300 to 550 seconds) can foster undesirable secondary reactions, such as over-cracking or repolymerization of the target

volatile compounds (Tripathi, Sahu, and Ganesan, 2016). On the other hand, the very short residence times (<30 seconds) typical of intermediate and fast pyrolysis (Bridgwater, 2012) may not allow sufficient time for certain desirable reactions to complete, especially when a catalyst is used. Thus, optimizing the residence time is crucial to strike a balance between minimizing unwanted secondary reactions and providing enough time for catalyzed reactions to occur (Yildiz et al., 2016). For catalytic pyrolysis, volatile residence times in the intermediate pyrolysis range often offer a suitable compromise (Veses et al., 2014).

2.8.6 Fast Pyrolysis

Fast pyrolysis is a prominent method for biofuel production and is considered one of the most efficient ways to convert biomass. However, bio-oil, or pyrolysis oil, often suffers from several drawbacks, including low calorific value, poor thermal stability, high corrosiveness, and high viscosity, which restrict its direct use. To overcome these limitations, developing a technology to reduce the oxygen content in bio-oils is essential (Charusiri and Vitidsant, 2017, Gollakota et al., 2016). CFP (Catalytic Fast Pyrolysis), which integrates catalytic upgrading with biomass pyrolysis in a single reactor, is gaining prominence as a crucial method for improving the quality of bio-oil. Typically, biomass CFP involves rapidly heating the biomass to temperatures between 500–600°C for a brief period of 1–2 seconds, followed by the rapid cooling of the reactor to room temperature (Liang et al., 2021). Figure 2.5 shows simplified pyrolysis chemistry mechanism with an acid catalyst.

2.8.7 Particle Size

The size of biomass particles is a critical factor in pyrolysis, as it influences the rate at which heat is transferred to the material. This is especially significant in fast pyrolysis, which requires high rates of heating and heat transfer (Bridgwater, 2003). As the particle size increases, bio-oil yields typically decrease, while the yields of char and gas tend to increase. Larger particles create greater resistance to heat transfer from the surface to the core, causing the inner portions of the biomass to heat more slowly than the outer layers, thereby favouring char formation (Encinar, Gonzalez, and Gonzalez, 2000). Additionally, as particle size increases, the volatiles stay inside the particles longer, which makes them more prone to secondary reactions, leading to higher char and gas production. For achieving rapid heating rates in fast pyrolysis (> 10 °C/s), particles smaller than 1 mm are needed (Tripathi, Sahu, and Ganesan, 2016). While it requires energy to reduce particle size, it is often advantageous to use larger particles (> 1 mm)

during pyrolysis. However, when catalysts are used with biomass, the particle size should be adjusted to enhance contact between the biomass and catalyst to facilitate the catalytic process (see Section 2.6.2). The process of pyrolysis that incorporates a catalyst to improve product quality is known as catalytic pyrolysis (CP), which is further discussed in Section 2.9.

2.9 Catalytic Pyrolysis

Several approaches have been explored to upgrade bio-oil and improve its fuel properties. The most widely applied methods include catalytic pyrolysis (CP) and hydro-treating. Catalysts facilitate oxygen removal by breaking down oxygenated compounds like carbon monoxide (through decarbonylation), carbon dioxide (via decarboxylation), and water (via dehydration), thus enhancing the quality of the bio-oil. In hydro-treating, bio-oil from thermal pyrolysis is treated with excess hydrogen in the presence of catalysts to reduce its oxygen content. While this method is effective at deoxygenating the oil, it is still under development, and it remains costly due to the need for high pressure and the expensive nature of hydrogen (Marinangeli et al., 2005; Thegarid et al., 2014).

This research proposes using catalysts with deoxygenating properties during the pyrolysis process to enhance bio-oil quality and make it more suitable for blending with petroleum refinery feedstocks. By removing oxygen, the calorific value (HHV) of the bio-oil is increased. However, while catalysts can improve the bio-oil, they tend to reduce the overall bio-oil yield by converting part of it into permanent gases through cracking reactions. Additionally, organic deposits, often referred to as coke, accumulate on the catalyst surface (Thegarid et al., 2014). The ideal catalyst should be stable, easy to regenerate, inexpensive, and efficient at both deoxygenation and improving HHV. Different catalyst configurations can be used in pyrolysis, and these are described in Section 2.9.1.

2.9.1 Catalyst Configurations

Two main configurations for catalysts in pyrolysis are in situ and ex situ, as described in the review by Yildiz et al. (2016). In the in-situ configuration, the biomass and catalyst are mixed directly in the pyrolysis reactor. At the operating temperature of the reactor, the catalyst becomes active and immediately reacts with the volatiles it contacts. Conversely, the ex-situ configuration places the biomass in a primary reactor, where pyrolysis occurs. The produced volatiles then pass through a separate catalyst bed in a secondary reactor, where they undergo further upgrading (Yildiz et al., 2016). These two reactors can operate at distinct temperatures,

optimized for specific reactions. However, this setup requires additional energy for the secondary reactor, leading to reduced energy efficiency, and ex situ systems tend to be more expensive to build (Yildiz et al., 2016).

The configuration choice also influences catalyst recycling capabilities (Yildiz et al., 2016). In ex situ systems, the char is separated from the catalyst, making recycling simpler by removing organic materials from the catalyst surface, followed by potential reactivation. In in situ systems, however, separating the catalyst from the char presents a technical challenge. One method to recover the catalyst is by combusting the char to retrieve the inorganic catalyst, though the purity of the recovered catalyst is influenced by the biomass's ash content. Alternatively, the catalyst-char mixture can be used as a soil amendment, depending on the catalyst type, potentially offering benefits like improving soil nutrition or neutralizing it (Samac and Tesfaye, 2003; Zimdahl, 2015).

A comparison of the two configurations showed similar outcomes, suggesting that the need for a secondary reactor could be avoided if there is sufficient mixing and contact time during the process (Imran et al., 2014). While mixing and contact time may be inadequate in small-scale tests, they are generally sufficient in larger reactors like auger reactors (Veses et al., 2014). In in situ configurations, there are two primary methods of mixing the catalyst, which are detailed further below.

2.9.2 Catalyst Mixing for in situ Pyrolysis

According to the literature, two common methods are used to mix feedstock and catalysts: impregnating the biomass with the catalyst or dry mixing the two. Dry mixing involves mechanically blending the biomass and catalyst particles. In impregnation, the catalyst particles are dissolved in water to create a catalyst solution. The biomass is then immersed in this solution, and the mixture is stirred to form a homogeneous slurry, which is subsequently dried to yield the impregnated feedstock (Patwardhan et al., 2010).

Impregnation is primarily used in studies involving water-soluble metal salts as catalysts. It has been suggested that metal cations mainly interact with oxygenated groups in hemicelluloses during impregnation (F. X. Collard et al., 2012). These metals are well dispersed and make close contact with the biomass (Richardson et al., 2010). This close contact, combined with the catalytic cracking of volatiles, may also affect certain primary reactions within the biomass structure (Patwardhan et al., 2010). However, the drying process required for impregnation

consumes energy, reducing the overall energy efficiency of the method. Furthermore, when the catalyst is not soluble, such intimate contact has not been observed, making the benefits of impregnation less clear. The ratio of catalyst to biomass in the mixture also impacts the pyrolysis process, which is discussed in the following section.

2.9.2.1 Char yield in in situ catalytic pyrolysis

In the context of in situ catalytic pyrolysis, the addition of a catalyst does not appear to have a major effect on char yield, as the biomass and catalyst do not make intimate contact, meaning the primary reactions are unlikely to be significantly altered. Lin et al. (2010) and Veses et al. (2014) both noted modest increases in char yield, from 25.3% to 27.9% and from 25% to 27%, respectively, upon the introduction of CaO. On the other hand, Chen et al. (2017) observed a slight reduction in char yield, dropping from 27% to 25%, following catalyst addition. Stefanidis et al. (2011), however, found a more notable rise in char yield, from 22.89% to 27.50% and 29.55%, with the inclusion of MgO and Al2O3. They suggested that the increase was due to coke formation on the catalyst surface. There is some uncertainty, however, regarding whether all studies used the same method or criteria for measuring char yield, especially in terms of including or excluding the catalyst. In general, though, it can be concluded that the impact of catalyst addition on char yield during in situ catalytic pyrolysis is minimal.

2.9.3 Catalyst to Biomass Ratio

The ratio of catalyst to biomass (C/B) plays a crucial role in determining the yields of pyrolysis products. When high catalyst-to-biomass ratios exceeding 1:1 (i.e., more than 50 wt.% catalyst) are used, a decrease in bio-oil yield is observed, alongside increases in the yields of gas and char (Veses et al., 2015; Chen et al., 2017; Russell et al., 2017). However, the quality of the bio-oil improves, especially in terms of reduced oxygen content and increased energy density.

The presence of large amounts of catalyst is thought to enhance the cracking of vapors, which results in a higher proportion of non-condensable gases (Yildiz et al., 2016). Additionally, the catalyst can promote secondary reactions, leading to the formation of high-molecular-weight compounds (recombination), which may create carbonaceous deposits and consequently increase char production.

When the C/B ratio was altered from 1:3 to 3:1, the char yield increased from 27% to 44% (on a catalyst-free basis) (Veses et al., 2015). At lower catalyst concentrations, the surface area available for the active catalyst is restricted, which results in some volatiles leaving the reactor without undergoing sufficient reforming, leading to less deoxygenation. Therefore, for an efficient and cost-effective catalytic pyrolysis (CP) process, the C/B ratio should be optimized within the range of 0:1 to 1:1 (0–50 wt.% catalyst).

2.9.4 Catalyst Selection

Various types of catalysts can influence different pyrolysis pathways, leading to diverse effects on the yields and properties of the products (Shadangi and Mohanty 2014b). Catalysts exhibit selectivity for specific chemical bonds and compounds, meaning that the choice of catalyst has a significant impact on both the yield and composition of the bio-oil.

In the in-situ configuration, lignocellulosic biomass has been subjected to pyrolysis with a range of catalysts. This section provides an overview of these catalysts, with a particular focus on their ability to deoxygenate bio-oil. This is typically achieved through processes such as decarboxylation, decarbonylation, and dehydration, all of which contribute to an increase in the higher heating value (HHV) of the bio-oil. However, enhancing bio-oil quality through deoxygenation usually leads to a reduction in the yield of the organic fraction, as CO_2, CO, and H_2O are produced during this process.

2.9.4.1 Zeolites

Zeolites, which are solid-acid aluminosilicates with microporous structures, have been widely investigated for bio-oil upgrading due to their comparable use in the petroleum refining process. Various studies have explored the application of different zeolite catalysts, such as ZSM-5, HZSM-5, H-Y, and H-mordenite, to enhance the quality of biomass pyrolysis vapors (Adjaye and Bakhshi, 1995; Lappas et al., 2002; Zhang et al., 2014). According to Adjaye and Bakhshi (1995), the best results were obtained with HZSM-5 in upgrading fast pyrolysis bio-oil. However, only 33.6% of the initial bio-oil was recovered as organic products, with up to 16% of the bio-oil converted into coke deposits on the catalyst surface. Furthermore, small-pore zeolites tend to increase the production of water and gases, which leads to a reduction in the yield of liquid organic products (Liang et al., 2021).

Zeolite catalysts, with their acidic sites, promote aromatization processes that produce aromatic compounds like benzene, toluene, and xylene (BTX). These reactions can also generate polycyclic aromatic hydrocarbons (PAHs), which serve as precursors for the formation of coke on the catalyst surface (Stefanidis et al., 2016). The buildup of coke leads to catalyst deactivation and a decrease in the yield of the desired liquid products (Du, Valla, and Bollas, 2010; Stefanidis et al., 2016). Furthermore, a high concentration of aromatic compounds in the bio-oil negatively impacts combustion efficiency due to their inherent stability.

Another significant limitation of zeolite catalysts is their irreversible deactivation, which occurs when the catalyst undergoes de-alumination, a process triggered by the water produced during pyrolysis and catalytic dehydration (Serrano-Ruiz and Dumesic, 2012). According to Paasikallio et al. (2014), alkali and alkaline earth metals (AAEMs) in the biomass can also deactivate the HZSM-5 catalyst irreversibly by replacing the protons at the catalyst's acid sites. This behavior makes zeolites less suitable for use in the in situ catalytic pyrolysis configuration, where the biomass and catalyst are in direct contact.

2.9.4.2 Metal Oxides

Metal oxides are known to enhance the quality of bio-oil by promoting deoxygenation and increasing its higher heating value (HHV). In particular, catalysts like Al_2O_3, CaO, and MgO have been the focus of several studies due to their relatively low cost (Veses et al., 2014). Research has highlighted the deoxygenation capabilities of these metal oxides during the pyrolysis of seeds (Pütün, 2010; Shadangi and Mohanty, 2014a; Shadangi and Mohanty, 2014b). When seeds are pyrolyzed, bio-oils with HHVs ranging from 40 to 43 MJ/kg, which are similar to those of fossil fuels, are produced. However, these high HHVs are partly attributed to the seeds' low oxygen content and the higher concentrations of extractives and fats, which are found in seeds compared to lignocellulosic biomass. As a result, while seed-derived bio-oils have a higher HHV, they are not directly comparable to those from lignocellulosic sources. Nonetheless, the same metal oxides—Al_2O_3, CaO, and MgO—have also been shown to improve the quality of bio-oils produced from lignocellulosic materials by reducing their oxygen content and increasing their HHV.

In some of the studies reviewed (Veses et al., 2014), the pyrolysis liquid was separated into two distinct phases via decanting. These included an organic phase, primarily composed of organic compounds, and an aqueous phase rich in water. In cases where the two-phase liquid

was not observed, the water content in the liquid was measured to determine the yield of pyrolytic water. Pyrolytic water refers to the water generated through the dehydration reactions occurring during pyrolysis and does not include the biomass's initial moisture. The organic yield in the bio-oil was then determined by subtracting the water yield from the total liquid yield.

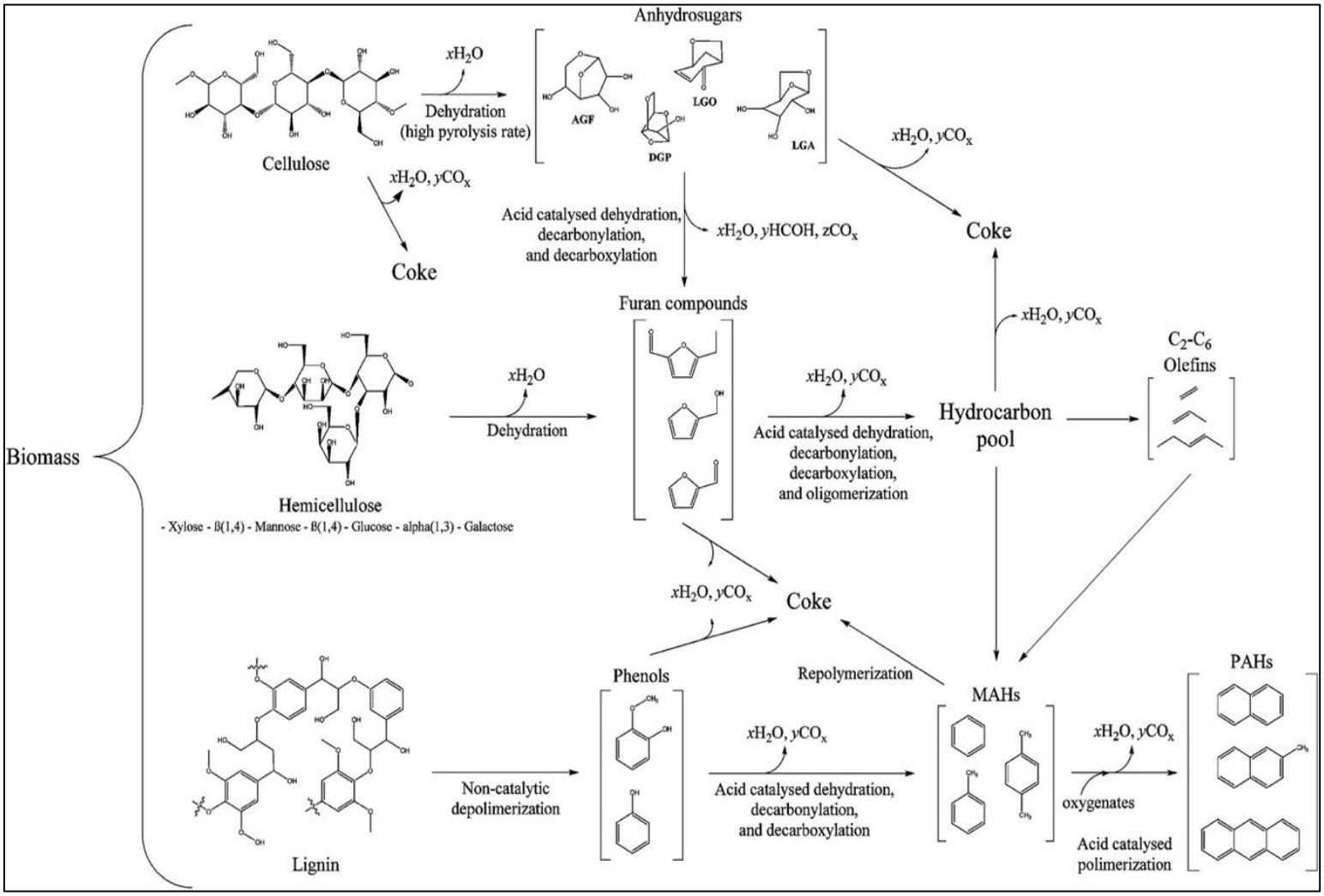

Figure 2. 5: Schematic of biomass pyrolysis chemistry with acid catalysts (Yildiz et al., 2014).

2.10 Summary of Relevant Literature

Table 2. 5: Summary of fast pyrolysis studies for different biomass.

Biomass (catalyst)	Reactor	Operating Parameters				Optimum Temp. (°C)	Yield (wt.%)	Ref.
		Temp. (°C)	HR (°C/min)	BPS (mm)	N_2 FR (mL/min)			
Walnut shells	PBR	375-750	273.58	0.5-1.5	1.6	500	BO: 44.7 BC: 37.6 BG: 40.4	Shah et al. (2021)
Wheat straw	FBR	400-600	5	1-3	2.5-4.5	500	BO: 44.0 BC: 32.0 BG: 25.0	Rathore et al. (2020)
Corncob	PBR	300-450	20	0.5-2	50	450	BO: 47.3 BC: 24.0 BG: 28.7	Biswas et al. (2017)
Rice straw	PBR	300-450	20	0.5-2	50	450	BO: 38.1 BC: 35.0 BG: 26.9	Biswas et al. (2017)
Anchusa azurea	PBR	350-550	100	0.6	100	450	BO: 31.3 BC: 30.0 BG: 30.0	Aysu et al. (2016)

2.11 Upgrading of Bio-oil

Considering the properties of bio-oil, it is evident that the fuel quality of bio-oil is lower than that of petroleum fuels. Recently, there are several studies that have been done on the upgradation of bio-oil.

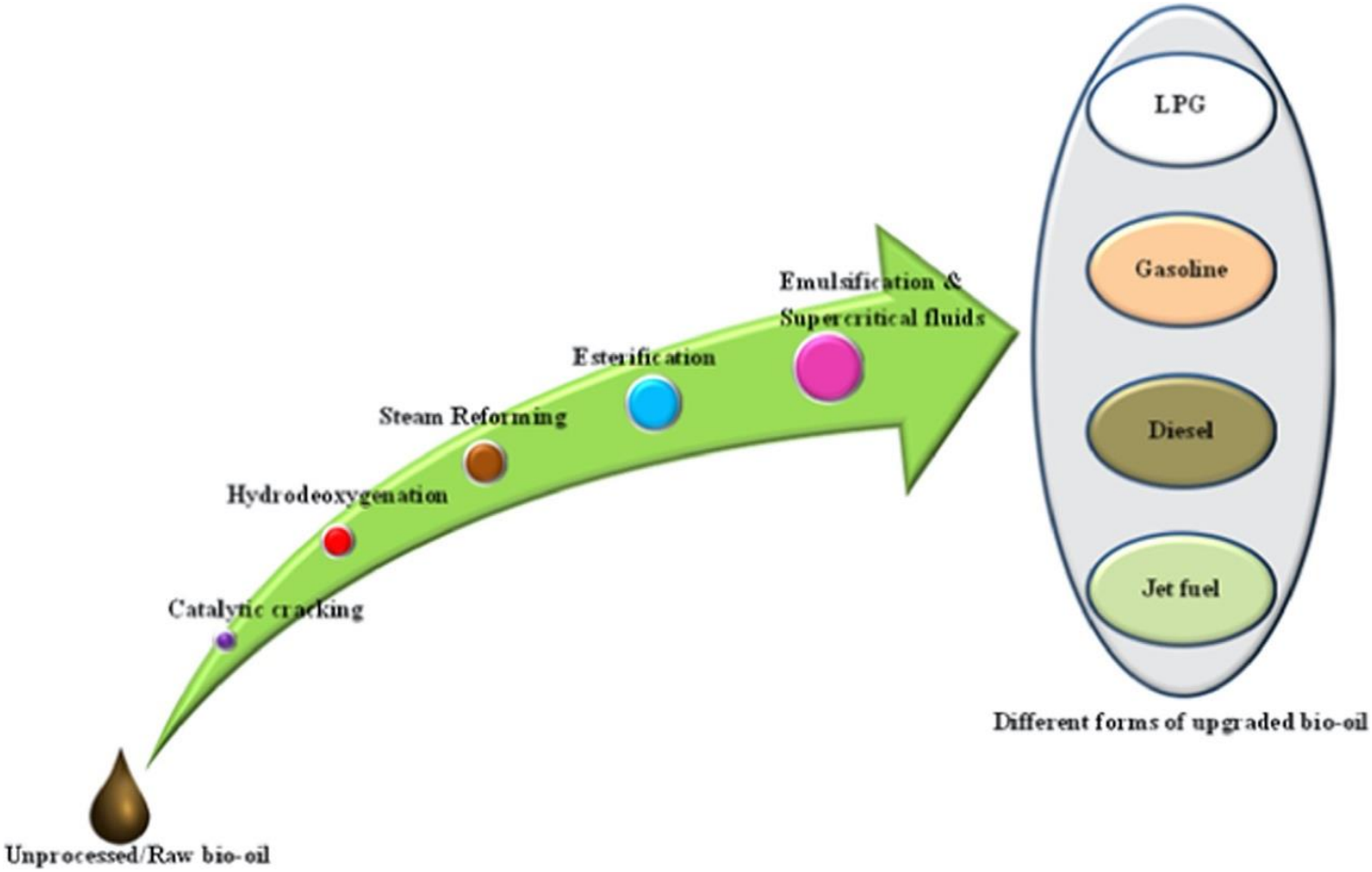

Figure 2. 6: Evolution of bio-oil upgrading techniques/methods (Gollakota et al., 2016).

Table 2. 6: Upgrading techniques of bio-oil with their advantages and disadvantages (Xiu and Shahbazi 2012).

Upgrading techniques	Process conditions	Advantages	Disadvantages
Hydrotreating	Temperature: ~500 °C	Commercialized	High coking (8–25%)
	Pressure: Low		Poor quality of fuels obtained
	Chemical: H_2/CO		
	Catalyst: HZSM-5 CoMo, NiMo		
Hydrocracking	Temperature: >350 °C	Makes larger quantities of light products	Need complicated equipment
	Pressure: 100–2000 psi		Reactor clogging
	Chemical: H_2/CO		Catalyst deactivation
	Catalyst: Ni/Al_2O_3-TiO_2		
Steam reforming	Temperature: 800–900 °C	Produces H_2 as a fuel	Complicated
	Catalyst: Ni		Require steady, dependable, and fully developed reactors
Supercritical fluids	Chemical: Alcohol, acetone, ethyl acetate, glycerol	High oil yield	Solvent is expensive
		Good fuel quality (lower oxygen content, lower viscosity)	
Esterification	Chemical: Alcohol	Simple	Solvents required
	Catalyst: Solid acid/base	Low cost of solvents	Mechanisms involved in adding solvent are not quite understood yet
		Reduces bio-oil viscosity	
Emulsification	Chemical: Surfactant	Simple	Requires high energy for production
		Less corrosive	

2.11.1 Esterification

Esterification of bio-oils with low molecular weight alcohols is an effective approach to improve their qualities (Gollakota et al., 2016). In the last few years, a lot of work has been done to upgrade the bio-oils by esterification (Cui et al., 2010, Zhang et al., 2006). Zhang et al. (2006) demonstrated the solid acid/base catalyst to esterify the bio-oil under atmospheric pressure and found that the acidity, density, heating value, and storage stability of the bio-oil improved remarkably.

2.12 Solvent-Assisted Biomass Conversion Processes

In biomass-related processes, subcritical and supercritical fluids have been employed in the transesterification, liquefaction, and gasification of biomass materials. Several studies have explored the enhancement of hydrothermal liquefaction (HTL) by utilizing water under supercritical conditions, where it serves both as a reactant and catalyst (Akhtar and Amin, 2011, Toor et al., 2011). Water exhibits unique properties like lower viscosity and increased solubility of organic compounds under sub- and supercritical conditions. These conditions create an ideal environment for rapid, uniform, and efficient chemical reactions (Toor et al., 2011). Additionally, the decrease in water's dielectric constant under supercritical conditions enhances its ability to dissolve free fatty acids which are hydrophobic organic compounds.

Supercritical transesterification is a non-catalytic transesterification process for biodiesel production. Supercritical alcohols can be used as an alternative technology to produce biodiesel via transesterification without catalyst addition (Anitescu and Bruno, 2012). The reaction mixture is heated to the critical temperature and pressure of the alcohol in this process. Researchers have used supercritical transesterification for a catalyst-free, highly efficient biodiesel production process to overcome the problems of homogenous/heterogeneous catalytic processes (Tan and Lee, 2011, Anitescu and Bruno, 2012).

Researchers are exploring the use of sub and supercritical water (SCW) in biomass gasification to avoid the costly and energy-intensive feed pre-treatment required in conventional methods (Guo et al., 2010). Operating under supercritical conditions removes barriers to mass transfer between phases, significantly enhancing the solubility of permanent gases and organic compounds in SCW during biomass gasification. This method, conducted at temperatures from 550 to 700°C, promotes high reaction rates, achieving complete gasification without adding catalysts (Guo et al., 2010, Azadi and Farnood, 2011).

2.12.1 Solvent-Assisted Bio-oil Upgrading

Polar solvents like acetone, ethanol, and methanol have been instrumental for over a decade in stabilizing the viscosity of bio-oil, which contains a high oxygen content (Bridgwater, 2012b). Specifically, methanol has proven effective in enhancing the uniformity of bio-oil, reducing its viscosity, and improving stability (Si et al., 2017). Compared to conventional organic solvents, supercritical fluid (SCF) solvents offer significant advantages in bio-oil treatment processes. These solvents capitalize on the unique properties associated with the supercritical state, such

as adjustable solvent strength and favourable transport properties, which facilitate the efficient separation of products from by-products and enable the recovery of homogeneous catalysts (Jessop and Leitner, 2008). Table 2.6 outlines the organic and inorganic compounds that are frequently utilized as supercritical fluids (SCFs) in bio-oil upgrading processes.

The objective of this section is to briefly explore the reported effects of these fluids on the process of supercritical bio-oil upgrading.

Table 2. 7: Frequently used solvents during bio-oil upgrading processes.

Solvents	Critical Parameters		
	Pressure (MPa)	Temperature (K)	Density (kg/m^3)
Ethanol	6.137	514.0	274.2
Methanol	8.084	512.3	273.8
Water	22.064	647.1	322.0
Carbon dioxide	7.383	304.2	468.2
1-butanol	4.414	563.1	271.5

Crude bio-oil contains reactive intermediates that can undergo polymerization reactions, leading to the formation of larger molecules and, ultimately, the production of coke (Xu et al., 2015). Subcritical and supercritical alcohols, noted for their unique hydrogen-donating ability, play a crucial role in preventing the repolymerization of reactive intermediates and subsequent coke formation. These fluids utilize unique solvation and dispersion mechanisms, uncommon in liquid-phase reactions, to effectively mitigate coke formation during bio-oil upgrading (Brand et al., 2013, Prajitno et al., 2016, Li et al., 2011). By encapsulating low-molecular-weight reactive intermediates with solvent molecules or dispersing them within the supercritical medium, these fluids prevent repolymerization and the deposition of coke. Specifically, supercritical ethanol and methanol are noted for their high alcoholysis capabilities, which enhance their ability to suppress coke formation during solvent-assisted bio-oil upgrading (Li et al., 2011, Zhang et al., 2012).

Bio-oil subjected to treatment with supercritical alcohols (ethanol, methanol, or 1-butanol) demonstrates enhanced properties characterized by reduced levels of highly reactive and corrosive compounds such as acids, aldehydes, ketones, and phenols, which typically have high oxygen content (Prajitno et al., 2016, Chen et al., 2014c, Xu et al., 2014). Concurrently, this process enriches the concentration of stable compounds including alcohols, esters, and ethers. Methanol and ethanol have demonstrated effectiveness in reducing oxygen concentration through hydrodeoxygenation, decarboxylation, and decarbonylation reactions [19, 20, 24].

Bio-oil treated with supercritical ethanol and methanol shows a notable decrease in oxygen concentration and O/C ratios compared to the original bio-oil (Prajitno et al., 2016, Li et al., 2011). Moreover, supercritical fluids (SCFs) reduce the acidity levels in crude bio-oil by serving as reactants in esterification processes. Using supercritical fluids increases the carbon and hydrogen content and the H/C ratio in the upgraded bio-oil compared to untreated bio-oil. This high hydrocarbon content enhances the co-processing compatibility of bio-oil with hydrocarbon fuels. Reducing the O/C ratio offers several advantages, including enhanced stability of bio-oil, reduced acidity (and consequently, reduced corrosiveness), increased heating value, and inhibited repolymerization and tar formation (Prajitno et al., 2016, Xu et al., 2014). Supercritical ethanol and methanol can engage in esterification reactions with organic acids present in bio-oil, forming non-corrosive and less reactive species such as ethyl esters and methyl esters (Li et al., 2011, Zhang et al., 2014b). Prajitno et al. (2016) reported that bio-oil treated with supercritical ethanol showed a substantial decrease in oxygen content, reducing it to 12.6 wt% from the original 26.8 wt% in fast pyrolysis bio-oil. Supercritical CO_2 ($scCO_2$) is highly effective in enhancing the heating value of crude bio-oil by extracting water, resulting in an upgraded bio-oil with a significantly increased calorific value. According to Cui et al. (2010) the treatment of crude bio-oil with supercritical CO_2 led to an increase of 83% in heating value. Carbon dioxide is highly favoured as a supercritical fluid primarily because of its low critical parameters (Ramsey et al., 2009).

Bio-oil upgraded in supercritical ethanol, methanol, 1-butanol, and CO_2 exhibits a higher heating value compared to the original bio-oil. This enhancement is primarily attributed to reducing or removing unfavourable components with high oxygen content. The solvent-assisted bio-oil upgrading technique remains open for optimization to achieve optimal operating parameters, considering energy costs and process efficiency. The following section will examine catalyst incorporation during solvent-assisted bio-oil upgrading.

2.12.2 Catalytic Solvent-Assisted Bio-oil Upgrading

Researchers have explored various methods to enhance bio-oil treatment processes. While catalysts improve reaction rates and yield, homogeneous catalytic reactions necessitate costly and energy-intensive separation processes. In contrast, heterogeneous catalytic reactions involve extended reaction times and expensive catalysts (Shende et al., 2019, Wildschut et al., 2009). To address these challenges, alternative approaches like incorporating supercritical fluids (SCFs) and cheap catalyst development have been developed to address these challenges

in bio-oil upgrading. Table 2.7 presents a consolidated overview of the research data pertaining to bio-oil upgrading.

Studies of bio-oil upgrading have utilized sulphided NiMo and CoMo catalysts for hydrodeoxygenation, aiming to achieve high activity, oxygen removal, and high yields without coke formation (Horáček and Kubička, 2017). However, these catalysts are prone to sulphur contamination and rapid deactivation. As an alternative, precious metal catalysts such as supported Pd, Pt, and Ru have been employed due to their superior performance in enhancing hydrodeoxygenation efficiency and increasing yields compared to traditional hydrotreatment catalysts (Zhang et al., 2021, Capunitan and Capareda, 2014, Wildschut et al., 2009).

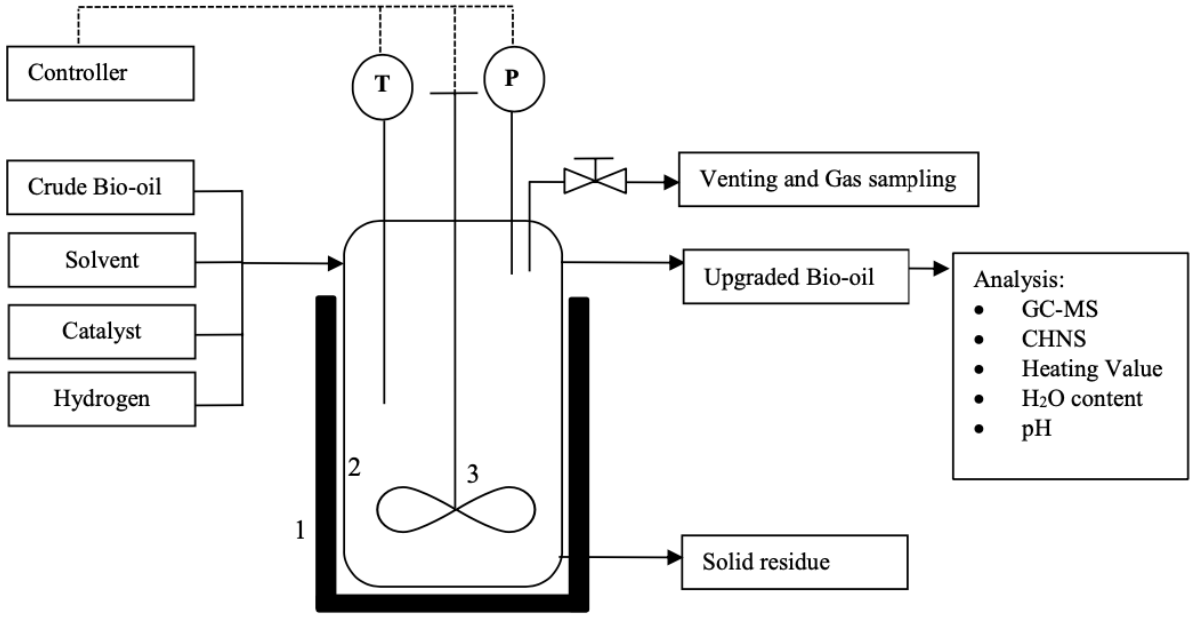

Figure 2. 7: Schematic presentation of bio-oil upgrading in stirred tank reactor (fixed volume).

In the last decade, there has been considerable research on bio-oil upgrading, exemplified in Figure 2.7, which outlines a typical process using supercritical solvents as documented in the literature.

2.12.2.1 Precious metals catalysts - Ruthenium

Ruthenium-based catalysts are noted for their efficacy in modifying the elemental composition of bio-oil through hydrogenation, deoxygenation, and denitrogenation processes. In a study done by Bai et al. (2014), Ru/C demonstrated superior performance in deoxygenation

compared to 15 other catalysts, including Pd and Pt. The upgraded oil produced by Ru/C had the lowest O/C molar ratio and the highest carbon content among the catalysts tested.

To enable the storage and transportation of bio-oil, it is essential to reduce its acidity, as bio-oil with a Total Acid Number (TAN) exceeding the ASTM specification of 0.50 mg KOH/g, according to ASTM D 6751-07a, can lead to operational problems and corrosion during storage (Chen et al., 2014b). The Total Acid Number (TAN) is a measure of bio-oil acidity, determined by the amount of potassium hydroxide (KOH) in milligrams needed to neutralize one gram of the oil. In the study conducted by Bai et al. (2014), the oil upgraded using the Ru/C catalyst exhibited the lowest Total Acid Number (TAN) compared to several other catalysts, including Pt/C and Pd/C. Oh et al. (2015) conducted a study investigating the impact of Ru/C and Pt/C catalysts on the hydrodeoxygenation of bio-oil. Their findings revealed that while both Ru/C and Pt/C treatments achieved complete removal of acidic components, the Ru/C upgraded oil exhibited a 59% reduction in Total Acid Number (TAN) from the original bio-oil, whereas Pt/C resulted in a 54% reduction.

Ruthenium (Ru) is frequently chosen as an active metal catalyst for bio-oil upgrading due to its superior hydrocracking abilities (Qu et al., 2021). Tang et al. (2010) found that using ruthenium (Ru) as an active metal catalyst for bio-oil upgrading offers significant advantages due to its high hydrocracking capabilities. This catalyst enhances oil yield and heating value while minimizing solid residue production. Specifically, bio-oil treated with supercritical ethanol and Ru catalyst showed markedly lower solid residue and higher oil yield and heating value compared to treatments using ZrO2/SBA-15, SO42-/ZrO2/SBA-15 catalysts, or supercritical ethanol alone (without catalyst). According to Chen et al. (2014c), Ru/C and Ru/HZSM-5 were found to produce bio-oils with higher oil content compared to bio-oils treated with Pd/C and Pt/C, indicating an enhancement in bio-oil yield. Yao et al. (2015) observed that the introduction of Ru into acidic catalysts promoted the hydrocracking of pyrolytic lignin while inhibiting polymerization and condensation reactions. As a result, this significantly increased the yield of oil. In another study, Ahmadi et al. (2016) compared the effects of CoMo and Ru/C catalysts and reported that the Ru/C catalyst resulted in the highest oil yield and minimal coke formation, with less than 1% by weight. Duan et al. (2016) reported that during bio-oil upgrading in supercritical water (SCW), the presence of Ru/C catalyst led to reduced coke formation. This effect was attributed to the catalyst promoting hydrogenation of coke precursors and inhibiting polymerization and condensation reactions. Among the

single-component and precious metal catalysts studied, Bai et al. (2014) found that oil upgraded with Ru/C exhibited the highest oil yield and the highest heating value (45.1 MJ/kg). This value was slightly higher than that of petroleum diesel (44.8 MJ/kg). Similarly, among 11 different catalysts tested, including Pt/C and Pd/C, Zhang et al. (2014a) identified Ru/C as the most effective catalyst for biocrude upgrading. They noted that Ru/C was unique in its ability to promote denitrogenation. Furthermore, biocrude upgraded using this catalyst exhibited the lowest sulphur content, high hydrocarbon content, and HHV. Xu et al. (2015) investigated the upgrading of pre-treated algal oil in supercritical water (SCW) using two-component catalyst mixtures, with Ru/C as the reference catalyst. They observed that while these mixtures offered benefits such as enhanced hydrogenation during bio-oil upgrading, their efficacy in deoxygenation was inferior to that of Ru/C as the sole catalyst. Likewise, Chen et al. (2014c) observed that the highest relative concentration of desired products was attained using Ru/C catalysts. The authors noted that Ru demonstrated superior hydrogenation capability compared to Pd and Pt, which potentially explains the enhanced upgrading performance observed with Ru/C.

Table 2. 8: Summary of bio-oil upgrading results.

Catalyst	Conditions	Observations	Ref
Ru/C (5wt%)	Batch reactor: Bio-oil (FR), 29 MPa, 330 ^{0}C (230–340 ^{0}C), 4 hrs, $R_{c:f}$ = 1:20	HHV_{TO} = 35.8 MJ/kg X_{TO} = 28% $X_{COKE} \leq$ 5% $(O/H/C)_{TO}$ = 15.5, 10.3, 74.2	de Miguel Mercader et al. (2010)
Ru/C (5wt%)	Batch reactor: Bio-oil (Beechwood): Step 1: 250 ^{0}C, 10 MPa and 4hrs $R_{c:f}$ = 1:31.5 Step 2: 20 MPa, 350 ^{0}C, 4 hrs, $R_{c:f}$ = 1:31.5	Step 2: HHV_{TO} = 43 MJ/kg X_{TO} = 17.5% X_{COKE} = 5% $(O/H/C)_{TO}$ = 11.6, 9.3, 79.1 DOD = 90wt%	Wildschut et al. (2009)
CoMo/C (1.9, 7.5) (3.5, 11.5)	Batch reactor: Algea HTL biocrude: 400 ^{0}C, 6.895 MPa and 5hrs $R_{c:f}$ = 1:70	H_2/kg of O = 47.7 $(O/H/C/N)_{Liq}$ = 7.05/11.0/75.2/3.01 HHV_{Liq} = 44 MJ/kg X_{Liq} = 74wt% X_{Wax} = 7wt%	Roy et al. (2022)
Ru/C (5wt%)	Packed Bed reactor: Bio-oil (Pine sawdust): Diethyl Ether extract LHSV = 0.4 h^{-1} 300–390 ^{0}C, 10 MPa	HHV = 41MJ/kg X_{oil} = 49% X_{COKE} = 1% $(O/H/C/N)_{oil}$ = 10.2/12.2/75.0/0.44	Kim et al. (2018)

Ru/C (5wt%)	Batch reactor: Bio-oil (Corn stover), 12.5 MPa, 200 ^{0}C and 300 ^{0}C, 4 hrs.	300 ^{0}C HHV = 39.0 MJ/kg X_{oil} = 54.4% DOD = 25.5% $(O/H/C/N/S)_{oil}$ = 8.80/9.69/78.6/2.6/0.40 200 ^{0}C $(O/H/C/N/S)_{oil}$ = 11.0/8.85/77.3/2.31/0.37 DOD = 7.4%	Capunitan and Capareda (2014)
Ru/C (5wt%)+1-butanol (1:1)-Feed:Solvent	Batch reactor: Bio-oil (Pine sawdust), 8.8-11.5 MPa, 250-300 ^{0}C, 3hrs.	250 ^{0}C HHV = 29.5 MJ/kg X_{oil} = 84.6% X_{COKE} = 0.3% DOD = 46.0% $(O/H/C/N)_{oil}$ = 24.7/10.5/64.3/0.2 280 ^{0}C HHV = 30.5 MJ/kg X_{oil} = 76.5% X_{COKE} = 0.3% $(O/H/C/N)_{oil}$ = 21.4/10.6/67.5/0.3 DOD = 53% 300 ^{0}C HHV = 32 MJ/kg X_{oil} = 69.4% X_{COKE} = 0.2% $(O/H/C/N)_{oil}$ = 14.5/11.3/72.4/0.2 DOD = 68%	(Xu et al., 2014)
Ru/C (5wt%) and Pt/C (5wt%) Ethanol (4:1)-Feed:Solvent	Batch reactor: Bio-oil (Miscanthus sinensis), 3 MPa, 250, 300 & 350 ^{0}C at 30, 45, and 60 min for each Temperature.	350 ^{0}C-Pt/C-45 min HHV = 27.8 MJ/kg X_{oil} = 34.9% DOD = 73.7% $(O/H/C/N/S)_{oil}$ = 20.1/9.0/70.7/0.2/0.0	(Oh et al., 2015)
Pd/C Ethanol (4:1)-Feed:Solvent	Batch reactor: Bio-oil (poplar wood), 3 MPa, 250-370 ^{0}C at 40-120 min	350 ^{0}C-60 min-2wt% catalyst HHV = 37.4 MJ/kg $(O/H/C/N)_{oil}$ = 18.2/8.1/73.0/0.8	(Kim et al., 2014)
Co; Zn; Co-Zn on HZSM-5 Methanol (1:1)-Feed:Solvent	Batch reactor: Bio-oil (pine sawdust), 500 psig, 300 ^{0}C, 5hrs	10%Co10%Zn/HZSM-5 HHV = 31.98 MJ/kg 5%Co15%Zn/HZSM-5 X_{oil} = 22.13% 20%Co/HZSM-5 H_2O=3.61	(Cheng et al., 2017)

This work aims to apply subcritical conditions for methanol, ethanol, and isopropyl alcohol and supercritical conditions for ethyl ether to stabilize the bio-oil organic phase before severe hydrotreatment. This approach is adopted to mitigate the effects of polymerization and the

impossibility of catalyst recovery that occurs during conventional mild hydrotreatment processes of bio-oil. The bio-oil stabilization approach of the current study is shown in Figure 2.8.

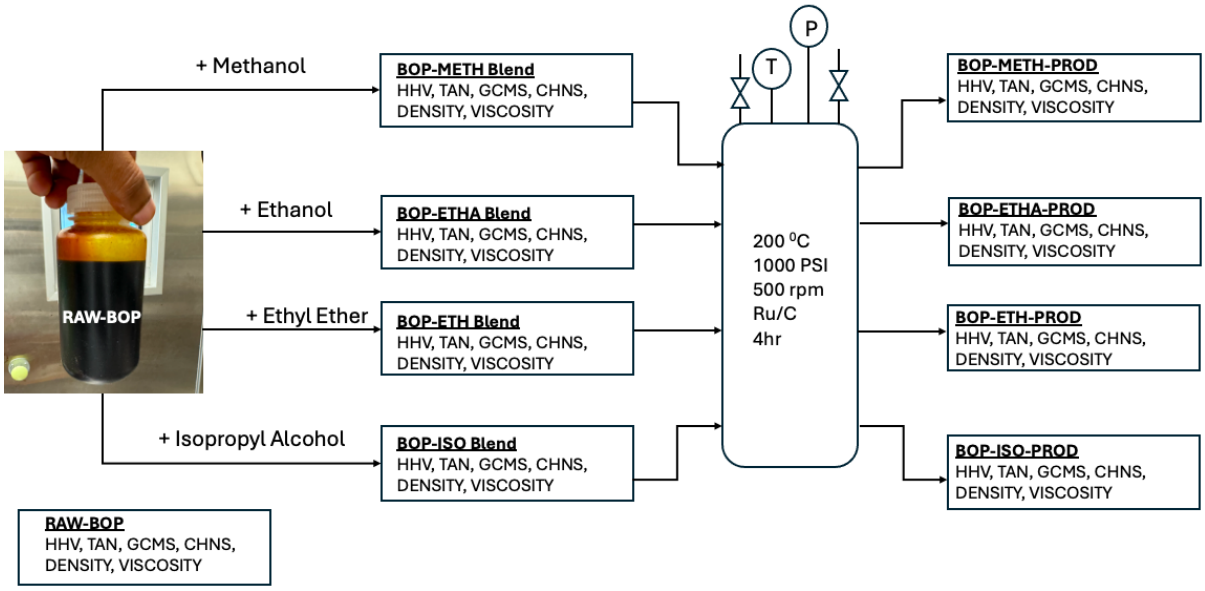

Figure 2. 8: Solvent-assisted bio-oil stabilization approach of the current study.

CHAPTER 3

3. Catalytic and Non-Catalytic Fast Pyrolysis of Giant Reed Biomass in a Fixed Bed Reactor

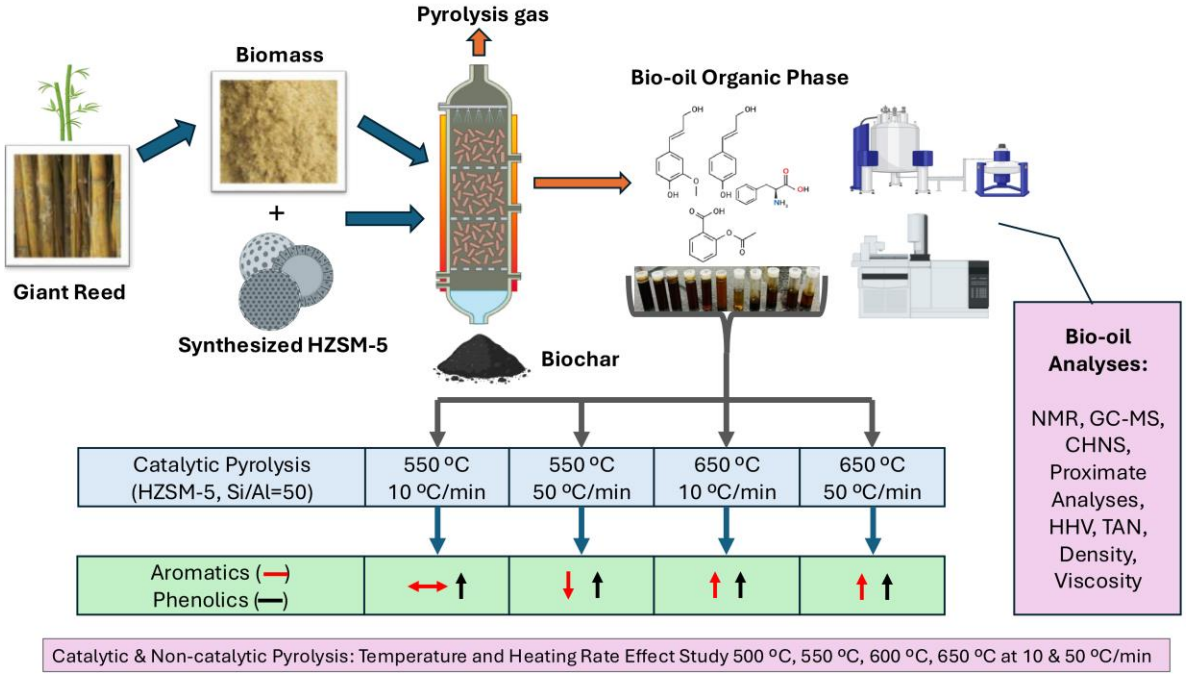

Abstract

A comparative study of catalytic and non-catalytic fast pyrolysis of giant reed was performed in a packed bed reactor. Giant reed was subjected to fast pyrolysis at 500-650 °C with heating rates of 10 and 50 °C/min, using a synthesized HZSM-5 (Si/Al=50) zeolite catalyst. Bio-oil properties were determined via gas chromatography-mass spectrometric detector (GC-MS), nuclear magnetic resonance (NMR), viscosity, total acid number (TAN), density, higher heating value (HHV), and proximate/ultimate analyses. Biomass and catalyst characterization included proximate/ultimate analysis (biomass) and pyridine adsorption infrared spectroscopy (Py-IR), Brunauer-Emmett-Teller (BET), and X-ray diffraction (XRD) (catalyst). The results indicated that the presence of the HZSM-5 catalyst significantly improves the quality of the pyrolysis oil. Catalytic pyrolysis consistently yielded bio-oil with lower moisture content and higher carbon content than non-catalytic pyrolysis. At the temperature of 550 °C and 10 °C/min, the HHV of the catalytic pyrolysis product was 23.0 MJ/kg compared to 21.3 MJ/kg for non-catalytic pyrolysis. Applying the HZSM-5 catalyst at 650 °C and 50 °C/min significantly enhances the production of aromatic hydrocarbons and phenolic compounds while reducing the presence of undesirable oxygenates in the bio-oil. However, this observation is a

trade-off to lower bio-oil yields and high energy consumption. As a result, 550 °C and 10 °C/min is a considered operating condition for bio-oil production using giant reed as feedstock.

Keywords: Fast Pyrolysis; Biofuels; Bio-oil; Zeolite; Giant Reed; Catalytic Pyrolysis.

3.1 Introduction

In response to the increasing global imperative for sustainable and renewable energy resources, there has been a substantial acceleration in research directed towards the utilization of biomass as a substitute for fossil fuels. Among the wide array of biomass feedstocks, *Arundo donax* (Giant Reed) is considered a promising candidate for biofuel production due to its fast growth rate, high yield, and adaptability to poor soil conditions (Ortega et al., 2024, Pilu et al., 2012, Ge et al., 2016, Ramsurrun and Surroop, 2019, Cappelli et al., 2021). Giant Reed species make it to the top 100 most invasive plant species globally, as stated by the International Union for the Conservation of Nature (Lowe et al., 2000). Furthermore, as an invasive species, Giant Reed is also regarded as a potential solution for biomass production while aiding in controlling its spread (Smith et al., 2013). Thermochemical conversion methods, particularly pyrolysis, have shown great potential in converting biomass into bio-oil, which is regarded as a viable alternative to conventional petroleum-derived fuels upon further treatment (Wang and Wu, 2023, Awasthi et al., 2023, Zhang and Brown, 2019, Lahijani et al., 2022, Gollakota et al., 2016). Pyrolysis involves the thermal decomposition of biomass in the absence of oxygen, producing bio-oil, syngas, and char. The product yields are influenced by the type of the pyrolysis process i.e. either fast, slow or flash. Fast pyrolysis is generally considered more advantageous for bio-oil production. This is because its primary goal is to maximize liquid yield, making it more efficient for producing bio-oil as a fuel or chemical feedstock. The rapid heating rates and short vapor residence times in fast pyrolysis minimize secondary reactions and prevent further decomposition of the bio-oil, leading to a higher yield compared to slow pyrolysis. Despite its potential, pyrolysis bio-oil often suffers from high oxygen content, low stability, and poor calorific value, limiting its direct use as a fuel (Fermoso et al., 2017, Gollakota et al., 2016, Wang et al., 2013, Liu et al., 2014, Khan et al., 2022). To overcome these challenges, catalytic pyrolysis has gained significant attention for improving bio-oil quality by reducing oxygenated compounds and promoting the formation of more stable and energy-dense hydrocarbons (Mortensen et al., 2011, Kariim et al., 2023, Tawalbeh et al., 2021, Qiu et al., 2018). In catalytic fast pyrolysis (CFP), catalysts are essential for selectively removing oxygen from bio-oils, helping convert reactive oxygenates into stable, chemically

robust compounds (Liu et al., 2020b). A wide range of catalysts including metal oxides, inorganic salts, zeolites, mesoporous silica, and carbon-based materials have been extensively studied for their effectiveness in improving bio-oil quality (Bhoi et al., 2020, Chen et al., 2019). Among these options, zeolite catalysts are particularly notable. Unlike many other catalyst types, which often reduce bio-oil yield significantly, zeolites achieve improvements in bio-oil quality while maintaining a more favourable yield (Rezaei et al., 2014). This unique advantage has positioned zeolite catalysts as a focal point in CFP research, with their ongoing development deemed critical to advancing bio-oil production technology. Zeolites such as HZSM-5 are widely recognized for their ability to deoxygenate bio-oil, increase aromatic hydrocarbon yield, and improve the stability of the produced liquid (Valle et al., 2022). Furthermore, HZSM-5 zeolite has demonstrated strong catalytic activity for the conversion of biomass into high-value chemicals and bio-oil with a reduced oxygen content (Promsampao et al., 2022, Chiosso et al., 2023, Shun et al., 2013, Liang et al., 2021, Taarning et al., 2011, Wang et al., 2016, Shao et al., 2017). The use of HZSM-5 in catalytic pyrolysis has been extensively studied with several biomass feedstocks such as wood, agricultural residues, and municipal waste. Studies have shown that this catalyst facilitates the deoxygenation of pyrolysis vapours, leading to bio-oil with lower oxygen content and higher calorific value, making it more suitable for direct fuel applications (Sebestyén et al., 2017, Mullen and Boateng, 2015, Dai et al., 2018, Chang et al., 2018, Zhang et al., 2016, French and Czernik, 2010, Valizadeh et al., 2022, Park et al., 2015, Yathavan and Agblevor, 2013). Additionally, metal-doping techniques (such as with Cr, Fe, and Zn) have been applied to HZSM-5 to further modify its activity, improving the selectivity toward light olefins and aromatic products (Chiosso et al., 2023). These modifications are essential to optimize catalytic performance and selectivity, which is crucial for scaling up the process for biofuel production. However, while extensive research exists on the catalytic pyrolysis of various biomass types using HZSM-5, studies focusing on Giant Reed as a feedstock remain scarce, leaving a notable gap in the literature. Given its high biomass yield and invasiveness, Giant Reed represents an underexplored yet valuable source for bio-oil production, especially when coupled with catalytic enhancement. This study addresses the gap by investigating the catalytic and non-catalytic fast pyrolysis of Giant Reed biomass in a fixed bed reactor. Specifically, we examine the effects of temperature and heating rate on the bio-oil yield and composition with a constant catalyst loading of HZSM-5. In addition, we employ nuclear magnetic resonance (NMR) spectroscopy to analyze the organic phase of the produced bio-oil, providing a detailed compositional analysis that has received limited attention in previous studies. This approach not only expands the understanding of Giant Reed's potential

as a biofuel feedstock but also contributes valuable insights into the catalytic effects of HZSM-5 on bio-oil quality and yield.

3.2 Materials and Methods

3.2.1 Sample Harvesting and Preparation

Giant Reed (Arundo donax) was harvested in-land (terrestrial) in Ladysmith marginal land in Kwa-Zulu Natal, South Africa (28.5631^0 S, 29.7810^0 E). Giant reed height from the ground was 2-6 m. The culm of the A. donax was considered in the current study. The culm was cut into short pieces and then dried for 24 h at 105 °C. The oven-dried biomass was ground by a micro plant grinder, followed by sieving to a particle size range of 0.5-2 mm.

3.2.2 Catalyst Preparation

3.2.2.1 Chemicals

To synthesize HZSM-5 with a Si/Al molar ratio of 50, the following chemicals were use, sodium silicate as the silicon source (Si as SiO_2, Na as Na_2O), aluminium sulfate as the aluminum source (Al as Al_2O_3), sodium hydroxide (NaOH, 97%) for pH adjustment, tetrapropylammonium bromide (TPABr) as a structure-directing agent (SDA), sulfuric acid (H_2SO_4, 98%) for pH control, and ammonium nitrate (NH_4NO_3) for ion exchange. All chemicals were purchased from Sigma-Aldrich, USA.

3.2.2.2 Catalyst Synthesis

The HZSM-5 catalyst synthesis followed a molar composition of $50SiO_2{:}1Al_2O_3{:}5TPABr{:}2.5Na_2O{:}2000H_2O$. Initially, sodium silicate and sodium hydroxide were dissolved in deionized water to form the silica solution. Separately, aluminium sulfate was also dissolved in deionized water and continuously stirred under ambient conditions to form alumina solution. Similarly, the SDA (TPABr) was dissolved in deionized water to form SDA solution. After preparing the solutions for gel synthesis, silica solution was mixed with the SDA solution under continuous vigorous stirring for 1 hr at 1000 rpm to thoroughly hydrolyze the components. The alumina solution was then added into the mixture and vigorously stirred for 5 hrs until the gel was formed. The pH value of the gel was adjusted to 10.5 by dropwise addition of 3 mL sulfuric acid. The final gel solution was allowed to age for

12 hrs at room temperature. The gel was then transferred into a Teflon-lined stainless-steel autoclave reactor for hydrothermal crystallization at 180 ºC for 24 hrs under autogenous pressure. Following the crystallization stage, the resulting precursor (ZMS-5 with template) was separated by filtration, thoroughly washed with deionized water, and dried at 110 ºC for 24 hrs. The dried product was calcined at 550 ºC for 5 hrs to eliminate organic template and obtain the sodium form ZSM-5 (Na-ZSM-5). The prepared Na-ZSM-5 was subjected to ion exchange at 80 ºC for 3 hrs with 1M solution of ammonium nitrate to obtain the ammonium form (NH_4^+-ZSM-5). The ion exchange step was repeated three times to ensure complete exchange of ions. Upon completion of the ion exchange step, the sample was filtered, washed with deionized water, and dried at 110 ºC for 24 hrs. Finally, the ammonium form was calcined for 5 hrs at 550 ºC to breakdown ammonium ions (form ammonia gas) and convert the catalyst to its active acidic form (H-ZSM-5).

3.2.3 Catalyst Characterization

3.2.3.1. Py-IR

The acidity profile of the synthesized catalyst was evaluated using pyridine adsorption infrared spectroscopy (Py-IR) on a Nicolet 6700 infrared spectrometer. This instrument operates with a resolution of 4 cm^{-1}, a precision of 0.01 cm^{-1}, and performs 32 scans. A sample with a mass of 1.50×10^{-2} g was initially degassed at 400 °C under high vacuum for 2 hours, followed by pyridine adsorption at ambient temperature. The sample was then subjected to desorption at 150 and 350 °C for 10 minutes each to capture the respective infrared spectra. Pyridine adsorption on zeolite acid sites produces characteristic bands in the 1300–1700 cm−1 region, corresponding to Brønsted and Lewis acid sites. The Brønsted to Lewis acid sites (B/L) ratio was calculated based on the integrated intensities of the pyridine adsorption bands at 1545 cm^{-1} (Brønsted acid sites) and 1450 cm^{-1} (Lewis acid sites), using their respective extinction coefficients (ε_B = 1.67 cm/μmol, ε_L= 2.22 cm/μmol) (Emeis, 1993). Additionally, the concentration of acid sites was determined by applying the following equation derived from De Beer's law:

$$C = \frac{A}{\varepsilon} \times \frac{s}{m} \times 10^3 \qquad (3.1)$$

Where C is the concentration of acid sites ($\mu mol.g^{-1}$), A is the band area (cm^{-1}), m is the mass wafer (mg), S is the wafer surface (2 cm^2), and ε is the molar extinction coefficient (cm/μmol).

3.2.3.2. X-ray Diffraction (XRD)

Phase analysis of the prepared catalyst was performed using X-ray diffraction (XRD) on a Bruker D8 Advance diffractometer with Cu Kα radiation (λ = 1.5418 Å) at 40 kV and 40 mA. The X-ray beam was incident at an angle of 5°, providing a penetration depth of less than 1.3 μm, assuming a completely flat surface. The data were collected in the 5° to 50° 2θ range, with a scan speed of 4° min^{-1} using a LYNXEYE detector. The setup enabled accurate phase identification and characterization of the catalyst structure.

3.2.3.3. Brunauer-Emmett-Teller (BET)

The N2 adsorption/desorption isotherms of the catalyst were obtained using a Micromeritics Tristar II 3020. Prior to analysis, the samples were degassed at 150 °C under vacuum for 3 hours to eliminate moisture and residual gases, followed by measurements at −195 °C with nitrogen as the adsorbate. The specific surface area was calculated using the BET method, the total pore volume was determined at a relative pressure of P/P0 = 0.995, and the pore size distribution was derived using the Brunauer-Joyner-Halenda (BJH) model.

3.2.4 Analytical Methods

Elemental analysis (CHNS) was performed using an Elementar Vario Micro Select, according to ASTM D5373 and ASTM D5291. The oxygen content was determined by difference, and the results were reported on a dry basis. The moisture content of bio-oil was measured by the Karl Fischer Titration method. Total Acid Number (TAN) was measured by a Mettler T50 autotitrator using a Total Acid Number Titration Solvent Mixture and 0.1M KOH 2-propanol as the titrating reagent (titrant), according to ASTM D664-07. The viscosity (kinetic and dynamic) and density were measured using the Anton Paar Instrument (SVM Standard method) at 40 ^{0}C. Biomass moisture and ash content were determined according to ASTM D4442-07 and E 1755-01, respectively. The volatiles were determined according to ASTM E872, and fixed carbon content was determined by difference. The thermal degradation profile of the biomass was evaluated using a Thermogravimetric Analyzer (TGA5500) under a nitrogen atmosphere, spanning a temperature range of 25 to 800°C with a heating rate of 10°C/min. Platinum HT pans were utilized for sample loading, and a ramping procedure was employed during the analysis. The weight loss data as a function of temperature were subsequently analyzed to assess the thermochemical decomposition characteristics of the biomass. A bomb calorimeter was used to determine the higher heating values of biomass and bio-oil organic

phase. A muffle furnace was used during the oxidation processes. The chemical functional groups of organic phase bio-oil were identified using a ^{13}C NMR. The chemical composition of organic phase bio-oil was analyzed by gas chromatography coupled with a mass spectrometric detector (GCMS). The experiments were carried out on an Agilent 5977C GC/MSD with helium gas as a carrier gas. National Institute of Standards and Technology (NIST) spectral library was used to identify the chemical compounds. To mitigate potential damage to the GC column from the complex matrix of bio-oil, a rigorous sample preparation protocol was implemented. This involved weighing (approx. 20 mg of bio-oil) and diluting with 2 ml methanol to reduce viscosity and concentration, followed by filtration through a JT Baker Nylon syringe filter with a 0.2 μm pore size. This pre-treatment effectively minimized the introduction of non-volatile and particulate components into the GCMS system, ensuring the integrity and longevity of the analytical column. The filtered sample was injected, and the inlet temperature was set to 280 ^0C at a split ratio of 10:1. The column temperature was held at 50 ^0C for 5 min, then heated to 280 ^0C at a ramping rate of 10 ^0C/min with a 5 min holding time. A synthesized catalyst, HZSM-5, was employed in this study and applied as received.

3.2.5 Semi-Batch Pyrolysis Setup and Procedure

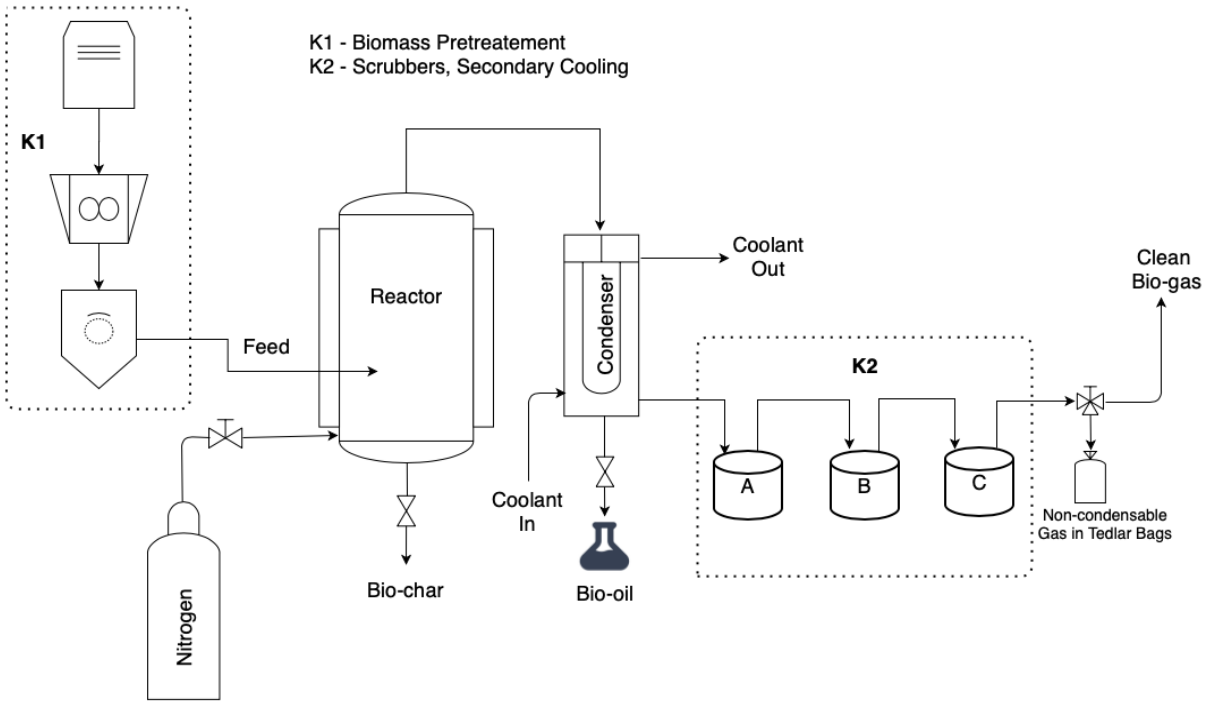

Figure 3. 1: Schematic representation of semi-batch fast pyrolysis unit.

Pyrolysis experiments were performed in a 1.5 L stainless steel fixed bed reactor (FBR). The representation of the pyrolysis system is shown in Figure 3.1. For a typical catalytic experimental run, 60 g of pretreated biomass at a catalyst ratio of 3 wt% was loaded into the reactor. This was followed by purging with nitrogen at 2 l/min to remove unwanted oxygen in the pyrolysis system. The reactor loaded with biomass and catalyst was weighed and inserted into the furnace. The nitrogen flow rate during the reaction was maintained at 2 l/min to maintain an inert atmosphere. A 3kW electrical heater equipped with a temperature control panel was used as a heat source during the pyrolysis reaction. The furnace was heated from room temperature to the desired setpoint temperature of 550 ^{0}C at a heating rate of 1 ^{0}C/min. Condensable vapors from the pyrolysis reactor were cooled in a two-series condensing system using cold water as a cooling medium. The cooling water was continuously circulated at 5 l/min using a submersible pump. Ice cubes were added to the circulating water to maintain the temperature at 5 ^{0}C. The bio-oil was collected in two product bottles connected in series. Non-condensable gases were collected in 0.5 L Tedlar bags (CEL Scientific) 15 min after the pyrolysis reaction for compositional analyses was started. The pyrolysis reaction was allowed to run until no gas was coming out of the exhaust line, with an average reaction time of 45 ± 5 min per run. At the end of each experiment, the reactor was allowed to cool down to room temperature, and the reactor with biochar was weighed. The percentage yields of the bio-oil organic phase (BOP%), aqueous phase (BAP%), biochar (BC%), and non-condensable gases (BG%) were calculated by the following equations:

$$\mathrm{BOP\%} = \frac{\mathrm{m_{bop}}}{\mathrm{m_{bm}}} \times 100 \qquad (3.2)$$

$$\mathrm{BAP\%} = \frac{\mathrm{m_{bap}}}{\mathrm{m_{bm}}} \times 100 \qquad (3.3)$$

$$\mathrm{BC\%} = \frac{\mathrm{m_{bc}}}{\mathrm{m_{bm}}} \times 100 \qquad (3.4)$$

Where, m_{bop}, m_{bm}, m_{bap}, and m_{bc} are the masses of the organic phase, biomass, aqueous phase, and biochar, respectively. The principle of mass conservation was used to determine the pyrolysis gas production yield according to the following equation;

$$\mathrm{BG\%} = 100 - \mathrm{BC\%} - (\mathrm{BOP\%} + \mathrm{BAP\%}) \qquad (3.5)$$

3.3 Results and Discussion

3.3.1 Characterization of feedstock

Table 3. 1: Characterization of Giant Reed biomass.

Parameter	Giant Reed
Proximate Analysis (wt%)[db]	
Moisture Content[b]	5.540 ± 0.11
Volatile content	84.91 ± 0.63
Ash content	1.880 ± 0.01
Fixed carbon[a]	7.67
Ultimate Analysis (wt%)[db]	
Carbon	49.77 ± 0.150
Hydrogen	6.890 ± 0.130
Nitrogen	0.250 ± 0.036
Sulphur	0.080 ± 0.002
Oxygen[a]	43.01 ± 0.141
Calorific Value (MJ/kg)	18.85 ± 0.053

[db] dry basis, [a] determined by difference.

The characterization results (Table 3.1) of giant reed biomass reveal its potential as a feedstock for bio-oil production via fast pyrolysis. With a high volatile matter content (84.91 wt%) and moderate caloric value (18.85 MJ/kg), giant reed biomass offers promising bio-oil yield and quality prospects. Despite its relatively higher ash content of 1.88 wt% compared to woody biomass (0.2-0.5 wt%) (Yildiz et al., 2015, Febrero et al., 2015), giant reed biomass still presents a viable option for bio-oil production, with its low nitrogen (0.25 wt%) and sulphur (0.08 wt%) contents indicating minimal emissions concerns. The elemental composition further supports the suitability of giant reed biomass for producing bio-oil, with carbon comprising the majority of its composition at 49.77 wt%. This suggests the potential for yielding carbon-rich bio-oil during fast pyrolysis, contributing to higher energy content. The oxygen content is observed to be 43.01 wt%, which is relatively high and may lead to the formation of oxygenated compounds in bio-oil. This provides opportunities for bio-oil valorization through downstream upgrading processes such as hydrodeoxygenation. Overall, giant reed biomass offers favourable characteristics for bio-oil production, particularly in terms

of its high volatile matter content and carbon-rich composition. The current research focuses on optimizing pyrolysis conditions (temperature and heating rate) to maximize bio-oil yield and improve quality while minimizing undesired by-product formation.

3.3.2 Thermal Degradation of Feedstock

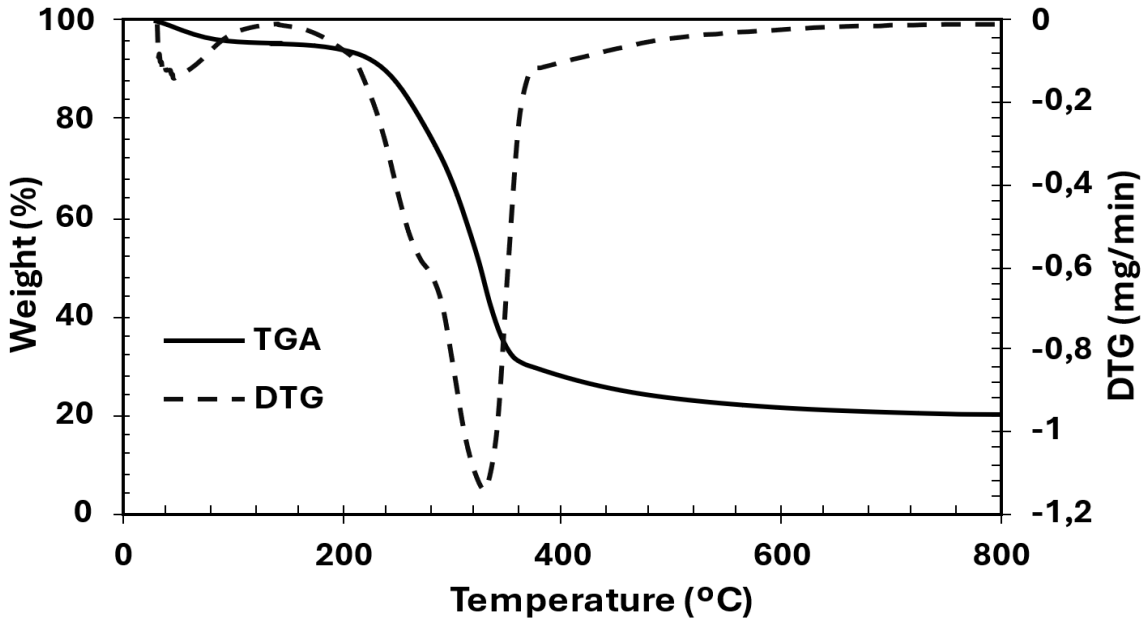

Figure 3. 2: Thermal degradation behaviour of Giant Reed biomass.

The thermogravimetric analysis (TGA) and differential thermogravimetry (DTG) profiles provide valuable insights into the pyrolysis reaction temperature range and the thermal degradation behaviour of various biomass materials. Figure 3.2 illustrates the TGA and DTG profiles for giant reed biomass, which exhibit three distinct stages of mass loss. The initial degradation stage, occurring between 26°C and 120°C, is attributed to the removal of moisture and the volatilization of light extractives, with an average mass loss of 5.50 wt%. The second stage corresponds to the thermal degradation of cellulose and hemicellulose (holocellulose), occurring within an average temperature range of 220°C to 360°C. The decomposition temperatures for pure cellulose, hemicellulose, and lignin are reported as 315°C–400°C, 220°C–315°C, and 150°C–900°C, respectively (Yang et al., 2007). Notably, the decomposition of hemicellulose occurs prior to the onset of cellulose degradation, beginning at approximately 220 °C (Bessa et al., 2020). Cellulose exhibits a higher degradation temperature than hemicellulose due to its linear polymer structure composed of glucose units, which lacks branching, thereby enhancing its thermal stability and structural integrity. During the second

stage of pyrolysis (active pyrolysis stage), an average mass loss of approximately 65 wt% is observed, during which some lipids and proteins also undergo thermal decomposition. The final stage, occurring between 385°C and 800°C, represents the continued degradation of lignin and the carbonization of cross-linked sugars, resulting in an average mass loss of 10 wt%. Lignin, characterized by aromatic rings with numerous branches interconnected by strong chemical bonds, exhibits a broad degradation temperature range (Suárez et al., 2023, Yang et al., 2007). The degradation of the remaining carbonaceous material in the biomass occurs during lignin decomposition, extending to the final temperature of 800°C. These materials are the primary contributors to char formation (Cheng et al., 2015). After thermal degradation, the residual weight percentage was 20%. The DTG profile revealed a secondary minor shoulder, observed immediately after the dehydration phase (26–120°C), which is attributed to the degradation of hemicellulose. The temperature range for hemicellulose degradation partially overlaps with that of cellulose, resulting in a shoulder on the weight loss rate curve rather than a distinct peak (Grønli et al., 2002). The DTG profile reveals that hemicellulose degradation occurs between 220°C and 323°C. The degradation of cellulose is marked by distinct peaks within the 300°C to 400°C temperature range. Furthermore, biomass harvested in the autumn, which typically contains higher concentrations of low molecular weight compounds like resins and oils, may undergo faster holocellulose degradation (Shezi et al., 2024). Lower hemicellulose content leads to more pronounced cellulose degradation peaks. As a result, holocellulose can decompose concurrently, creating a more distinct peak (Saffe et al., 2019). The temperature at which the maximum mass loss rate occurred was 331°C, primarily attributed to the higher cellulose content. Additionally, the observed temperature for maximum mass loss in giant reed aligns with the findings of Huang et al. (2015). Following cellulose degradation, lignin decomposition occurs during passive pyrolysis within the temperature range of 400°C to 800°C. In this phase, lignin undergoes thermal degradation without a distinct peak, likely due to the relatively small mass loss, which results in a minimal reaction rate. The maximum thermal degradation rate (−dm/dT) observed for giant reed biomass was 1.18 mg/min, as shown in Figure 3.2.

3.3.3 HZSM-5 Phase Structure

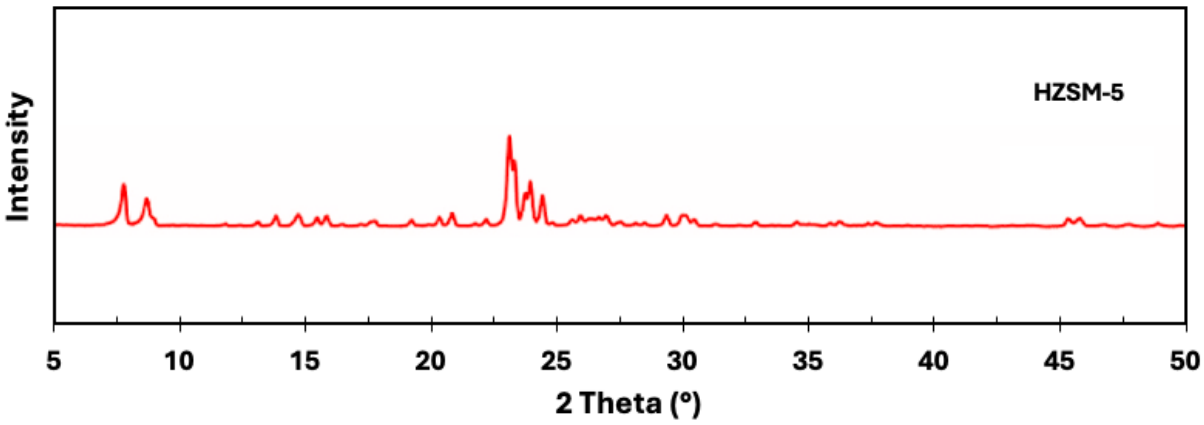

Figure 3. 3: XRD pattern of synthesized HZSM-5 catalyst

The X-ray diffraction (XRD) pattern of the catalyst, displayed in Figure 3.3, reveals no additional diffraction peaks apart from the typical Mobil Five (MFI) peaks characteristic of the HZSM-5 zeolite structure, occurring at 7–9° and 23–25° for 2θ, specifically at 7.95°, 8.85°, 23.17°, 24.00°, and 24.48°. The analysis of the peaks in the 23–25° range indicates that the crystallinity of the catalyst remains unchanged, which is consistent with previously reported results (Park et al., 2022, Guo et al., 2022). Furthermore, the peaks within the range of 23–25° are also an indication that HZSM-5 (Si/Al = 50) catalyst was successfully synthesized.

3.3.4 Specific Surface Area of HZSM-5 Catalyst

Table 3. 2: HZSM-5 surface properties.

Catalyst	S_{BET} (m^2/g)[a]	S_{ext} (m^2/g)[b]	V_{total} (cm^3/g)	V_{micro} (cm^3/g)[c]	V_{meso} (cm^3/g)[d]	Pore Size (nm)[e]
HZSM-5	423.3	38.4	0.258	0.169	0.089	5.6

[a] Determined by BET equation

[b] Determined by *t*-plot method and Harkins-Jura equation

[c] t-plot micropore volume

[d] $V_{meso} = V_{total}$ (at $P/P_0 = 0.995$) – V_{micro}

[e] BJH desorption average pore diameter between 20 Å and 500 Å

The synthesized HZSM-5 catalyst with a Si/Al ratio of 50 exhibited a BET surface area of 423.3 m²/g as tabulated in Table 2. This value is remarkably consistent with the surface area of 425 m²/g reported by Ding et al. (2018) for HZSM-5 with the same Si/Al ratio, albeit derived

from a purchased ZSM-5 precursor and subjected to a slightly shorter calcination time of 4 hours at 550°C. This close agreement suggests that the synthesis method employed in this work yielded a material with comparable surface area characteristics despite the use of synthesized ZSM-5 rather than a commercial one. Furthermore, a BET surface area of 423.3 m^2/g is indicative of a well-developed porous structure. However, the surface area obtained in this study is notably higher than the 350 m^2/g reported by Rahman et al. (2020) for a purchased ZSM-5 with a lower Si/Al ratio of 46. This difference is expected, as it is well-established that higher Si/Al ratios generally lead to increased surface areas in ZSM-5 zeolites due to the higher framework density of silicates. When comparing with Rajaei et al. (2021), despite having the same Si/Al ratio of 50, the surface area obtained in this work (423.3 m^2/g) is slightly higher than their reported value of 405 m^2/g. This variation could be attributed to the different calcination protocols employed. Rajaei et al. (2021) calcined the ZSM-5 overnight at a lower temperature of 110°C, while in the present study, calcination was carried out at 550°C for 5 hours. The higher calcination temperature used in this work might have resulted in a more complete removal of organic template molecules, leading to a more accessible pore structure and a higher surface area. The external surface area (S_{ext}) of 38.4 m^2/g in Table 2 suggested that a significant portion of the surface area is exposed for catalytic reactions. The total pore volume (V_{total}) is 0.258 cm^3/g, with a distribution of micropores (V_{micro} = 0.169 cm^3/g) and mesopores (V_{meso} = 0.089 cm^3/g). The pore volume of the synthesized HZSM-5 (0.258 cm^3/g) is considerably lower than the value of 0.418 cm^3/g reported by Rajaei et al. (2021). This discrepancy could be a consequence of variations in the synthesis procedure, particularly in the degree of micropore development or the presence of any mesopores or macropores. The difference in pore size (5.6 nm in this work vs. 4.15 nm in Rajaei et al. (2021)) also supports the possibility of structural variations. The average pore size of 5.6 nm highlights a mesoporous structure, which is advantageous for facilitating the diffusion of reactants and products during in situ pyrolysis (Liu et al., 2020a). In summary, the synthesized HZSM-5 in this study exhibits comparable surface area to literature values for similar Si/Al ratios, with minor variations likely arising from differences in synthesis and activation procedures. The observed differences in pore volume and size compared to Rajaei et al. (2021) highlight the sensitivity of these properties to the specific synthesis conditions employed. Nonetheless, the observed textural features are expected to enhance the catalyst's performance by providing a high surface area for active site availability, along with a suitable pore network to accommodate the reaction intermediates and promote efficient catalytic activity.

3.3.5 Acidity of HZSM-5 Catalyst

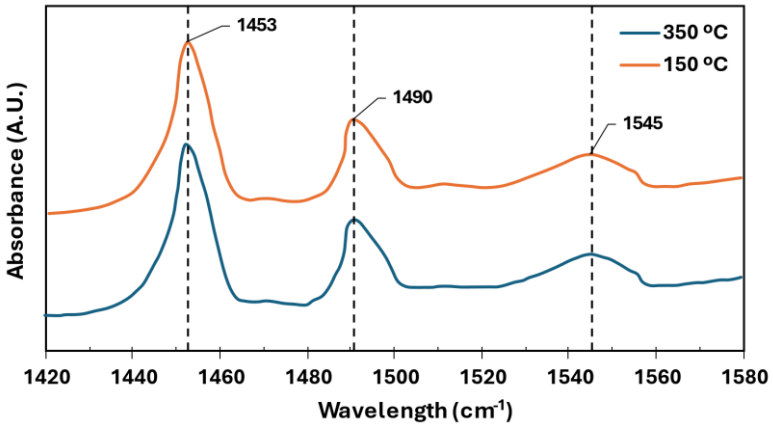

Figure 3. 4: Py-IR spectra of HZSM-5 catalyst.

Table 3. 3: Distribution of Lewis acid sites and Brønsted acid sites of HZSM-5 catalyst.

Catalyst	Brønsted Acid Sites (mmol/g)			Lewis Acid Sites (mmol/g)			B/L
	150 °C	350 °C	Total	150 °C	350 °C	Total	
HZSM-5	0.403	0.288	0.691	0.023	0.013	0.036	19.19

Acidity variations of the catalyst produced by the Py-IR were shown in Figure 3.4 and Table 3.3. The HZSM-5 catalyst (Si/Al = 50), activated by calcination at 550°C for 6 hours, was characterized by its Brønsted and Lewis acid site distribution using in situ pyridine adsorption infrared (Py-IR) spectroscopy. The Py-IR spectra revealed three distinct peaks corresponding to both Brønsted and Lewis acid sites as shown in Figure..: a peak at 1545 cm^{-1} for Brønsted acid sites (BAS), attributed to the pyridinium ion formed upon pyridine adsorption, and a peak at 1453 cm^{-1} for Lewis acid sites (LAS), corresponding to pyridine coordination with Lewis acid centres on the catalyst. The peak at 1490 cm^{-1} was ascribed to the combined action of BAS and LAS. The detailed distribution results of BAS and LAS were tabulated in Table 3.3.

The catalyst exhibited a total of 0.691 mmol/g of Brønsted acid sites and 0.036 mmol/g of Lewis acid sites, resulting in a Brønsted-to-Lewis acid site ratio (B/L) of 19.19. This ratio indicates a significant dominance of Brønsted acidity, which is typical for HZSM-5 catalysts with higher Si/Al ratios, where the lower concentration of framework aluminium favours the formation of Brønsted acid sites over Lewis sites (Le et al., 2020). The high B/L ratio observed in this study is consistent with previous research indicating that HZSM-5 catalysts with high

Si/Al ratio (Si/Al = 50) typically exhibit a higher concentration of Brønsted acid sites (Guo et al., 2022). Wang et al. (2021) demonstrated that HZSM-5 catalysts with high Si/Al ratios, are characterized by a strong dominance of Brønsted acidity, which enhances their ability to catalyze protonation and cleavage of C-C and C-O bonds, key steps in biomass pyrolysis.

The high Brønsted acidity of the HZSM-5 catalyst is particularly advantageous for biomass pyrolysis, where the protonation of biomass-derived oxygenates is critical for the formation of smaller hydrocarbons and valuable bio-oil components. As reported by Rahman et al. (2018), Brønsted acid sites are key to driving the dehydration, cracking, and cyclization reactions that convert biomass intermediates into aromatic hydrocarbons. The low Lewis acid site concentration in the present catalyst, which contributes just 0.036 mmol/g overall, helps minimize side reactions like oligomerization and coking (Yarulina et al., 2018). HZSM-5 catalysts with high Si/Al ratios tend to exhibit lower Lewis acidity, likely due to the reduced number of Al sites available for coordination with pyridine (Rahman et al., 2018). This lack of excess Lewis acidity is beneficial in biomass pyrolysis, as it reduces unwanted side reactions and helps maintain a higher yield of volatile bio-oil products. Furthermore, higher Si/Al ratios result in more stability at higher temperatures whereas lower Si/Al ratios result in more acidity which enhances catalytic performance through increased acidity with a trade-off of poor catalyst stability at higher temperatures (due to framework degradation). The acidity profile observed in this study aligns with the findings of previous study on HZSM-5 catalysts with similar Si/Al ratios (Guo et al., 2022). Whereas a study done by Park et al. (2022) reported contrasting BAS and LAS results which was attributed to different catalyst synthesis and activation conditions. Zhang et al. (2020) found that the total number of Brønsted and Lewis acid sites decreased with increasing the Si/Al ratio which was attributed to a decrease in the number of strong Brønsted acid sites. The current study applied an Si/Al ratio of 50 to offer a balance between stability and catalytic performance during pyrolysis.

3.3.2 Effect of Temperature: Non-Catalytic vs Catalytic

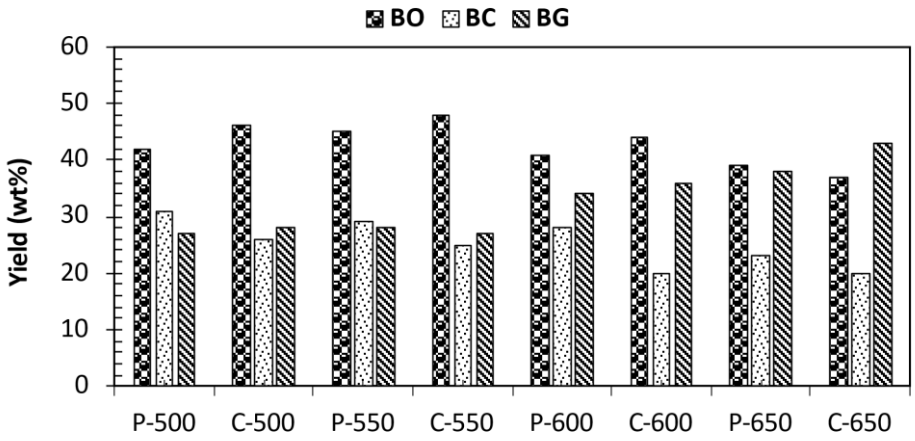

Figure 3. 5: Effect of temperature during catalytic (C) and non-catalytic (P) fast pyrolysis of Giant Reed biomass.

The data in Figure 3.5 indicates catalytic pyrolysis (denoted as "C") and non-catalytic pyrolysis (denoted as "P") across the temperature range of 500-650 °C at a heating rate of 10 °C/min. The presence of the HZSM-5 catalyst and the operating temperature of the pyrolysis process significantly influences bio-oil (BO) production. Catalytic pyrolysis consistently yields higher bio-oil quantities than non-catalytic pyrolysis, particularly at lower temperatures (500 °C and 550 °C). This phenomenon can be attributed to the catalytic cracking and reforming reactions facilitated by the HZSM-5 catalyst (Shun et al., 2013), which promotes the conversion of complex biomass compounds into lighter, more volatile species, thus increasing bio-oil yields. As the temperature rises to 650 °C, the differences in bio-oil yields between catalytic and non-catalytic processes diminish, suggesting that higher temperatures may promote secondary reactions less influenced by the catalyst. Biochar (BC) production exhibits an inverse relationship with temperature, where higher temperatures lead to lower biochar yields, as seen in Figure 5. This phenomenon is observed in both catalytic and non-catalytic pyrolysis processes. At lower temperatures (500 °C and 550 °C), catalytic pyrolysis tends to yield less biochar compared to non-catalytic pyrolysis, suggesting that the presence of the HZSM-5 catalyst promotes the conversion of biomass into other products, such as bio-oil and pyrolysis gas. However, as the temperature increases, the overall biochar production decreases due to increased thermal decomposition and volatilization of biomass components. Therefore, while the HZSM-5 catalyst influences the distribution of pyrolysis products, temperature remains the primary factor governing biochar formation in lignocellulosic biomass pyrolysis. Pyrolysis gas (BG) production is significantly enhanced by catalytic presence, particularly at higher temperatures (600 °C and 650 °C). The HZSM-5 catalyst promotes gasification reactions by

facilitating catalytic cracking and reforming of biomass components (Imran et al., 2018, Balagurumurthy et al., 2015), leading to increased pyrolysis gas yields. However, at lower temperatures (500 °C and 550 °C), the difference in pyrolysis gas yields between catalytic and non-catalytic processes are less pronounced, suggesting that temperature plays a more significant role in pyrolysis gas production under these conditions, possibly through thermal decomposition reactions.

3.3.3 Bio-oil Analyses: Proximate, Ultimate, and Properties

Table 3. 4: Characterization of bio-oil produced from catalytic and non-catalytic fast pyrolysis of Giant Reed biomass.

Parameters	P-550U	C-550U-5	C-550H-5	P-650U	C-650U-5	C-650H-5
Ultimate Analysis (wt%)[db]						
Carbon	65.55 ± 0.49	67.41 ± 0.23	67.25 ± 0.24	66.01 ± 0.02	68.65 ± 0.01	68.35 ± 0.22
Hydrogen	7.88 ± 0.13	7.99 ± 0.01	8.71 ± 0.03	7.89 ± 0.01	8.09 ± 0.03	8.45 ± 0.01
Nitrogen	0.19 ± 0.02	0.20 ± 0.01	0.13 ± 0.01	0.09 ± 0.01	0.08 ± 0.01	0.09 ± 0.01
Sulphur	0.04 ± 0.02	0.03 ± 0.02	0.01 ± 0.02	0.04 ± 0.02	0.02 ± 0.02	0.02 ± 0.03
Oxygen[a]	26.34 ± 0.45	24.37 ± 0.43	23.9 ± 0.25	25.97 ± 0.22	23.16 ± 0.51	23.09 ± 0.44
C/H ratio	8.32 ± 0.02	8.437 ± 0.01	7.721 ± 0.07	8.366 ± 0.01	8.486 ± 0.01	8.089 ± 0.0
H/C ratio	0.12 ± 0.00	0.119 ± 0.00	0.130 ± 0.00	0.120 ± 0.00	0.118 ± 0.00	0.124 ± 0.0
O/C	0.40 ± 0.00	0.362 ± 0.00	0.355 ± 0.01	0.393 ± 0.00	0.337 ± 0.00	0.338 ± 0.0
Properties						
Moisture Content[b]	9.65 ± 0.31	9.09 ± 0.011	8.96 ± 0.13	9.45 ± 0.13	8.99 ± 0.11	8.85 ± 0.22
Density (g/cm^3, 40 ^{0}C)[ar]	1.18 ± 0.00	1.15 ± 0.00	1.13 ± 0.00	1.14 ± 0.00	1.13 ± 0.00	1.09 ± 0.00
K. Viscosity (mm^2/s, 40 ^{0}C)[ar]	51.25 ± 1.11	51.22 ± 1.3	50.02 ± 1.2	49.69 ± 1.5	49.99 ± 1.3	50.11 ± 1.4
TAN (mgKOH/g)[ar]	61.35 ± 1.5	59.88 ± 1.0	59.01 ± 1.4	57.33 ± 2.3	57.65 ± 1.7	56.55 ± 1.4
HHV (MJ/kg)	21.3 ± 0.02	23.0 ± 0.03	24.5 ± 0.03	21.8 ± 0.01	23.8 ± 0.07	24.7 ± 0.04

[db] dry basis, [a] determined by difference, [ar] as received & [b] wet basis

The pyrolysis of biomass was investigated under both non-catalytic and catalytic conditions (Table 3.4) using HZSM-5 catalyst at 550 and 650 °C, with heating rates of 10 °C/min (U) and 50 °C/min (H). The results indicate that the presence of the HZSM-5 catalyst significantly improves the quality of the pyrolysis oil. Catalytic pyrolysis consistently yielded bio-oil with lower moisture content and higher carbon content than non-catalytic pyrolysis. At 550°C and 10°C/min, the carbon content increased from 65.55 wt% in non-catalytic pyrolysis to 67.41 wt% in catalytic pyrolysis, and at 650° C and 10 °C/min, it increased from 66.01 wt% to 68.65 wt%. The oxygen-to-carbon (O/C) ratio decreased significantly in catalytic runs, indicating enhanced deoxygenation, with values dropping from 0.393 to 0.337 at 650 °C and 10 °C/min. The carbon-to-hydrogen (C/H) ratio shows a modest increase, reflecting the formation of aromatic hydrocarbons favoured by the catalytic action of HZSM-5. The non-catalytic

pyrolysis at 550 and 650 °C with a heating rate of 50 °C/min produced a lower bio-oil yield and a higher proportion of biochar and non-condensable gases. This was attributed to incomplete thermal degradation of biomass and insufficient time for secondary reactions that convert intermediate products into higher-quality bio-oil (Rahman et al., 2018). Higher Heating Value (HHV) improvements were also notable in catalytic pyrolysis bio-oil. At 550 °C and 10 °C/min, the HHV of the catalytic pyrolysis product was 23.0 MJ/kg compared to 21.3 MJ/kg for non-catalytic pyrolysis. The HHV reached up to 24.7 MJ/kg at 650 °C and 50 °C/min of the catalytic pyrolysis. These enhancements in HHV values are primarily attributed to the higher carbon and lower oxygen content observed in the catalytic products, leading to more energy-dense bio-oils. The HZSM-5 catalyst enhances the pyrolysis process through several mechanisms: its acidic sites promote the cracking of larger biomass molecules into more minor, more volatile compounds; its shape-selectivity favours the formation of aromatic hydrocarbons; and it facilitates deoxygenation reactions, reducing the O/C ratio and increasing the carbon content (Rahman et al., 2018, Shun et al., 2013, Liu et al., 2014). The temperature and heating rate also play critical roles in determining the product composition and quality. Higher temperatures and faster heating rates enhance thermal cracking and deoxygenation, producing more volatile, energy-rich compounds. These findings emphasize the potential of catalytic pyrolysis for producing high-quality bio-oils and highlight the importance of optimizing pyrolysis conditions to maximize product quality. From the investigated conditions, it is evident that catalytic 550°C and 10 °C/min are optimal when considering bio-oil yield and energy costs.

3.3.4 GCMS Analysis of Bio-oil

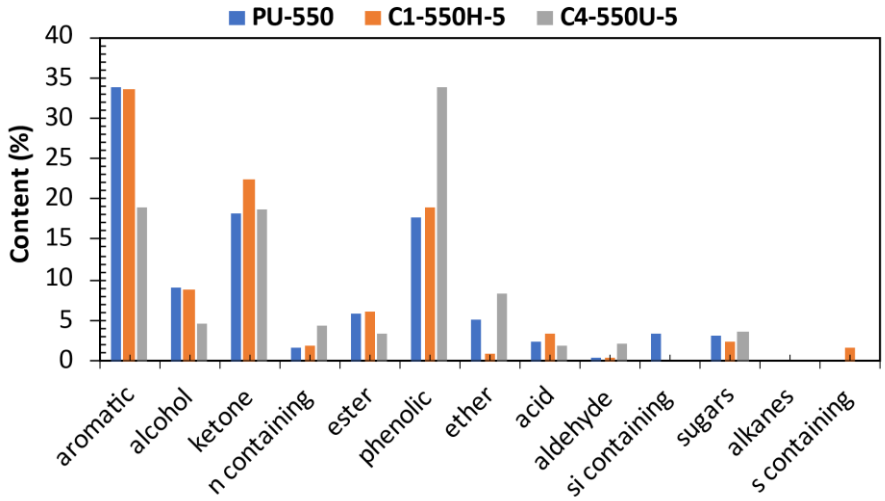

Figure 3. 6: GCMS analysis of bio-oil at different heating rates for 550 ^{0}C.

The GC-MS analysis (Figure 3.6) of bio-oil derived from giant reed pyrolysis at 550 °C, under non-catalytic (P) conditions and using HZSM-5 catalyst (C) with heating rates of 10 °C/min (U) and 50 °C/min (H), reveals significant variations in chemical composition due to variations in catalytic activity and heating rate. Non-catalytic pyrolysis produces bio-oil rich in aromatics (33.7%), ketones (18.16%), and phenolics (17.74%), reflecting partial degradation of biomass components (holocellulose and lignin). The use of HZSM-5 at 50 °C/min maintains similar aromatic content (33.49%) but increases ketones (22.3%) and esters (6.11%) while reducing ethers (0.8%), indicating enhanced deoxygenation and stable oxygenated product formation through cracking and dehydration (Valle et al., 2022). In contrast, at 10 °C/min, there is a marked increase in phenolics (33.93%) and a reduction in aromatics (19.01%), suggesting that the slower heating rate allows more extensive catalytic conversion of lignin-derived intermediates into phenolics. The variations in alcohols, ketones, and acids further reflect the selective catalytic pathways influenced by heating rates, highlighting the catalyst's role in directing biomass conversion towards desirable bio-oil compositions.

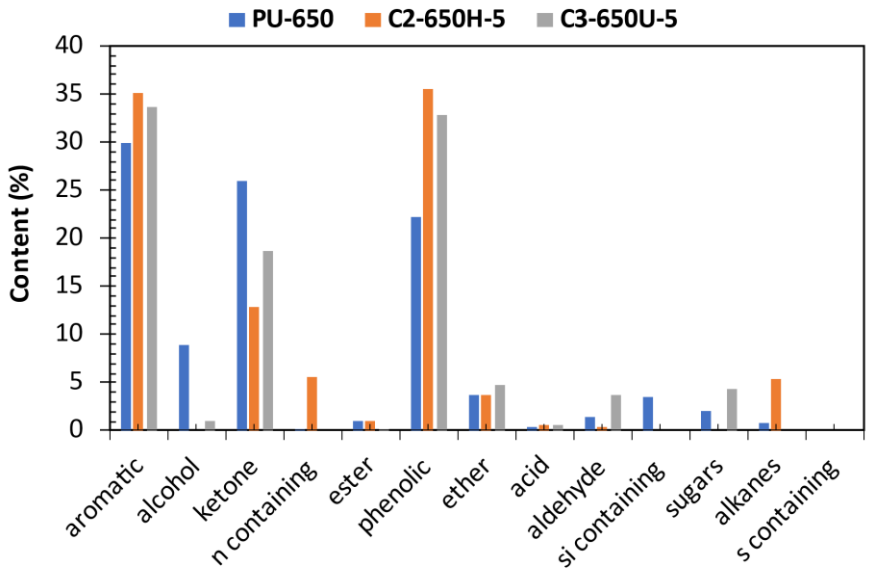

Figure 3. 7: GCMS analysis of bio-oil at different heating rates for 650 ^{0}C.

The GC-MS analyses (Figure 3.7) of bio-oil produced from the pyrolysis of lignocellulosic biomass at 650°C reveal significant insights into the effect of HZSM-5 catalysis and varying heating rates. The non-catalytic pyrolysis results show a diverse distribution of products, with significant amounts of aromatics (29.99%), ketones (25.87%), and phenolics (22.31%), alongside minor quantities of alcohols, esters, ethers, aldehydes, acids, and sugars. This

indicates extensive thermal decomposition of the biomass, with notable contributions from lignin-derived phenolic compounds and oxygenated degradation products from cellulose and hemicellulose. When employing HZSM-5 as a catalyst, the product distribution shifts markedly, reflecting the catalyst's strong deoxygenation and aromatization capabilities. At a heating rate of 50 °C/min, the bio-oil exhibits a higher aromatic content (35.14%) and phenolics (35.52%), while oxygenated compounds such as alcohols and ketones decrease significantly. This suggests that the catalyst effectively promotes the formation of stable aromatic hydrocarbons and phenolic compounds through acid-catalyzed deoxygenation reactions, such as dehydration, decarboxylation, and decarbonylation (Valle et al., 2022). The minimal presence of esters, ethers, aldehydes, acids, and the complete absence of sugars further underscore the efficient catalytic conversion processes facilitated by the zeolite's acidic sites. At a slower heating rate of 10 °C/min, the bio-oil still demonstrates enhanced aromatic content (33.71%) and phenolics (32.75%) compared to the non-catalytic run, though slightly lower than at the faster heating rate. The increase in ketones (18.68%) and the presence of some alcohols, aldehydes, and sugars suggest that the slower heating rate leads to less complete deoxygenation and conversion of intermediate products. This can be attributed to prolonged exposure of the biomass to intermediate temperatures, resulting in different reaction pathways and less efficient catalytic performance compared to the faster heating rate. The application of HZSM-5 catalyst at 650°C and 50 °C/min significantly enhances the production of aromatic hydrocarbons and phenolic compounds while reducing the presence of undesirable oxygenates in the bio-oil. However, this observation is a trade-off to lower bio-oil yields, as a result, 550°C and 10 °C/min is considered an optimal operating condition for bio-oil production. These findings highlight the critical role of optimized pyrolysis conditions in maximizing the yield of desired products and improving the quality of bio-oil before downstream processing (hydrodeoxygenation) to obtain hydrocarbon-rich bio-oil. Further refinement of the hydrotreated bio-oil leads to the production of jet fuel, gasoline, lubricants, solvents, and resins, among other petrochemical products.

3.3.5. ^{13}C NMR Analysis of Bio-oil

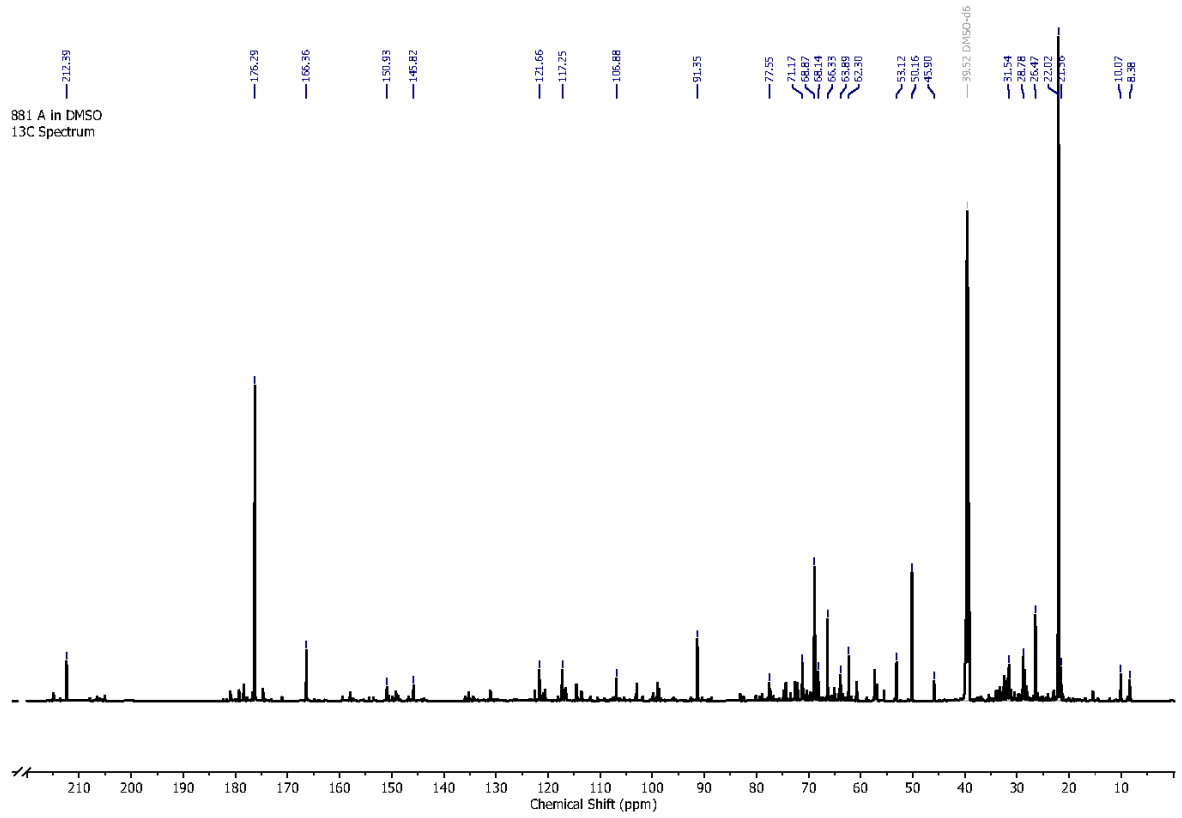

Figure 3. 8: ^{13}C NMR of bio-oil produced from non-catalytic fast pyrolysis of Giant reed biomass at 550 ^{0}C and 10 ^{0}C/min.

The carbonyl region peaks in the NMR spectrum (Figure 3.8) provide valuable molecular-level dynamics governing the pyrolysis kinetics and product distributions, ultimately, providing insights for optimizing the pyrolysis process for desired bio-oil quality. The observed peaks in the carbonyl region (160-220 ppm) of the NMR spectrum offer valuable insights into the chemical transformations occurring during the thermal decomposition of giant reed at 550 °C. At 212.39 ppm, a peak indicative of a carbonyl carbon, often associated with ketones or aldehydes, suggests the formation of carbonyl-containing compounds as intermediates or products of biomass pyrolysis. This peak could arise from the degradation of cellulose, hemicellulose, or lignin components within the giant reed biomass. The peak at 176.29 ppm, associated with a carbonyl carbon likely originating from carboxylic acids, esters, or amides, suggests the formation of oxygenated functional groups during pyrolysis, thus imparting distinct chemical attributes to the resulting bio-oil fractions. The high-intensity peak at 176.29 supports the prospect of high oxygen content in the bio-oil due to the significant presence of oxygenates. Furthermore, the presence of peaks at 165.36 and 165.82 ppm, signifying carbonyl

carbons within conjugated systems such as esters or amides, suggests the occurrence of more complex chemical reactions, possibly involving condensation or polymerization at 550 °C.

The aromatic and olefinic carbon region (120-160 ppm) of the NMR spectrum at 550°C suggests the formation of aromatic compounds and unsaturated hydrocarbons during the thermal decomposition of giant reed. These compounds likely originate from the degradation of lignin, cellulose, and hemicellulose components. Notably, signals at 150.93 and 149.92 ppm denote the presence of aromatic carbons, suggesting the involvement of aromatic functionalities potentially substituted with electron-withdrawing groups. Additionally, peaks observed at 121.46, 117.25, and 106.88 ppm are indicative of aromatic or olefinic carbons. These findings imply the presence of conjugated double bonds or aromatic rings, which are characteristic features of unsaturated hydrocarbons or aromatic compounds. In the oxygenated carbon region, signals between 91-77 ppm indicate the presence of carbons bonded to oxygen, suggesting the presence of alcohol or ether functional groups in the bio-oil. The additional peaks observed around 68-66 ppm further support this indication of alcohols or ethers. The formation of alcohols or ethers was attributed to various reaction pathways, including dehydration, deoxygenation, and condensation reactions involving reactive intermediates produced during pyrolysis.

In the aliphatic carbon region, peaks below 50 ppm are consistent with simple alkyl chains, including methyl and methylene groups. These observations collectively suggest the presence of oxygenated functional groups and aliphatic chains in the bio-oil, likely originating from the degradation of biomass constituents during pyrolysis at 550°C. Furthermore, These alkyl chains are likely remnants of the alkyl side chains present in biomass constituents such as fatty acids or lipids, which undergo thermal cleavage during pyrolysis. The peak at 39.52 ppm in the NMR spectrum (Figure 3.8) corresponds to the solvent peak from DMSO-d6, used as the solvent for sample dissolution.

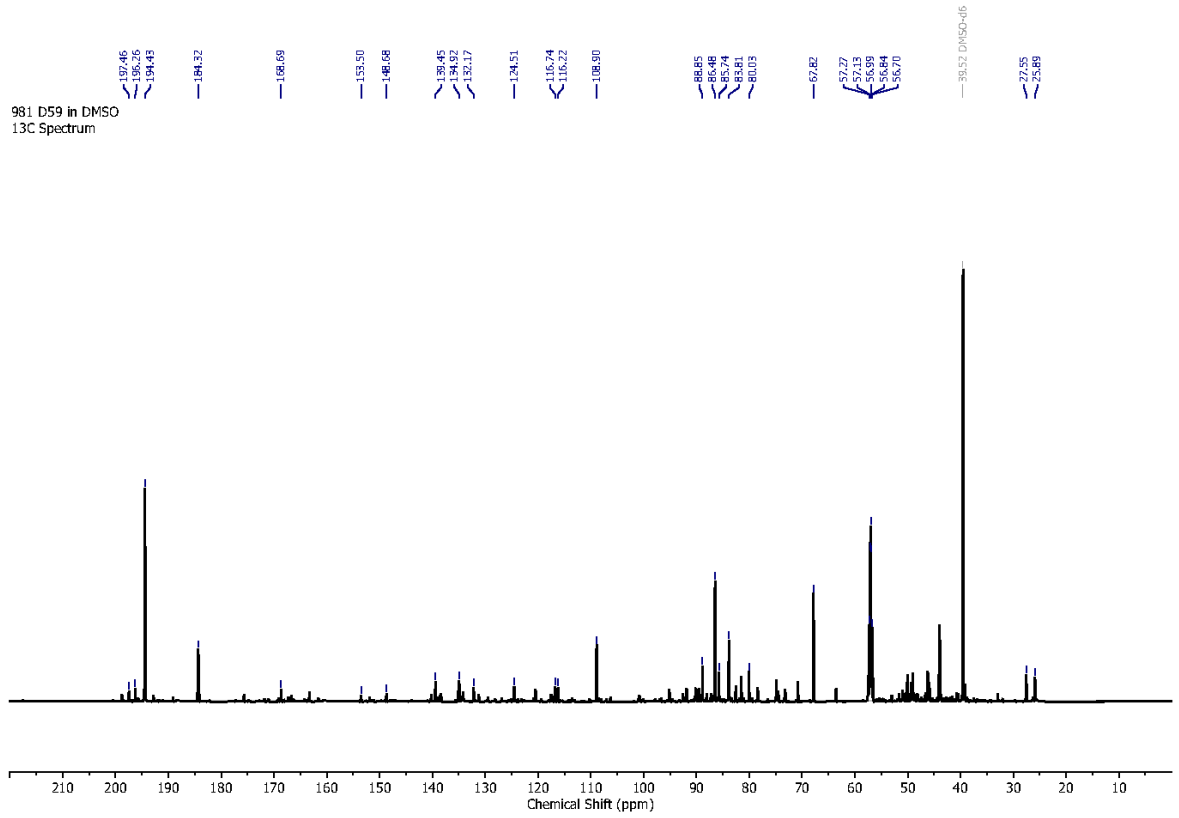

Figure 3. 9: ^{13}C NMR of bio-oil produced from non-catalytic fast pyrolysis of Giant reed biomass at 650 ^{0}C and 10 ^{0}C/min.

The 212.39 ppm peak is absent at 650 ºC, suggesting that the aldehydes or conjugate ketones observed at 550 ^{0}C are no longer present at the higher temperature, owing to further thermal decomposition and transformation into other compounds. The peak at 194.26 ppm in Figure 3.9 indicates a shift toward different ketone structures, possibly more stable (less conjugated) than those observed at 550 ^{0}C. The shift from 165.36 ppm (550 ºC) to 184.32 ppm (650 ºC) indicates the formation of cyclic anhydrides or stable carboxylic acid derivatives. Furthermore, higher pyrolysis temperatures can result in further decomposition and oxidation of aldehydes into carbon monoxide (CO) and carbon dioxide (CO_2) (Jiang et al., 2012). This possible occurrence is also supported by higher gas yields that are observed in Figure 3.5.

The higher number of peaks observed in the aromatic zone (120-160 ppm) of the ^{13}C NMR spectrum for the bio-oil produced at 650 ºC (Figure 3.9) compared to that at 550 ºC (Figure 3.8) can be primarily attributed to the elevated temperatures during pyrolysis. At 650 ºC, the increased thermal energy facilitates various chemical transformations conducive to the formation of aromatic compounds. Firstly, higher temperatures promote the dehydration, dehydrogenation, and cyclization of precursor molecules, resulting in the generation of

aromatic rings from aliphatic structures. Additionally, thermal cracking processes become more pronounced, leading to the fragmentation of larger molecules into smaller aromatic units. The formation of polycyclic aromatic hydrocarbons (PAHs) and other complex aromatic structures is also favoured at higher temperatures due to the increased likelihood of cross-linking and condensation reactions (Gao et al., 2016, Newalkar et al., 2014). Consequently, the combination of these mechanisms results in a more diverse array of aromatic compounds present in the bio-oil produced at 650 ºC, manifesting as a greater number of distinct peaks within the aromatic region of the ^{13}C NMR spectrum.

The comparison of ^{13}C NMR spectra between bio-oil samples produced at 550 ºC and 650 ºC reveals substantial alterations in chemical composition and structural complexity as a consequence of varying pyrolysis temperatures. Notably, the shift in chemical shift ranges from 50 ppm to 85 ppm at 550 ºC to 55 ppm to 100 ppm at 650 ºC suggests the emergence of more diverse chemical species, particularly encompassing aromatic carbons, and potentially more highly substituted aliphatic carbons. This expansion in chemical diversity is further highlighted by the heightened intensity and pronounced nature of peaks observed at 650 ºC (Figure 3.9), indicative of increased abundance or concentration of certain chemical fractions. The pronounced presence of aromatic carbons, known for their stability suggests a prominent role of aromatization pathways facilitated by higher temperatures. Concurrently, the broader chemical shift range at 650 ºC signifies the formation of complex molecules, including cyclic structures and heterocyclic compounds, reflective of the extensive pyrolysis reactions occurring at elevated temperatures.

The similar ^{13}C NMR spectral shifts observed when using the HZSM-5 catalyst and varying the heating rates between 10 °C/min and 50 °C/min at both 550 °C and 650 °C suggest that the catalyst's influence on the pyrolysis process is robust against changes in heating rate (Figures 3.10 and 3.11). HZSM-5, with its strong acidity and shape-selective properties, efficiently facilitates the conversion of biomass components into aromatic hydrocarbons, regardless of the rate at which the temperature is increased (Liu et al., 2014). This catalytic activity likely ensures that key reactions, such as deoxygenation, cracking, and aromatization, proceed effectively, producing a similar distribution of chemical species. The consistency in ^{13}C NMR shifts indicates that the thermal pathways and reaction mechanisms induced by HZSM-5 remain stable over a range of heating rates. Consequently, the catalyst's performance in directing the formation of complex aromatic and aliphatic compounds is maintained, resulting in analogous

chemical compositions of the bio-oil. This finding highlights the versatility and reliability of HZSM-5 in biomass pyrolysis, highlighting its potential for use in various pyrolysis conditions to achieve consistent and desirable bio-oil properties for energy and material applications.

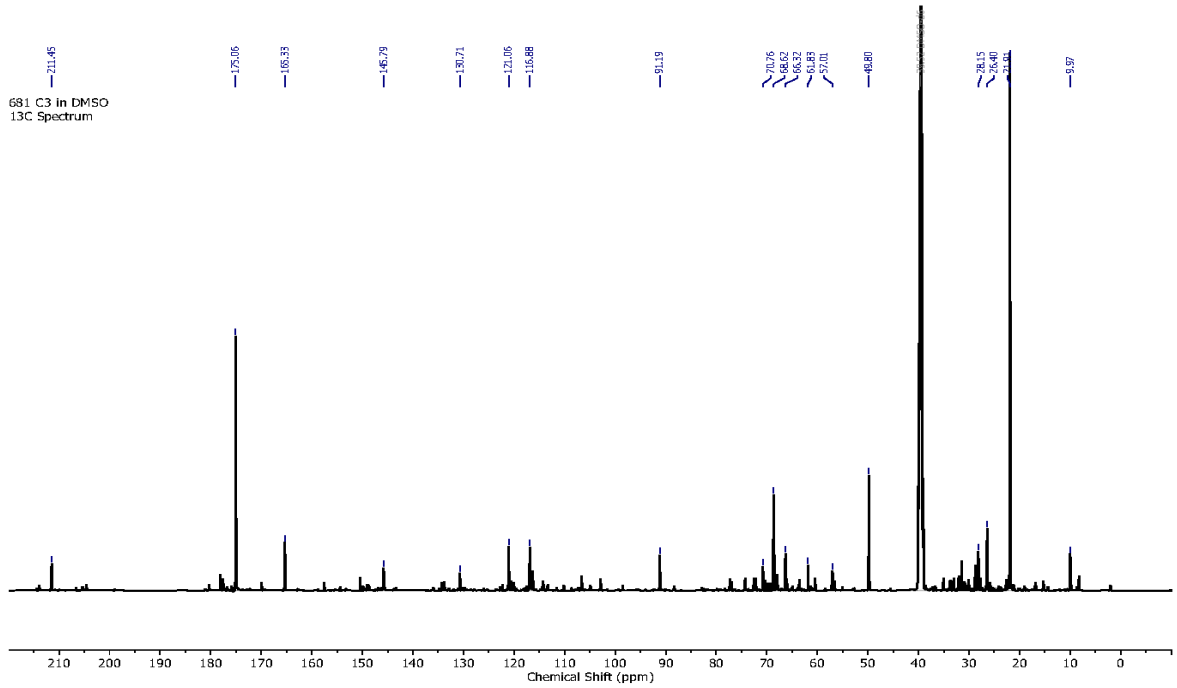

Figure 3. 10: ^{13}C NMR of bio-oil produced from catalytic fast pyrolysis of Giant reed biomass at 650 ^{0}C and 10 ^{0}C/min.

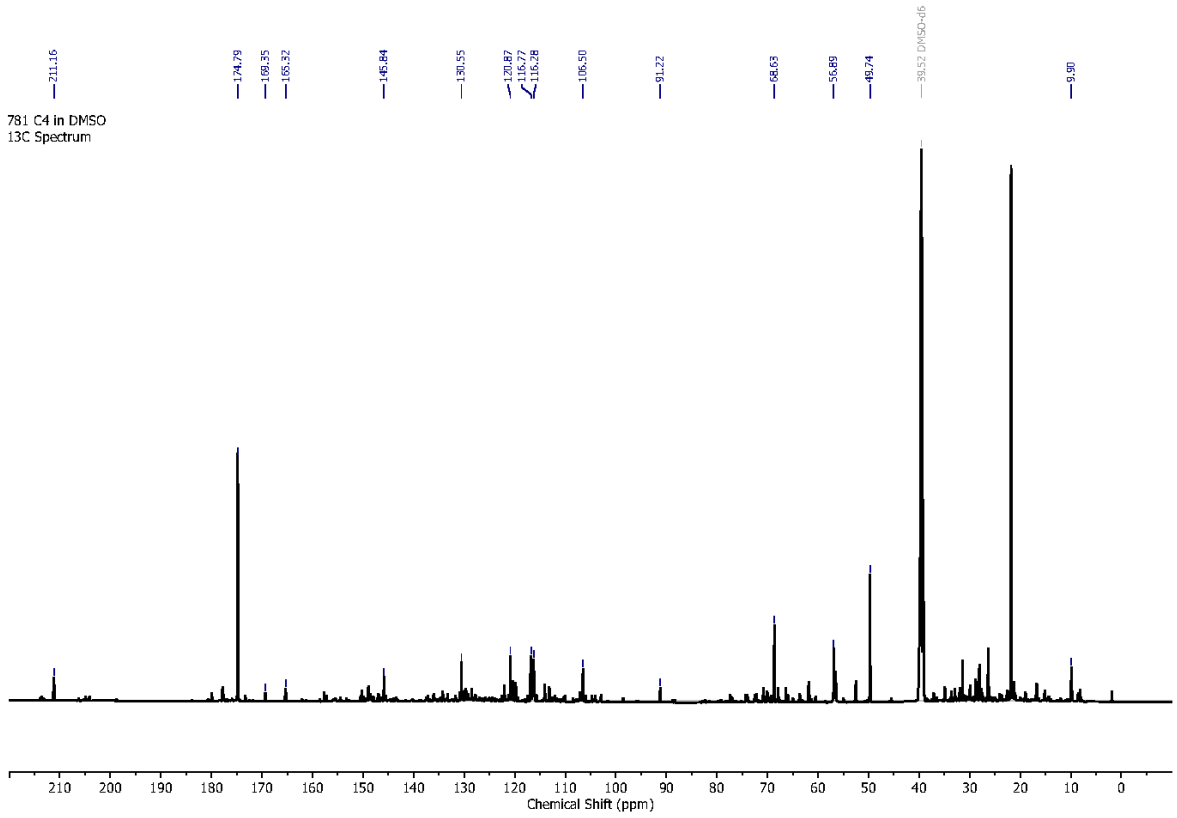

Figure 3. 11: ^{13}C NMR of bio-oil produced from catalytic fast pyrolysis of Giant reed biomass at 550 ^{0}C and 10 ^{0}C/min.

3.3.6. Van Krevelen Plot

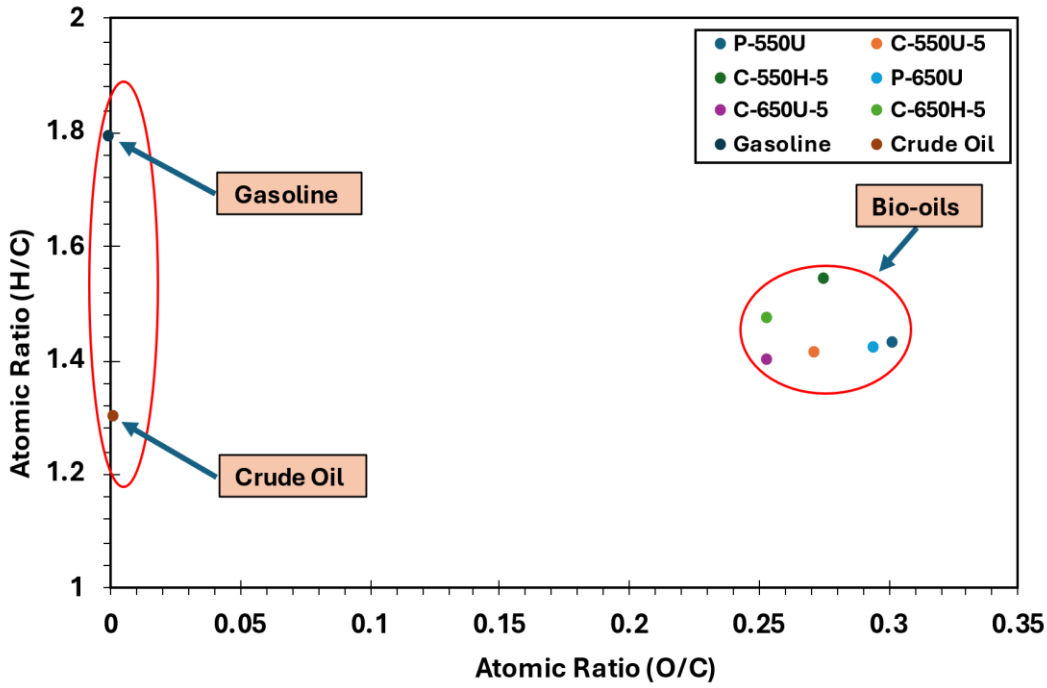

Figure 3. 12: Van Krevelen plot of catalytic and non-catalytic bio-oils versus conversional gasoline and crude oil.

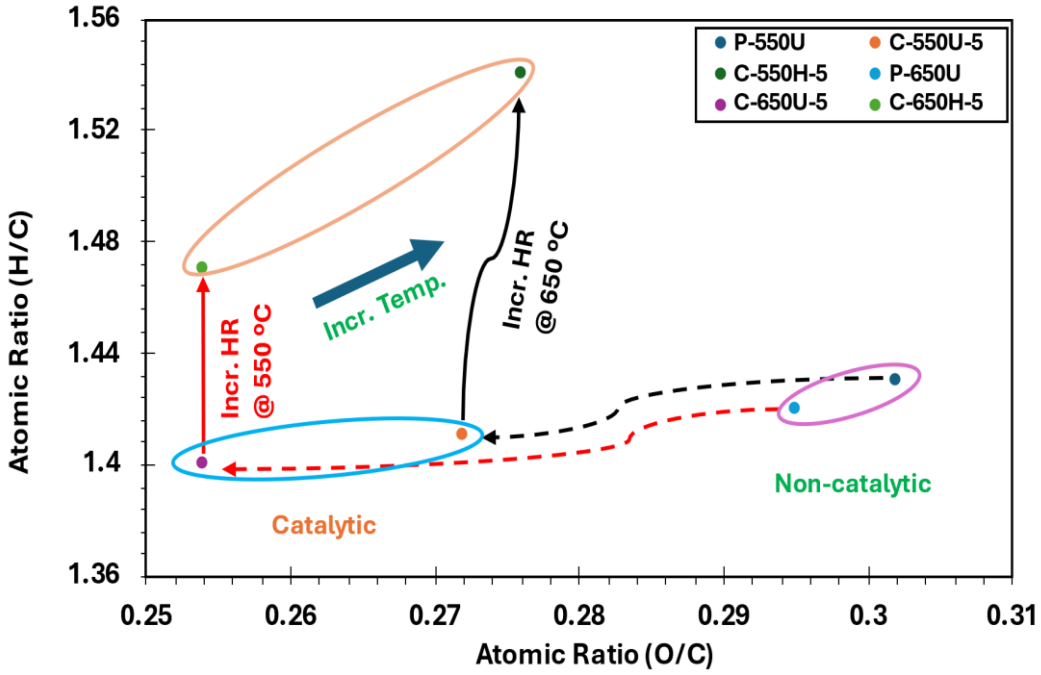

Figure 3. 13: Zoom in of Van Krevelen plot of catalytic and non-catalytic bio-oils at different temperatures and heating rates. [Incr. = Increase, HR = Heating Rate, Temp. = Temperature].

The Van Krevelen plots in Figures 3.12 and 3.13 analyses of bio-oil derived from giant reed catalytic and non-catalytic pyrolysis revealed distinct trends influenced by temperature, catalyst presence, and heating rate, further elucidated by the complementary GC-MS analysis. Notably, all samples exhibited relatively low H/C ratios, ranging from 1.40 to 1.54, consistent with the GC-MS results indicating a high abundance of aromatics, phenolics, and ketones. The H/C ratios of the bio-oil (1.40-1.54) were intermediate to crude oil (1.30) and gasoline (1.79) as seen in Figure 12b. Ideally, higher H/C ratios are preferred for lower carbon monoxide (CO) emissions and greater fuel efficiency (Shezi et al., 2024). However, the bio-oil's lower values, relative to gasoline, point to a higher aromatic content, which can lessen its reactivity. Additionally, although bio-oil has higher H/C ratio compared to conversional crude oil, oxygen removal remains a major hurdle in enhancing the heating value of bio-oil. The O/C ratios, spanning 0.254 to 0.302 in Figures 3.12 and 3.13, suggested the presence of significant oxygen-containing functional groups, which were primarily identified as phenolics and ketones in the GC-MS analysis. An increase in pyrolysis temperature from 550 °C to 650 °C resulted in a consistent decrease in O/C ratios for both non-catalytic (P-550U to P-650U) and catalytic runs, demonstrating enhanced deoxygenation at higher temperatures. This observation aligns with potential transformations of phenolic compounds, such as the removal of hydroxyl groups,

which would decrease the O/C ratio. The catalytic pyrolysis, evidenced by samples C-550U-5, C-550H-5, C-650U-5, and C-650H-5, consistently yielded lower O/C ratios compared to their non-catalytic counterparts (P-550U and P-650U), highlighting the HZSM-5 effectiveness in promoting deoxygenation. This is supported by the GC-MS data, which likely showed a reduction in specific phenolic compounds in catalytic runs, indicating a shift towards less oxygenated aromatics. Furthermore, the heating rate during catalytic pyrolysis influenced the H/C ratio; samples subjected to a higher heating rate (50 °C/min, C-550H-5 and C-650H-5) exhibited slightly elevated H/C ratios compared to those at 10 °C/min (C-550U-5 and C-650U-5). This suggests that faster heating rates may favour the formation of more aliphatic side chains on aromatic compounds, or potentially the formation of less condensed aromatic structures, as seen in the slight increase in H/C. The observed higher O/C ratios in the catalytic bio-oil, when contrasted with crude oil and gasoline as seen in Figure 3.12, demonstrate a less advanced fuel composition, indicating a considerable proportion of polar oxygenates that influence its chemical reactivity and suitability as a biofuel. Furthermore, Figure 3.12 clearly indicate that deoxygenation of bio-oil organic phase is the vital process that will enhance bio-oil into biofuel. The analyses underscore the importance of optimizing pyrolysis conditions to tailor bio-oil composition for specific applications, with lower O/C ratios generally correlating with improved fuel properties. The prevalence of phenolics and aromatics, highlights the influence of lignin degradation during giant reed pyrolysis.

3.4 Conclusions

The pyrolysis of biomass was investigated under both non-catalytic and catalytic conditions using HZSM-5 catalyst at 550 and 650 °C, with heating rates of 10 °C/min (U) and 50 °C/min (H). The results indicate that the presence of the HZSM-5 catalyst significantly improves the quality of the pyrolysis oil. Catalytic pyrolysis consistently yielded bio-oil with lower moisture content and higher carbon content than non-catalytic pyrolysis. This phenomenon can be attributed to the catalytic cracking and reforming reactions facilitated by the HZSM-5 catalyst. At lower temperatures (500 °C and 550 °C), catalytic pyrolysis tends to yield less bio-char compared to non-catalytic pyrolysis, suggesting that the presence of the HZSM-5 catalyst promotes the conversion of biomass into other products, such as bio-oil and pyrolysis gas. However, as the temperature increases, the overall biochar production decreases due to increased thermal decomposition and volatilization of biomass components. Pyrolysis gas (BG) production was significantly enhanced by catalytic presence, particularly at higher temperatures (600 °C and 650 °C). The carbon-to-hydrogen (C/H) ratio showed a modest

increase, reflecting the formation of aromatic hydrocarbons, favoured by the catalytic action of HZSM-5. The non-catalytic pyrolysis at 550 and 650 °C with a heating rate of 50 °C/min produced a lower bio-oil yield and a higher proportion of biochar and non-condensable gases. This was attributed to incomplete thermal degradation of biomass and insufficient time for secondary reactions that convert intermediate products into higher-quality bio-oil. Higher Heating Value (HHV) improvements were also notable in catalytic pyrolysis bio-oil. At 550 °C and 10 °C/min, the HHV of the catalytic pyrolysis product was 23.0 MJ/kg compared to 21.3 MJ/kg for non-catalytic pyrolysis. The HHV reached up to 24.7 MJ/kg at 650 °C and 50 °C/min of the catalytic pyrolysis. These enhancements in HHV values are primarily attributed to the higher carbon and lower oxygen content observed in the catalytic products, leading to more energy-dense bio-oils. The application of the HZSM-5 catalyst at 650°C and 50 °C/min significantly enhances the production of aromatic hydrocarbons and phenolic compounds while reducing the presence of undesirable oxygenates in the bio-oil. However, this observation is a trade-off to lower bio-oil yields and high energy consumption, as a result, 550 °C and 10 °C/min is considered an optimal operating condition for bio-oil production.

CHAPTER 4

4. Seasonal Harvesting Impact on Biomass Fuel Properties and Pyrolysis-Derived Bio-Oil Organic Phase Composition

4.1 Abstract

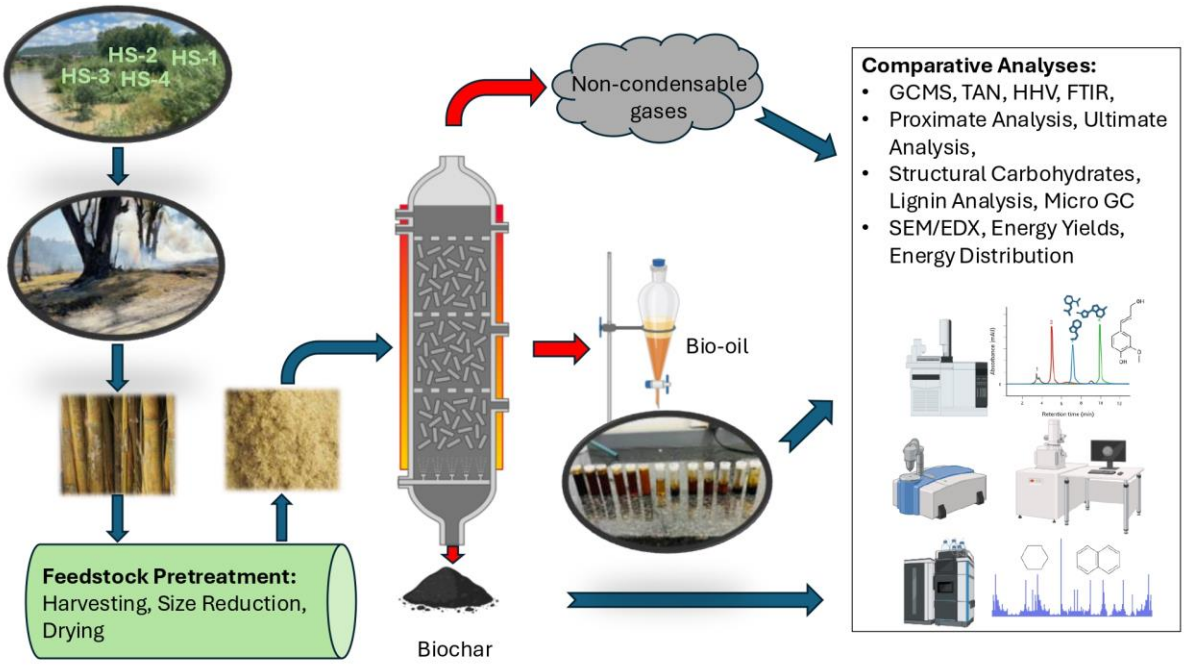

Figure 4. 1: Typical graphical Typical graphical abstract.

Thermochemical conversion of giant reed biomass during periodic variations has been carried out in a semi-batch tubular reactor at 550 ^{0}C. This study was carried out after the incineration of giant reed along the riverbanks. Four periodic variations, late spring (HS-4), late summer (HS-1), late autumn (HS-2), and late winter (HS-3) were considered to investigate the effect of harvest time on biomass fuel properties, pyrolysis product distribution, non-condensable gas characterization, and bio-oil organic phase (BOP) fuel properties. The considered biomasses herein had average calorific values of 18.86 ± 0.05, 19.73 ± 0.05, 19.23 ± 0.04, and 18.44 ± 0.04 MJ/kg during HS-1, HS-2, HS-3, and HS-4, respectively. The biomass, bio-oil organic phase, biochar, and pyrolysis gas were characterized using thermogravimetric analysis (TGA), gas chromatography-mass spectroscopy (GCMS), Fourier transform infrared spectroscopy (FTIR), micro-GC, and scanning electron microscopy (SEM/EDS). The organic phase of bio-oil was isolated using a 125 ml separating funnel, allowing natural stratification of the immiscible phases. BOP yield increased from 5 to 11 wt% during HS-4 and HS-3, respectively.

Higher heating values (HHV) of the BOP ranged from 19.4 ± 0.03 to 22.6 ± 0.02 MJ/kg in relation to the active growth stage and senescence-dormant phase. Physical and chemical properties (TAN, density, viscosity, water content, and CHNS) and chemical compound groups of organic phase bio-oil were analyzed. The produced BOP was rich in phenolics for all considered periods. The effect of harvest time showed that biomass and bio-oil organic phase fuel properties are improved during the senescence-dormant period. As a result, giant reed biomass should be harvested during autumn to avoid incineration that releases carbon dioxide into the atmosphere and will also reduce the occurrence of artificial flooding.
Keywords: biochar, biofuels, biomass, bio-oil, fast pyrolysis, Giant Reed, harvest seasons, invasive species.

4.2 Introduction

The continued use of fossil fuels poses a severe challenge because of the world's limited supply, energy insecurity, and environmental concerns over global warming due to the production of greenhouse gases (Fernandez et al., 2021, Patel et al., 2020). Inevitably, the world will run out of oil that can be mined and burned in the long term. Sustainable energy transport and infrastructure are the endpoint. Dependence on fossil fuels is dangerous and poses a great threat to biodiversity, thus attaining sustainable energy transport and infrastructure is critical. Additionally, dependence on fossil fuels for energy has tampered with the natural carbon cycle. It is well known that the natural carbon cycle has existed for millions of years and there was no urgency around it. The problem started when extra carbon was added to the natural carbon cycle through human activities, and the net result is that the carbon in the atmosphere is increasing over time. It is much more than that can be absorbed by the ecosystem. As a result, it has become evident that energy should be renewable, cost-effective, convenient, safe, and sustainable. Nowadays, it is considered feasible and promising to convert biomass via thermochemical processes into petrochemicals and biofuels (Çağlar and Demirbaş, 2002). These processes use various biomasses that can be processed into a wide range of products, offering great productivity. In thermochemical conversion, the primary techniques include pyrolysis, liquefaction, gasification, and combustion (Awasthi et al., 2023). Among the aforementioned thermochemical techniques, pyrolysis is the most preferred approach that is cost-effective and easy to use for the production of biofuels and petrochemicals from biomass. This technique is categorized into slow, fast, and flash pyrolysis (Pawar et al., 2020). The choice of pyrolysis type to employ depends on the desired product distribution. Fast pyrolysis

is known to be a good choice when high bio-oil yields are desired, while slow and flash are selective to higher yields of biochar and biogas, respectively. The bio-oil from fast pyrolysis is a potential source of a variety of valuable petrochemicals, however, due to undesired properties, it is incompatible with direct application as an engine fuel (Lohitharn and Shanks, 2009). Low heating value and high-water content, acidity, and corrosiveness are well-known limitations of raw bio-oil. The aforementioned drawbacks of raw bio-oil are attributed to the presence of oxygenated compounds such as phenols, alcohols, furans, water, acids, ketones, and aldehydes (Auersvald et al., 2019, Oasmaa et al., 2012). Giant Reed species make it to the top 100 most invasive plant species around the globe, as stated by the International Union for the Conservation of Nature (Lowe et al., 2000). This plant species has been allowed to grow without definitive and sustainable control in many parts of the world. Giant Reed is well suited to subtropical and warm temperate regions and found in the Mediterranean basin for thousands of years (Ba et al., 2020, Saikia et al., 2015). The significance of Giant Reed is justified as a non-food crop not only because of its high biomass yields, low agronomic input, and low production costs but also because of its versatility. At present, there is no effective control measure for dealing with the extensive amount of invasive Giant Reed. Incinerating it directly is the adopted technique to dispose of it, however this results in the release of harmful gases which are, carbon monoxide, carbon dioxide, nitrogen oxides, and fine particulate matter (Corno et al., 2014). South Africa is no exception for not being able to deal with the invasive nature of Giant Reed. Artificial flooding was witnessed in Ladysmith (a semi-rural area in South Africa) in February 2021 which had a significant impact as it led to damage of property, loss of jobs, loss of shelter, and loss of cattle among other impacts. The concentration of Giant Reed is high in Ladysmith (in riverbanks and in-land). During the flood the stems and rhizomes of Giant Reed deposit in the drainage systems and under bridges resulting in the blocking of waterways, structural damage, and hazards to bridges and other structures (Ba et al., 2020). The attempts to apply biological and burning methodologies to control the invasiveness of the non-food plant add no value compared to utilizing the plant for bioenergy generation. Patel and Kumar (2016), investigated the pyrolysis of gigantic reed grass using TG-MS. The authors concluded that energy grass has a stronger thermochemical reactivity and a quicker devolatilization. Giant Reed has the potential to be a sustainable biorefinery feedstock, due to its fast growth rate, composition, and is available year-round. The current study will be looking at pyrolyzing Giant Reed and characterizing the products. Furthermore, to the best of the author's knowledge, there is no study available in the literature on how the fuel properties of Giant Reed vary based on different harvest seasons after incineration from the previous year.

The objective of this study was to investigate the effect of periodic variations on the fuel properties of Giant Reed and assess its influence on pyrolysis product yield, quality, and distribution.

4.3 Materials and Methods

4.3.1 Sample Harvesting and Preparation

Giant Reed (Arundo donax) was harvested from the banks of Klip River in Ladysmith, Kwa-Zulu Natal, South Africa (28.5631^0 S, 29.7810^0 E). The harvesting was done in four different seasons, namely late spring (October), late summer (January), late autumn (April), and late winter (July) denoting HS-4, HS-1, HS-2, and HS-3, respectively. HS-4 and HS-1 were aligned with the active growth stage whereas HS-2 and HS-3 were aligned with the senescence-dormant phase. Giant reed height from the ground was 2-6 m. The culm of the A. donax was considered in the current study. The culm was cut into short pieces and then dried for 24 h at 105 °C. The oven-dried biomass was grinded by a micro plant grinder followed by sieving to a particle size range of 0.5-2 mm.

4.4 Estimation of Biomass Structural Composition

4.4.1 Acid Insoluble Lignin

The Klason lignin was estimated by following the NREL method (Sluiter et al., 2008, Sluiter et al., 2005). Briefly, 10 g of biomass was loaded into the extraction crucible for a sequential water and ethanol extraction process. After extraction, 0.3 g of biomass was loaded into pressure tubes to conduct acid hydrolysis using 72% sulfuric acid. Klason lignin (KL), was determined through filtration and oxidation following the acid hydrolysis.

4.4.2 Detergent Fibre Method

Van Soest method (Van Soest et al., 1991) was adopted to estimate the quantities of cellulose, hemicellulose, and lignin. The method involves the determination of acid detergent fibre (ADF), acid detergent lignin (ADL), and neutral detergent fibre (NDF) as follows:

4.4.3 ADF Technique

To determine acid detergent fibre (ADF), 1 g of dried biomass and 100 mL of an acid detergent solution containing cetyltrimethylammonium bromide (CTAB) and 0.5 M H_2SO_4 were added to a flat bottom flask. After the mixture began to boil, it was refluxed for 1 hr. The residue was

washed with hot distilled water and acetone and then dried at 105 ± 5 °C until its weight remained constant.

$$\%\text{ADF} = \frac{m_{C+ADF} - m_C}{m_{bm}} \times 100 \quad (4.1)$$

4.4.4 ADL Technique

Acid detergent lignin (ADL) was determined by digesting ADF for with 72 % H_2SO_4 for 3 hr. Digested ADF was then washed with hot deionized water through a filtering crucible. The residue was dried at 105 ± 5 °C until constant weight was achieved, followed by oxidation at 550 °C for 5 hr.

$$\%\text{ADL} = \frac{m_{C+ADL} - m_C}{m_{bm}} \times 100 \quad (4.2)$$

The ash content was determined from the residue after 5 hr oxidation at 550 ^{0}C.

$$\%\text{ASH} = \frac{m_{C+ASH} - m_C}{m_{bm}} \times 100 \quad (4.3)$$

4.4.5 NDF Technique

Ethylene Diamine Tetra Acetate acid and sodium dodecyl sulphate were used to prepare neutral detergent solutions (NDF). After the mixture began to boil, it was refluxed for 1 hr. The residue was subjected to sequential rinsing, starting with hot deionized water followed by acetone, and then dried at 105 ± 5 °C until its weight remained constant.

$$\%\text{NDF} = \frac{m_{C+NDF} - m_C}{m_{bm}} \times 100 \quad (4.4)$$

Based on NDF, ADF, and ADL, the contents of cellulose, hemicellulose, and lignin were computed as follows:

$$\text{Hemicellulose} = \text{NDF} - \text{ADF} \quad (4.5)$$

$$\text{Cellulose} = \text{ADF} - \text{ADL} \quad (4.6)$$

$$\text{Lignin} = \text{ADL} - \text{Ash} \quad (4.7)$$

$$\text{Others} = 100 - \text{NDF} \quad (4.8)$$

Others are inclusive of extractives, proteins, and lipids.

4.5 Analytical Methods

Elemental analysis (CHNS) was performed using an Elementar Vario Micro Select, according to ASTM D5373 and ASTM D5291. The oxygen content was determined by difference, and the results were reported on a dry basis. The moisture content of bio-oil was measured by Karl Fischer Titration method. Total Acid Number (TAN) was measured by a Mettler T50 auto titrator using a Total Acid Number Titration Solvent Mixture and 0.1M KOH 2-propanol as the titrating reagent (titrant), according to ASTM D664-07. The viscosity (kinetic and dynamic) and density were measured using the Anton Paar Instrument (SVM Standard method) at 40 ^{0}C. Biomass moisture content and ash content were determined according to ASTM D4442-07 and E1755-01, respectively. The volatiles were determined according to ASTM E872, and fixed carbon content was determined by difference. A bomb calorimeter was used to determine the higher heating values of biomass and bio-oil organic phase. SEM/EDS was used to determine the contents of silicates and potassium on the internal and external surfaces of biomass. A muffle furnace was used during the oxidation processes. The thermal degradation behaviour of biomass was carried out using a Thermogravimetric analyzer (TGA5500) under the nitrogen atmosphere for a temperature range of 25-800 ^{0}C at a heating rate of 10 ^{0}C/min. Platinum HT pan types were used for sample loading and a ramp procedure was employed. The data on weight loss of biomass as a function of temperature was used to interpret thermochemical decomposition behaviour. The chemical functional groups of biomass and organic phase bio-oil were identified by using a Fourier Transform Infrared spectroscopy (FTIR) at a range of 4000-400 cm^{-1}. The spectra were generated using the FTIR-ATR, Thermo Fisher Scientific Smart ITX (Nicolet iSO10) spectrometer. Biogas chemical composition was analyzed using Agilent 490 4-channel Micro GC, with helium and argon as carrier gases for different channels. The calibration curves were initiated using a standard gas mixture of hydrogen (H_2), nitrogen (N_2), carbon monoxide (CO), carbon dioxide (CO_2), oxygen (O_2), ethene (C_2H_4), ethane (C_2H_6), and methane (CH_4). The "others (C_xH_y)" on the biogas balance was obtained by difference, i.e., non-quantified gases were classified as others. The chemical composition of organic phase bio-oil was analyzed by gas chromatography coupled with a mass spectrometric detector (GCMS). The experiments were carried out on an Agilent 5977C GC/MSD with helium gas as a carrier gas. National Institute of Standards and Technology (NIST) spectral library was used to identify the chemical compounds. The samples were weighed and diluted with 2 ml of methanol then filtered through JT Baker Nylon syringe filter (0.2 μm). The filtered sample was injected, and the inlet temperature was set to 280 ^{0}C at a split ratio of 10:1. The

column temperature was held at 50 ^{0}C for 5 min, then heated to 280 ^{0}C at a ramping rate of 10 ^{0}C/min with a 5 min holding time.

4.6 Semi-Batch Pyrolysis Setup and Procedure

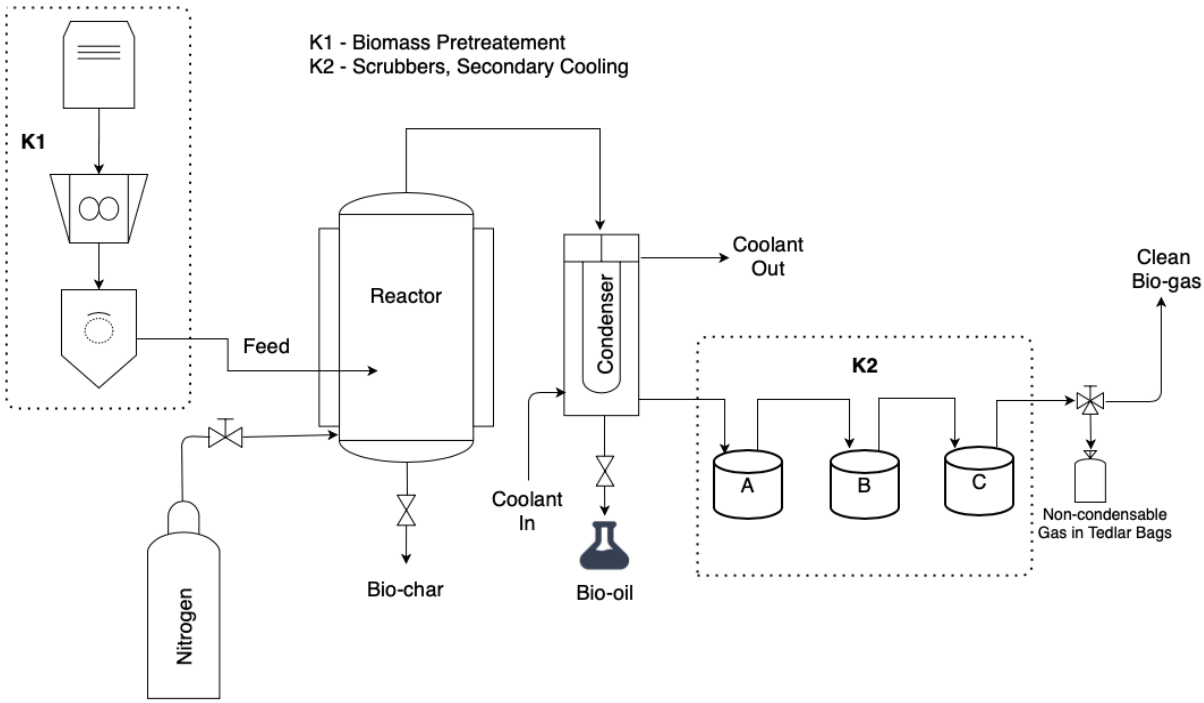

Figure 4. 2: Schematic representation of semi-batch fast pyrolysis unit.

Pyrolysis experiments were performed in a 1.5 L stainless steel fixed bed reactor (FBR). The representation of the pyrolysis system is shown in Figure 4.2. For a typical experimental run, 60 g of pretreated biomass was loaded into the reactor, followed by purging with nitrogen at 2 l/min to remove unwanted oxygen in the pyrolysis system. The nitrogen flow rate during the reaction was maintained at 2 l/min to maintain an inert atmosphere. A 3kW electrical heater equipped with a temperature control panel was used as a heat source during the pyrolysis reaction. The furnace was heated from room temperature to the desired setpoint temperature of 550 ^{0}C at a heating rate of 5 ^{0}C/min. Condensable vapors from the pyrolysis reactor were cooled in a two-series condensing system using cold water as a cooling medium. The cooling water was continuously circulated at 5 l/min using a submersible pump. Ice cubes were added to the circulating water to maintain the temperature at 5 ^{0}C. The bio-oil was collected in two product bottles connected in series. Non-condensable gases were collected in 0.5 L Tedlar bags (CEL Scientific) 15 min after the pyrolysis reaction for compositional analyses was started. The pyrolysis reaction was allowed to run until no gas was coming out of the exhaust line with an

average reaction time of 45 ± 5 min per run. At the end of each experiment, the reactor was allowed to cool down to room temperature, and the reactor with biochar was weighed. The percentage yields of the bio-oil organic phase (BOP%), aqueous phase (BAP%), biochar (BC%), and biogas (BG%) were calculated by the following equations:

$$\mathrm{BOP\%} = \frac{\mathrm{m_{bop}}}{\mathrm{m_{bm}}} \times 100 \quad (4.9)$$

$$\mathrm{BAP\%} = \frac{\mathrm{m_{bap}}}{\mathrm{m_{bm}}} \times 100 \quad (4.10)$$

$$\mathrm{BC\%} = \frac{\mathrm{m_{bc}}}{\mathrm{m_{bm}}} \times 100 \quad (4.11)$$

Where, m_{bop}, m_{bm}, m_{bap}, and m_{bc} are the masses of the organic phase, biomass, aqueous phase, and biochar, respectively. The principle of mass conservation was used to determine the biogas production yield according to the following equation;

$$\mathrm{BG\%} = 100 - \mathrm{BC\%} - (\mathrm{BOP\%} + \mathrm{BAP\%}) \quad (4.12)$$

Energy density and distribution were determined for the bio-oil organic phase after the thermochemical conversion of biomass via fast pyrolysis, were, X_P, HHV_P, HHV_B are the product yield, and heating values of product and biomass, respectively.

$$\mathrm{Energy\ Density} = \mathrm{X_P HHV_P}(1 - \mathrm{M_C}) \quad (4.13)$$

$$\%\mathrm{Energy\ Distribution} = \frac{\mathrm{HHV_P}}{\mathrm{HHV_B}} \times 100 \quad (4.14)$$

4.7. Bio-oil Phase Separation

This study employed a conventional separation technique to isolate the aqueous (BAP) and organic (BOP) phases of bio-oil for quantification and analysis. Given their immiscibility, the two phases naturally stratified, with the aqueous phase on top and the denser organic phase settling at the bottom. A 125 ml separating funnel (conical and graduated with PTFE stopcock) separated the two immiscible phases. The organic phase, being heavier, was collected by carefully opening the stopcock at the bottom of the funnel until all of the phase was transferred into a flask, after which the stopcock was closed. Weights were measured to determine the

yields of each phase, with the organic phase subjected to further analysis in accordance with the study's objectives. Numerous researchers have performed exceptional work in employing solvent extraction methods for phase separation (Ahmed and Kishore, 2024, Ahmed and Kishore, 2023a, Ahmed and Kishore, 2023b, David and Kopac, 2018, Park et al., 2016, Das and Goud, 2021, Aravind et al., 2023). However, this research specifically aimed to retain the original properties of the BOP, thus avoiding solvent use. Moreover, many studies focusing on solvent extraction prioritize improving the BOP properties, which was different from the objective of this work; therefore, only conventional separation was deemed necessary. The aqueous phase primarily contained water-soluble compounds, while the organic phase was predominantly rich in water-insoluble phenolics, highlighting the distinct chemical compositions of the two fractions.

4.7 Results and Discussion

4.7.1 Composition of Biomass

The quality of the fuel is highly dependent on the raw material used. Hence, it is crucial to select feedstock with excellent fuel characteristics that are fit for generating bioenergy. Fuel query parameters, such as ash content, fixed carbon, calorific value, and volatile matter content, will determine the operational attributes and performance of the fuel.

Table 4. 1: Ultimate analysis and higher heating values (HHV) of Giant Reed.

Parameter	Periodic Variations			
	HS-1	HS-2	HS-3	HS-4
Ultimate Analysis (wt%)[db]				
Carbon	48.61 ± 0.14	49.69 ± 0.16	49.72 ± 0.14	48.20 ± 0.13
Hydrogen	6.54 ± 0.16	6.37 ± 0.18	6.30 ± 0.18	6.58 ± 0.18
Nitrogen	0.28 ± 0.05	0.29 ± 0.03	0.240 ± 0.03	0.204 ± 0.04
Sulphur	0.025 ± 0.00	0.039 ± 0.01	0.03 ± 0.01	0.015 ± 0.01
Oxygen	44.55 ± 0.20	43.61 ± 0.29	43.71 ± 0.25	45.00 ± 0.23
C/H	7.74 ± 0.17	7.80 ± 0.20	7.89 ± 0.20	7.33 ± 0.18
H/C	0.13 ± 0.00	0.13 ± 0.00	0.13 ± 0.00	0.14 ± 0.00
O/C	0.84 ± 0.44	0.88 ± 0.43	0.88 ± 0.42	0.93 ± 0.51
HHV (MJ/kg)[db]	18.86 ± 0.05	19.73 ± 0.05	19.23 ± 0.04	18.44 ± 0.04

[db] dry basis.

The elemental composition analysis indicated variations in biomass characteristics over different seasons, as tabulated in Table 4.1. Carbon, a primary component, demonstrates marginal fluctuations across seasons, with the highest concentration observed during HS-2 at 49.69 ± 0.16 wt% and the lowest in HS-4 at 48.20 ± 0.13 wt%. Hydrogen content, essential for energy yield, exhibits analogous trends, peaking in HS-1 at 6.54 ± 0.16 wt% and decreasing in HS-3 to 6.30 ± 0.18 wt%. Nitrogen exhibits minor variability and exhibits heightened levels in HS-2 at 0.29 ± 0.03 wt%. Sulphur content, pertinent for fuel quality, notably varies, with HS-2 showing the highest concentration at 0.039 ± 0.01 wt%. The low sulphur and nitrogen contents indicate the possibility of improved quality of bio-oil, i.e., it will result in low emissions of sulphur and nitrogen oxides when burnt. Oxygen, pivotal for combustion characteristics, showcases fluctuations, with the highest levels recorded in HS-4 at 45.00 ± 0.23 wt%.

Additionally, C/H and H/C ratios remain relatively constant, indicating consistent C-H relationships. Conversely, the O/C ratio demonstrates slight variability, with the highest values in HS-4 at 0.93 ± 0.51 wt%. Furthermore, higher heating value (HHV) displays seasonal fluctuations, reaching a high in HS-2 at 19.73 ± 0.05 MJ/kg and decreasing in HS-4 to 18.44 ± 0.04 MJ/kg. The variations in heating values were mainly attributed to the high and low oxygen content in HS-4 and HS-2, respectively. The heating value of cane biomass is higher than grass biomass and comparable to woody biomass (Nordin, 1994). This supports the utilization of giant reed biomass for bioenergy applications and directly indicates that HS-2 and HS-3 seasons are enough for Giant Reed to reach a high level of HHV. The observed elemental shifts highlighted the significance of biomass pyrolysis aligned with seasonal variations for optimal bio-oil quality and yield.

Table 4. 2: Proximate analysis of Giant Reed.

Parameter	Periodic Variations			
	HS-1	HS-2	HS-3	HS-4
Proximate Analysis (wt%)				
Moisture Content[a]	6.14 ± 0.16	5.23 ± 0.13	4.32 ± 0.14	6.21 ± 0.14
Volatile Content[db]	86.5 ± 0.73	86,8 ± 0.70	87.2 ± 0.61	85.8 ± 0.58
Ash Content[db]	4.69 ± 0.04	2.01 ± 0.02	1.95 ± 0.02	6.10 ± 0.03
Fixed Carbon[db]	8.81	11.2	10.9	8.10

[a] is wet basis, and [db] is dry basis.

The volatile content of biomass increased from 85.8 ± 0.58 to 87.2 ± 0.61 wt% during HS-4 and HS-3, respectively, as seen in Table 4.2. The higher volatile content in HS-3 indicated that biomass can release more volatile compounds during pyrolysis, which results in higher bio-oil yields. Meanwhile, the moisture content decreased from 6.21 ± 0.14 to 4.32 ± 0.14 wt%. Compared to biomass harvested during other seasons, the lower moisture content seen during HS-3 indicated that biomass harvested in this season may require less energy for drying before pyrolysis. The observed trend in moisture content variations coincides with the results of Liu et al. (2016). Lower moisture content in biomass is essential for reducing transportation and storage costs; thus, HS-2 and HS-3 are optimal harvest seasons for low moisture content. The volatile content is 86.8 ± 0.70 wt% in HS-2, slightly increasing compared to the HS-1 season (86.5 ± 0.73 wt%).

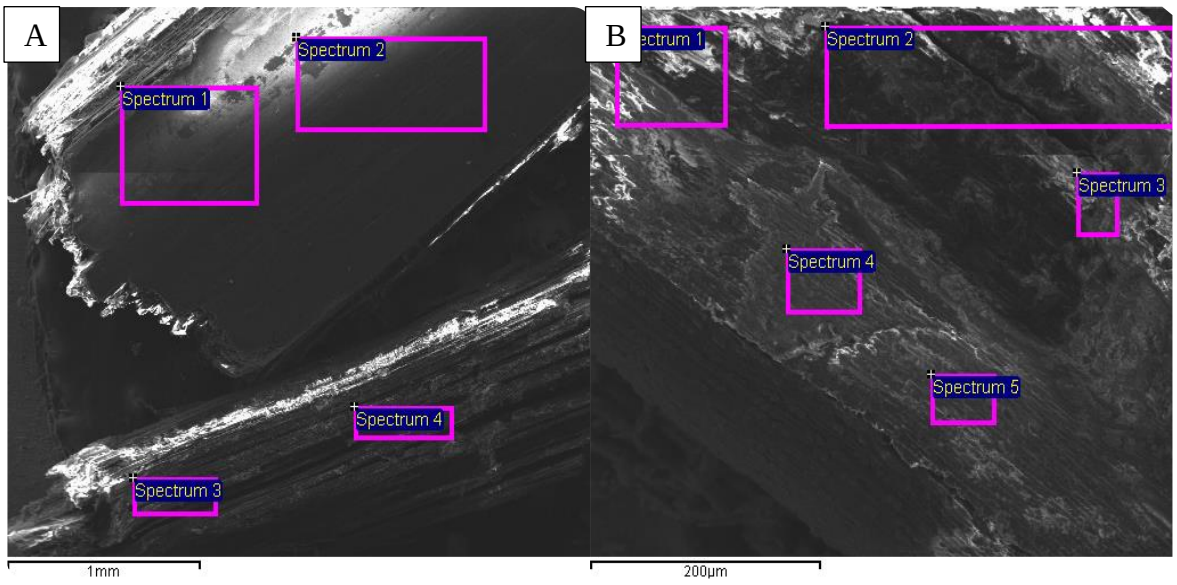

Figure 4. 3: SEM/EDS of Giant Reed, A: external and B: internal.

The ash content data shows significant variations across the different seasonal variations (HS-1 to HS-4). In HS-1, the ash content is 4.69 ± 0.04 wt%, while in HS-2, it decreases substantially to 2.01 ± 0.02 wt%. Similarly, in HS-3, the ash content further reduces to 1.95 ± 0.02 wt%, followed by a notable increase in HS-4 to 6.1 ± 0.03 wt%. These variations in ash content show changes in the mineral composition (inorganics) of the biomass, likely influenced by factors such as soil conditions, and weather patterns. Additionally, the variations in ash content can be attributed to the translocation of nutrients from the above-ground plant to the roots at the end of the growing season (Smith and Slater, 2011). The observed trend of the ash content correlates with the presence of silicates and potassium, as seen in Table 4.3. The

inorganics (silicates and potassium) were higher at the external surface than the internal surface. Silicates and potassium were highest during HS-4 and HS-1 on both internal and external surfaces, coinciding with the ash content. The spectrum of biomass surfaces is shown in Figure 4.3. Higher inorganics were observed during the growing season, in contrast to the dormant phase.

Table 4. 3: Internal and external surface elements of Giant Reed according to SEM/EDS spectrums.

Culm Surface	Periodic Variations			
	HS-1	HS-2	HS-3	HS-4
External (wt%)[wb]				
Carbon	44.2 ± 3.50	46.5 ± 2.50	47.6 ± 1.70	44.9 ± 3.10
Oxygen	38.5 ± 1.58	38.6 ± 1.77	37.5 ± 1.60	37.9 ± 1.55
Silicates	16.3 ± 0.55	14.14 ± 0.71	14.3 ± 0.69	16.3 ± 0.40
Potassium	1.01 ± 0.01	0.81 ± 0.03	0.73 ± 0.04	0.96 ± 0.01
Internal (wt%)[wb]				
Carbon	55.0 ± 3.15	56.2 ± 4.16	56.9 ± 3.62	54.2 ± 3.02
Oxygen	42.8 ± 2.46	42.7 ± 3.58	42.0 ± 3.37	43.1 ± 2.68
Silicates	2.10 ± 0.45	1.09 ± 0.55	1.06 ± 0.58	2.43 ± 0.47
Potassium	0.10 ± 0.04	0.08 ± 0.05	0.07 ± 0.03	0.29 ± 0.04

[wb] wet basis.

Giant reed starts to senescence in autumn/winter or lose their foliage, which results in biomass loss (Liu et al., 2016). Similarly, switchgrass, miscanthus, and reed canary plants experience biomass loss of around 20% in the autumn/winter season (Monti et al., 2008). Giant reed foliage contains more inorganics, which results in higher ash content (Ge et al., 2016). Hence, the current study only focused on the culm/stem of the giant reed. In contrast to HS-4 and HS-1, fouling problems during pyrolysis due to high inorganics are minimal for HS-3 and HS-2. Higher ash content is undesirable as it directly influences the yield and quality of bio-oil. Reduction in ash content correlates with increased organic content, thus improving bio-oil quality post-pyrolysis. The fixed carbon content shows discernible fluctuations across the seasonal variations (HS-1 to HS-4). Notably, in HS-1, the fixed carbon content is 8.81 wt%, showcasing a moderate level. This is succeeded by an increase to 11.2 wt% in HS-2, indicating a higher carbonaceous composition. Conversely, during the HS-3, a slight decrement to 10.9

wt% is observed, although remaining relatively high. Subsequently, in HS-4, there is a noteworthy decline to 8.10 wt%. These variations could be attributed to intrinsic changes in biomass composition, environmental conditions, and growth patterns across seasons. Fixed carbon content is a pivotal determinant of biochar yield and quality, with higher levels typically correlating with enhanced carbon sequestration potential and thermochemical conversion efficiency. HS-3 and HS-2 are associated with periods of dormancy, hence the observed trends in the biomass proximate analyses. On the other hand, HS-4 and HS-1 are associated with the growing season. The aforementioned results show that HS-3 and HS-2 are desirable harvest seasons for Giant Reed for thermochemical conversion applications when bio-oil is the desired product.

4.7.2 Structural Components of Giant Reed at Different Seasons

The fibrous composition, described by Neutral Detergent Fibre (NDF) and Acid Detergent Fibre (ADF) content, exhibits notable seasonal variability across the studied seasons (HS-1 to HS-4), as seen in Table 4.4. During HS-1, NDF content registers at 76.2 ± 1.96 wt%, indicative of a substantial presence of cellulose, hemicellulose, and lignin constituents in biomass. Conversely, ADF content is lower at 52.25 ± 1.41 wt%, suggesting a relatively lesser quantity of holocellulose. Transitioning to HS-2, both NDF and ADF contents exhibit a decline, with NDF recording 67.53 ± 1.95 wt% and ADF at 48.54 ± 1.28 wt%. The observed decline was attributed to seasonal variations in plant growth and composition. A comparable trend is observed in the subsequent HS-3 season, where NDF content decreased to 63.75 ± 1.98 wt% and ADF to 47.03 ± 1.21 wt%, indicating a continued reduction in fibrous structural components. Nonetheless, during HS-4, there was a resurgence in fibrous content, with NDF rising to 79.3 ± 1.93 wt% and ADF to 53.97 ± 1.28 wt%, reflecting a return to higher cellulose and hemicellulose levels. The observed variations emphasize the influence of seasonal factors on biomass structural composition, which is crucial for optimizing the pyrolysis process. The fibrous materials play a pivotal role in determining product distribution and properties.

Table 4. 4: Structural components and neutral fibres of Giant Reed.

Parameter	Periodic Variations			
	HS-1	HS-2	HS-3	HS-4
Fibres (wt%)[db]				
NDF	76.2 ± 1.96	67.53 ± 1.95	63.75 ± 1.98	79.3 ± 1.93
ADF	52.25 ± 1.41	48.54 ± 1.28	47.03 ± 1.21	53.97 ± 1.28
Components (wt%)[db]				
Klason Lignin[ef]	15.9 ± 0.93	18.2 ± 0.88	19.5 ± 0.99	12.7 ± 0.89
Lignin	8.46 ± 1.10	12.23 ± 1.08	12.68 ± 1.09	5.11 ± 1.08
Cellulose	38.1 ± 0.27	34.29 ± 0.18	32.4 ± 0.10	40.75 ± 0.17
Hemicellulose	23.95 ± 0.55	18.99 ± 0.67	16.72 ± 0.77	25.33 ± 0.65
Others	23.8	32.47	36.25	20.7

Others = 100-NDF

[ef] extractives free, [db] is dry basis.

Several trends were observed in analyzing biomass components across the four seasons (HS-4 to HS-3) (Table 4.4). Klason lignin content shows variability, with the highest value observed in HS-3 at 19.5 wt% and the lowest in HS-4 at 12.7 wt%. This indicates potential seasonal influences on lignin accumulation. Cellulose content varies across seasons, with the highest value in HS-1 at 38.1 wt% and the lowest in HS-3 at 32.4%, reflecting seasonal changes in plant growth and development. Similarly, hemicellulose content shows fluctuations, with the highest value in HS-1 (23.95 wt%) and the lowest in HS-3 (16.72 wt%), suggesting seasonal variations in hemicellulose composition. Cellulose and hemicellulose tend to decline as Giant Reed matures. However, hemicellulose decreased significantly from HS-4 to HS-3, which was attributed to the lignification effect. These fluctuations reflect seasonal influences on biomass composition, which impacts its suitability for bio-oil production via pyrolysis. In a study done by Neto et al. (1997), the authors found that the culm of giant reed had 3 wt% ash, 17.2 wt% lignin, and 58.8 wt% holocellulose. The giant reed was approximately 6-7 months old, however, the authors did not report the harvest season. Their results were close to HS-2. Suárez et al. (2023), reported cellulose, hemicellulose, and lignin estimations of 38 ± 3.7, 42.4 ± 1.3, and 32.4 ± 2.7 wt%, respectively, for giant reed with a diameter of 2-3 cm and a height of 4-5 m. Another study done by Liu et al. (2016), showed polymer estimations over four months.

The cellulose ranged between 29 to 31 wt%, hemicellulose ranged between 14 to 16 wt%, and lignin ranged from 16 to 18 wt%.

4.7.3 FTIR of Giant Reed at Different Seasons

The identification of biomass functional groups aids in elucidating the chemical structure of the biomass sample, providing crucial information for its characterization and application during thermochemical conversion. The FTIR spectrum of biomass samples is shown in Figure 4.4.

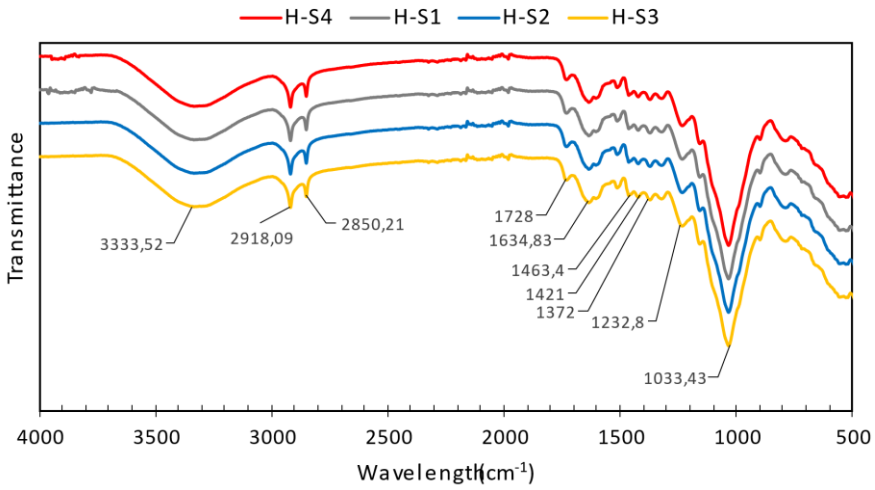

Figure 4. 4: FTIR spectre of Giant Reed at different periodic variations.

The functional groups present in biomass can be identified by the different peaks as seen on the spectrum. The broad peak 3333.52 cm^{-1} represents the O-H stretching vibrations of lignin and cellulose present in the biomass sample. In contrast, the peaks at 2918.09 and 2850.21 cm^{-1} are the C-H stretching vibrations i.e., aliphatic compounds in the hemicellulose (Suárez et al., 2023, Chikouche et al., 2015). The peak at 1728 cm^{-1} originates from C=O stretching vibration of oxygen double bonds due to hemicellulose. The C=O stretching was due to lignin and hemicellulose (Bessa et al., 2020). The aldehyde functionalities are mainly derived from xylose. The peaks at 1634.83 and 1463.4 cm^{-1} may pertain to N-H bending, C=C stretching, and C-H bending vibrations, respectively. The peaks 1421 and 1372 cm^{-1} are due to O-H bending and S=O stretching resonances, respectively, thus, the biomass contains carboxylic acid and sulfonate/phenol functionalities. 1232.8 cm^{-1} represents C-O stretching vibrations of lignin and xylan, as well as syringyl ring breathing. The peak at 1033.43 cm^{-1} was attributed to stretching vibrations of S=O/C-N. The peak at 1033.43 cm^{-1} was also due to the presence of cellulose (Martínez-Sanz et al., 2018).

4.7.4 Thermal Degradation of Giant Reed at Different Seasons

The information on feasible pyrolysis reaction temperature range and thermal degradation behaviour for available biomass materials can be obtained from the thermogravimetric analysis (TGA) and differential thermogravimetry (DTG) profiles. Figures 4.5a and 4.5b represents the TGA and DTG of giant reed during various seasons (HS-4 to HS-3), respectively. The curves show three mass loss partitions/stages. The first stage of degradation represents the loss of moisture or volatilization of light extractives. In Figure 4a, it can be seen that moisture loss occurs between 26 to 120 ^{0}C across all seasons with an average loss of 5.48 wt%.

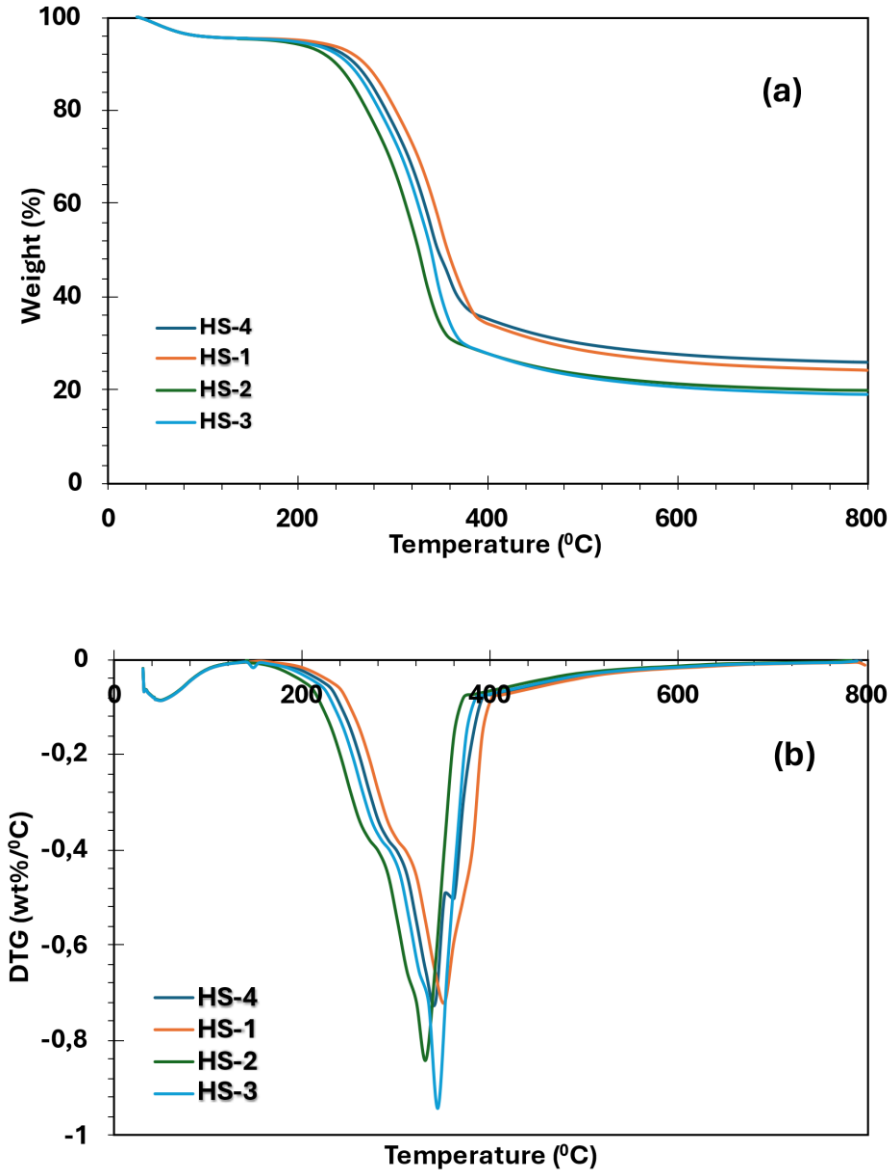

Figure 4. 5: Thermogravimetric analysis of giant reed biomass at different seasons (a) TGA and (b) DTG.

The second stage represents the degradation of cellulose and hemicellulose (holocellulose) at an average temperature range of 225 to 398 ^{0}C across all seasons. Pure cellulose, hemicellulose, and lignin have degradation temperatures of 315-400, 220-315, and 150-900 ^{0}C, respectively (Yang et al., 2007). The holocellulose degradation during HS-4 and HS-2 occurred at a range of 260-398 and 245-378 ^{0}C, respectively. Meanwhile, in HS-3 and HS-1, the degradation of holocellulose was seen at 225-360 and 260-380 ^{0}C, respectively. That said, it is worth noting that hemicellulose decomposition occurs before cellulose degradation starts at a temperature of 220 ^{0}C (Bessa et al., 2020). Cellulose degrades at a higher temperature than hemicellulose due to the long polymer of glucose with no branches, thus strengthening its structure and thermal stability. During the second stage, the highest mass loss of around 70 wt% on average is observed, and active pyrolysis takes place. Hence, some lipids and proteins are also degraded during this stage. The observed mass loss during the second stage corroborates with the estimated values of holocellulose in this current study, although it may include proteins and lipids. The last stage (380-800 ^{0}C) is the continuation of lignin decomposition and carbonization of cross-linked sugar, giving an average weight loss of 10-11 wt% across all seasons. Lignin is composed of aromatic rings with numerous branches bonded by strong chemical bonds; hence the degradation temperature of lignin covers a wide range (Suárez et al., 2023, Yang et al., 2007). The degradation of other remaining carbonaceous material in biomass is possible during lignin decomposition, going into the final temperature of 800 ^{0}C. These are the main contributors to the char formation (Cheng et al., 2015). The residual weight percentages observed after thermal degradation for the different harvest seasons were HS-1 at 24%, HS-2 at 20%, HS-3 at 19%, and HS-4 at 26%. These results indicate variability in thermal stability among the growth stages, with HS-4 exhibiting the highest residual weight, suggestive of greater char retention and high presence of inorganics, while HS-3 showed the lowest residual mass. In Figure 4b, the DTG plot reveals secondary small shoulders observed after the dehydration phase (26-120 ^{0}C), which signify hemicellulose degradation. The temperature range for hemicellulose degradation partially coincides with that of cellulose degradation, resulting in the weight loss rate curve exhibiting a shoulder rather than a distinct peak (Grønli et al., 2002). The profiles in Figure 4b indicate that hemicellulose degradation across all seasonal samples occurs within a temperature range of 220-323 ^{0}C. The prominent peaks within the temperature range of 300-400 ^{0}C signified the degradation of cellulose for all seasons. However, it is worth noting that cellulose degradation started at different temperatures, which was attributed to variations in the structural composition of each biomass sample. Furthermore, high concentrations of low molecular weight compounds (resins and oils) can contribute to

faster holocellulose degradation during HS-2 and HS-3 seasons, associated with autumn and winter harvesting. Hence, the order of degradation for holocellulose was HS-2<HS-3<HS-4<HS-1. Lower hemicellulose contents result in more prominent cellulose peaks. Holocellulose can then decompose simultaneously, forming a more prominent peak (Saffe et al., 2019). The temperatures for maximum mass loss rate are 351, 331, 344, and 341 ^{0}C for HS-1, HS-2, HS-3, and HS-4, respectively. These maximum mass losses are mainly associated with higher cellulose contents. Furthermore, the observed temperatures of maximum mass loss for giant reed, coincide with the results of Huang et al. (2015). After cellulose degradation, lignin decomposition follows (passive pyrolysis) at a temperature range of 400-800 ^{0}C. During this phase, lignin decomposes without a characteristic peak, possibly due to slight mass loss, which translates to a minimal reaction rate. Thermal degradation rates ($-dW/dT$), illustrated in Figure 4b, increase from the growing stages (HS-1 and HS-4) to senescence (HS-2), subsequently transitioning into the dormant stage (HS-3). Consequently, the growing stages exhibit a delayed thermal degradation response.

4.7.5 Pyrolysis Product Distribution

Pyrolysis products showed variations that reflect seasonal influences, as seen in Figure 4.6. HS-1 and HS-4 showed the highest bio-oil yields at 42.3 ± 0,95 and 42 ± 0.81 wt%, respectively. Meanwhile, HS-2 and HS-3 yields were averaging at 41 wt%. However, there was a significant difference in the production of aqueous and organic phases, which comprise total liquid yield. HS-1 and HS-4 resulted in higher yields of aqueous phase in contrast to HS-2 and HS-3.

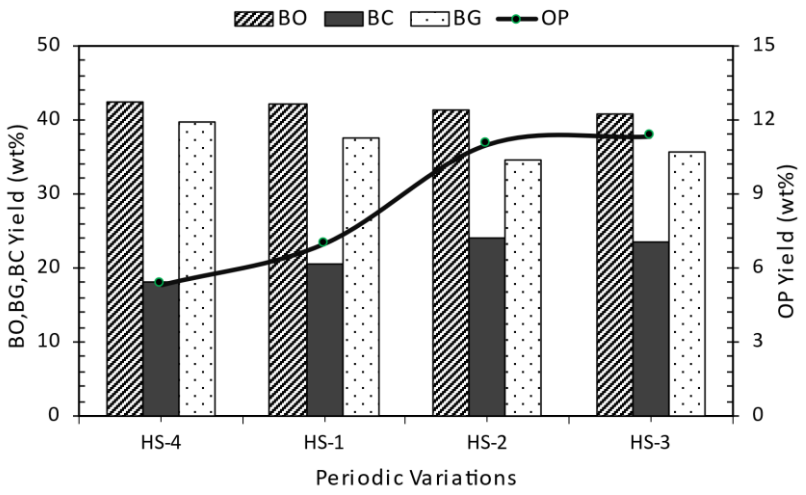

Figure 4. 6: Thermochemical conversion products of Giant Reed biomass.

Conversely, the organic phase demonstrated the opposite trend, with higher yields in HS-2 and HS-3 at 11 ± 0.43 and 11.3 ± 0.42 wt%, respectively (Figure 2.6). The disparity in aqueous and organic phase yields could arise from varied biomass compositions affecting phase separation efficiencies during pyrolysis. HS-1 and HS-4 may yield higher aqueous fractions due to elevated moisture content, while HS-2 and HS-3 exhibit greater organic phase yields, possibly due to differences in extractable organic compounds. Furthermore, the observed increase in the aqueous phase during HS-4 and HS-1 could also be attributed to higher oxygen content. High oxygen content promotes dehydration reactions during pyrolysis, which forms water as a product (Rangel et al., 2023). Biochar production was the highest during HS-2 and HS-3, averaging at 24 wt%. Meanwhile, HS-1 and HS-4 yields were slightly lower at 20.5 ± 0.67 and 18 ± 0.76 wt%, respectively. The elevated biochar yields in HS-2 and HS-3 were attributed to potential factors such as higher lignin content and denser biomass structure (increased fixed carbon content), which favours biochar formation during pyrolysis. Biogas yield ranged from 35 to 49 wt%, with the highest yield obtained during HS-4 (39.7 ± 1.71 wt%) and the lowest yield in HS-2 (34.7 ± 1.81 wt%). Higher volatile content in HS-1 and HS-2 correlated with increased biogas yields due to greater gasification potential during pyrolysis. This results in higher gas production, contrasting with lower volatile content in HS-3 and HS-4, which leads to reduced biogas yields. In the current study, biochar was lower than biogas for all seasons, this observation was in contrast with the work reported by Temiz et al. (2013). The authors reported liquid, solid, and gas yields of 45, 30, and 25 wt% during the thermal degradation of giant reed. These disparities were attributed to different operating conditions during pyrolysis.

4.7.6 Properties of Bio-oil Organic Phase

The analysis of bio-oil samples collected during different seasonal variations (HS-1, HS-2, HS-3, and HS-4) are tabulated in Table 4.5. These analyses exhibited discrepancies in both proximate and ultimate composition. Moisture content showed a slight variation, with HS-4 displaying the highest value at 9.95 ± 0.05 wt% as expected since biomass was harvested during semi-early stages of growth.

Table 4. 5: Proximate, ultimate analysis and properties of BOP.

Parameter	Periodic Variations				
	Gasoline	HS-1	HS-2	HS-3	HS-4
Ultimate Analysis (wt%)[db]					
Carbon	86.00	65.00 ± 0.75	71.18 ± 0.75	69.65 ± 0.70	63.78 ± 0.73
Hydrogen	12.80	7.84 ± 0.08	7.83 ± 0.08	7.99 ± 0.08	7.34 ± 0.07
Nitrogen	0.000	0.24 ± 0.04	0.55 ± 0.02	0.52 ± 0.03	0.12 ± 0.02
Sulphur	1.000	0.06 ± 0.02	0.01 ± 0.02	0.04 ± 0.02	0.14 ± 0.03
Oxygen	< 0.20	26.86 ± 0.67	20.44 ± 0.66	21.8 ± 0.53	28.62 ± 0.67
H/C	1.790	1.45 ± 0.00	1.32 ± 0.00	1.38 ± 0.00	1.38 ± 0.00
O/C	0.002	0.31 ± 0.00	0.22 ± 0.01	0.23 ± 0.00	0.34 ± 0.00
Properties[ar]					
Moisture Content[a]	***	9.80 ± 0.15	9.82 ± 0.14	9.79 ± 0.19	9.95 ± 0.05
K. Viscosity (**cSt**) 40°C	0.5 @ 20°C	66.6 ± 1.05	53.2 ± 1.15	54.4 ± 1.24	67.8 ± 1.35
Density (g/cm^3) 40°C	0.76 @15°C	1.18 ± 0.00	1.14 ± 0.00	1.14 ± 0.00	1.18 ± 0.00
TAN (mgKOH/g)	0.05–0.2	58.1 ± 1.26	54.3 ± 1.25	53.2 ± 1.23	59.2 ± 1.31
D. Viscosity (mPa.s) 40°C	0.38 @15°C	78.4 ± 1.05	60.6 ± 1.15	62.0 ± 1.24	80.0 ± 1.35
HHV (MJ/kg)[db]	45.70	20.8 ± 0.03	22.6 ± 0.04	22.0 ± 0.02	19.4 ± 0.03

[ar] is as received, [db] dry basis, [a] wet basis.

Pertaining to the ultimate analysis, significant differences were noted in the carbon, hydrogen, nitrogen, sulphur, and oxygen content across all seasons. HS-2 exhibited the highest carbon content at 71.18 ± 0.75 wt%, while HS-4 had the highest oxygen content at 28.62 ± 0.67 wt%. Hydrogen content varied from 7.34 ± 0.07 wt% in HS-4 to 7.99 ± 0.08 wt% in HS-3. Nitrogen content ranged from 0.12 ± 0.02 wt% in HS-4 to 0.55 ± 0.02 wt% in HS-2, with considerable disparity. The properties of the bio-oil samples, i.e. kinematic viscosity, density, total acid number (TAN), dynamic viscosity, and higher heating value (HHV), also varied with seasons. HS-1 and HS-4 demonstrated higher TAN values at 58.1 ± 1.26 and 59.2 ± 1.31 mgKOH/g, respectively, compared to HS-2 (54.3 ± 1.25) and HS-3 (53.2 ± 1.23), indicating differences in acidity levels. The reed harvested during the dormant phase showed lower acidity when compared to the one harvested during the active growth phase. HS-2 and HS-3 showed low kinematic viscosity at 53.2 ± 1.15 and 54.4 ± 1.24 mm2/s, respectively. Conversely, higher viscosity was observed during HS-4 and HS-1. Meanwhile, the density consistent for HS-4 and HS-1, followed by another consistency between HS-2 and HS-3. Additionally, HHV values were higher for HS-2 and HS-3 when compared to HS-1 and HS-4, suggesting variations in the energy content of the bio-oil samples. It ranged from 19.4 ± 0.03 MJ/kg in HS-4 to 22.6 ± 0.04 MJ/kg in HS-2. These variations in HHV were correlated with the variations in bio-oil oxygen

and water contents. The results emphasized the significant impact of seasonal variations on the composition and properties of bio-oil. Hence, it is evident that HS-2 and HS-3 showed improved quality of bio-oil when compared to HS-1 and HS-4.

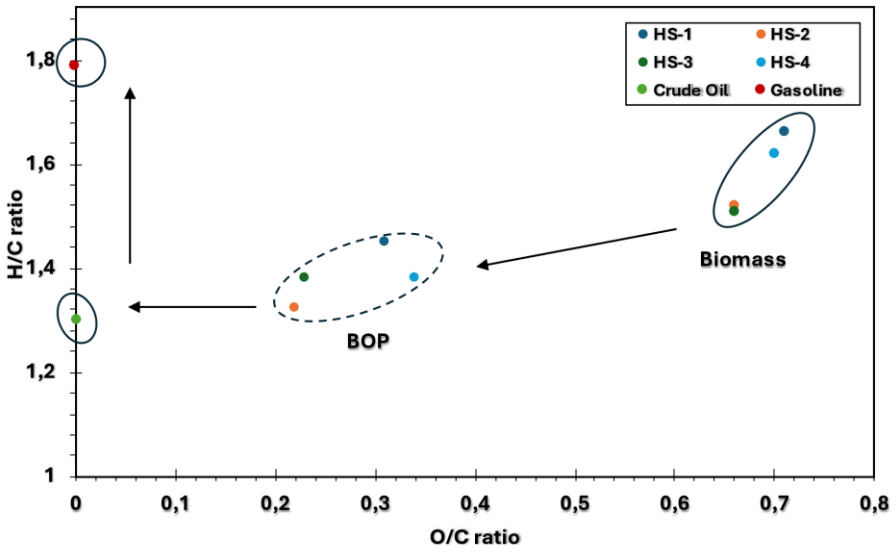

Figure 4. 7: Van Krevelen plot of giant reed biomass and bio-oil organic phase (BOP) compared to crude oil and gasoline.

The Van Krevelen plot (Figure 4.7) is a powerful tool for assessing the molecular composition of various fuels, specifically through the analysis of hydrogen-to-carbon (H/C) and oxygen-to-carbon (O/C) molar ratios. This study evaluated and compared the ratios for biomass and bio-oil organic phase (BOP) to crude oil and gasoline across different harvest seasons (HS-4 to HS-3). The BOP exhibits a range of O/C ratios from 0.22 to 0.34 and H/C ratios from 1.32 to 1.45. Crude oil presents an O/C ratio of 0.0017 and an H/C ratio of 1.3, reflecting its highly carbon-rich and low-oxygen nature (Panwar and Paul, 2021). Similarly, gasoline has an O/C ratio of 0 and an H/C ratio of 1.79, emphasizing its complete removal of oxygen, which is characteristic of refined petroleum products (Hu and Gholizadeh, 2020). The lowest O/C ratio for BOP was obtained during the senescence-dormant phase (HS-2 and HS-3).

Although this study did not focus on upgrading BOP to fuel-range hydrocarbons, comparing the O/C and H/C ratios to crude oil and gasoline was necessary to understand the best BOP based on seasonal variations. The O/C ratios indicated that BOP retains a significant oxygen

content compared to conventional fossil fuels, which typically have much lower O/C ratios. Furthermore, the O/C and H/C ratios also highlighted the loss of functional groups that contain oxygen and hydrogen, such as -OH, -COOH, and -CH_3, likely due to dehydration and deoxygenation reactions during pyrolysis. The low O/C ratio correlated with the reduction of oxygen-containing functional groups through the decrease in oxygen content from the active growth stage (HS-4 and HS-1) to the senescence-dormant phase (HS-2 and HS-3). The higher O/C ratios in BOP compared to both crude oil and gasoline indicate a less mature fuel composition, suggesting that BOP may still contain a significant proportion of polar functional groups, which can influence its reactivity and suitability as a biofuel. This is consistent with previous findings highlighting that bio-oil hydroxyl and carboxyl functional groups contribute to higher oxygen content (Bridgwater, 2012a).

The H/C ratios of BOP in the current study ranged from 1.32 to 1.45; these are lower than those of gasoline (1.79) but comparable to crude oil (1.3). Higher H/C ratios are desired for the fuel to be more efficient through reducing CO emissions. Whereas lower H/C ratios are undesirable since it translates to more aromatics, thus making bio-oil less reactive. This also induces more coking during bio-oil upgrading via hydrodeoxygenation. The lower H/C ratio in BOP indicated a higher degree of unsaturation and potential functionalization than gasoline, primarily composed of saturated hydrocarbons. The reduced H/C ratios for BOP were attributed to hydrogen being transformed into water and recovered in the aqueous phase of bio-oil. Other compounds that carry hydrogen away from the organic phase into the aqueous phase include alcohols, carboxylic acids, aldehydes, and ketones.

Additionally, some hydrogen was also lost through non-condensable gases and biochar. This characteristic suggests that while BOP may be suitable for energy applications, further upgrading or refining may be necessary to improve its fuel properties, particularly regarding stability and energy density. Since only BOP was considered in the current study, it supported the prospect of decreasing H/C ratios. The Van Krevelen plot analysis revealed that the BOP retains a higher O/C ratio and lower H/C ratio than gasoline and crude oil, indicating its potential for further refinement to enhance fuel quality.

4.7.7 GCMS Analysis of Bio-oil Organic Phase

The GCMS analysis of bio-oil samples obtained during seasonal variations revealed significant distinctions in the composition and distribution of organic compounds (Figure 4.8). The identified compounds were grouped as aldehydes, ketones, furans, phenolics, olefins, sugars,

and others. Furthermore, “others” were a classification of other compound groups in bio-oil, namely, amines, aromatics, esters, acids, alcohols, aliphatic, ethers, organosilicon, nitriles, nucleoside, alkoxysilanes, and cyclopentanetriols.

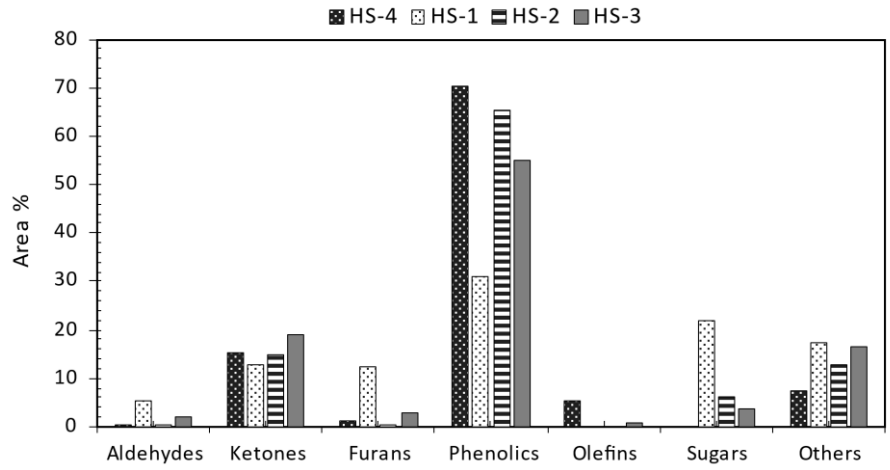

Figure 4. 8: Functional groups of BOP as detected by the GCMS.

Pyrolysis incorporates complex reactions owing to the degradation of hemicellulose, cellulose, and lignin. Decomposition of cellulose and hemicellulose forms 1-hydroxy-2- propanone, acetic acid, anhydro sugars, furans, and levoglucosan, among other compounds. While phenolics, aldehydes, ketones, guaiacols, alcohols, and carboxylic acids come from the lignin decomposition (Guilhaume et al., 2021). Aldehydes were significantly higher during HS-1 at 5.46% compared to 0.31% during HS-4. This observation indicates potential differences in biomass degradation kinetics that favoured the formation of aldehyde compounds during HS-1. Phenolics demonstrated significant variability across seasons, with HS-4 exhibiting the highest content at 70.49% and HS-1 showing the lowest at 31.1%. This was reflective of seasonal fluctuations in lignin and cellulose compositions. Bio-oil from HS-4 was mainly in the aqueous phase. Hence the high area% of phenolics in Figure 8 was mainly due to polar phenolic compounds. In HS-2 and HS-3, the phenolic compounds were relatively high at 65.21 and 55%, respectively. Phenolic content decreased with plant maturity which was a surprise since phenolics are mainly derived from lignin and lignification stops during dormant phases. This signified that the distribution of pyrolysis products is highly influenced by the constituent structure of the biomass (Azeez et al., 2010). The application of phenols includes the manufacturing of renewable resin when extracted and can potentially replace conventional petroleum-based phenol. Ketones showed relatively consistent levels across all seasons, with HS-3 exhibiting the highest percentage at 18.79% followed by HS-4 at 15.29%. These compounds form esters when oxidized. Phenolics and ketones are oxygenated compounds that

contribute significantly to lowering the heating value of bio-oil (Arazo et al., 2017). Furan derivatives were elevated in HS-1 (12.31%) followed by HS-3 at 3%, suggesting variations in biomass characteristics over various seasons. However, during HS-2 and HS-4, furans remained relatively flat at 0.49 and 1.28%, respectively. Furans are typical products of cellulose and lignin decomposition, similar to phenolics (Cheng et al., 2015). Olefins were predominantly present in HS-4, constituting 5.32% of the composition. This was indicative of potential differences in the thermal degradation pathways of biomass constituents that favoured the formation of these compounds in HS-4.

The sugars were highest in HS-1 at 21.87% which was due to the degradation of biomass carbohydrates during pyrolysis. In HS-2 and HS-3, the sugars were 6.36 and 3.71%, respectively. Meanwhile, during HS-4, no sugar compound was detected. The main sugar compound that was obtained in bio-oils was levoglucosan from the decomposition of cellulose. It is formed during a depolymerization reaction due to transglycosylation at a temperature of 300 ^{0}C (Azeez et al., 2010). The observed decrease in sugars was attributed to fission and disproportionation which leads to the formation of furans and acids. Additionally, the high content of inorganics which promotes glucose fragmentation rather than polymerization also contributes to sugar compound reduction. 1,4:3,6-Dianhydro-α-d-glucopyranose, the dehydrated form of levoglucosan was also obtained in bio-oils during HS-1, HS-2, and HS-3. From these results, it is evident that bio-oil compounds vary with different seasons. Hence, it is crucial to determine the desired product before harvesting biomass for thermochemical conversion.

4.7.8 GCMS analysis on the distribution of "Others"

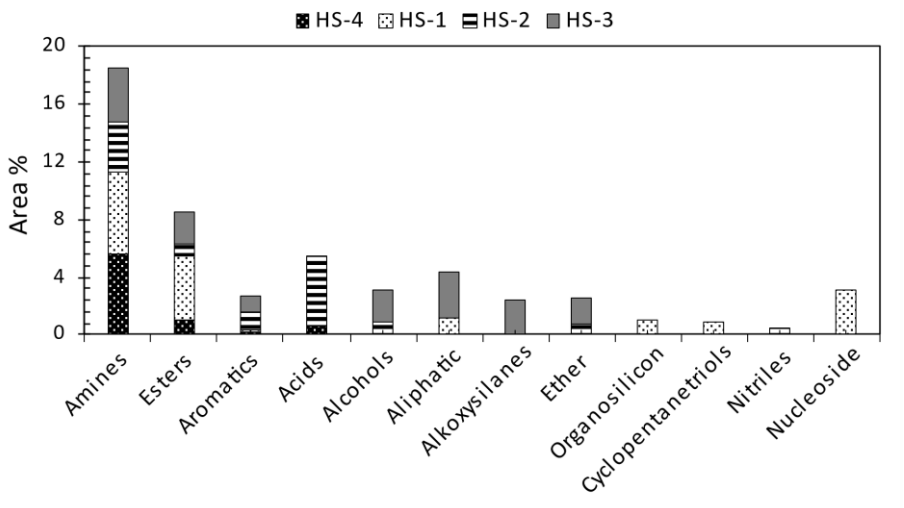

Figure 4. 9: Distribution of "Others" functional groups detected by the GCMS.

The “others” compounds are shown in Figure 4.9, which further showcases the compound groups for different seasons. The alcohols were found in HS-2 and HS-3 at 0.87 and 2.22%, respectively. Similarly, the ether groups were 0.72 and 1.83% for HS-2 and HS-3, respectively. The amine and ester groups were present in all seasons; however HS-1 was rich in esters, and HS-4 was rich in amines. The increase in esters and amines was HS-1>HS-3>HS-4>HS-2 and HS-1>HS-4>HS-3>HS-2, respectively. The acids dominated during HS-2 at 4.96% followed by 0.58% in HS-4. Aliphatic compounds, on the other hand, were present in HS-1 and HS-3 at 1.24 and 3.06%, respectively. Acid compounds and their derivatives are formed due to the decomposition of hemicellulose. The nitrogenous compounds were attributed to the heterocyclic ring-containing compounds in the biomass (Kumar et al., 2022b). Amines were attributed to the significance of nitrogen atoms during plant growth. Amines are not desirable as fuel; however, amine solvents are essential in scrubbing carbon dioxide from flue gas via amine-based post-combustion capture (PCC), thus preventing air pollution. The presence of various compounds highlighted the complex nature of bio-oil composition and the relationship of factors influencing pyrolysis products during different seasons.

4.7.9 Energy Density of Bio-oil Organic Phase

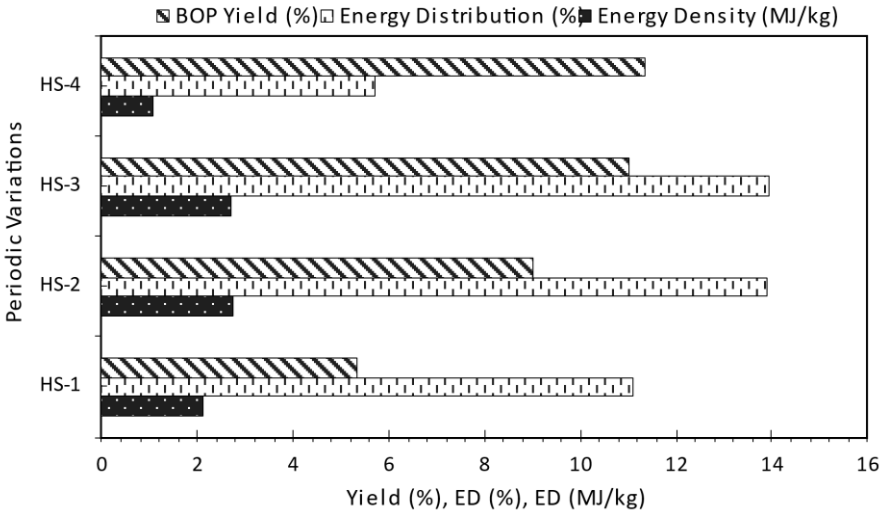

Figure 4. 10: Energy density and distribution of BOP.

The biomass energy distribution (Figure 4.10) of the bio-oil organic phase was determined from the ratio of the heating values. The energy density gives the biomass energy share respective to the bio-oil organic phase. As previously discussed, the highest organic phase yield was obtained during HS-3 and HS-2, while the lowest yield was observed in HS-4. The high

organic phase yields correlated with high lignin content during HS-3 and HS-2. On energy distribution, approximately 14% of initial HHV was converted into the organic phase during HS-3 and HS-2. Meanwhile, 5.72 and 11% of the initial HHV were converted into the organic phase during HS-4 and HS-1, respectively. The HHV values of BOP correlated with the variations in BOP oxygen and water contents. The results emphasized the significant impact of seasonal variations on the composition and properties of bio-oil. Hence, it was evident that HS-2 and HS-3 showed improved BOP energy content compared to HS-1 and HS-4. From an energy yield perspective, it is crucial to recognize that the calculation of percentage energy density may be erroneous if the yield of the pyrolysis liquid is solely attributed to the organic phase without correctly differentiating between the organic and aqueous phases. This increases energy density percentages, accounting for the aqueous phase yield. Furthermore, the pyrolysis liquid phases have distinct heating values; thus, it is necessary to account for organic phase yield when determining the energy density. The aqueous phase needs to be accounted for separately due to distinct heating values compared to the organic phase.

4.7.10 Characterization of Biogas

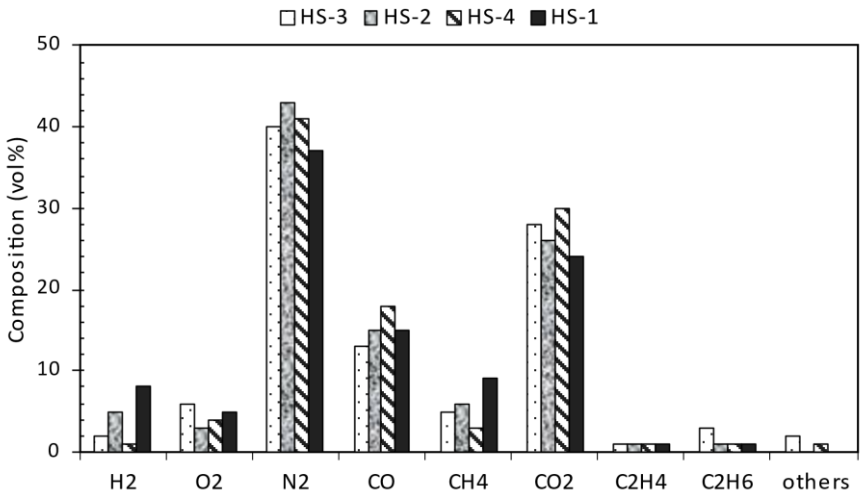

Figure 4. 11: Biogas distribution during thermochemical conversion of Giant Reed.

The biogas/non-condensable gases were collected and analysed during the degradation of biomass at different seasonal variations (HS-4 to HS-3). The results of the analysed biogas samples are shown in Figure 4.11. The analysis of the biogas mixture identified the following gases: hydrogen (H_2), nitrogen (N_2), carbon monoxide (CO), carbon dioxide (CO_2), oxygen (O_2), ethene (C_2H_4), ethane (C_2H_6), others (C_xH_y), and methane (CH_4). Based on the identified gases, nitrogen, carbon monoxide, carbon dioxide, and methane were the predominant gases.

Nitrogen had the highest concentration by volume when compared to other gases, and this was attributed to nitrogen being used as the carrier gas during pyrolysis. Carbon dioxide and carbon monoxide had the highest concentration by volume during HS-4. Meanwhile, during HS-1, the highest concentration of hydrogen was observed and the lowest carbon dioxide concentration when compared to other seasons. The release of carbon dioxide during the thermal degradation of biomass is mainly attributed to the holocellulose and lignin (Yang et al., 2007). In addition, degradation of monosaccharide and polysaccharide fractions of hemicellulose are the dominant contributors to the formation of carbon monoxide and carbon dioxide (Gaur and Reed, 2020). Another contributor to the increase of carbon dioxide and carbon monoxide is the oxidation of biochar (Baker et al., 2005, Lee SeongBeom and Fasina, 2009). This explains the highest CO_2 and CO during HS-4 (growing phase).

4.8 Conclusions

Harvest time significantly impacts the fuel properties of lignocellulosic biomass, specifically giant reed. Elemental analysis revealed that carbon and hydrogen contents remained relatively stable, while inorganic materials peaked during the active growth stage (HS-1 and HS-4), contributing to higher ash content. Thermogravimetric behaviour also supported the prospect of higher inorganics during active growth stages. The HHV values of biomass increased from 18.44 ± 0.04 to 19.73 ± 0.05 MJ/kg from the active growth to the senescence-dormant phase (HS-2 and HS-3). While holocellulose content decreased, lignin content increased, with fixed carbon being the highest during the senescence-dormant phase. Higher ash content correlated with lower bio-oil organic phase and pyrolysis gas yields, while lower ash content yielded higher yields. The organic phase yield increased from the active growth stage to the senescence-dormant phase, significantly linked to lignification ($R^2 = 0.97$). Properties of the bio-oil organic phase improved during the senescence-dormant period, with viscosity and total acid number decreasing alongside increasing HHV values. The O/C ratio varied, reaching its lowest during the senescence-dormant phase. The HHV values of the BOP ranged from 19.4 ± 0.03 to 22.6 ± 0.02 MJ/kg during active growth to senescence-dormant periods. Therefore, harvesting giant reed in autumn optimizes biomass and BOP properties, minimizes carbon emissions from incineration, and mitigates flooding issues from dormant plant blockages.

CHAPTER 5

5. Isothermal Pyrolysis of Bamboo and Pinewood Biomass: Product Characterization and Comparative Study in a Fluidized Bed Reactor

5.1 Abstract

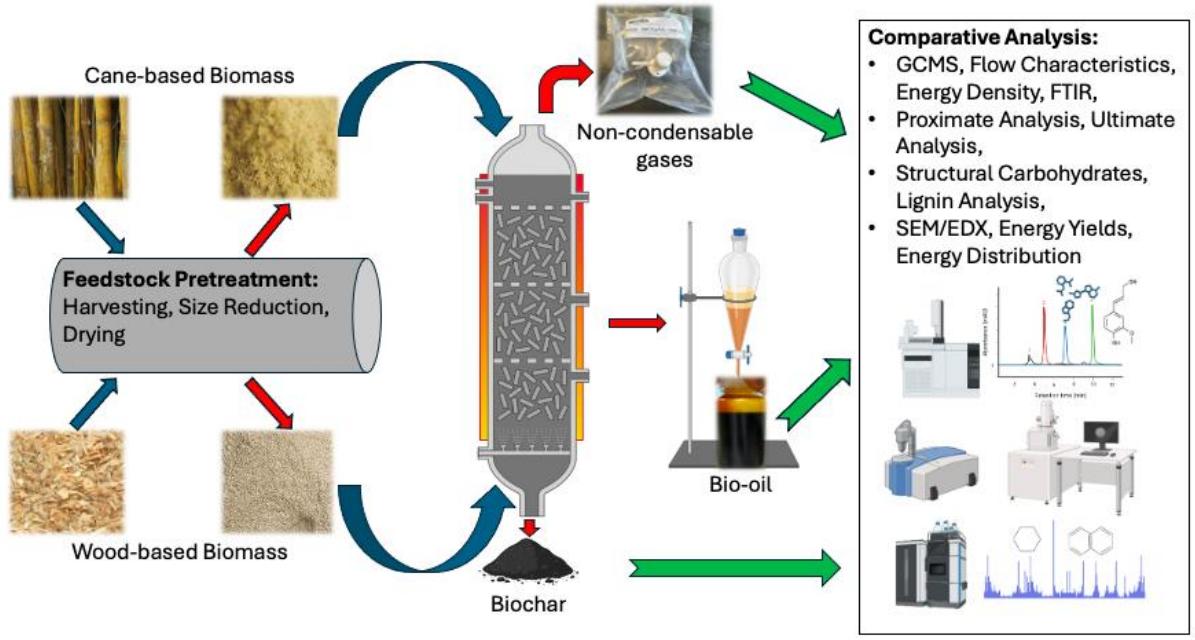

Fast pyrolysis of biomass is crucial for sustainable biofuel production, necessitating thorough characterization of feedstocks to optimize thermal conversion technologies. This study investigated the isothermal pyrolysis of bamboo and pinewood biomass in a sand-fluidized bed reactor, aiming to assess biomass suitability for commercial bio-oil production. The pyrolysis products and biomass species were characterized through proximate and ultimate analyses, along with GCMS, FTIR, SEM/EDX, and structural analysis to assess their chemical and physical properties. Results indicated that pine bio-oil possesses superior energy density, with a higher calorific value (20.38 MJ/kg) compared to bamboo (18.70 MJ/kg). Pine biomass yielded greater organic phase bio-oil (BOP) at 13 wt%, while bamboo produced 9 wt%. Energy yields were also notable, with pine exhibiting an energy yield of 15% for bio-oil organic phase (EBOP), compared to 11% for bamboo. The fibrous nature of bamboo biomass resulted in less reacted biomass at constant reaction time due to flow resistance during pyrolysis. Pine bio-oil organic phase (P-BOP) demonstrated a higher heating value (23.90 MJ/kg) than bamboo (B-BOP). The findings suggest that while both biomass types are viable renewable energy sources, pine biomass is more favourable for commercialization due to its superior energy properties and efficiency in pyrolysis.

Keywords: biomass, bio-oil, fast pyrolysis, biofuels.

5.2 Introduction

The significant environmental degradation caused by climate change, mainly due to extensive fossil fuel consumption, has prompted increased interest in bio-based fuels as potential alternatives. This shift aims to decrease dependence on fossil fuels overall (Fernandez et al., 2021, Patel et al., 2020). As a result, it has become evident that energy should be renewable, cost-effective, convenient, safe, and sustainable. Nowadays, it is considered feasible and promising to convert biomass via thermochemical processes into petrochemicals and biofuels (Çağlar and Demirbaş, 2002). These processes use various biomasses that can be processed into a wide range of products, offering great productivity. While virtually all plant biomass can undergo pyrolysis, certain species exhibit more excellent suitability than others under similar operational conditions (Hoang et al., 2021). Energy crops such as bamboo and Giant Reed have gained enormous exploration for future energy production due to their high economic value, short rotation, high productivity, and improvement for sustainable management. Bamboo is considered invasive in other parts of the world, especially the running type bamboo, thus its application in biofuel production is vital for the efficient use of marginal lands (Cappelli et al., 2021). Currently, there is no effective control measure for dealing with the extensive amount of invasive energy crops. Incinerating it directly is the adopted technique to dispose of it, however this results in the release of harmful gases which are, carbon monoxide, carbon dioxide, nitrogen oxides, and fine particulate matter (Corno et al., 2014). The attempts to apply biological and burning methodologies to control the invasiveness of the non-food energy crops add no value compared to utilizing the plants for bioenergy generation. Patel and Kumar (2016), investigated the pyrolysis of gigantic reed grass using thermogravimetry-mass spectrometry (TG-MS). The authors concluded that energy grass has a stronger thermochemical reactivity and a quicker devolatilization. Woody biomass, on the other hand, is known for its low ash content when compared to energy crops. Pinewood is among the most abundant biomass sources in the world and extensive work has been done in producing bio-oil and biochar via thermochemical conversion technologies (Trubetskaya et al., 2023, Newalkar et al., 2014, Yildiz et al., 2015, Mishra et al., 2015, DeSisto et al., 2010, Oudenhoven et al., 2016, Varma and Mondal, 2018, Tran et al., 2021). In forested areas, logs are often harvested for fuelwood or incinerated in open settings once dry, to clear space for alternative forest activities. Wood shavings and residuals from sawmills are similarly combusted as a method of disposal (Azeez et al., 2010). The emissions resulting from combustion exacerbate environmental challenges related to climate change. Optimal utilization of biomass for

bioenergy production holds considerable promise in addressing global energy demands and economic issues in developing countries. In thermochemical conversion, the primary techniques include pyrolysis, liquefaction, gasification, and combustion (Awasthi et al., 2023). Among the aforementioned thermochemical techniques, pyrolysis is the preferred approach, as it is cost-effective and easy to use for the production of biofuels and petrochemicals from biomass. This technique is categorized into slow, fast, and flash pyrolysis (Pawar et al., 2020). The choice of pyrolysis type to employ depends on the desired product distribution. Fast pyrolysis is a good choice when high bio-oil yields are desired, while slow and flash are selective to higher yields of biochar and biogas, respectively. Fast pyrolysis of biomass represents a pivotal avenue for biofuel production, recognized as environmentally viable for future energy needs. Comprehensive knowledge of biomass pyrolysis characterization and its derived products is essential for the design of thermal conversion technology systems and for selecting appropriate feedstock species for efficient biofuel production (Dayton and Foust, 2019). Therefore, thorough characterization of the parent feedstock is fundamental in pyrolysis technology. While extensive research has been conducted on the pyrolysis of bamboo and pine biomass individually, limited studies have examined the pyrolysis of these materials when continuously fed into a reactor for bulk bio-oil production. This is particularly critical for advancing large-scale bio-oil production, yet this area has largely been overlooked in the existing literature. In particular, the effects of fibrous feedstocks, such as bamboo, in continuous feeding setups remain underexplored. In the current work, two biomass species were characterized and pyrolyzed in a sand-fluidized bed reactor to determine their suitability for commercial bio-oil production. Other pyrolysis products were also characterized to assess their potential as sources of bioenergy. The comparative isothermal fast pyrolysis study of cane-based biomass and wood-based biomass for the production and characterization of bio-oil in a sand-fluidized bed reactor has not been done to the best of the authors' knowledge. This study uses *N. Henon* bamboo, a highly invasive species that has not been widely examined in thermochemical conversion applications. In contrast, *Moso* bamboo is the most commonly studied species(Dong and Xiong, 2014, Jiang et al., 2012, Dong et al., 2018, Chen et al., 2014a, Qin et al., 2024, Liu et al., 2013, Lei et al., 2024, Tong et al., 2020, Liang et al., 2018). The introduction of *N. Henon* bamboo as a feedstock for pyrolysis represents a novel approach in biomass research. The key research question guiding this study is: How does the pyrolysis behaviour of bamboo compare to pine biomass under similar conditions? This study addresses these gaps by conducting a comprehensive analysis of bamboo and pine biomass under

identical pyrolysis conditions, with a focus on the impact of feedstock properties on bio-oil yield and composition.

5.3 Materials and Methods

5.3.1 Sample Harvesting and Preparation

Bamboo (*Phyllostachys nigra 'Henon'*) and pinewood biomass were obtained from Auburn University, USA. Bamboo was harvested during summer having a height of 4-6 m, and a diameter of 5 cm. The pinewood considered in this study was longleaf pine (*Pinus palustris*) and was felled, debarked, and ground into small chips to be stored in the biomass storage warehouse. In preparation for pyrolysis experiments, biomass was dried for 24 hr at 105 ºC. The oven-dried biomass was grinded by a hammer mill (C.S. Bell Co., model 10HBLPK, Tiffin, OH, USA) prior to sieving. Sieve shaker was used to obtain the desired particle size range of 0.6-1 mm.

5.3.2 Biomass Characterization

Elemental analysis (CHNS) was performed using an Elementar Vario Micro Select, according to ASTM D5373. Biomass moisture content and ash content were determined according to ASTM D4442-07 and E1755-01, respectively. The volatiles were determined according to ASTM E872, and fixed carbon content was determined by difference. A thermolyne (Thermo Scientific) furnace was used during the oxidation process. Thermal degradation behavior of biomass was carried out using a Thermogravimetric analyzer (TGA5500/Discovery Series) under the nitrogen atmosphere for a temperature range of 25–800 ^{0}C at a heating rate of 10 ^{0}C/min. Platinum HT pan types were used for sample loading, and a ramp procedure was employed. Lignin and structural carbohydrates were estimated by following the National Renewable Energy Laboratory method (NREL) (Sluiter et al., 2008, Sluiter et al., 2005, Sluiter et al., 2012). Briefly, 10 g of biomass was loaded into the extraction crucible for a sequential water and ethanol extraction process. After extraction, 0.3 g of biomass was loaded into pressure tubes to conduct acid hydrolysis using 72% sulfuric acid, diluted with deionized water, and autoclaved for 1 hr. Vacuum filtration was used to separate solids and liquid using filtering crucibles. The solid residue was heated to 105 ± 5 ^{0}C to determine the dry residue weight followed by oxidation at 575 ± 25 ^{0}C to determine Klason lignin (AIL). Using the filtrate, the acid soluble lignin (ASL) was determined using a UV/Vis Spectrophotometer (Thermo Scientific, Orion Aquamate AQ8100). Sugars were analyzed using by high performance liquid chromatography (HPLC) (Agilent Technologies 1260) using BioRad HPX-87P column. The

chemical functional groups of biomass was identified by using a Fourier Transform Infrared spectroscopy (FTIR) at a range of 4000–400 cm^{-1}. The spectra were generated using the FTIR-ATR, Thermo Fisher Scientific Smart ITX (Nicolet iSO10) spectrometer.

5.3.3 Fast Pyrolysis with Fluidized Bed Reactor

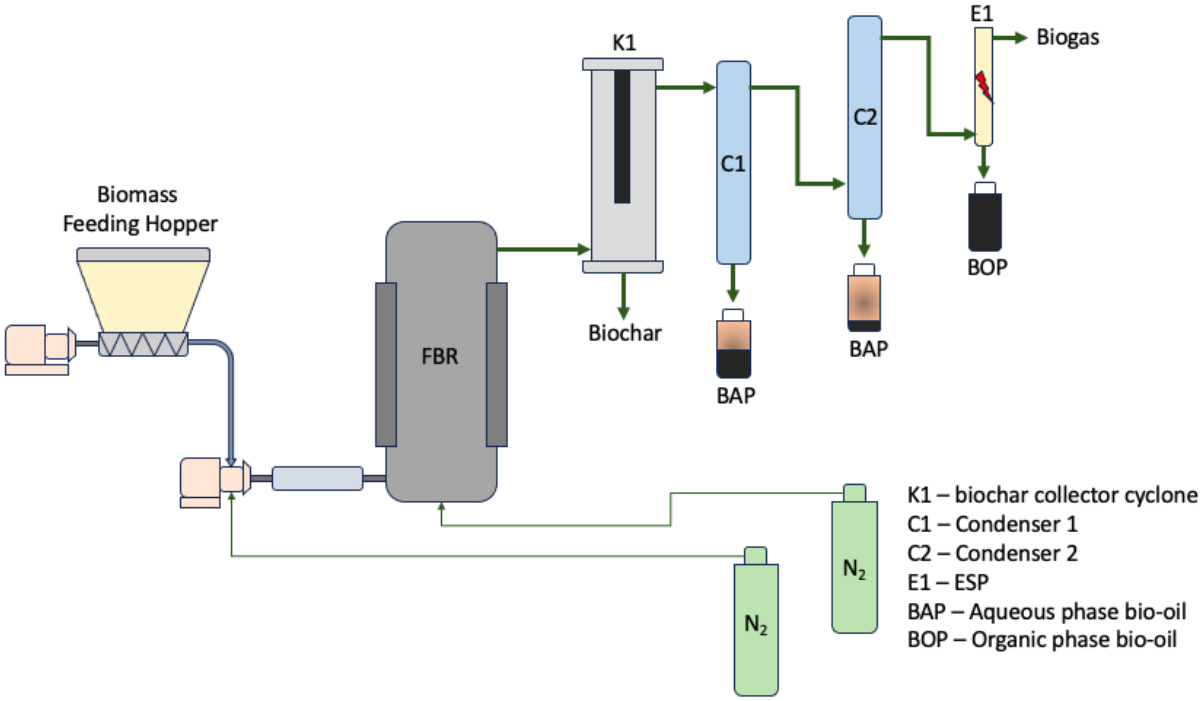

Figure 5. 1: Schematic diagram for fast pyrolysis in a Fluidized Bed Reactor (FBR).

The fast pyrolysis runs were conducted using a fluidized gas-solid reactor developed by the Bioenergy Laboratory of Auburn University (Auburn, AL, USA) as shown in Figure 5.1. Pinewood or bamboo biomass was loaded into the hopper. White fine silica sand (1235 ± 0.5 g) was used to fluidize the bed and enhance the heat transfer within the reactor. The sand was sieved to a desired particle size of 0.3–0.22 mm and then was loaded into the reactor. The pyrolysis system is comprised of a hopper (screw auger/airlock feeding), fluidized bed reactor (FBR), hot filtration unit, and condensing system that is equipped with an electrostatic precipitator (ESP). The reactor and char filter were preheated to the desired temperature before starting each run using electrical heaters. Once the desired temperatures were reached, the system was purged with nitrogen gas for 13 ± 2 min to ensure an inert atmosphere. Two nitrogen lines with flowrates 34 standard litres per minute (SLPM) and 6 ± 1 SLPM for fluidization and backflow prevention were used, respectively. A superficial velocity of 0.032 m/s was used, which was sufficient to maintain adequate fluidization in the FBR reactor. The reactor temperature was allowed to reach 595 ± 18 ^{0}C before feeding the biomass. Then

biomass was conveyed into the reactor at a rate of 27 g/min by a screw auger that is mechanically controlled by Weigh Feeder Controller (C-702, ACRISON). Each pyrolysis run was allowed to run for 2 hrs at a temperature of 544 ± 33 ^{0}C in replicates of three. The reactor, pipelines, and char filter were properly insulated to minimize any heat loss to the surroundings that can result in undesired condensation taking place before reaching the cooling system. The cooling medium was ethylene glycol at 2 ± 0.5 ^{0}C and 1.2 bar with a pumping capacity flowrate (PCF) of 40 L/min from a recirculating chiller (Julabo, FL2503, USA). Non-condensable gases were collected in 1 L Tedlar bags (RESTEK) after 20 min of starting the pyrolysis reaction for compositional analyses. Biochar was collected and weighed. The sand and biochar balance were used to correctly determine the amount of biochar obtained from the char filter and the reactor. The total weight of biogas was determined by mass balance after the pyrolysis reaction. The vapors from the reactor passed through the char filter where biochar was collected. Thereafter, the liquid product (aqueous phase) was condensed by two condensers in series. The organic phase bio-oil was precipitated from the non-condensable gases (NCGs) using one ESP. Bio-oil was continuously obtained and weighed for the duration of the reaction using Nalgene bottles style 2104 (B9157 and B9407, Sigma-Aldrich) for sample collection. The bio-oil collected from the ESP was classified as the bio-oil organic phase (BOP) and was used for hydrotreating experiments. The percentage yields of the bio-oil organic phase (BOP%), aqueous phase (BAP%), biochar (BC%), and pyrolysis gas (BG%) were calculated by the following equations:

$$\mathrm{BOP\%} = \frac{\mathrm{m_{bop}}}{\mathrm{m_{bm}}} \times 100 \qquad (5.1)$$

$$\mathrm{BAP\%} = \frac{\mathrm{m_{bap}}}{\mathrm{m_{bm}}} \times 100 \qquad (5.2)$$

$$\mathrm{BC\%} = \frac{\mathrm{m_{bc}}}{\mathrm{m_{bm}}} \times 100 \qquad (5.3)$$

Where, m_{bop}, m_{bm}, m_{bap}, and m_{bc} are the masses of the organic phase, biomass, aqueous phase, and biochar, respectively. The principle of mass conservation was used to determine the biogas production yield according to the following equation;

$$\mathrm{BG\%} = 100 - \mathrm{BC\%} - (\mathrm{BOP\%} + \mathrm{BAP\%}) \qquad (5.4)$$

5.3.4 Product Characterization

Elemental analysis (CHNS) was performed using an Elementar Vario Micro Select, according to ASTM D5373 and ASTM D5291. The oxygen content was determined by difference, and the results were reported on a dry basis. The moisture content of bio-oil was measured by Karl Fischer Titration by using Aquastar (combititrant 5 keto, volumetric KFT for aldehydes and ketones) as a titrator/reagent and Apura (combi-solvent keto, volumetric KFT, ca.5mg H_2O) as a solvent. Total Acid Number (TAN) was measured by a Mettler T50 autotitrator using a Total Acid Number Titration Solvent Mixture and 0.1M KOH 2-propanol as the titrating reagent (titrant), according to ASTM D664-07. SEM/EDX was used to determine the inorganic contents/elements of biochar. A bomb calorimeter (IKA C200 calorimeter, IKA Works, Wilmington, N.C.) was used to determine the higher heating values of biomass and bio-oil organic phase. The ash content was determined according to ASTM D 482, where a BOP sample was ignited and allowed combust until only carbon material and ash (inorganics) remained in the vessel. In order to reduce the carbonaceous residue to ash, the ignited sample was heated at 775 ± 25 ^{0}C for 20 min in a muffle furnace. Following oxidation, the sample was cooled to room temperature in a desiccator and then weighed. The viscosity (kinetic and dynamic) and density were measured using the Anton Paar Instrument (SVM Standard method) at 40 ^{0}C. Biogas chemical composition was analyzed using Agilent 490 4-channel Micro GC, with helium and argon as carrier gases for different channels. The calibration curves were initiated using a standard gas mixture of hydrogen (H_2), carbon monoxide (CO), carbon dioxide (CO_2), and methane (CH_4). The "others (C_xH_y)" on the biogas balance was obtained by difference, i.e., non-quantified gases were classified as others. The chemical composition of organic phase bio-oil was analyzed by gas chromatography coupled with a mass spectrometric detector (GCMS). The experiments were carried out on an Agilent 5977C GC/MSD with helium gas as a carrier gas. National Institute of Standards and Technology (NIST) spectral library was used to identify the chemical compounds. Briefly, the samples were weighed and then diluted with 2 ml of methanol. Following dilution and continuous shaking for complete mixing, the sample was filtered through JT Baker Nylon syringe filter (0.2 μm). The filtered sample was injected, and the inlet temperature was set to 280 ^{0}C at a split ratio of 10:1. The column temperature was held at 50 ^{0}C for 5 min, then heated to 280 ^{0}C at a ramping rate of 10 ^{0}C/min with a 5 min holding time. Thermal behavior of the spent catalyst was used to examine carbon deposition on the catalyst. TG-50H detector with an alumina cell was used for examination at a heating rate of 10 ^{0}C/min and a holding temperature of 800 ^{0}C (2 min) under the air atmosphere (20 ml/min).

5.4 Results and Discussion

5.4.1 Biomass Characterization: Proximate and Ultimate Analysis

Table 5. 1: Proximate and ultimate analysis of lignocellulosic biomass.

Parameter	Bamboo	Pine
Proximate Analysis (wt%)[db]		
Moisture Content[a]	4.010 ± 0.13	6.760 ± 0.28
Volatile Content	85.90 ± 0.70	92.50 ± 0.60
Ash Content	1.970 ± 0.02	0.330 ± 0.07
Fixed Carbon[b]	12.13	7.17
Ultimate Analysis (wt%)[db]		
Carbon	48.97 ± 0.170	51.16 ± 0.130
Hydrogen	6.280 ± 0.180	7.052 ± 0.160
Nitrogen	0.280 ± 0.047	0.043 ± 0.011
Sulphur	0.030 ± 0.009	0.020 ± 0.010
Oxygen	44.49 ± 0.160	41.73 ± 0.010
HHV (MJ/kg)	18.70 ± 0.045	20.38 ± 0.054

[db] dry basis, [b] calculated by difference, [a] wet basis

The characterization results from the proximate and ultimate analyses provide valuable insights into the suitability of bamboo and pine as feedstocks for pyrolysis-based bio-oil production (Table 5.1). Proximate analysis reveals critical parameters such as moisture, volatile matter, ash, and fixed carbon contents, which significantly influence pyrolysis behaviour and product distribution. Bamboo demonstrates a lower moisture content (4.01 wt%) compared to pine (6.76 wt%), indicating a higher energy efficiency. Pine, however, exhibits higher volatiles (92.50 wt%) compared to bamboo (85.90 wt%), suggesting a greater potential for bio-oil yield. Moreover, bamboo presents a higher fixed carbon content (12.13 wt%) compared to pine (7.17 wt%), indicating a propensity for more stable pyrolysis reactions and potentially higher biochar yields. The 41% decline in fixed carbon for pine biomass was attributed to low ash content and high volatiles. Bamboo is nutrient-rich and tends to absorb minerals from the ground, which results in high inorganics that contribute to high ash content as shown by a 2% ash content compared to 0.3% for pine. Jung et al. (2008) reported an ash content of 1.7 wt% for bamboo, while Kato et al. (2014) found the ash to be 1.25 wt% for bamboo. The observed discrepancies in ash content can be attributed to geographical origin, different species of bamboo, and harvest

season. High mineral absorption for bamboo contributes to high levels of nitrogen and sulphur contents (Hu et al., 2017, Satya et al., 2012, Guiotoku et al., 2024). Hence, pine biomass is anticipated to emit minimal sulphur and nitrogen oxides during bio-oil synthesis, reinforcing its environmental compatibility over bamboo biomass. In the ultimate analysis, bamboo displays slightly lower carbon (48.97 wt%) and hydrogen (6.280 wt%) contents compared to pine (carbon: 51.16 wt%; hydrogen: 7.052 wt%). However, bamboo demonstrates a higher nitrogen content (0.280 wt%) compared to pine (0.043 wt%). Both bamboo and pine show minimal sulphur content, with bamboo slightly higher at 0.030 wt% compared to pine at 0.020 wt%. Bamboo appears to have a higher oxygen content (44.49 wt%) compared to pine (41.73 wt%). The high oxygen content of bamboo biomass correlated with its low heating value. These results indicated that bamboo contains more oxygenated compounds than pine biomass with a lower oxygen content. Considering calorific values, pine exhibits a higher (8% higher) calorific value (20.38 MJ/kg) compared to bamboo (18.70 MJ/kg), indicating differences in energy content per unit mass. Other biomass sources such as coconut and cassava rhizomes have HHVs of 17.77 and 23.67 MJ/kg, respectively (Landrat et al., 2022). Despite bamboo's lower calorific value, its lower moisture content and higher fixed carbon content suggest it may still offer favourable characteristics during pyrolysis, particularly in terms of process efficiency and biochar yield. However, the higher volatile matter content in pine indicates a potentially higher bio-oil yield, making it a superior source for bio-oil production over bamboo.

5.4.2 Biomass Structural Composition

The biomass structural composition significantly influences the product distribution and quality of bio-oil during pyrolysis. The biomass structural composition data is tabulated in Table 2. Pine biomass exhibits lower water and ethanol extractives at 1.52 and 1.72 wt%, respectively, in contrast to bamboo with higher values of 6.15 and 1.88 wt%, respectively. These extractives results signify that bamboo biomass has the potential to yield more bio-oil aqueous phase than pine biomass. Despite the higher water extractives content in bamboo, which suggests higher bio-oil aqueous phase yields, the actual yields are influenced by various factors beyond extractives content. As previously stated that volatiles content have a significant influence on bio-oil organic phase yield, Asadullah et al. (2008) stated that volatile matter is converted to bio-oil upon condensation, hence low volatiles for bamboo biomass support the prospect of low bio-oil yield. Other factors such as the contents of lignin and carbohydrates (holocellulose) which affect reaction pathways during pyrolysis play a significant role.

Table 5. 2: Structural composition of pine and bamboo biomass.

Components	Pine	Bamboo
Extractives (wt%)[db]		
Water	1.52 ± 0.05	6.15 ± 0.03
Ethanol	1.72 ± 0.02	1.88 ± 0.04
Lignin (wt%)[db,e]		
Klason (AIL)	9.367 ± 0.04	16.63 ± 0.05
Acid Soluble Lignin (ASL)	12.38 ± 0.07	12.51 ± 0.03
Carbohydrates (wt%)[db,e]		
Glucose	43.50 ± 0.03	43.07 ± 0.09
Xylose	35.47 ± 0.08	32.86 ± 0.05
Galactose	16.04 ± 0.02	15.51 ± 0.01
Arabinose	2.045 ± 0.17	1.673 ± 0.23
Mannose	2.063 ± 0.13	1.690 ± 0.11

[db] dry basis, [e] extractive free

The UV-Vis spectrophotometric analysis revealed distinct absorbance peaks for lignin in pine and bamboo biomass samples, with values of 0.51396 and 1.08148, respectively, at 280 nm (Figure 5.2). This wavelength corresponds to the typical absorbance range for lignin, attributed to its aromatic rings which exhibit strong absorbance around 280 nm (Crestini and Argyropoulos, 1998, Silverstein et al., 2014, Ghaffar and Fan, 2013, Stark et al., 2016, Cogulet et al., 2016). Although carbohydrates generally absorb in the 190–210 nm range (Ding et al., 2008, Martínez Montero et al., 2004, Kurzyna-Szklarek et al., 2022), the current study specifically targeted lignin detection; hence, an absorbance range of 194–354 nm was selected. The significantly higher absorbance in bamboo suggests a relatively higher lignin content compared to pine, potentially impacting its degradation characteristics and suitability in biofuel applications.

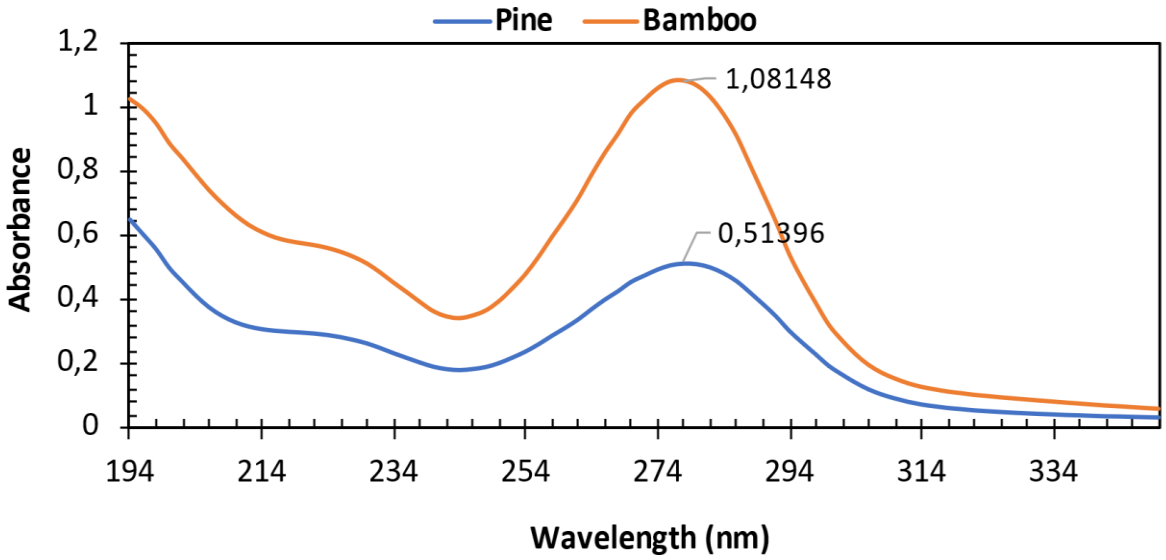

Figure 5. 2: Absorbance peaks of pine and bamboo biomass after acid hydrolysis.

The Klason lignin content in bamboo (16.63 wt%) is associated with increased phenolic compound production in the bio-oil, making bamboo biomass favourable for bio-oil with phenolic compounds. Conversely, lower lignin content for pine biomass (9.37 wt%) may result in lower phenolic compound yields. The acid-soluble lignin (ASL) exhibits consistent values between pine and bamboo biomass with an absolute error of 1%. Carbohydrates profile for pine biomass include glucose (43.50 wt%), xylose (35.47 wt%), galactose (16.04 wt%), arabinose (2.045 wt%), and mannose (2.063 wt%). Meanwhile, bamboo biomass exhibits glucose (43.07 wt%), xylose (32.86 wt%), galactose (15.51 wt%), arabinose (1.673 wt%), and mannose (1.690 wt%). The distribution of these components influences the composition of the resulting bio-oil. Different carbohydrates undergo varied thermal degradation pathways during pyrolysis, affecting bio-oil quality (Ansari et al., 2019, Chen et al., 2019). The glucose content was comparable among the two considered biomasses with an absolute error of 0.95% relative to pine. The mannose and galactose contents were marginally distinct, with an absolute error of 18% relative to pine. Xylose deviated slightly with an absolute error of 2.8% relative to pine, which signifies that xylose content in pine is 2.8% higher than that in bamboo. The overall estimates of lignin and holocellulose were 21.75 and 78.97 wt% for pine and 29.14 and 75.93 wt% for bamboo, respectively. Guiotoku et al. (2024) carried out bamboo characterization, and the lignin and holocellulose values were closely correlated with the results of this study. Conversely, Kato et al. (2014) reported Klason lignin of 24.37 wt% and holocellulose of 65.66 wt% for bamboo. This was attributed to harvest season, bamboo specie, and geographical location. Ferreira-Santos et al. (2020) reported 29.7 wt% holocellulose, and 41.05 wt% Klason

lignin for pine. Correspondingly, Santos et al. (2021) obtained 39.3 wt% holocellulose and Klason lignin of 46.2 wt% for pine. Hence, it is evident that the investigated pine specie was rich in lignin. The "others" content, which includes proteins and lipids, was higher for bamboo biomass (5.2 wt%) in contrast to pine biomass (0.9 wt%). These results indicate that pine biomass can produce furans due to its high xylose content, while both biomasses may produce levoglucosan due to high glucose content.

5.4.3 Biomass FTIR

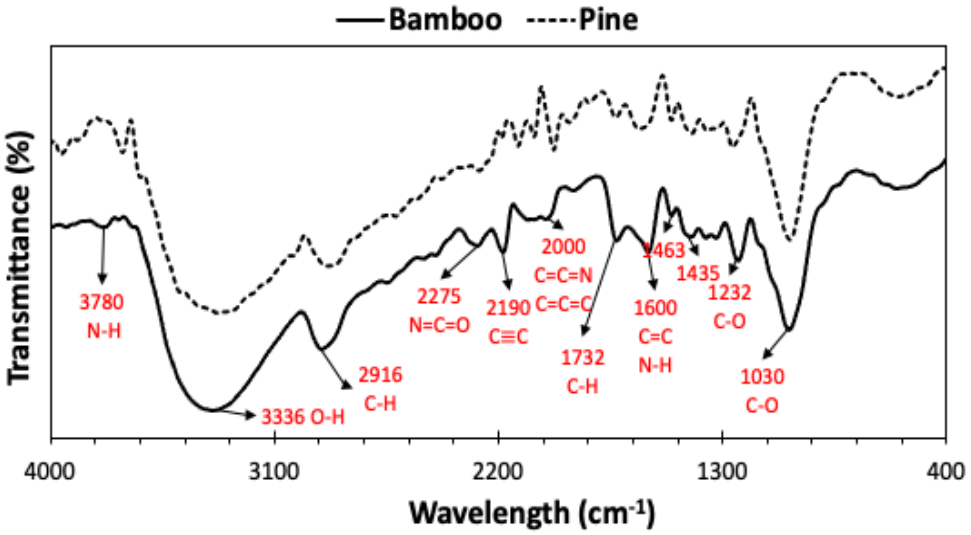

Figure 5. 3: FTIR profiles of pine and bamboo biomass.

The categorization of biomass functional groups assists in understanding the chemical composition of the biomass sample, offering crucial insights for its analysis and utilization in thermochemical processes. Figure 5.3 illustrates the FTIR spectrum of biomass samples (bamboo and pine), revealing various functional groups through distinctive peaks. The broad peak observed at 3336 cm^{-1} denotes the O-H stretching vibrations of lignin and cellulose in the biomass. Similarly, the peaks at 2916 cm^{-1} signify the C-H stretching vibrations, indicating the presence of aliphatic compounds in the hemicellulose (Suárez et al., 2023, Chikouche et al., 2015). The peak at 1732 cm^{-1} originates from the C-H and C=O stretching vibration of oxygen double bonds in hemicellulose, which is also contributed by lignin (Bessa et al., 2020). Aldehyde functionalities, mainly derived from xylose, are indicated by 1435 and 1463 cm^{-1} peaks, which may also relate to N-H bending, C=C stretching, and C-H bending vibrations. Bamboo biomass exhibits a significant presence of nitrogenous compounds compared to pine biomass as seen in Figure 5.3. The peaks for these compounds were prominent in the bamboo biomass. Peaks observed between 1200, and 1600 cm^{-1} suggest O-H bending and S=O

stretching resonances, hinting at carboxylic acid and sulfonate/phenol functionalities in the biomass. The peak at 1232 cm^{-1} signifies C-O stretching vibrations of lignin and xylan, along with syringyl ring breathing. The peak at 1030 cm^{-1} is associated with stretching vibrations of S=O/C-N functionalities (inorganics in biomass). Additionally, peak 1030 cm^{-1} was also attributed to the presence of cellulose I crystalline and C-O bonding (Martínez-Sanz et al., 2018, Rosdiana et al., 2020).

5.4.4 Fast Pyrolysis Product Distribution

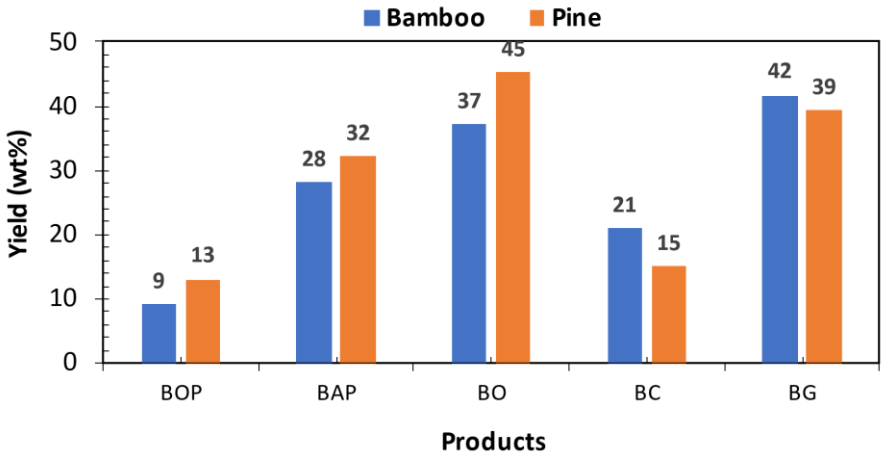

Figure 5. 4: Fast pyrolysis product yields. [BOP: bio-oil organic phase, BAP: bio-oil aqueous phase, BO: bio-oil, BC: biochar, and BG: pyrolysis gas].

The influence of different biomass (pine and bamboo) on the pyrolysis product distribution (biochar, bio-oil, and gas) was examined and plotted in Figure 5.4. Pine and bamboo biomass were subjected to pyrolysis at 550 °C to examine the effect of woody and cane-based biomass on product distribution. Moreover, bio-oil yield can only be accurate if the two phases are quantified separately. In the present study bio-oil phases were quantified separately. It is observed that the bio-oil organic phase (BOP) yield was higher for pine biomass at 13 wt% in contrast to bamboo biomass (9 wt%). The bio-oil yields for pine and bamboo were 45% and 37% by weight, respectively. In a study by Varma and Mondal (2018), a bio-oil yield of 43.76% was achieved at 550°C from pinewood biomass. Correspondingly, Chen et al. (2015) reported a bio-oil yield of 36.6% by weight at 500°C from bamboo biomass. These findings align closely with the trends observed in the current study.

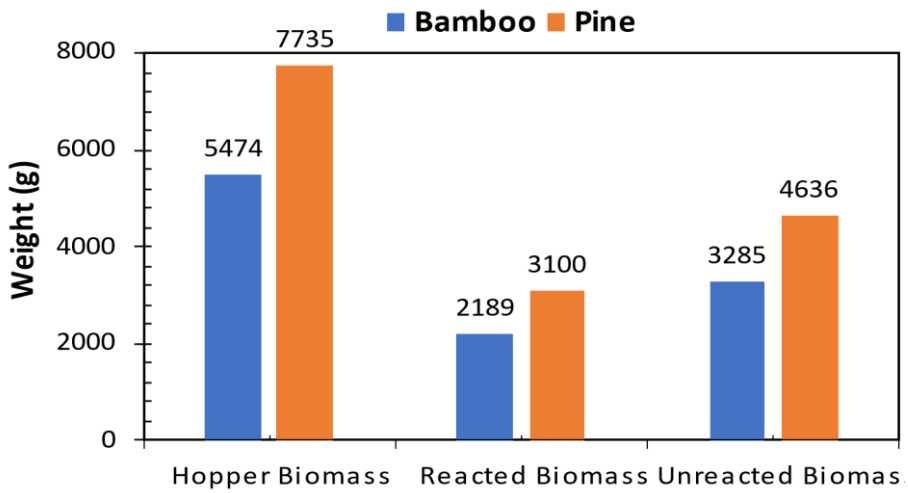

Figure 5. 5: Biomass balance for fast pyrolysis in a Fluidized Bed Reactor.

The primary decomposition reactions of the pine and bamboo biomasses were somehow comparable, with the only distinction arising from the reacted biomass. The mass difference between the initial (hopper biomass) and the final (unreacted biomass) was classified as reacted biomass. The fibrous nature of bamboo biomass resulted in less reacted biomass at constant reaction time due to flow resistance during pyrolysis (Figure 5.5). Bamboo pyrolysis is subjected to high operating costs due to prolonged reaction times, leading to higher energy utilization. Bamboo biomass resulted in biochar and pyrolysis gas yields of 21 and 42 wt%, respectively, at low reacted biomass, which correlated to high fixed carbon content and extractives. These outcomes suggest that bamboo pyrolysis results in continued cracking of the products at a temperature of 550 °C, as indicated by higher non-condensable gas yields of CO_2, CO, and CH_4 (Leite et al., 2018) (Figure 5.4). A similar trend was noted by Fahmi et al. (2008), who attributed it to the presence of inorganic compounds (ash) in the biomass. The authors found that higher inorganic content led to a reduction in bio-oil yield, accompanied by increased yields of biochar and pyrolysis gases. In this study, as shown in Table 5.1, the ash content of pine biomass is approximately 83% lower than that of bamboo, which accounts for the observed lower biochar and pyrolysis gas yields for bamboo.

5.4.5 BOP Characterization: Proximate, Ultimate, and Properties

The analyses of bio-oil samples collected during the thermal degradation of bamboo and pine biomass are tabulated in Table 5.3. These analyses exhibited discrepancies in both proximate and ultimate composition. Moisture content showed a slight variation, with bamboo displaying the higher value at 9.82 ± 0.135 wt% with an absolute error of 0.3 % relative to pine moisture

content. The observed high moisture content for bamboo bio-oil coincides with the high yield of aqueous phase (Figure 5.4). Ash content refers to the inorganic material left behind after the combustion of a fuel. In this study, the ash content in BOPs ranged from 0.029 wt% for pine to 0.21 wt% for bamboo. These results suggest that bamboo BOP contain a higher level of inorganic material compared to pine BOP. The difference in ash content is attributed to bamboo's greater ability to absorb minerals, resulting in higher inorganic concentrations. Furthermore, the data show that higher ash content in biomass leads to an increase in ash content in the bio-oil organic phase. Elevated ash levels in liquid fuels like bio-oil can cause several operational issues, including increased wear on pumps and injectors, as well as the formation of deposits and corrosion in combustion systems. These problems are mainly due to the presence of alkali metals in the ash.

Table 5. 3: Proximate, ultimate, and properties of bio-oil organic phase.

Parameter	**Bamboo**	**Pine**
Ultimate Analysis (wt%)[db]		
Carbon	70.82 ± 0.75	64.54 ± 0.45
Hydrogen	7.910 ± 0.08	7.820 ± 0.02
Nitrogen	0.540 ± 0.02	0.180 ± 0.07
Sulphur	0.020 ± 0.02	0.040 ± 0.02
Oxygen	21.11 ± 0.67	27.42 ± 0.55
C/H	8.90 ± 0.76	8.252 ± 0.82
H/C	0.11 ± 0.01	0.121 ± 0.01
O/C	0.30 ± 0.19	0.425 ± 0.22
Properties[ar]		
K. Viscosity (mm^2/s) 40 ^oC	53.25 ± 1.15	67.85 ± 1.25
Moisture Content (wt%)[a]	9.82 ± 0.135	9.79 ± 0.180
Ash Content (wt%)[db]	0.210 ± 0.01	0.029 ± 0.00
Density (g/cm^3) 40 ^oC	1.14 ± 0.00	1.18 ± 0.00
Dynamic Viscosity (mPa.s)[ar]	60.71 ± 1.31	80.06 ± 1.47
TAN (mgKOH/g)	54.13 ± 1.24	63.85 ± 2.25
HHV (MJ/kg)[db]	22.89 ± 0.04	23.90 ± 0.06

[a] wet basis, [db] dry basis, [ar] as received

The ultimate analysis exhibits significant differences in the carbon, nitrogen, sulphur, and oxygen contents for pine and bamboo organic phase bio-oils. The hydrogen content, on the other hand, remained relatively constant with an absolute error of 1.1%. Bamboo bio-oil exhibited the highest carbon content at 70.42 ± 0.75 wt%, while pine bio-oil showed the highest oxygen content at 27.42 ± 0.55 wt%. The carbon content of pine bio-oil is 8.3% lower than that of bamboo. Meanwhile, the oxygen content of bamboo bio-oil is 23% lower than that of pine bio-oil. Considering the 0.3% absolute error in the moisture content, it is evident that pine bio-oil contained more oxygenated compounds than bamboo bio-oil. Pine bio-oil exhibits lower nitrogen content (0.18 ± 0.07 wt%) than bamboo bio-oil (0.54 ± 0.02 wt%). These results suggest that pine bio-oil has a lower tendency to produce air-polluting impurities, such as nitrogen oxides. The sulphur content is lower for bamboo bio-oil at 0.02 ± 0.02 wt% and 50% higher for pine bio-oil. The high nitrogen content for bamboo bio-oil was attributed to nutrient absorption by bamboo plants (Ohyama, 2010, Leghari et al., 2016), considering the significance of nitrogen for plant growth, especially for cane-based biomass (energy crops). The properties of the bio-oil samples, i.e., kinematic viscosity, density, total acid number (TAN), dynamic viscosity, and higher heating value (HHV), also varied for pine and bamboo bio-oils. Pine bio-oil demonstrated higher TAN and viscosity values at 63.85 ± 2.45 mgKOH/g and 67.85 ± 1.25 mm2/s, respectively, compared to bamboo bio-oil at 54.13 ± 1.24 mgKOH/g and 53.25 ± 1.15 mm2/s, indicating differences in acidity levels as well flow characteristics. The cane-based bio-oil exhibits lower acidity when compared to wood-based bio-oil. This was attributed to different structural compositions in biomass, which influences the bio-oil quality (Ansari et al., 2019). Meanwhile, the density of pine bio-oil is 1.18 g/cm^3, whereas the density of bamboo bio-oil showed a 3.4% deviation from the pine bio-oil. The density values were somewhat close to the ones reported in literature for grape bagasse (Demiral and Ayan, 2011), coconut shell (Rout et al., 2016), cassava rhizome (Suttibak et al., 2012), rice husk (Lu et al., 2008), and palm tree (Abnisa et al., 2013). The HHV values exhibited a higher value for pine bio-oil (23.90 ± 0.06 MJ/kg) when compared to bamboo bio-oil (22.89 ± 0.04 MJ/kg), suggesting variations in the energy content of the bio-oil samples. The observed disparity between the heating values was insignificant, as indicated by the absolute error of 4.2 % relative to pine bio-oil. In a study conducted by Hassan et al. (2009), the authors reported a density of 1.18 g/cm³ and a HHV of 22.49 MJ/kg for bio-oil derived from pine biomass. These values are consistent with the findings obtained in the present study. Khuenkaeo and Tippayawong (2020) reported a HHV of 20.24 MJ/kg for bio-oil from bamboo residues, which contrasts with the value obtained in this study. This discrepancy is likely due to differences in biomass

characteristics, operating conditions and the type of pyrolysis reactor used. Cane-based bio-oil showed improved fuel properties when compared to wood-based bio-oil. These improvements, however, come with trade-offs, such as high inorganics in the cane-based biomass, which will result in higher ash content in the bio-oil. Moreover, the presence of impurities such as sulphur in the bio-oil is advantageous during hydrotreating when using sulphided catalysts (Xu et al., 2013, Auersvald et al., 2019). This will negate the need for an external sulphur source, such as hydrogen sulphide, in order to keep the catalyst active. Hence, the choice of bio-oil source is somehow dependent on the chosen method of bio-oil stabilizing and upgrading techniques.

5.4.6 Bio-oil Organic Phase GCMS

To assess the distribution of products across different samples, the compounds identified via GC-MS were categorized into six groups based on their functional groups: phenols, esters, ketones, aldehydes, sugar derivatives, and furans. Figure 5.6 summarizes the proportional amounts of compound classes in the bio-oil organic phase (BOP). Each group's total proportional area (%) was determined by summing each compound's proportional area (%) within that category.

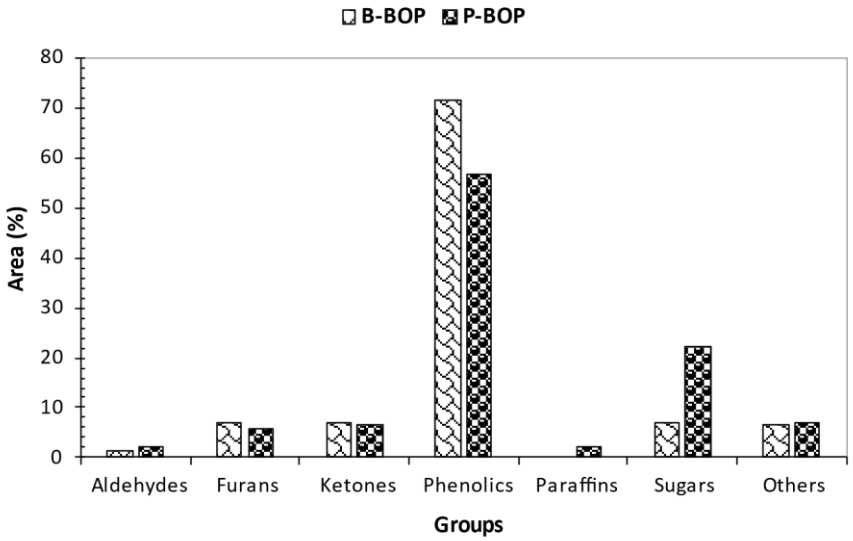

Figure 5. 6: GCMS analysis of bio-oil organic phase for pine (P-BOP) and bamboo (B-BOP).

Pyrolysis incorporates complex reactions owing to the degradation of hemicellulose, cellulose, and lignin. Decomposition of cellulose and hemicellulose forms 1-hydroxy-2- propanone, acetic acid, anhydro sugars, furans, and levoglucosan, among other compounds. While phenolics, aldehydes, ketones, guaiacols, alcohols, and carboxylic acids come from the lignin decomposition (Guilhaume et al., 2021). Phenolic compounds were prominent groups in the

bio-oil for both pine and bamboo biomass. However, bamboo exhibited higher phenolics with an absolute error of 21% relative to pine phenolics. These results were attributed to higher lignin content for bamboo than pine biomass (Table 5.2). Bio-based phenols could be used as renewable resin when extracted and can potentially replace conventional petroleum-based phenol. Ketones are present in both biomass at consistent proportions. These compounds tend to form esters when oxidized. Phenolics and ketones are oxygenated compounds that contribute significantly to lowering the heating value of bio-oil (Arazo et al., 2017). Moreover, Phenolics and furans are typical products of cellulose and lignin decomposition (Cheng et al., 2015). Acid compounds (classified under "others" in Figure 5.6) and their derivatives are formed due to the decomposition of hemicellulose. The nitrogenous compounds were attributed to the heterocyclic ring-containing compounds in the biomass (Kumar et al., 2022b). Bamboo biomass showed the presence of amines, which was attributed to strong nutrient absorption during plant growth. Amines are not desirable as fuel; however, amine solvents are essential in absorbing carbon dioxide from flue gas via amine-based post-combustion capture (PCC), thus preventing air pollution (Wang et al., 2015, Bernhardsen and Knuutila, 2017). Pine exhibited heightened sugars content when compared to bamboo. The main sugar compound that was obtained in bio-oils was levoglucosan from the decomposition of cellulose. It is formed during a depolymerization reaction due to transglycosylation at a temperature of 300 ^{0}C (Azeez et al., 2010). The observed decrease in sugars for bamboo was attributed to fission and disproportionation, which leads to the formation of furans and acids. Additionally, the high content of inorganics in bamboo, which promotes glucose fragmentation rather than polymerization, also contributes to sugar compound reduction. 1,4:3,6-Dianhydro-α-d-glucopyranose, the dehydrated form of levoglucosan, and D-Allose were also obtained in bio-oils. This signified that the constituent structure of biomass highly influences the distribution of pyrolysis products (Azeez et al., 2010).

5.4.7 Bio-oil Organic Phase FTIR

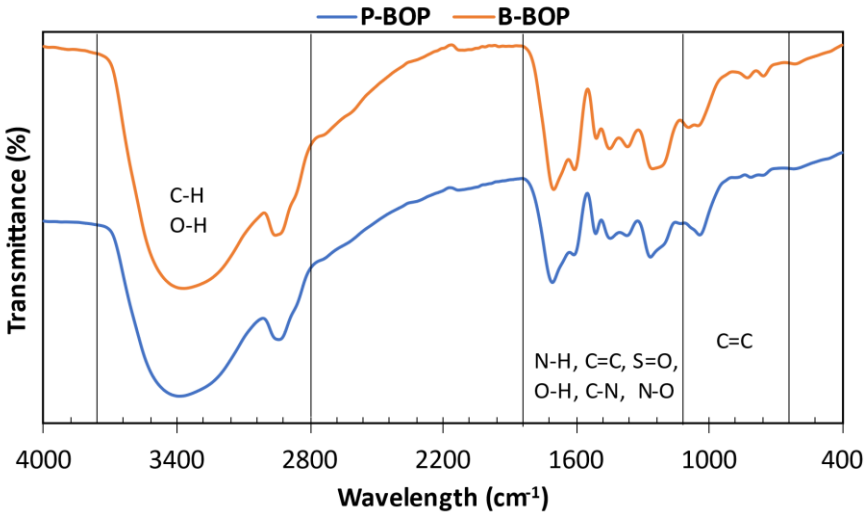

Figure 5. 7: FTIR spectres of bio-oil organic phase for pine (P-BOP) and bamboo (B-BOP).

FT-IR spectroscopy, as outlined by Lievens et al. (2013), serves as a potent analytical tool for elucidating the functional groups present in pyrolysis bio-oils. The infrared spectra of bio-oil samples from pine and bamboo biomass after thermal degradation are shown in Figure 5.7. Analysis of the infrared spectra of bio-oil samples derived from pine and bamboo biomass reveals that both types of biomass yield bio-oils containing similar functional groups. However, it is noteworthy that bamboo biomass, due to its higher nutrient absorption during growth, may contain more inorganic compounds. Spectral analysis indicates the presence of key functional groups, including C=O, C=C, C–O, C–H, and O–H bonds, within the spectral ranges of 3000–3500 cm^{-1} and 800–1750 cm^{-1}. These functional groups suggest the presence of alcohols, phenols, aromatics, and acids in the bio-oil, which aligns with findings from GC–MS analysis. Furthermore, the FT-IR spectra in the range of 1490–1850 cm^{-1} offer detailed insights into various carbonyl groups present in the bio-oil, as reported Lievens et al. (2013). Considering that biomass mainly comprises CHO chemical compounds derived from cellulose, hemicellulose, and lignin (Cho et al., 2020), these results underscore the potential for producing value-added products through the pyrolysis of pine and bamboo biomass. Moreover, the organic phase of the bio-oil presents promising opportunities for enhancement through hydrotreatment.

5.4.8 Biochar Characterization

Table 5. 4: Proximate, ultimate and energy density of biochar.

Parameter	Bamboo	Pine
Proximate Analysis (wt%)[db]		
Moisture Content[a]	0.174 ± 0.160	0.014 ± 0.002
Volatile Content	13.52 ± 0.233	17.27 ± 0.243
Ash Content	74.07 ± 1.597	55.56 ± 1.821
Fixed Carbon[b]	12.41	27.17
Ultimate Analysis (wt%)[db]		
Carbon	65.55 ± 3.12	67.76 ± 6.10
Hydrogen	2.134 ± 0.13	2.658 ± 0.18
Nitrogen	0.401 ± 0.04	0.127 ± 0.01
Sulphur	0.036 ± 0.04	0.007 ± 0.01
Oxygen	32.06 ± 2.85	29.47 ± 6.70
O/C	0.488 ± 0.02	0.430 ± 0.06
H/C	0.033 ± 0.00	0.039 ± 0.00
Calorific Value (MJ/kg)[db]	23.03 ± 0.01	24.24 ± 0.02

[db] dry basis, [a] wet basis, [b] determined by difference

Table 5.4 indicates the proximate and ultimate analysis of the biochar for bamboo and pine after the thermal degradation process in the fluidized bed reactor. The proximate and ultimate analyses of bamboo and pine biomass subjected to pyrolysis in a fluidized bed reactor yield valuable insights into their respective biochar characteristics. Bamboo exhibits a lower moisture content at 0.174 wt% than pine (0.014 wt%), indicating a potentially higher efficiency due to reduced energy requirements for moisture removal. However, such a low moisture content could potentially eliminate the requirement for supplementary drying, contingent upon compliance with specified biochar quality standards. Pine demonstrates a higher volatile content at 17.27 wt% compared to bamboo (13.52 wt%), suggesting greater combustible matter in pine biochar. Additionally, bamboo biochar contains significantly higher ash content (74.07 wt%) compared to pine (55.56 wt%), owing to variations in mineral composition. Pine biochar exhibits superior fixed carbon content (27.17 wt%) compared to bamboo at 12.41 wt%, indicating a higher potential for stable carbon sequestration. Although both biochar exhibit almost comparable carbon content, pine biochar demonstrates marginally higher hydrogen

(2.658 wt%) and lower oxygen (29.47 wt%) content, contributing to its slightly elevated calorific value (24.24 MJ/kg) compared to bamboo biochar (23.03 MJ/kg). Therefore, considering its lower moisture content, higher volatile matter, and favourable fixed carbon content, pine biomass emerges as the preferred choice for biochar production in fluidized bed reactor pyrolysis processes. Furthermore, the biochar produced has substantial potential for generating heat and power through methods such as boilers, gasifiers, and furnaces. Additionally, it offers diverse applications, including its use as fertilizer, activated carbon, and for enhancing catalytic processes, as cited in references (Sakhiya et al., 2020, Lyu et al., 2020, Qian et al., 2015, Cha et al., 2016, Wang et al., 2019, Do Minh et al., 2020, Hu et al., 2021, Kumar et al., 2022a).

5.4.9 Van Krevelen Plot

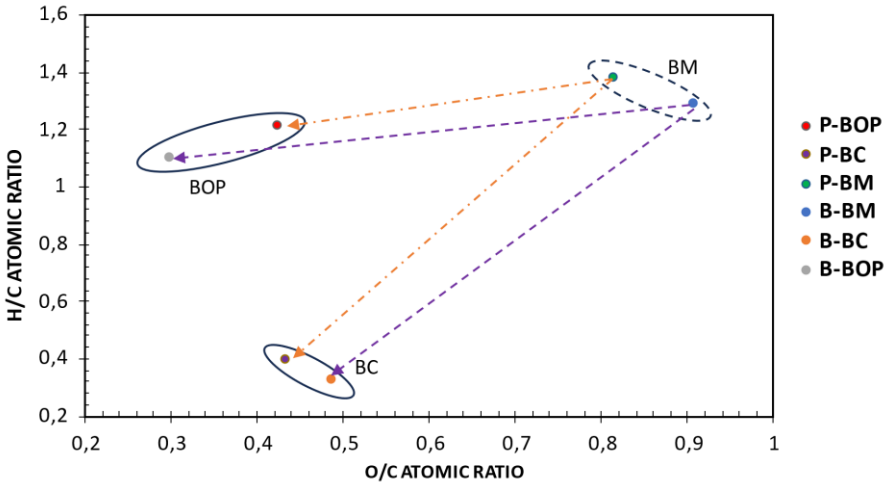

Figure 5. 8: Van Krevelen Plot of pine (P) and bamboo (B) for biomass (BM), biochar (BC), and bio-oil organic phase (BOP).

The atomic ratio of hydrogen/carbon (H/C) and oxygen/carbon (O/C) of pine (P) and bamboo (B) biomass (BM), biochar (BC), and bio-oil organic phase (BOP) were evaluated and compared as shown in the Van Krevelen diagram in Figure 5.8. This plot tracks changes in the molecular composition of feedstocks during pyrolysis, offering insight into the evolution of product distribution and the degree of aromaticity in the material ("Van Krevelen, 1993). In pyrolysis, the van Krevelen plot is often used to understand the progression from biomass or other organic materials to pyrolytic products, such as bio-oils and pyrolysis gases. It shows how the H/C and O/C ratios change as a function of temperature and reaction conditions. Van Krevelen (1993) first discussed the concept in relation to the combustion and pyrolysis of organic materials, particularly coals. The plot highlighted three distinct regions for biomass,

biochar, and bio-oil organic phase, with the biomass at the top right corner and the bio-oil organic phase at the lower left corner. Higher H/C ratios are desired for the fuel to be more efficient through the reduction of CO emissions. Pine bio-oil resulted in higher H/C and O/C ratios, while bamboo bio-oil exhibited lower H/C and O/C ratios. These results imply that pine bio-oil is more efficient in reducing CO emissions during bio-oil stabilization and hydrotreatment. Pine biochar exhibited higher H/C and lower O/C ratios. Meanwhile, bamboo bio-oil exhibited higher O/C and lower H/C ratios. The decreased H/C ratios observed in the pine and bamboo bio-char samples suggest that higher levels of aromatic compounds were formed in the bio-char structures due to hydration, decarboxylation, and decarbonylation during processing at the operating temperature. Consequently, this process enriched the bio-char with carbon, resulting in a surface that is highly resistant to water (Rajapaksha et al., 2016, Liu et al., 2015, Qin et al., 2020, Kumar et al., 2022a).

5.4.10 SEM/EDX of Biochar

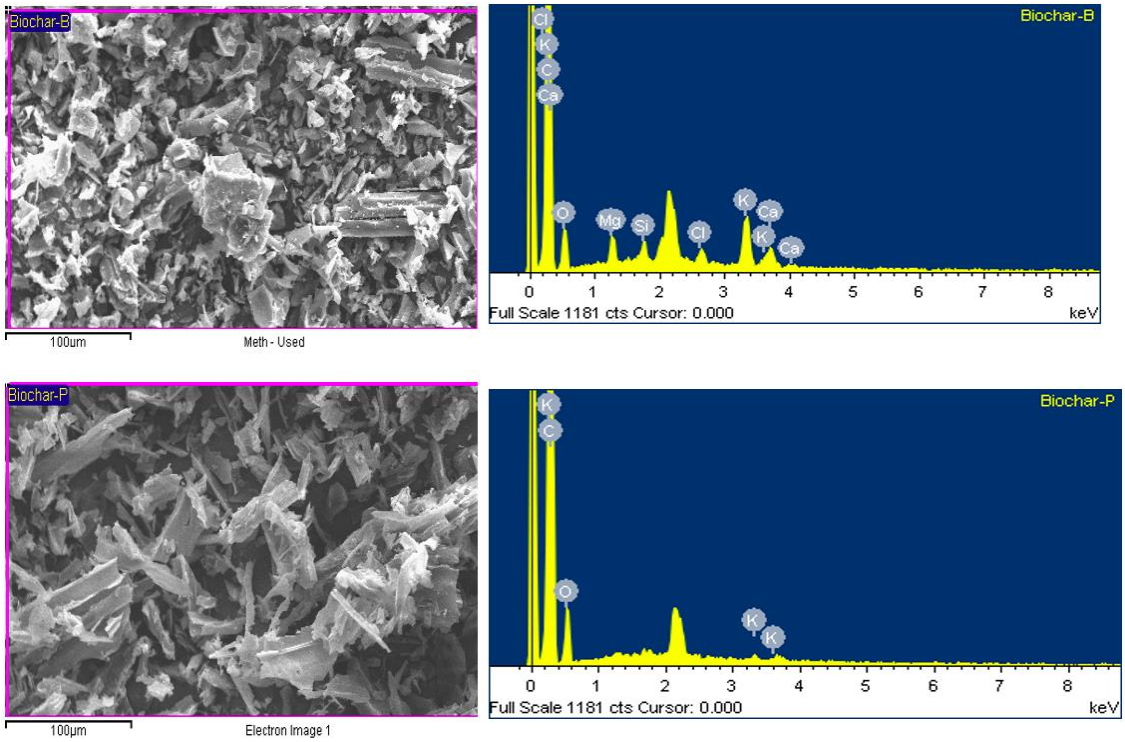

Figure 5. 9: SEM/EDX of bamboo biochar (Biochar-B) and pine biochar (Biochar-P).

The SEM/EDX analysis (Figure 5.9) of biochar derived from bamboo and pine biomass demonstrates distinct differences in their elemental compositions, which have significant implications for their respective applications. Bamboo biochar exhibits a diverse range of elements with the presence of carbon (C), oxygen (O), potassium (K), calcium (Ca),

magnesium (Mg), silicates (Si), and traces of chlorine (Cl). The substantial carbon content confirms effective carbonization during pyrolysis, while the diverse mineral content, including high levels of potassium, calcium, and magnesium, indicates a significant ash component (Correa et al., 2019). This composition suggests that bamboo biochar has enhanced capabilities for soil amendment, including improved pH buffering, nutrient supply, and potential soil fertility benefits due to calcium's liming effects and potassium and magnesium's fertilizing properties. Applying biochar to soil resulted in mineral phases adhering to its surface, which made the elemental composition more complex. This effect is likely due to the biochar's carboxylic and phenolic functional groups, which can bond with multi-valent cations such as Si^{2+}, Al^{3+}, and Fe^{3+}, creating organo-mineral complexes. These organo-minerals typically boost soil nutrient transformation and adsorption. Biochar with finer particles and high internal porosity are expected to improve soil quality significantly (Ma et al., 2016). The presence of silicates may further enhance the biochar's mechanical strength and stability. In contrast, pine biochar contains primarily carbon, oxygen, potassium, and hydrogen, with fewer mineral elements. The carbon content indicates successful pyrolysis, but the reduced presence of calcium, magnesium, and silicate limits its potential as a multifunctional soil conditioner. SEM/EDX analysis revealed that the surface of biochar is rich in various nutrients. It can serve as an adsorbent in water purification processes and enhance soil fertility. Additionally, because of its high pH, biochar is effective for soil amendment, helping to neutralize soil acidity and raise the soil pH. Pine biochar's more straightforward mineral composition may be preferable in applications requiring minimal alteration of soil mineral content, while bamboo biochar's broader mineral profile positions it as a more versatile option for comprehensive soil and environmental management strategies.

5.4.11 Energy Yield and Gas Analysis

The gas compositions, including hydrogen (H_2), methane (CH_4), carbon monoxide (CO), carbon dioxide (CO_2), and others (C_XH_Y), along with the energy yields resulting from thermal degradation experiments on pine and bamboo biomass, are depicted in figure 5.10. Methane production is attributed to lignin deformation occurring at the operating pyrolysis temperature. The methane yield is 10.5% for bamboo and 11% for pine. Moreover, cellulose composition features a significant presence of the –HCOH segment, the decomposition of which could yield -H and -CO or -CH and -OH (Glasser et al., 2012). Combining -CH with numerous -H atoms produce CH_4, while CO_2 forms by combining -CO with -OH or an oxygen radical. Studies indicate that lignin deformation and cracking release more hydrogen and methane compared to

cellulose and hemicellulose (Moon et al., 2015, Capunitan and Capareda, 2012, González et al., 2003, Santos et al., 2020, Janković et al., 2019, Tan et al., 2017). Furthermore, water gas shift reaction is also an attribute to the formation of hydrogen and carbon dioxide. This is because cellulose contains more OH and C–O compounds, hemicellulose comprises higher levels of C=O organic compounds, whereas lignin is rich in aromatic rings and O–CH_3 functional groups. Gas analysis reveals that carbon monoxide is the primary compound in bamboo and pine pyrolysis gases at 550°C (32.5% and 33.1%, respectively). The reverse water gas reaction ($H_2 + CO_2 = CO + H_2O$) may occur, resulting in a more significant generation of CO while reducing the quantities of H_2 and CO_2 (Wang and Nakamura, 2010). Carbon dioxide, regarded as an inert gas (excluded in the biogas energy content), is the second highest component at 27.8% for bamboo and 28.3% for pine, likely due to decarbonylation and decarboxylation reactions increasing CO levels. Cracking the bond between the C1 carbon atom and two oxygen atoms in the gluconic unit of cellulose may produce CO_2 (Mettler et al., 2012). The substantial presence of hydrogen (19.3% for bamboo and 18.75% for pine) in the pyrolysis gas indicates its potential as a hydrogen source for downstream bio-oil hydrotreating to meet fuel standards. The dehydrogenation reactions result in the formation of H_2. Furthermore, the breakdown of lignin, release hydrogen gas as some of its structures decompose (Azadi et al., 2013).

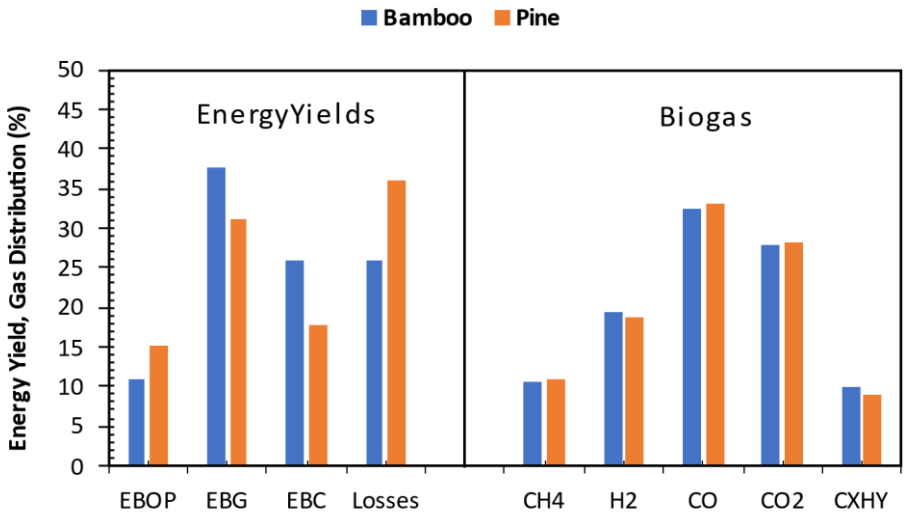

Figure 5. 10: Pyrolysis gas analysis and energy yields for bio-oil organic phase (EBOP), pyrolysis gas (EBG), biochar (EBC), and losses.

It is observed that the pine energy yield for the bio-oil organic phase (EBOP) is higher than that of bamboo, at 15% and 11%, respectively. This can be explained by the better energy value

and higher oil production for pine biomass (Figure 5.10). Biogas had the highest energy fraction among the product energy yields, with bamboo and pine biogas at 38% and 31%, respectively. The second highest energy yield was observed for biochar, with bamboo at 26% and pine at 18%. The yields of the pyrolysis products correlated with the observed energy yields despite biogas having the lowest heating values and higher yields. The determined heating values for biogas were 16.76 and 16.35 MJ/kg for bamboo and pine, respectively. It is worth noting that bio-oil organic phase energy yield did not incorporate the aqueous phase, which is usually quantified as bio-oil yield. During the continuous pyrolysis process, some organic bio-oil ends up in the aqueous phase. For this work, only the pure organic phase was considered, i.e,. ESP oil. The trade-off to the aforementioned procedure is the addition of losses. The observed energy losses were from 26% to 36% for bamboo and pine, respectively. Bamboo most efficiently converted 74% of the feedstock energy into pyrolysis products. The observed losses were primarily due to the consideration of organic bio-oil only. Additionally, some organic bio-oil couldn't be retrieved from the condensing unit due to the complexities involved in collecting all the resulting liquid yield. Consequently, a portion of bio-oil energy was lost, impacting the process's efficiency in terms of energy yields.

5.5 Conclusions

A comparative study employing isothermal fast pyrolysis in a sand-fluidized bed reactor investigated bamboo and pine biomass for the production and characterization of bio-oil and associated by-products. Pine bio-oil exhibited superior energy density compared to bamboo bio-oil, indicating variations in their energy content. Consequently, pine bio-oil emerges as more favourable for commercialization, considering bamboo's higher flow resistance during fluidized bed reactor pyrolysis and the higher heating value (HHV) of pine bio-oil. Bio-oils are viable for fuel applications and chemical production following refining and enhancement processes. Bamboo bio-oil displayed lower acidity, attributed to differing biomass structural compositions. Pine bio-oil demonstrated higher H/C and O/C ratios, whereas bamboo bio-oil exhibited lower ratios, suggesting pine bio-oil's potential efficacy in reducing CO emissions during stabilization and hydrotreatment. Spectroscopic and chromatographic analyses revealed numerous oxygenated compounds in the bio-oils. With its elevated carbon content and HHV of 24.24 MJ/kg, pine biochar holds promise for energy applications and as a precursor in activated carbon production. Gaseous products included carbon monoxide and hydrogen, which are suitable for fuel applications or conversion into liquid fuels, with hydrogen particularly valuable for bio-oil upgrading. Pine biomass yielded a higher energy yield for the

bio-oil organic phase (EBOP) than bamboo, at 15% and 11%, respectively, attributable to superior energy content and enhanced oil yield from pine biomass. The study concludes that pine and bamboo biomass are viable renewable energy sources, contingent upon efficiently utilizing all pyrolysis products.

CHAPTER 6

6. Stabilization of Bio-Oil Organic Phase via Solvent-Assisted Hydrotreating: Investigating the Influence of Various Solvents

6.1 Abstract

Conventional mild hydrotreatment processes of bio-oil present significant challenges of high degree of polymerization, low oil yield, high coke formation, and poor catalyst recovery. To address these challenges, the study looked into investigating and enhancing the properties of raw bio-oil organic phase samples via a solvent-assisted stabilization approach using methanol (METH), ethanol (ETHA), isopropyl alcohol (IPA), and ethyl ether (ETH). Solvents like methanol (METH) and ethanol (ETH), which are highly polar, yielded higher oil fractions (64% and 62% respectively) compared to less polar solvents like ethyl ether (DME) at 59%. Isopropyl alcohol (IPA), with intermediate polarity, achieved a balanced oil yield of 63%, indicating its ability to dissolve both polar and non-polar components. The moisture reduction in stabilized bio-oils followed the order: IPA > ETH > METH > DME, with IPA showing the highest reduction due to its structural characteristics facilitating dehydration. Viscosity reduction varied with IPA > ETH > DME > METH. Carbon recovery in stabilized bio-oils ranged from 65% to 75% for DME, ETH, and METH and was 71% for IPA. The heating values of stabilized bio-oils ranged from 28 to 29 MJ/kg, with IPA-stabilized bio-oil showing the highest value (29.05 ± 0.06 MJ/kg). METH demonstrated high efficiency (74.8%) in stabilizing bio-oil, attributed to its strong hydrogen-donating capability. ETH followed closely at 69.5%, indicating its comparable performance in bio-oil stabilization. With moderate efficiency (69.3%), IPA presents a balanced alternative considering its molecular structure and hydrogen solubility. In contrast, DME exhibited lower efficiency (63.6%) due to its weaker hydrogenation capability and propensity for undesired side reactions. The study suggests that subcritical conditions up to 200°C are adequate for METH, ETH, and IPA in bio-oil stabilization, comparable to results obtained under supercritical conditions.

Keywords: Biomass, Bio-oil stabilization, Solvents, Mild hydrodeoxygenation, Dehydration.

6.2 Introduction

Alternative energy sources like biomass have gained considerable attention due to global concerns such as dwindling fossil fuel reserves, rapid population growth, rising energy needs, and fluctuations in crude oil prices. Biomass can be a renewable resource to produce gaseous, liquid, and solid biofuels (Sánchez et al., 2019). Second-generation feedstocks, predominantly composed of lignin and cellulose from sources like forest product residues, represent a sustainable substitute for first-generation feedstocks that do not raise issues related to food security. Nowadays, it is considered feasible and promising to convert biomass via thermochemical processes into petrochemicals and biofuels (Çağlar and Demirbaş, 2002). These processes use various biomasses that can be processed into a wide range of products, offering great productivity. In thermochemical conversion, the primary techniques include pyrolysis, liquefaction, gasification, and combustion (Awasthi et al., 2023). Among the aforementioned thermochemical techniques, pyrolysis is the most preferred approach that is cost-effective and easy to use for the production of biofuels and petrochemicals from biomass. This technique is categorized into slow, fast, and flash pyrolysis (Pawar et al., 2020). The choice of pyrolysis type to employ depends on the desired product distribution. Fast pyrolysis is a good choice when high bio-oil yields are desired, while slow and flash are selective to higher yields of biochar and biogas, respectively. The bio-oil from fast pyrolysis is a potential source of various valuable petrochemicals. However, due to undesired properties, it is incompatible with direct application as an engine fuel (Lohitharn and Shanks, 2009). Low heating value and high water content, acidity, and corrosiveness are well-known limitations of raw bio-oil. The aforementioned drawbacks of raw bio-oil are attributed to the presence of oxygenated compounds such as phenols, alcohols, furans, water, acids, ketones, and aldehydes (Auersvald et al., 2019, Oasmaa et al., 2012). Consequently, eliminating oxygenates is adopted to improve the quality of raw bio-oil (Garba et al., 2018). Conventional upgrading technologies include hydrotreatment, catalytic cracking, and steam reforming, with the former being the most efficient due to high yields of fuel-range hydrocarbons (Gollakota et al., 2016, Auersvald et al., 2019). Furthermore, the hydrotreating process has already been commercialized in crude oil refineries to upgrade the distillates. Thus, bio-oil upgrading via hydrotreating is economically and commercially viable. Researchers have explored numerous hydrotreating catalysts globally. These catalysts include sulfided metals (NiMo, CoMo, and NiW), reduced noble (Pg, Pt, and Ru), and transition (Co, Fe, Mo, Ni, and Cu) metals with selected support carriers. The well-known supports are alumina-based (Al_2O_3), silica-based (SiO_2), titanium-

based (SiO_2), and carbon-based (C) (Shumeiko et al., 2020, Mortensen et al., 2011, Elkasabi et al., 2014, Gholizadeh et al., 2016). Alumina-based support is considered unsuitable for application during the hydrotreatment of raw bio-oil due to the formation of boehmite (AlO(OH)), which is yielded due to high water content in raw bio-oil (Capunitan and Capareda, 2014). Hence, neutral support such as carbon is a convenient option during the hydrotreatment of raw bio-oil (Mortensen et al., 2011). Noble metal-based catalysts have higher catalytic activity than transition metal catalysts for hydrotreating, thus providing simplified operating conditions (Cordero-Lanzac et al., 2021, Ardiyanti et al., 2011). Metal sulphide catalysts have also proven their robust industrial application for upgrading heavy petroleum fractions, with bimetallic phases such as sulphidde NiMo, being more effective when compared to monometallic due to the synergy effect (Shumeiko et al., 2020). Nonetheless, sulphided metal catalysts (NiMo and CoMo) have a significant potential drawback of deactivation due to low sulphur content in raw bio-oil (Capunitan and Capareda, 2014). The hydrotreatment process for upgrading bio-oil has been extensively studied and shown to reduce the effectively oxygenates, thereby enhancing the quality and stability of bio-oil (Han et al., 2019). Conventionally, hydrotreatment of bio-oil is carried out in two stages, with the first stage (mild conditions) serving to stabilize the bio-oil and the second stage (severe conditions) to upgrade the bio-oil by increasing the energy density via the elimination of oxygenates and reduction in moisture content. However, during the first stage, there are still drawbacks, such as polymerization, low oil yield, and poor catalyst recovery. Hence, during the second stage (350–450°C, 5–15 MPa), significant gas and char formation as by-products are observed due to the aforementioned drawbacks of the conventional mild hydrotreatment process. This has spurred research efforts toward developing hydrotreatment processes that eliminate polymerization and poor catalyst recovery while enhancing bio-oil properties. Hence, in this work, a solvent-assisted bio-oil stabilization technique has been carried out to address the aforementioned drawbacks of the conventional first-stage hydrotreatment process.

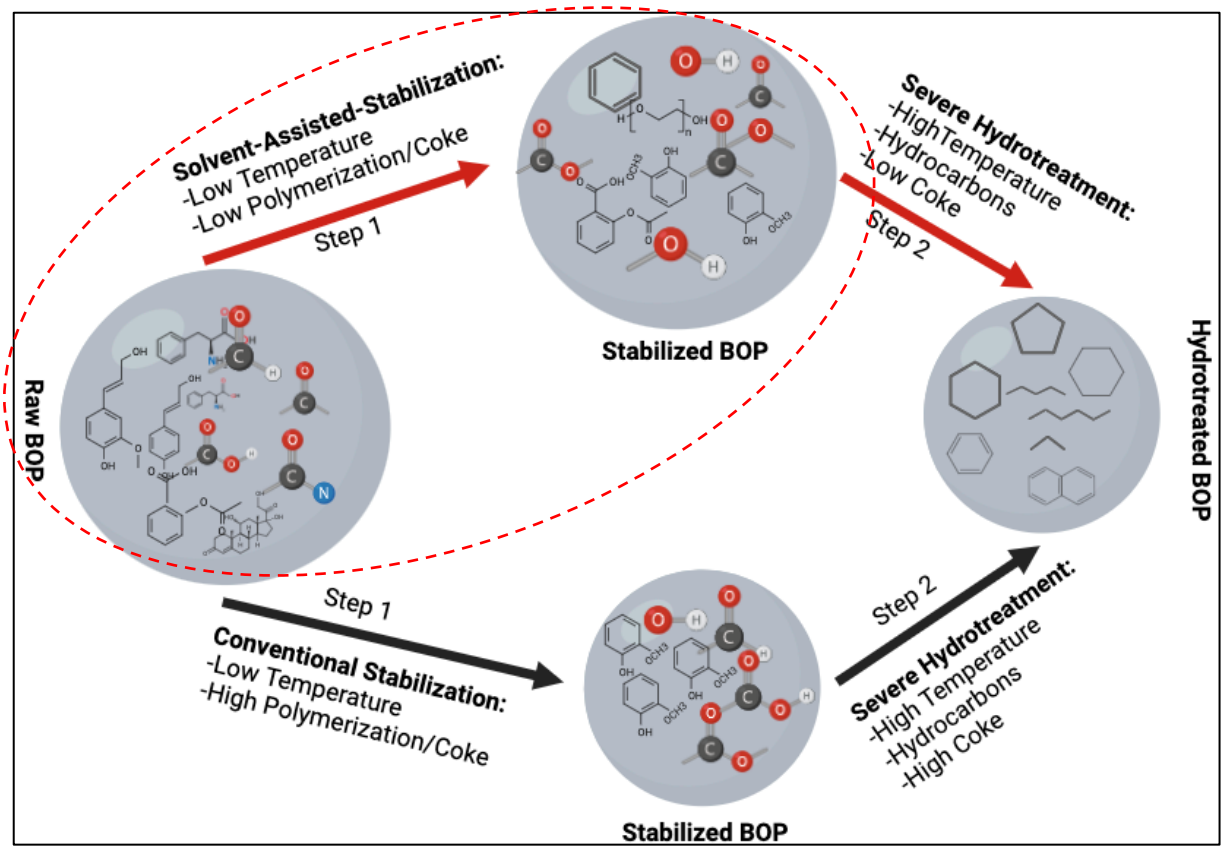

Figure 6. 1: Typical rationale of the proposed solvent-assisted bio-oil organic phase stabilization.

The main goal of adopting the solvent-assisted stabilizing technique of bio-oil is to eliminate compounds responsible for coking (aldehydes and furans) and reduce the degree of polymerization. Typical rationale of the proposed process is shown in Figure 6.1. Although oxygen is undesired in the treated product, completely removing oxygen from bio-oil is very complex, especially under mild conditions. Hence, this study focused more on the properties of the stabilized bio-oil, namely density, viscosity, total acid number (TAN), elemental analysis, degree of deoxygenation, degree of dehydration, moisture content reduction, and energy efficiency.

6.3 Materials and Methods

6.3.1 Materials

A commercially available catalyst, Ru/C, procured from Sigma/Aldrich, was employed in this study. The catalyst contained 5 wt% metal loading, a BET surface area of 686.55 m2/g, and a pore diameter of 3.3 nm, and it was utilized without any prior treatment. i.e., used as received. Methanol (METH), ethanol (ETH), ethyl ether (DME), and isopropyl alcohol (IPA) were used

as solvents in the current work. The bio-oil organic phase was produced from the thermal degradation of pinewood biomass in a fluidized reactor.

6.3.2 Fast Pyrolysis Procedure

The fast pyrolysis runs were conducted using a fluidized gas-solid reactor developed by the Bioenergy Laboratory of Auburn University (Auburn, AL, USA). Pinewood (7.75 ± 0,19 kg) biomass was loaded into the hopper. White fine silica sand (1235 ± 0.5 g) was used to fluidize the bed and enhance the heat transfer within the reactor. The sand was sieved to a desired particle size of 0.3–0.22 mm and then was loaded into the reactor. Once the desired temperatures were reached, the system was purged with nitrogen gas for 13 ± 2 min to ensure an inert atmosphere. Two nitrogen lines with flowrates 34 SLPM and 6 ± 1 SLPM for reactor and backflow prevention were used, respectively. The reactor temperature was allowed to reach 595 ± 18 ^{0}C before feeding the biomass. Then biomass was conveyed into the reactor at a rate of 27 g/min by a screw auger that is mechanically controlled by Weigh Feeder Controller (C-702, ACRISON). Pyrolysis runs were allowed to run for 2 hrs at a temperature of 544 ± 33 ^{0}C. The reactor, pipelines, and cyclone were adequately insulated to minimize any heat loss to the surroundings that can result in undesired condensation taking place before reaching the cooling system. The cooling medium was ethylene glycol at 2 ± 0.5 ^{0}C and 1.2 bar with a PCF rate of 40 L/min from a recirculating chiller (Julabo, FL2503, USA). The vapors from the reactor passed through the cyclone, where biochar was collected. Thereafter, the liquid product (aqueous phase) was condensed by two condensers in series. The organic phase bio-oil was precipitated from the non-condensable gases (NCGs) using one electrostatic precipitator (ESP). Bio-oil was continuously obtained and weighed for the duration of the reaction using Nalgene bottles style 2104 (B9157 and B9407, Sigma-Aldrich) for sample collection. The bio-oil collected from the ESP was classified as the bio-oil organic phase (BOP) and was used for hydrotreating experiments.

6.3.3 BOP Stabilization Procedure

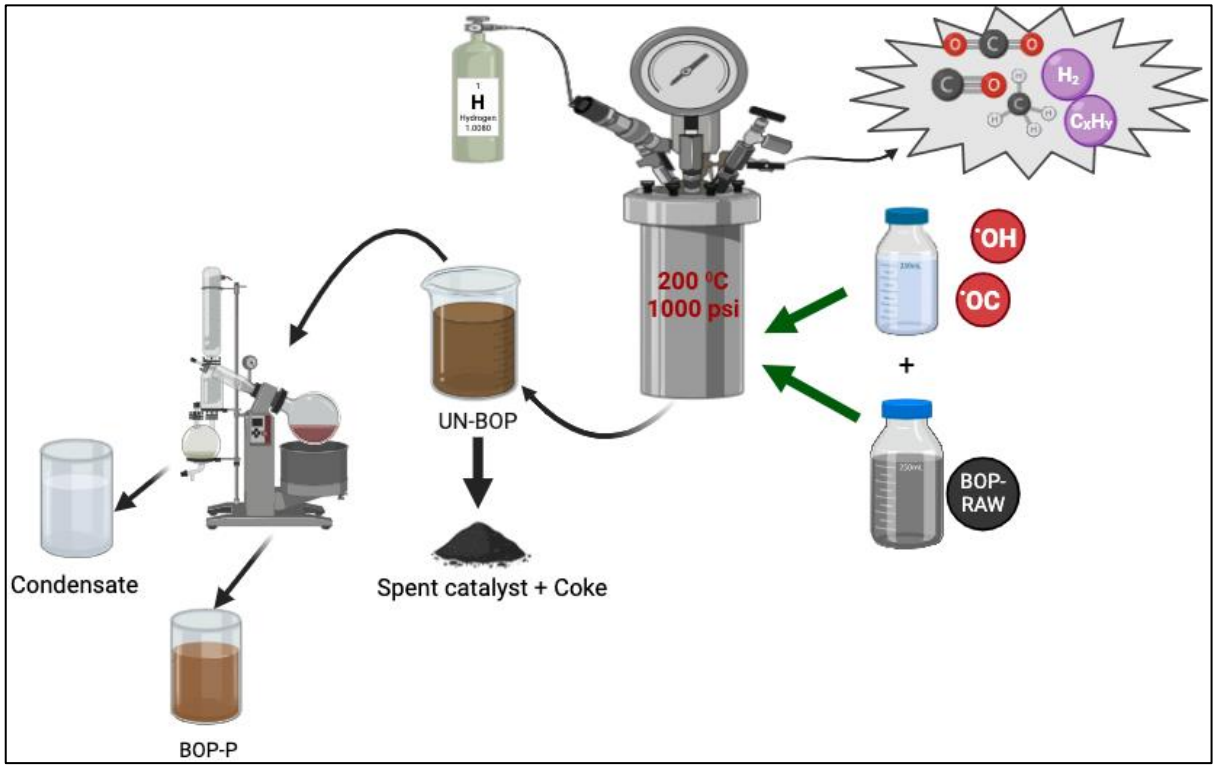

Figure 6. 2: Schematic flow of solvent-assisted bio-oil organic phase stabilization.

This investigation explored the stabilization (mild hydrodeoxygenation) of bio-oil using various solvents. The schematic flow of the solvent-assisted approach is shown in Figure 6.2. The first step was blending bio-oil with each solvent to obtain a feed to the stabilization system. The bio-oil-alcohol feed blends were prepared by taking a 80% by weight sample of bio-oil and mixing it with 20% by weight of solvent in a glass container. To achieve homogeneity, the mixture was placed onto the vortex mixer for 3 ± 1 min. The feed blends and the desired amount of catalyst were transferred into the 450 ml stirred Parr reactor. The feed-to-catalyst ratio was 70:1. The reactor was sealed cautiously to avoid damaging the nuts. Following reactor sealing, a leak test was conducted under 1500 psi of hydrogen with a holding time of 4 minutes. The leak test was performed three times to incorporate sufficient purging of the system. Upon confirming no leaks, hydrogen was released to displace residual air, and the reactor was vacuumed. The reactor was pressurized to 1000 psi for the stabilization experiments, and the temperature was ramped up to the set point with stirring at 500 rpm. The set point temperature was 200 0C, with a retention time of 4 hours, exclusive of heating. After each experimental run, the reactor was allowed to cool down to room temperature. The final pressure was recorded, and the gas sample was collected using a 1 L Tedlar bag (RESTEK). The final mass

of the reactor with stabilized oil was weighed. Liquid products were then collected, and catalyst particles were separated via centrifugation. Coke products and used catalysts were recovered via vacuum filtration and rinsed with feed solvent. The solid-free liquid product was separated using a rotary evaporator to obtain the stabilized bio-oil. The percentage yields after bio-oil stabilization were calculated by the following equations:

$$\text{Liquid Yield} = \frac{\text{Liquid product(g)}}{\text{Bio} - \text{oil(g)} + \text{Solvent(g)}} \times 100 \qquad (6.1)$$

$$\text{Solids Yield} = \frac{\text{Solids product(g)}}{\text{Bio} - \text{oil(g)} + \text{Solvent(g)}} \times 100 \qquad (6.2)$$

$$\text{Gas Yield} = 100 - \text{liquid yield} - \text{solids yield} \qquad (6.3)$$

The degree of deoxygenation (DOD) and degree of dehydration (DOD^h) were determined by the following equations:

$$\text{DOD} = \left(1 - \frac{\text{Oxygen in product}}{\text{Oxygen in feed}}\right) \times 100 \qquad (6.4)$$

$$\text{DOD}^{\text{h}} = \left(1 - \frac{\text{MC}_\text{P}}{\text{MC}_\text{F}}\right) \times 100 \qquad (6.5)$$

$$\frac{\text{H}}{\text{C}_{\text{eff}}} = \frac{\text{H}}{\text{C}} - 2\left(\frac{\text{O}}{\text{C}}\right) \qquad (6.6)$$

Where MC_P and MC_F are moisture contents for stabilized bio-oil (BOP-P) and feed bio-oil (BOP-Raw), respectively. The ratio of H/C_{eff} is the effective carbon ratio that incorporates the removal of oxygen in the form of water.

6.3.4 Product characterization

Elemental analysis (CHNS) was performed using an Elementar Vario Micro Select, according to ASTM D5373 and ASTM D5291. The oxygen content was determined by difference, and the results were reported on a dry basis. The moisture content of bio-oil was measured by Karl Fischer Titration by using Aquastar (combititrant 5 keto, volumetric KFT for aldehydes and ketones) as a titrator/reagent and Apura (combi-solvent keto, volumetric KFT, ca.5mg H_2O) as a solvent. Total Acid Number (TAN) was measured by a Mettler T50 autotitrator using a Total

Acid Number Titration Solvent Mixture and 0.1M KOH 2-propanol as the titrating reagent (titrant), according to ASTM D664-07. Bomb calorimeter (IKA C200 calorimeter, IKA Works, Wilmington, N.C.) was used to determine the higher heating values of biomass and bio-oil organic phase. The viscosity (kinetic and dynamic) and density were measured using the Anton Paar Instrument (SVM Standard method) at 40 ^{0}C. The chemical composition of organic phase bio-oil was analyzed by gas chromatography coupled with a mass spectrometric detector (GCMS). The experiments were carried out on an Agilent 5977C GC/MSD with helium gas as a carrier gas. National Institute of Standards and Technology (NIST) spectral library was used to identify the chemical compounds. Briefly, the samples were weighed, diluted with 2 ml of methanol and the filtered through a JT baker Nylon syringe filter with a pore size of 0.2 μm. The filtered sample was injected, and the inlet temperature was set to 280 ^{0}C at a split ratio of 10:1. The column temperature was held at 50 ^{0}C for 5 min, then heated to 280 ^{0}C at a ramping rate of 10 ^{0}C/min with a 5 min holding time. Thermal behavior of the spent catalyst was used to examine carbon deposition on the catalyst. TG-50H detector with an alumina cell was used for examination at a heating rate of 10 ^{0}C/min and a holding temperature of 800 ^{0}C (2min) under the air atmosphere (20 ml/min).

6.4 Results and Discussion

6.4.1 Product Yields

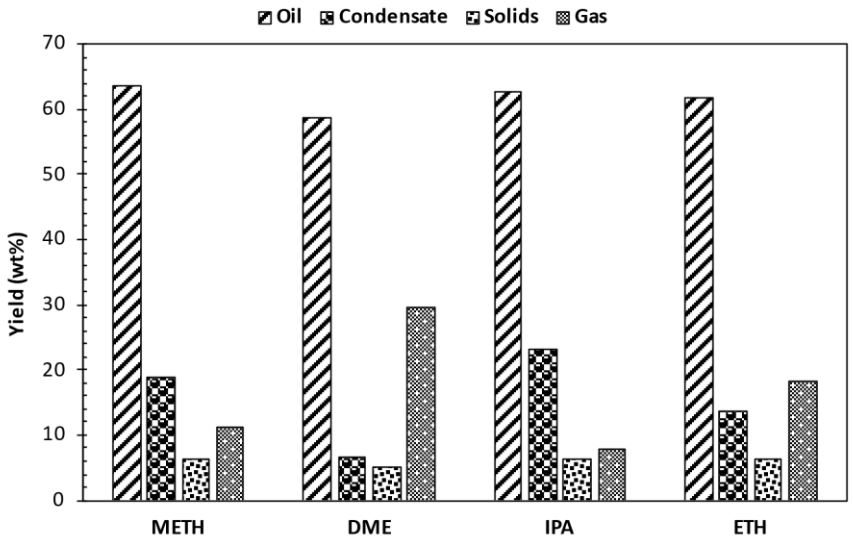

Figure 6. 3: Product distribution of solvent-assisted bio-oil organic phase stabilization.

The overall mass balance closure for liquid and solid components reached 80.90%, 90.75%, and 91.37% following the reactions with methanol, ethanol, and isopropanol, respectively (as shown in Figure 6.3). The solids incorporated tar; thus, crystallization was necessary. Filtration,

solvent washing and drying were adopted for crystallization to quantify solid yields. The tar loss was negligible as it represented less than 1% of the total stabilized bio-oil yield. The results of the bio-oil stabilization process with different solvents reveal distinct trends in product yields. Solvents with higher polarity, such as methanol (METH) and ethanol (ETH), demonstrate enhanced oil yields of 64% and 62%, respectively, compared to less polar solvents like ethyl ether (DME) with a yield of 59%. Hence, DME, possessing lower polarity, yielded a marginally lower oil fraction suggesting reduced affinity for polar compounds. This disparity reflects the ability of polar solvents to effectively solubilize polar compounds present in the bio-oil during solvent-assisted mild hydrotreatment. Isopropyl alcohol (IPA), with intermediate polarity, yields an oil fraction of 63%, suggesting a balanced ability to dissolve both polar and non-polar components. Conversely, DME yields the highest gas percentage at 30%, indicative of its propensity for vigorous hydrogenation reactions, followed by ethanol at 18%. The observed gas yield trend was DME>ETH>METH>IPA. Various reactions occur during the bio-oil upgrading process, including cracking, decarboxylation, decarbonylation, methanation, and hydrodenitrogenation, which can produce gaseous products (Ahamed et al., 2021). The observed increase in gas yield suggested that more of the DME-bio-oil underwent decomposition into gas products compared to METH, IPA, and ETH bio-oils. Furthermore, this was indicative that DME had a greater tendency than METH and IPA to promote cracking of the heavier molecular fractions of bio-oil and gas formation during the stabilization process. The increased DME activity may have caused higher mass losses due to the greater volatility of the resulting products. Additionally, the self-decomposition of solvents in their supercritical state may also contribute to some fractions of the gas products (Omar et al., 2019). Isopropyl alcohol, with its intermediate polarity, stands out for its elevated condensate yield of 23%, compared to the other solvents the observed trend was IPA>METH>ETH>DME. This suggests its potential to promote the formation of water molecules during mild hydrotreatment. The observed high yield of condensate for IPA correlated with the highest moisture content reduction of 8%. Solids yield remains relatively consistent across solvents, ranging from 5% to 6%, indicative of the robustness of the solvent-assisted hydrotreating process. It is worth noting that the solids wt% is inclusive of tar, which was accounted as losses, as a result, the solids are much lesser.

6.4.2 Physicochemical Properties of Raw, Blend and Stabilized BOP

Properties of treated bio-oil such as thermal stability, acidity, and heating value were enhanced by demoisturization or dehydration, hydrocracking, hydrogenation, and mild deoxygenation during stabilization of bio-oil. The solvent can also act as a co-reactant as indicated by variations in proximate and ultimate analysis (Table 6.1). After blending with each solvent, the properties of the raw bio-oil vary. As a result, bio-oil stabilization is highly affected by the choice of solvent used. The current study explores how the solvent affects bio-oil stability and quality; this was done by investing the differences in properties arising from the inclusion of different solvents during the solvent-assisted mild hydrotreatment process. The investigated parameters were density, viscosity, total acid number (TAN), elemental analysis, degree of deoxygenation, moisture content reduction, and energy efficiency. Since solvent addition affects raw properties, blending variations were also incorporated.

Table 6. 1: Physicochemical properties of raw, blend and stabilized bio-oil organic phase.

Parameters	BOP Blends				BOP-MILD-HDO				BOP
	METH	DME	IPA	ETH	METH	DME	IPA	ETH	
Ultimate Analysis (wt%)[db]									
Carbon	59.41 ± 0.69	64.83 ± 0.26	64.07 ± 0.74	59.83 ± 2.61	65.78 ± 0.01	67.12 ± 0.02	66.57 ± 0.15	67.44 ± 0.04	64.54 ± 0.45
Hydrogen	8.50 ± 0.12	8.50 ± 0.02	8.91 ± 0.19	8.30 ± 0.40	8.10 ± 0.01	7.77 ± 0.01	7.99 ± 0.00	8.30 ± 0.02	7.820 ± 0.02
Nitrogen	0.18 ± 0.03	0.09 ± 0.01	0.16 ± 0.02	0.16 ± 0.01	0.08 ± 0.00	0.07 ± 0.01	0.08 ± 0.01	0.06 ± 0.01	0.180 ± 0.07
Sulphur	0	0	0	0	0	0	0.04 ± 0.03	0.05 ± 0.07	0.040 ± 0.02
Oxygen[a]	31.9 ± 0.84	26.58 ± 0.24	26.85 ± 0.95	31.71 ± 3.00	26.04 ± 0.01	25.04 ± 0.02	25.32 ± 0.11	24.16 ± 0.14	27.42 ± 0.55
C/H ratio	6.99 ± 0.02	7.63 ± 0.01	7.19 ± 0.07	7.21 ± 0.03	8.12 ± 0.01	8.64 ± 0.01	8.33 ± 0.02	8.13 ± 0.02	8.252 ± 0.82
H/C ratio	0.143 ± 0.00	0.131 ± 0.00	0.139 ± 0.00	0.139 ± 0.00	0.123 ± 0.00	0.116 ± 0.00	0.120 ± 0.00	0.123 ± 0.00	0.121 ± 0.01
O/C	0.54 ± 0.00	0.41 ± 0.00	0.42 ± 0.01	0.53 ± 0.03	0.40 ± 0.00	0.37 ± 0.00	0.38 ± 0.00	0.36 ± 0.00	0.425 ± 0.43
Properties									
Moisture Content[b]	9.08 ± 0.36	9.09 ± 0.00	9.96 ± 0.03	9.94 ± 0.02	3.91 ± 0.02	2.60 ± 0.01	2.15 ± 0.23	3.38 ± 0.04	9.79 ± 0.180
Density (g/cm^3, 40^{0}C)[ar]	1.09 ± 0.00	1.08 ± 0.00	1.09 ± 0.00	1.08 ± 0.00	1.13 ± 0.00	1.14 ± 0.00	1.13 ± 0.00	1.13 ± 0.00	1.18 ± 0.00
K.Viscosity (mm^2/s,40^{0}C)[ar]	13.0 ± 1.14	13.3 ± 1.25	29.8 ± 1.77	19.9 ± 1.55	4.82 ± 1.65	5.90 ± 1.70	15.18 ± 1.50	12.25 ± 1.25	67.85 ± 1.25
D. Viscosity (mPa.s)[ar]	14.15 ± 1.34	14.63 ± 1.50	32.32 ± 2.02	21.59 ± 1.75	5.45 ± 1.85	6.71 ± 1.95	17.16 ± 1.75	13.85 ± 1.45	80.20 ± 1.50
TAN (mgKOH/g)[ar]	62.55 ± 2.00	63.99 ±1.88	64.03 ± 1.55	62.56 ± 1.55	23.78 ± 2.88	36.98 ± 1.47	28.55 ± 2.44	19.56 ± 1.55	63.85 ± 2.45
DOD-raw (%)[b]	n.d	n.d	n.d	n.d	19.03 ± 0.05	24.47 ± 0.05	24.64 ± 0.05	23.66 ± 0.04	n.d
DOD-blend(%)[b]	9.39 ± 0.03[f]	4.49 ± 0.05	1.95 ± 0.01	1.97 ± 0.04[f]	24.06 ± 0.05	18.86 ± 0.05	21.14 ± 0.05	29.17 ± 0.03	n.d
DOD^h (%)[b]	7.25 ± 0.02	7.15 ± 0.03	1.74 ± 0.02[k]	1.53 ± 0.03[k]	56.99 ± 0.01	71.45 ± 0.06	78.46 ± 0.04	66.05 ± 0.01	n.d
HHV (MJ/kg)	24.02 ± 0.04	26.66 ± 0.05	26.26 ± 0.02	25.59 ± 0.06	28.23 ± 0.04	28.83 ± 0.08	29.05 ± 0.06	28.86 ± 0.06	21.56 ± 0.06

[b] wet basis, [db] dry basis, [f] degree of oxygenation (-), [k] hydrous effect, DOD^o degree of deoxygenation, DOD^h degree of dehydration (-), [ar] as received, n.d not determined.

Table 6.1 presents a summary of findings from analyses including water content, density, viscosity, heating value, TAN, and CHNS. The bio-oil feed blends of METH and DME resulted in a reduction in moisture content in contrast to IPA and ETH feed blends. This phenomenon agreed with the observation made by Yu et al. (2007) on the METH feed blend, however, it differed for IPA and ETH feed blends. Yu et al. (2007) noted that blending bio-oil with methanol, ethanol, and isopropanol led to a decrease in water content. Pidtasang et al. (2016) attributed the reduction in moisture content to the dilution effect of anhydrous alcohols. Hence, the observed increases in moisture were attributed to the possible hydrous effect of IPA and METH. Following solvent-assisted bio-oil stabilization reactions, METH and ETH bio-oils

showed the highest water content due to esterification reactions between the solvents and bio-oil acids, generating water as a by-product. These results were confirmed by the GCMS analysis for METH and ETH stabilized bio-oils (Figure 6.6). Similarly, the observed acid number for all stabilized bio-oils was subsequently lower when compared to the raw bio-oil. The primary mechanism behind this reduction in acidity and subsequent pH improvement was attributed to ester formation as well as oligomer repolymerization, solvent hydrodeoxygenation, and hydrocracking during the stabilization process. This resultant water was lowest for DME as supported by observed low condensate yield (Figure 6.3). The lower gas yield (Figure 6.3) in bio-oil-IPA indicated that IPA didn't decompose to gas, keeping water content relatively low. Reducing moisture in bio-oil is important as it can prolong ignition delay and lower combustion rates in engines (Broumand et al., 2020). However, water in bio-oil can be advantageous by reducing viscosity. The reduction in moisture content after bio-oil stabilization was IPA>ETH>METH>DME as seen in Figure 6.4. The stabilized oil fractions are relatively dry, containing 2 to 4 wt% moisture. The stabilized bio-oil products exhibited lower kinematic viscosity with relatively consistent densities compared to the raw bio-oil, with no noticeable alteration in colour. The viscosity range from 4.82 ± 1.65 to 15.18 ± 1.50 mm^2/s for METH and IPA bio-oils, respectively. The decrease in viscosity was IPA>ETH>DME>METH.

6.4.3Energy Density and Moisture Content Reduction

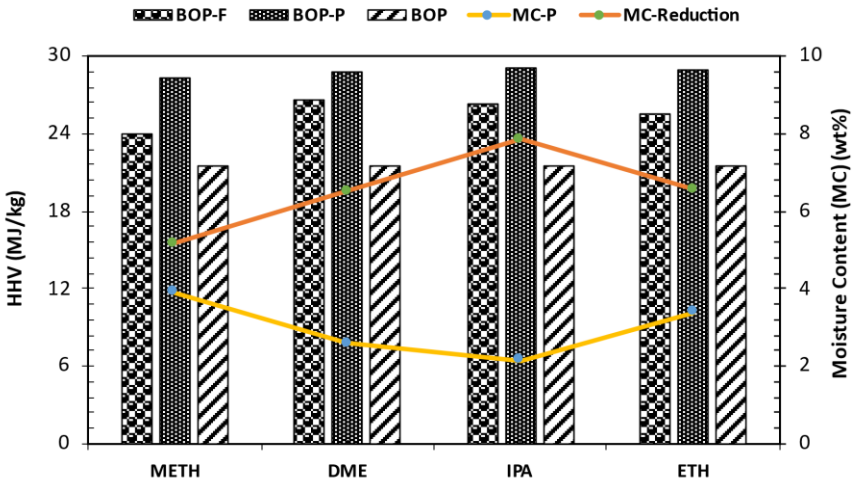

Figure 6. 4: Energy density and moisture content reduction of stabilized bio-oil organic phase.

The energy output of the raw bio-oil was 21.577 ± 0.06 MJ/kg. Improving this output is vital for better combustion efficiency in engines. Figure 6.4 illustrates minor changes in energy

output after stabilization of bio-oils compared to the respective blends as well as moisture content reduction. In the current study, the stabilization reactions don't significantly enhance the energy output compared to blending, although there is a significant drop in moisture content. The rise in energy output between the feed blends and the raw bio-oil correlated with the solvent:oil ratio of 1:6. The observed rises in energy outputs between blends and raw bio-oil was around 20% for all solvents. The results of energy outputs were indicative of highly oxygenated compounds in the stabilized bio-oil which was also evident on the GCMS and CHNS/O analyses. Increasing carbon (C) and hydrogen (H) levels while decreasing oxygen (O) results in higher energy density (Kumar et al., 2017). The DOD values were between 19 and 30% which correlated with the observed heating values. High oxygen content in the bio-oil decreases its energy output due to the reduction of available carbon which facilitates combustion. The stabilized bio-oils had heating values of 28-29 MJ/kg, with METH bio-oil having the lowest heating value at 28.23 ± 0.04 MJ/kg. The highest HHV was obtained for IPA-stabilized bio-oil with a 29.05 ± 0.06 MJ/kg value. The energy outputs of the blends and stabilized bio-oils increased corresponding to the energy content of the added solvents, with DME, IPA, and ETH showing the highest values due to superior properties over METH. Although there are increases in energy outputs for stabilized bio-oils, the values are relatively low compared to crude oil (45.54 MJ/kg) or conventional gasoline (46.54 MJ/kg). Nonetheless, the improvements in energy output compared to raw bio-oil suggest that solvent-assisted bio-oil stabilization is an effective method for enhancing bio-oil properties while eliminating the coking effect due to polymerization. Moreover, this study aimed to stabilize the bio-oil by improving its quality before severe treatment that potentially leads to the formation of fuel-rich hydrocarbons, thus the observed results of heating values align with the goals of the current study.

6.4.4 Degree of Deoxygenation and Carbon Recovery

The elemental analysis provided the weight percentages of carbon (C), hydrogen (H), nitrogen (N), and sulfur (S) in the sample, with the oxygen content (O) being derived by difference. The data presented in table 6.1 reveals a slight increase in C, H, and N contents for all stabilized bio-oils. The carbon retention/recovery for stabilized bio-oils ranged from 65 to 75% for DME and ETH&METH, respectively while it was 71% for IPA as seen in Figure 6.5. The oxygen content was moderately lower after stabilizing bio-oi, however, it was an anticipated outcome because mild hydrotreatment focuses more on stabilizing the bio-oil and converting compounds to corresponding alcohols, mainly xylenols. In addition to alcohol conversion,

solvent addition promotes the generation of ketones. Hence, the high oxygen content was attributed to the presence of oxygenated compounds such as ketones and phenol derivatives (such as xylenols) in the stabilized bio-oils.

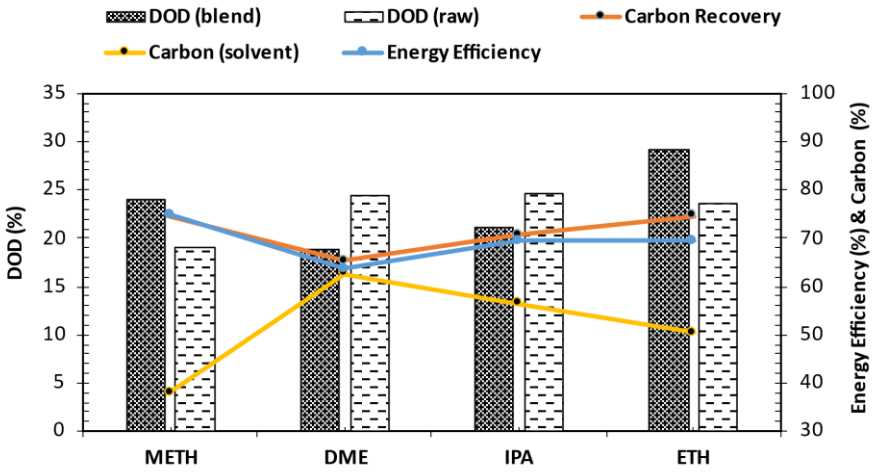

Figure 6. 5:Degree of deoxygenation, carbon recovery and energy efficiency of stabilized bio-oil organic phase [Carbon (solvent) is available carbon in the feed solvent].

The observed xylenol isomers in the stabilized bio-oil were attributed to applying the Ru/C catalyst which promotes isomerization (Liu et al., 2017). With all that being said, there was a reduction in oxygen after stabilizing the bio-oils regardless. The calculated results of DOD relative to feed blend (DOD blend) and raw bio-oil (DOD raw) are shown in Figure 6.5. Employing DME, IPA, and ETH as the solvents for stabilizing bio-oil resulted in DOD of 25%, while METH resulted in 19% relative to raw bio-oil. Conversely, relative to the feed blend, ETH and METH resulted in DOD of 29 and 24%, respectively. Meanwhile, for DME and IPA the DOD was 19 and 21%, respectively, relative to feed blend. Available carbon in the solvent is negatively correlated to the recovered carbon in the stabilized bio-oils as seen in figure 6.5. DME solvent has more available carbon, however, DME bio-oil carbon recovery is the lowest, which is indicative that most carbon is recovered in the gas phase due to the absence of hydroxyl groups that facilitate dehydration reactions and a high degree of volatility. The loss of carbon as solid and gas could be due to polymerization reactions and processes such as decarboxylation, decarbonylation, and methanation, respectively (Chia et al., 2020, Nolte and Shanks, 2017). Examining the energy efficiency results of treated bio-oils using various solvents during bio-oil stabilization reveals insights into the process dynamics. METH, with its high-efficiency rating of 74.8%, showcases its efficacy as a stabilizing solvent. Its strong hydrogen-donating capability likely facilitates effective hydrogenation reactions, leading to enhanced conversion rates and reduced energy consumption. ETH closely follows at 69.5%, owing to its comparable hydrogenation potential and conducive chemical interactions during

bio-oil stabilization. METH and ETH efficiency indicated their suitability for solvent assisted bio-oil stabilization processes. On the other hand, IPA, despite its moderate efficiency of 69.3%, presents a viable alternative, offering a balance between performance and cost considerations, potentially influenced by its molecular structure and hydrogen solubility. Conversely, DME's lower efficiency of 63.6% hints at limitations stemming from its weaker hydrogenation capability (due to the absence of the -OH group) and propensity for undesired side reactions. The results highlight the significance of solvent polarity and reactivity profiles in dictating energy efficiency of stabilized bio-oils.

6.4.5 GCMS Analysis of Stabilized BOP

GC-MS analysis was employed to identify and quantify the various molecular compounds found in both the raw bio-oil and the stabilized bio-oils. To assess the distribution of products across different samples, the compounds identified via GC-MS were categorized into six groups based on their functional groups: phenols, esters, ketones, aldehydes, sugar derivatives, and furans. Figure 6.6 presents a summary of the proportional amounts of compound classes in the raw bio-oil and the treated bio-oils. The total proportional area (%) of each group was determined by summing the proportional area (%) of each compound within that category. It's worth noting that the chromatographic peak area (%) of a compound is directly proportional to its concentration. Therefore, comparing the chromatographic peak area (%) of compounds allows for the examination of changes. For instance, the peak area (%) of phenol following each reaction can be compared to analyze the impacts of solvents during the stabilization of bio-oils. Moreover, the peak area (%) can be utilized to assess the variations in the relative content of the compound among the detected compounds.

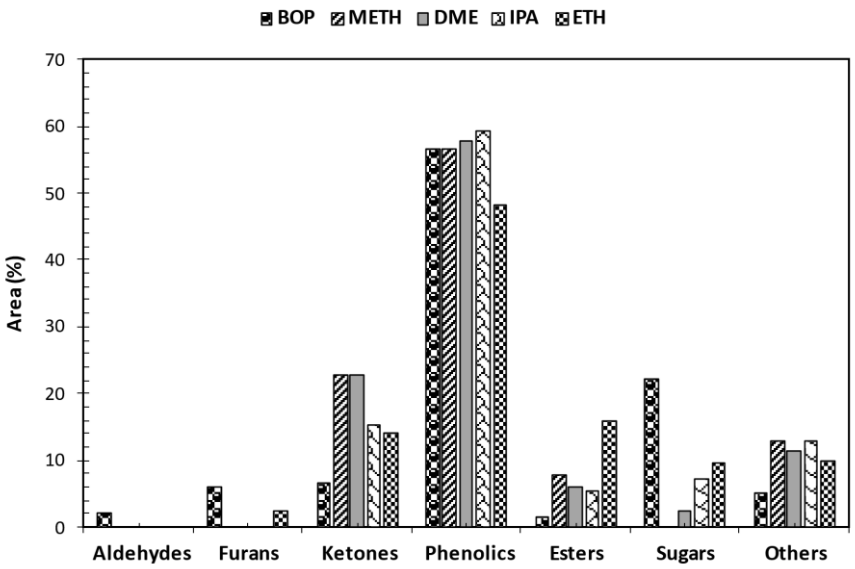

Figure 6. 6: GCMS analysis of raw and stabilized bio-oil organic phase using various solvents. [BOP-raw bio-oil organic phase].

Analyses of GC-MS for raw bio-oil (BOP) compared to stabilized bio-oils using various solvents, indicated distinct variations in compound composition expressed as area percentages. Notably, aldehydes are present in BOP (2%) but absent in all stabilized bio-oils, indicating efficient removal during solvent-assisted stabilization. Similarly, furans are notably reduced in stabilized bio-oils, with residual furans observed only in the ETH-treated bio-oil (3%). Ketones exhibit significant variation among the samples, with the highest concentration observed in the METH and DME-treated bio-oils (23%), followed by IPA (15%), and ETH (14%). This suggests solvent-dependent effects on ketone formation or preservation during bio-oil stabilization. Phenolics were significantly present in the stabilized bio-oils with concentrations ranging from 48 to 59%, however, the ETH stabilized bio-oil reduced phenolics and formed more esters. The abundance of phenolics after stabilizations was attributed to phenolics being converted to their corresponding derivatives. Hence, the presence of unsaturated double bonds within substituted groups of phenols, like 2-methoxy-4-(1-propenyl)-phenol, in the raw bio-oil was notably decreased, while phenols with saturated substituted groups, such as 2-methoxy-4-propyl-phenol, increased. This observation was attributed to the reduction of double bonds through bio-oil hydrotreating (Patel and Kumar, 2016). The rise in the proportion of 2-methoxy-4-propyl-phenol post-reactions was attributed to the conversion of 4-hydroxy-2-methoxycinnamaldehyde, which was undetectable post bio-oil stabilization. Furthermore, the rise in methoxy-phenolic compounds subsequent to the stabilization reactions, was attributed to depolymerization of the lignin fraction within the bio-oil (Remón et al., 2016). Removal or

conversion aldehydes in bio-oil is desirable due to their role in thermal instability and carbonaceous deposits formation. Aldehydes like 5-hydroxymethyl-2-furancarboxaldehyde (HMF), prevalent in raw bio-oil, were undetectable after bio-oil stabilization. The absence of sugars in METH-treated bio-oil and the varying concentrations in other stabilized bio-oils indicate selective removal or conversion of sugars during solvent-assisted bio-oil stabilization. These findings highlight the efficacy of solvent-assisted bio-oil stabilization in reducing oxygenates and also the effects on bio-oil composition. Such insights are crucial before severe hydrotreating of stabilized bio-oil to obtain hydrocarbon-rich products with diverse applications, ranging from biofuels to specialty chemicals. Compounds identified in the raw bio-oil comprise furfural, 2-methoxy-5-methyl-phenol, 1,2-Cyclopentanedione, D-Allose, 2-Furancarboxaldehyde, 5-methyl-, Benzenepropanol, 4-hydroxy-3-methoxy-, and Methacrylic acid, ethyl ester. Among these, phenolic derivatives, which originates from the lignin degradation, constituted the largest proportion (57 %) in the raw bio-oil, with components like 2-Methoxy-5-methylphenol, 1,2-Benzenediol, 4-methyl-, 2-Methoxy-4-vinylphenol, trans-Isoeugenol, and Phenol, 2-methyl-, being major contributors. Although the percentage of peak area isn't indicative of the actual compound content, it strongly suggests a significant presence of phenolic compounds in the crude bio-oil, consistent with findings from other studies (Lo et al., 2017, Kim and Choi, 2018, Bu et al., 2012, Pecha and Garcia-Perez, 2020).

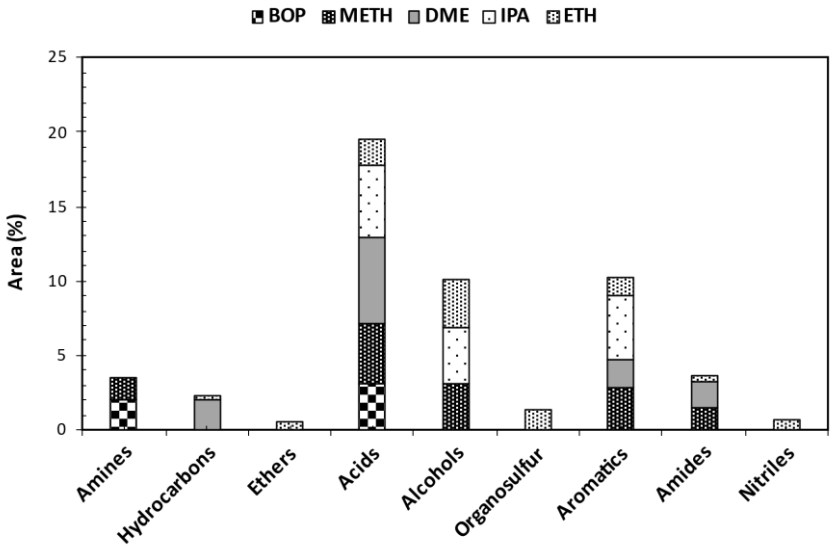

Figure 6. 7: " Others" GCMS analysis of raw and stabilized bio-oil organic phase using various solvents. [BOP-raw bio-oil organic phase].

Following the solvent-assisted bio-oil stabilization, the number of identified esters and their relative proportions notably increased compared to the raw bio-oil. Ester prevalence is preferable in fuel composition over acids due to their reduced corrosive impact on engine

surfaces. Esters can form via esterification reactions between bio-oil acids and corresponding alcohols (METH/ETH/IPA). Additionally, esters can arise from reactions between alcohol solvents and acids derived from intermediate products during the stabilization process. Solvents, like methanol and ethanol, have been shown to disrupt oligomer chains in crude bio-oil, leading to lower molecular weight compounds. The GCMS analysis in this study confirms this phenomenon. Ester product distribution altered after bio-oil reacted with each alcohol solvent. ETH stabilized bio-oil showed reduced acid compounds (Figure 6.7) which correlated with observed high ester presence in Figure 6.6. The METH, ETH and IPA stabilized bio-oils resulted in (Propanoic acid methyl ester, 9-Octadecenoic acid, methyl ester, Heptadecanoic acid, 16-methyl-, methyl ester, Butanoic acid, 3-methyl-2-oxo-, methyl ester, and Hexadecanoic acid, methyl ester), (Pentanoic acid, 4-oxo-, ethyl ester, Propanoic acid, 2-hydroxy-, ethyl ester, Butanoic acid, ethyl ester, Butanedioic acid, diethyl ester, Propanoic acid, 2-methyl-, 2-methylpropyl ester, Methacrylic acid, ethyl ester, Octadecanoic acid, ethyl ester, and Ethyl Oleate), and (Pentanoic acid, 4-oxo-, 1-methylethyl ester, and Propanoic acid, 2-methyl-, propyl ester), respectively. DME stabilized bio-oil resulted in nitrogen and sulphur containing compounds, these compounds are undesirable, and stabilizing the bio-oil also aims at removing these unwanted compounds. Aside from the undesired compounds, DME stabilized bio-oil also yielded esters (1,2-Ethanediol, monoacetate, Sulphurous acid, 2-pentyl pentyl ester, and 1,2-Propanediol, 1-acetate), however, esterification was not prominent when compared to METH,ETH, and IPA stabilization reactions. The observed ester detection in the stabilized bio-oils is ETH>METH>IPA>DME. The results are indicative that solvent-assisted bio-oil stabilization using methanol, ethanol, and isopropanol can facilitate ester formation.

6.4.6 Van Krevelen Plot of Raw, Blend and Stabilized BOP

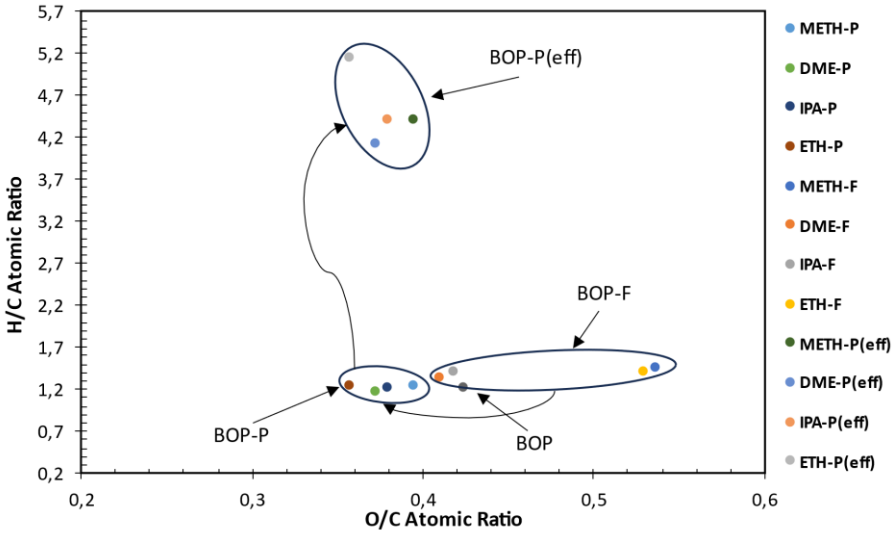

Figure 6. 8: Van Krevelen plot of raw, blend and stabilized bio-oil organic phase.[H/C_{eff} = H/C – 2(O/C), raw bio-oil (BOP), feed blends (-F), stabilized/effective bio-oils (-P/eff)]

Figure 6.8 depicts a Van Krevelen plot illustrating the raw bio-oil (BOP), feed blends (-F), stabilized/effective bio-oils (-P/eff). The graph reveals notable differences in elemental compositions and O/C ratios between the feed blends, with METH closely correlated to ETH. However, the O/C ratios in the stabilized bio-oils (BOP-P) from all experiments consistently fall within a narrow range of 0.36 to 0.40, significantly lower than those of the corresponding feed blends (BOP-F), while BOP was slightly above at 0.43. Solvent-assisted stabilization approach produced bio-oils with reduced O/C ratios and consistent H/C ratios relative to the raw bio-oil. Meanwhile, the METH and ETH feed blends resulted in higher O/C ratios and slight increases in H/C ratios. Conversely, DME and IPA feed blends had lower O/C ratios relative to the raw bio-oil. Higher H/C ratios are desirable for biofuel production, thus the lowered H/C ratios in the treated bio-oils do not indicate ineffective solvent-assisted stabilization. To assess the effectiveness of the solvent-assisted approach, the effective H/C ratio (H/Ceff) was adopted, which considers the removal of oxygen content in the form of water. This metric offers a superior evaluation of the chemical structure transformation, indicating that all experiments notably enhanced the H/Ceff value within a narrow range of 4.1 to 5.1, implying effective stabilization of raw bio-oil. The increase in H/Ceff ratio suggested dehydration reactions. These reactions are negatively correlated with the H/C ratio, hence the observed consistency in the H/C ratios. A decrease in O/C ratio was indicative of bio-oil deoxygenation (oxygen reduction). From these results it is evident that dehydration reactions

were highly favoured during the stabilization of bio-oil, with ETH solvent resulting in lower O/C and higher H/Ceff ratio when compared to other solvents.

6.4.7 Turnover Frequency Thermogravimetric Analysis of Catalyst

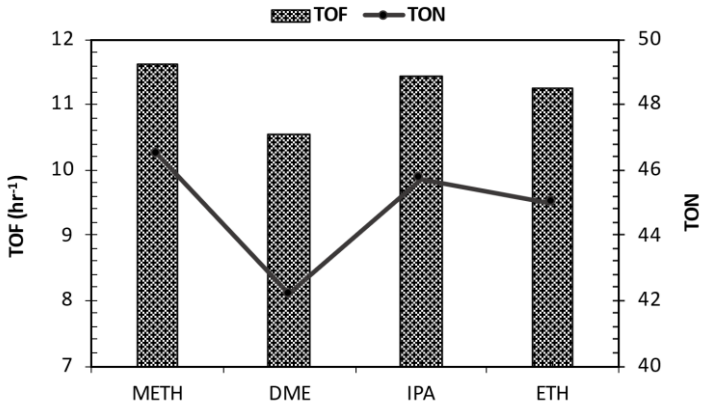

Figure 6. 9: Turnover frequency of catalyst during solvent-assisted bio-oil organic phase stabilization.

The analysis of turnover number (TON) and turnover frequency (TOF) data for Ru/C catalysts in the presence of different solvents during bio-oil stabilization reveals interesting insights into the catalytic performance (Figure 6.9). The TON values obtained for METH (46), DME (42), IPA (46), and ETH (45) indicate that these solvents contribute to almost comparable (with minimal variations) levels of catalytic efficiency in terms of product formation per gram of catalyst before deactivation. The lowest TON was observed after DME stabilization. The absence of hydroxyl groups on the DME solvent may have contributed to lower TON due to reduced solubility. This suggests that the choice of solvent may not significantly impact the overall catalytic activity of the Ru/C catalyst during bio-oil stabilization, however, DME was observed to be undesirable for bio-oil stabilization. Additionally, the calculated TOF values, which were derived from the TON values at a reaction time of 4 hrs, further support this observation, with METH exhibiting the highest TOF (11.6) and DME showing the lowest TOF (10.5). These findings suggest that while the solvents may have subtle effects on the kinetics of the stabilization reactions, they do not significantly alter the overall efficiency of the catalytic process as indicated by a 0 to 8.7% absolute error relative to the highest value.

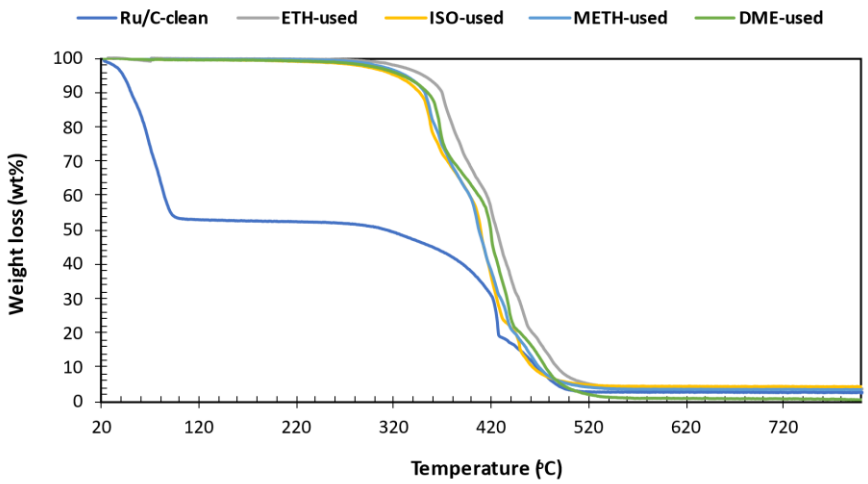

Figure 6. 10: Thermogravimetric analysis of clean and spent catalyst after solvent-assisted bio-oil organic phase stabilization.

Adopting solvent-assisted bio-oil stabilization provides several advantages for minimizing carbon deposition over conventional mild hydrotreatment processes (Figure 6.10). Coke, normally classified as an undesirable by-product in bio-oil's hydrocracking and hydrotreatment processes, typically results from the re-polymerization and excessive dehydration of oligomers (Omar et al., 2019, Zacher et al., 2014). In Figure 6.10 it is evident that the profiles were closely correlated, suggesting similar carbon deposits on spent catalysts. This was also supported by comparable solids yield post bio-oil stabilization reactions. Although the degradation profiles are almost equivalent, DME-used showed a high degree of coking as indicated by the highest mass degradation of 98%. The significant increase in weight loss for DME-used is attributed to the combustion of the extra carbon deposited on the catalyst surface. The high degree of coking for DME-used is attributed to the absence of the OH group and its high volatility. The elemental analysis of solids shows a carbon content of 95-98 wt%, and supports the prospect of carbon deposition via coke formation. Among the major advantages of adopting solvent-assisted bio-oil stabilization, coke reduction and depolymerization via enhanced solubility, improved mass transfer, and dilution effect are prominent. Furthermore, the successful stabilization of intermediates (aldehydes, furans and carboxylic acids) suppressed carbon deposition prospects for ETH-used, METH-used and ISO-used.

6.5 Conclusions

The study investigated how different solvents influence the stability and quality of bio-oil. By employing solvents with varying polarities during solvent-assisted mild hydrotreatment, significant differences in oil yields and properties were observed compared to conventional

methods. Solvents like methanol (METH) and ethanol (ETH), which are highly polar, yielded higher oil fractions (64% and 62% respectively) compared to less polar solvents like ethyl ether (DME) at 59%. This difference underscores the polar solvents' ability to solubilize polar compounds in bio-oil effectively. Isopropyl alcohol (IPA), with intermediate polarity, achieved a balanced oil yield of 63%, indicating its ability to dissolve both polar and non-polar components. The moisture reduction in stabilized bio-oils followed the order: IPA > ETH > METH > DME, with IPA showing the highest reduction due to its structural characteristics facilitating dehydration. The stabilized bio-oils exhibited lower viscosity and consistent densities compared to raw bio-oil, without significant colour alteration. Viscosity reduction varied with IPA > ETH > DME > METH. Carbon recovery in stabilized bio-oils ranged from 65% to 75% for DME, ETH, and METH, and was 71% for IPA. The heating values of stabilized bio-oils ranged from 28 to 29 MJ/kg, with IPA-stabilized bio-oil showing the highest value (29.05 ± 0.06 MJ/kg). The rise in energy output between the feed blends and the raw bio-oil correlated with the solvent:oil ratio of 1:6. The results of energy outputs were indicative of highly oxygenated compounds in the stabilized bio-oil which was also evident on the GCMS and CHNS/O analyses. Aldehydes like 5-hydroxymethyl-2-furancarboxaldehyde (HMF), prevalent in raw bio-oil, were undetectable after bio-oil stabilization. Energy outputs correlated with the energy content of added solvents, with DME, IPA, and ETH providing higher values than METH due to superior properties. METH demonstrated high efficiency (74.8%) in stabilizing bio-oil, attributed to its strong hydrogen-donating capability. ETH followed closely at 69.5%, indicating its comparable performance in bio-oil stabilization. IPA, with moderate efficiency (69.3%), presents a balanced alternative considering its molecular structure and hydrogen solubility. In contrast, DME exhibited lower efficiency (63.6%) due to its weaker hydrogenation capability and propensity for undesired side reactions. The study suggests that subcritical conditions up to 200°C are effective for methanol, ethanol, and isopropyl alcohol in bio-oil stabilization, comparable to results obtained under supercritical conditions. Stabilization reactions further improved bio-oil properties through processes like esterification and hydrogenation, enhancing physicochemical characteristics such as heating value and viscosity. Future research should focus on optimizing solvent recovery and reuse to improve the efficiency of bio-oil stabilization processes. This approach not only ensures sustainability but also maximizes the economic viability of bio-oil upgrading by minimizing resource consumption and waste generation.

CHAPTER 7

7. Conclusions and Recommendations

The depletion of conventional fossil fuel reserves, encompassing oil, gas, and coal, has heightened global concerns surrounding environmental sustainability and energy security. As a result, there has been a notable shift towards exploring alternative energy technologies and advancing sustainable products and processes. Biomass has emerged as a pivotal renewable feedstock in recent decades. Bio-oil derived from biomass presents a promising avenue for diverse applications in energy production, chemical synthesis, and as a potential energy carrier.

The overall research focused mainly on the utilization of lignocellulosic biomass, primarily sourced from invasive species, for the production of biofuels. By converting invasive plant species into valuable biofuels, the research aimed to address two critical issues: managing invasive species and developing sustainable energy sources. Furthermore, the research incorporated a bio-oil organic phase stabilization study to enhance bio-oil properties in preparation for the severe hydrotreatment stage.

7.1 Catalytic vs. Non-Catalytic Fast Pyrolysis of Giant Reed

The first study evaluated catalytic and non-catalytic fast pyrolysis of Giant Reed using HZSM-5 zeolite as a catalyst. The results indicated that the presence of the HZSM-5 catalyst significantly improves the quality of the pyrolysis oil. Catalytic pyrolysis consistently yielded bio-oil with lower moisture content and higher carbon content than non-catalytic pyrolysis. Catalytic pyrolysis, conducted at 550°C with a heating rate of 1 °C/s, yielded an increased higher heating value (HHV) of 23.0 MJ/kg for the bio-oil compared to 21.3 MJ/kg from non-catalytic pyrolysis. The application of HZSM-5 at 650°C and a heating rate of 5°C/s increased the production of aromatic hydrocarbons and phenolic compounds while reducing undesirable oxygenates. However, this led to lower bio-oil yields and higher energy consumption. Thus, the optimal conditions for maximizing bio-oil yield and quality were determined to be 550°C and a heating rate of 1°C/s, balancing bio-oil quality and energy efficiency. While Giant Reed demonstrates potential as a bio-oil feedstock, further optimization of pyrolysis parameters and upgrading techniques are necessary to improve bio-oil quality and economic feasibility. The study offers the following suggestions for future research.

Exploration of Alternative Catalysts: Investigate a wider range of zeolites and other catalytic materials, such as metal-supported catalysts or mixed oxide catalysts, to determine if they offer

improved catalytic performance in terms of bio-oil yield, composition, and stability compared to HZSM-5.

Catalyst Regeneration: Examine the feasibility of regenerating HZSM-5 and other potential catalysts to reduce operational costs and extend their useful life. Research will focus on effective regeneration methods and their impact on catalyst performance and bio-oil quality.

7.2 Seasonal Variations in Giant Reed Biomass

The second study explored the effect of seasonal variations on the fuel properties of Giant Reed biomass, aiming to optimize harvest timing to enhance bio-oil production and reduce artificial flooding risks. The HHV of the biomass increased from 18.44 ± 0.04 MJ/kg during the active growth stage to 19.73 ± 0.05 MJ/kg during the senescence-dormant phase. The active growth stage exhibited the highest ash content, which negatively impacted bio-oil yield due to increased slag formation. In contrast, the dormant phase, with lower ash content and higher fixed carbon, led to improved bio-oil yield. While Giant Reed pyrolysis averaged 41-42 wt% bio-oil, HS-1/HS-4 favoured aqueous phase production, and HS-2/HS-3 produced higher organic phase yields (around 11 wt%). The increase in the bio-oil organic phase correlated with the lignification effect significantly as shown by the R^2 value of 0.97. Higher heating values (HHV) of the bio-oil organic phase were in the range of 19.4 ± 0.03 to 22.6 ± 0.02 MJ/kg in relation to the active growth stage and senescence-dormant phase, respectively. The study recommended harvesting Giant Reed in autumn to optimize biomass quality and mitigate environmental impacts, including CO_2 emissions and flooding risks caused by dormant biomass. The study recommends exploring the following areas for future research.

Extended Seasonal Studies: Expand research to include a more comprehensive range of seasonal variations and geographic locations to better understand the effects of different climates and soil conditions on biomass properties and bio-oil production as well as quality.

Impact of Harvest Timing on Bio-Oil Upgrading: Investigate how the timing of biomass harvest affects subsequent bio-oil upgrading processes, including stabilization and refining. Assess how different harvest times influence the efficiency and effectiveness of the upgrading techniques.

Biomass Storage and Handling: Study the effects of different storage and handling practices on the quality and stability of Giant Reed biomass before pyrolysis. Determine how pre-pyrolysis storage conditions impact bio-oil yield and properties.

7.3 Comparative Analysis of Wood-Based and Cane-Based Biomass

The third study assessed bio-oil production from wood-based (pine) and cane-based (bamboo) biomass using a sand-fluidized bed reactor. Pine biomass produced bio-oil with a higher energy density compared to bamboo, with an energy yield for the bio-oil organic phase (EBOP) of 15% versus 11% for bamboo. Pine bio-oil demonstrated superior flow characteristics and a higher HHV, making it more suitable for commercial applications. Although lower in acidity, bamboo bio-oil presented higher flow resistance during pyrolysis. The study concluded that while both biomass types were viable, pine biomass was more advantageous for commercialization due to its superior energy content and processing efficiency. The study suggests the following areas for future research.:

Broader Biomass Comparisons: Inclusion of additional biomass types in comparative studies to identify other potential feedstocks with high energy yields and favourable pyrolysis characteristics.

Economic Feasibility and Scale-Up: Perform economic feasibility studies and scale-up assessments for pine and bamboo biomass pyrolysis. Analyze the cost-effectiveness, infrastructure requirements, and potential market applications for bio-oil derived from these feedstocks.

7.4 Stabilization of Raw Bio-Oil Using Solvent-Assisted Approach

The final study addressed the stabilization of raw bio-oil using various solvents, namely methanol (METH), ethanol (ETH), isopropyl alcohol (IPA), and ethyl ether (DME). Highly polar solvents such as METH and ETH achieved higher oil fractions of 64% and 62%, respectively, compared to the less polar DME at 59%. With intermediate polarity, IPA resulted in a 63% oil yield and exhibited the greatest reduction in moisture content and viscosity among the solvents tested. The moisture reduction in stabilized bio-oils followed the order: IPA > ETH > METH > DME. The lack of the hydroxyl group on the DME structure reduced its ability to promote dehydration. Carbon recovery in stabilized bio-oils ranged from 65% to 75%, with IPA achieving the highest recovery at 71%. The heating values of the stabilized bio-oils ranged

from 28 to 29 MJ/kg, with IPA-stabilized bio-oil reaching 29.05 ± 0.06 MJ/kg. The energy efficiency of stabilization followed the order: METH (74.8%) > ETH (69.5%) > IPA (69.3%) > DME (63.6%). Subcritical conditions up to 200°C were found to be effective for stabilization, providing results comparable to those obtained under supercritical conditions. The study offers the following recommendations for future research.

Evaluation of Additional Solvents and Methods: Test a broader range of solvents, including those with varying polarities and functionalities, to determine their effectiveness in stabilizing bio-oil. Investigate the use of solvent combinations or new stabilizing agents.

Long-Term Stability Studies: Study the long-term stability of bio-oil stabilized with different solvents to assess how well the properties of stabilized bio-oil are maintained over time. Investigate the potential for degradation or changes in quality during storage and handling.

This research provided significant advancements in understanding bio-oil production and stabilization. The findings demonstrated the benefits of catalytic pyrolysis with HZSM-5 for enhancing bio-oil quality, the impact of seasonal variations on biomass and bio-oil properties, the superior potential of pine over bamboo for commercial bio-oil production, and effective solvent-assisted approach for bio-oil stabilization.

8. REFERENCES

Abnisa, F., Arami-Niya, A., Daud, W. W., Sahu, J. & Noor, I. 2013. Utilization Of Oil Palm Tree Residues To Produce Bio-Oil And Bio-Char Via Pyrolysis. *Energy Conversion And Management,* 76**,** 1073-1082.

Ahamed, T. S., Anto, S., Mathimani, T., Brindhadevi, K. & Pugazhendhi, A. 2021. Upgrading Of Bio-Oil From Thermochemical Conversion Of Various Biomass–Mechanism, Challenges And Opportunities. *Fuel,* 287**,** 119329.

Ahmadi, S., Yuan, Z., Rohani, S. & Xu, C. C. 2016. Effects Of Nano-Structured Como Catalysts On Hydrodeoxygenation Of Fast Pyrolysis Oil In Supercritical Ethanol. *Catalysis Today,* 269**,** 182-194.

Ahmed, G. & Kishore, N. 2023a. Fuel Phase Extraction From Pyrolytic Liquid Of Azadirachta Indica Biomass Followed By Subsequent Characterization Of Pyrolysis Products. *Renewable Energy,* 219**,** 119460.

Ahmed, G. & Kishore, N. 2023b. Separation And Extensive Evaluation Of Properties Of Fuel And Non-Fuel Portions Of Pyrolytic Bio-Oil Obtained From Erythrina Indica Biomass. *Journal Of Renewable And Sustainable Energy,* 15.

Ahmed, G. & Kishore, N. 2024. Synergistic Effects On Properties Of Biofuel And Biochar Produced Through Co-Feed Pyrolysis Of Erythrina Indica And Azadirachta Indica Biomass. *Renewable Energy,* 227**,** 120508.

Akhtar, J. & Amin, N. A. S. 2011. A Review On Process Conditions For Optimum Bio-Oil Yield In Hydrothermal Liquefaction Of Biomass. *Renewable And Sustainable Energy Reviews,* 15**,** 1615-1624.

Anitescu, G. & Bruno, T. J. 2012. Fluid Properties Needed In Supercritical Transesterification Of Triglyceride Feedstocks To Biodiesel Fuels For Efficient And Clean Combustion–A Review. *The Journal Of Supercritical Fluids,* 63**,** 133-149.

Ansari, K. B., Arora, J. S., Chew, J. W., Dauenhauer, P. J. & Mushrif, S. H. 2019. Fast Pyrolysis Of Cellulose, Hemicellulose, And Lignin: Effect Of Operating Temperature On Bio-Oil Yield And Composition And Insights Into The Intrinsic Pyrolysis Chemistry. *Industrial & Engineering Chemistry Research,* 58**,** 15838-15852.

Aravind, S. V., Ahmed, G. & Kishore, N. 2023. Pyrolysis Of Delonix Regia Using Metal Oxide Catalysts And Solvent Effect On Fuel Fraction Of Bio-Oil. *Results In Engineering,* 17**,** 100876.

Arazo, R. O., Genuino, D. A. D., De Luna, M. D. G. & Capareda, S. C. 2017. Bio-Oil Production From Dry Sewage Sludge By Fast Pyrolysis In An Electrically-Heated Fluidized Bed Reactor. *Sustainable Environment Research,* 27**,** 7-14.

Ardiyanti, A., Gutierrez, A., Honkela, M., Krause, A. & Heeres, H. 2011. Hydrotreatment Of Wood-Based Pyrolysis Oil Using Zirconia-Supported Mono-And Bimetallic (Pt, Pd, Rh) Catalysts. *Applied Catalysis A: General,* 407**,** 56-66.

Asadullah, M., Rahman, M. A., Ali, M. M., Motin, M. A., Sultan, M. B., Alam, M. R. & Rahman, M. S. 2008. Jute Stick Pyrolysis For Bio-Oil Production In Fluidized Bed Reactor. *Bioresource Technology,* 99**,** 44-50.

Auersvald, M., Shumeiko, B., Staš, M., Kubička, D., Chudoba, J. & Šimáček, P. 2019. Quantitative Study Of Straw Bio-Oil Hydrodeoxygenation Over A Sulfided Nimo Catalyst. *Acs Sustainable Chemistry & Engineering,* 7**,** 7080-7093.

Awasthi, M. K., Sar, T., Gowd, S. C., Rajendran, K., Kumar, V., Sarsaiya, S., Li, Y., Sindhu, R., Binod, P. & Zhang, Z. 2023. A Comprehensive Review On Thermochemical, And Biochemical Conversion Methods Of Lignocellulosic Biomass Into Valuable End Product. *Fuel,* 342**,** 127790.

Aysu, T., Durak, H., Güner, S., Bengü, A. Ş. & Esim, N. 2016. Bio-Oil Production Via Catalytic Pyrolysis Of Anchusa Azurea: Effects Of Operating Conditions On Product Yields And Chromatographic Characterization. *Bioresource Technology,* 205**,** 7-14.

Azadi, P. & Farnood, R. 2011. Review Of Heterogeneous Catalysts For Sub-And Supercritical Water Gasification Of Biomass And Wastes. *International Journal Of Hydrogen Energy,* 36**,** 9529-9541.

Azadi, P., Inderwildi, O. R., Farnood, R. & King, D. A. 2013. Liquid Fuels, Hydrogen And Chemicals From Lignin: A Critical Review. *Renewable And Sustainable Energy Reviews,* 21**,** 506-523.

Azeez, A. M., Meier, D., Odermatt, J. R. & Willner, T. 2010. Fast Pyrolysis Of African And European Lignocellulosic Biomasses Using Py-Gc/Ms And Fluidized Bed Reactor. *Energy & Fuels,* 24**,** 2078-2085.

Ba, Y., Liu, F., Wang, X. & Yang, J. 2020. Pyrolysis Of C3 Energy Plant (Arundo Donax): Thermogravimetry, Mechanism, And Potential Evaluation. *Industrial Crops And Products,* 149**,** 112337.

Bai, X., Duan, P., Xu, Y., Zhang, A. & Savage, P. E. 2014. Hydrothermal Catalytic Processing Of Pretreated Algal Oil: A Catalyst Screening Study. *Fuel,* 120**,** 141-149.

Baker, R. R., Coburn, S., Liu, C. & Tetteh, J. 2005. Pyrolysis Of Saccharide Tobacco Ingredients: A Tga–Ftir Investigation. *Journal Of Analytical And Applied Pyrolysis,* 74**,** 171-180.

Balagurumurthy, B., Singh, R. & Bhaskar, T. 2015. Catalysts For Thermochemical Conversion Of Biomass. *Recent Advances In Thermo-Chemical Conversion Of Biomass.* Elsevier.

Balat, M., Balat, M., Kirtay, E. & Balat, H. 2009. Main Routes For The Thermo-Conversion Of Biomass Into Fuels And Chemicals. Part 1: Pyrolysis Systems. *Energy Conversion And Management,* 50**,** 3147-3157.

Bastos, R. R. C., Da Luz Corrêa, A. P., Da Luz, P. T. S., Da Rocha Filho, G. N., Zamian, J. R. & Da Conceição, L. R. V. 2020. Optimization Of Biodiesel Production Using Sulfonated Carbon-Based Catalyst From An Amazon Agro-Industrial Waste. *Energy Conversion And Management,* 205**,** 112457.

Bernhardsen, I. M. & Knuutila, H. K. 2017. A Review Of Potential Amine Solvents For Co2 Absorption Process: Absorption Capacity, Cyclic Capacity And Pka. *International Journal Of Greenhouse Gas Control,* 61**,** 27-48.

Bessa, W., Trache, D., Derradji, M., Ambar, H., Tarchoun, A. F., Benziane, M. & Guedouar, B. 2020. Characterization Of Raw And Treated Arundo Donax L. Cellulosic Fibers And Their Effect On The Curing Kinetics Of Bisphenol A-Based Benzoxazine. *International Journal Of Biological Macromolecules,* 164**,** 2931-2943.

Bhoi, P., Ouedraogo, A., Soloiu, V. & Quirino, R. 2020. Recent Advances On Catalysts For Improving Hydrocarbon Compounds In Bio-Oil Of Biomass Catalytic Pyrolysis. *Renewable And Sustainable Energy Reviews,* 121**,** 109676.
Bioenergy, I. 2006. Annual Report 2009. *International Energy Agency***,** 4-20.
Biswas, B., Pandey, N., Bisht, Y., Singh, R., Kumar, J. & Bhaskar, T. 2017. Pyrolysis Of Agricultural Biomass Residues: Comparative Study Of Corn Cob, Wheat Straw, Rice Straw And Rice Husk. *Bioresource Technology,* 237**,** 57-63.
Brand, S., Susanti, R. F., Kim, S. K., Lee, H.-S., Kim, J. & Sang, B.-I. 2013. Supercritical Ethanol As An Enhanced Medium For Lignocellulosic Biomass Liquefaction: Influence Of Physical Process Parameters. *Energy,* 59**,** 173-182.
Bridgwater, A. V. 2012a. Review Of Fast Pyrolysis Of Biomass And Product Upgrading. *Biomass And Bioenergy,* 38**,** 68-94.
Bridgwater, A. V. 2012b. Upgrading Biomass Fast Pyrolysis Liquids. *Environmental Progress & Sustainable Energy,* 31**,** 261-268.
Bridgwater, T. Biomass Pyrolysis. Iea Bioenergy Task, 2007.
Broumand, M., Albert-Green, S., Yun, S., Hong, Z. & Thomson, M. J. 2020. Spray Combustion Of Fast Pyrolysis Bio-Oils: Applications, Challenges, And Potential Solutions. *Progress In Energy And Combustion Science,* 79**,** 100834.
Bu, Q., Lei, H., Ren, S., Wang, L., Zhang, Q., Tang, J. & Ruan, R. 2012. Production Of Phenols And Biofuels By Catalytic Microwave Pyrolysis Of Lignocellulosic Biomass. *Bioresource Technology,* 108**,** 274-279.
Çağlar, A. & Demirbaş, A. 2002. Conversion Of Cotton Cocoon Shell To Hydrogen Rich Gaseous Products By Pyrolysis. *Energy Conversion And Management,* 43**,** 489-497.
Cappelli, G. A., Ginaldi, F., Fanchini, D., Corinzia, S. A., Cosentino, S. L. & Ceotto, E. 2021. Model-Based Assessment Of Giant Reed (Arundo Donax L.) Energy Yield In The Form Of Diverse Biofuels In Marginal Areas Of Italy. *Land,* 10**,** 548.
Capunitan, J. A. & Capareda, S. C. 2012. Assessing The Potential For Biofuel Production Of Corn Stover Pyrolysis Using A Pressurized Batch Reactor. *Fuel,* 95**,** 563-572.
Capunitan, J. A. & Capareda, S. C. 2014. Hydrotreatment Of Corn Stover Bio-Oil Using Noble Metal Catalysts. *Fuel Processing Technology,* 125**,** 190-199.
Cha, J. S., Park, S. H., Jung, S.-C., Ryu, C., Jeon, J.-K., Shin, M.-C. & Park, Y.-K. 2016. Production And Utilization Of Biochar: A Review. *Journal Of Industrial And Engineering Chemistry,* 40**,** 1-15.
Chang, R., Zhu, L., Jin, F., Fan, M., Liu, J., Jia, Q., Tang, C. & Li, Q. 2018. Production Of Bio-Based P-Xylene Via Catalytic Pyrolysis Of Biomass Over Metal Oxide-Modified Hzsm-5 Zeolites. *Journal Of Chemical Technology & Biotechnology,* 93**,** 3292-3301.
Charusiri, W. & Vitidsant, T. 2017. Upgrading Bio-Oil Produced From The Catalytic Pyrolysis Of Sugarcane (Saccharum Officinarum L) Straw Using Calcined Dolomite. *Sustainable Chemistry And Pharmacy,* 6**,** 114-123.
Chen, D., Liu, D., Zhang, H., Chen, Y. & Li, Q. 2015. Bamboo Pyrolysis Using Tg–Ftir And A Lab-Scale Reactor: Analysis Of Pyrolysis Behavior, Product Properties, And Carbon And Energy Yields. *Fuel,* 148**,** 79-86.

Chen, D., Zhou, J. & Zhang, Q. 2014a. Effects Of Heating Rate On Slow Pyrolysis Behavior, Kinetic Parameters And Products Properties Of Moso Bamboo. *Bioresource Technology,* 169**,** 313-319.
Chen, D., Zhou, J., Zhang, Q. & Zhu, X. 2014b. Evaluation Methods And Research Progresses In Bio-Oil Storage Stability. *Renewable And Sustainable Energy Reviews,* 40**,** 69-79.
Chen, W., Luo, Z., Yu, C., Li, G., Yang, Y. & Zhang, H. 2014c. Upgrading Of Bio-Oil In Supercritical Ethanol: Catalysts Screening, Solvent Recovery And Catalyst Stability Study. *The Journal Of Supercritical Fluids,* 95**,** 387-393.
Chen, X., Che, Q., Li, S., Liu, Z., Yang, H., Chen, Y., Wang, X., Shao, J. & Chen, H. 2019. Recent Developments In Lignocellulosic Biomass Catalytic Fast Pyrolysis: Strategies For The Optimization Of Bio-Oil Quality And Yield. *Fuel Processing Technology,* 196**,** 106180.
Cheng, L., Adhikari, S., Wang, Z. & Ding, Y. 2015. Dynamic Variation Of Fuel Properties Of Tonkin Cane (Pseudosasa Amabilis) During Maturation. *Energy & Fuels,* 29**,** 2408-2415.
Cheng, S., Wei, L., Julson, J., Muthukumarappan, K. & Kharel, P. R. 2017. Upgrading Pyrolysis Bio-Oil To Biofuel Over Bifunctional Co-Zn/Hzsm-5 Catalyst In Supercritical Methanol. *Energy Conversion And Management,* 147**,** 19-28.
Chia, J. W., Sawai, O. & Nunoura, T. 2020. Reaction Pathway Of Poly (Ethylene) Terephthalate Carbonization: Decomposition Behavior Based On Carbonized Product. *Waste Management,* 108**,** 62-69.
Chikouche, M. D. L., Merrouche, A., Azizi, A., Rokbi, M. & Walter, S. 2015. Influence Of Alkali Treatment On The Mechanical Properties Of New Cane Fibre/Polyester Composites. *Journal Of Reinforced Plastics And Composites,* 34**,** 1329-1339.
Chiosso, M. E., Crespo, I., Merlo, A. B. & Valle, B. 2023. Metal-Doped Hzsm-5 Zeolite Catalysts For Catalytic Cracking Of Raw Bio-Oil: Exploring Activity Toward Value-Added Products. *Catalysts,* 13**,** 1198.
Cho, E. J., Trinh, L. T. P., Song, Y., Lee, Y. G. & Bae, H.-J. 2020. Bioconversion Of Biomass Waste Into High Value Chemicals. *Bioresource Technology,* 298**,** 122386.
Cogulet, A., Blanchet, P. & Landry, V. 2016. Wood Degradation Under Uv Irradiation: A Lignin Characterization. *Journal Of Photochemistry And Photobiology B: Biology,* 158**,** 184-191.
Collard, F.-X. & Blin, J. 2014. A Review On Pyrolysis Of Biomass Constituents: Mechanisms And Composition Of The Products Obtained From The Conversion Of Cellulose, Hemicelluloses And Lignin. *Renewable And Sustainable Energy Reviews,* 38**,** 594-608.
Cordero-Lanzac, T., Rodriguez-Mirasol, J., Cordero, T. & Bilbao, J. 2021. Advances And Challenges In The Valorization Of Bio-Oil: Hydrodeoxygenation Using Carbon-Supported Catalysts. *Energy & Fuels,* 35**,** 17008-17031.
Corno, L., Pilu, R. & Adani, F. 2014. Arundo Donax L.: A Non-Food Crop For Bioenergy And Bio-Compound Production. *Biotechnology Advances,* 32**,** 1535-1549.
Correa, C. R., Hehr, T., Voglhuber-Slavinsky, A., Rauscher, Y. & Kruse, A. 2019. Pyrolysis Vs. Hydrothermal Carbonization: Understanding The Effect Of Biomass Structural Components And Inorganic Compounds On The Char Properties. *Journal Of Analytical And Applied Pyrolysis,* 140**,** 137-147.

Crestini, C. & Argyropoulos, D. S. 1998. The Early Oxidative Biodegradation Steps Of Residual Kraft Lignin Models With Laccase. *Bioorganic & Medicinal Chemistry,* 6**,** 2161-2169.
Cui, H.-Y., Wang, J.-H., Zhuo, S.-P., Li, Z.-H., Wang, L.-H. & Yi, W.-M. 2010. Upgrading Bio-Oil By Esterification Under Supercritical Co2 Conditions. *Journal Of Fuel Chemistry And Technology,* 38**,** 673-678.
Dai, G., Wang, S., Huang, S. & Zou, Q. 2018. Enhancement Of Aromatics Production From Catalytic Pyrolysis Of Biomass Over Hzsm-5 Modified By Chemical Liquid Deposition. *Journal Of Analytical And Applied Pyrolysis,* 134**,** 439-445.
Das, S. & Goud, V. V. 2021. Rsm-Optimised Slow Pyrolysis Of Rice Husk For Bio-Oil Production And Its Upgradation. *Energy,* 225**,** 120161.
David, E. & Kopac, J. 2018. Pyrolysis Of Rapeseed Oil Cake In A Fixed Bed Reactor To Produce Bio-Oil. *Journal Of Analytical And Applied Pyrolysis,* 134**,** 495-502.
Dayton, D. C. & Foust, T. D. 2019. *Analytical Methods For Biomass Characterization And Conversion,* Elsevier.
De Miguel Mercader, F., Groeneveld, M., Kersten, S., Way, N., Schaverien, C. & Hogendoorn, J. 2010. Production Of Advanced Biofuels: Co-Processing Of Upgraded Pyrolysis Oil In Standard Refinery Units. *Applied Catalysis B: Environmental,* 96**,** 57-66.
Demiral, İ. & Ayan, E. A. 2011. Pyrolysis Of Grape Bagasse: Effect Of Pyrolysis Conditions On The Product Yields And Characterization Of The Liquid Product. *Bioresource Technology,* 102**,** 3946-3951.
Desisto, W. J., Hill, N., Beis, S. H., Mukkamala, S., Joseph, J., Baker, C., Ong, T.-H., Stemmler, E. A., Wheeler, M. C. & Frederick, B. G. 2010. Fast Pyrolysis Of Pine Sawdust In A Fluidized-Bed Reactor. *Energy & Fuels,* 24**,** 2642-2651.
Dhanavath, K. N., Shah, K., Bankupalli, S., Bhargava, S. K. & Parthasarathy, R. 2017. Derivation Of Optimum Operating Conditions For The Slow Pyrolysis Of Mahua Press Seed Cake In A Fixed Bed Batch Reactor For Bio–Oil Production. *Journal Of Environmental Chemical Engineering,* 5**,** 4051-4063.
Dhyani, V., Awasthi, A., Kumar, J. & Bhaskar, T. 2017. Pyrolysis Of Sorghum Straw: Effect Of Temperature And Reaction Environment On The Product Behavior. *J. Energy Environ. Sustainability***,** 64-69.
Ding, C., Wang, L., Tian, C., Li, Y., Sun, Z., Wang, H., Suo, Y. & You, J. 2008. Lc-Dad-Esi-Ms Characterization Of Carbohydrates Using A New Labeling Reagent. *Chromatographia,* 68**,** 893-902.
Ding, K., Zhong, Z., Wang, J., Zhang, B., Fan, L., Liu, S., Wang, Y., Liu, Y., Zhong, D. & Chen, P. 2018. Improving Hydrocarbon Yield From Catalytic Fast Co-Pyrolysis Of Hemicellulose And Plastic In The Dual-Catalyst Bed Of Cao And Hzsm-5. *Bioresource Technology,* 261**,** 86-92.
Do Minh, T., Song, J., Deb, A., Cha, L., Srivastava, V. & Sillanpää, M. 2020. Biochar Based Catalysts For The Abatement Of Emerging Pollutants: A Review. *Chemical Engineering Journal,* 394**,** 124856.
Dong, Q., Niu, M., Bi, D., Liu, W., Gu, X. & Lu, C. 2018. Microwave-Assisted Catalytic Pyrolysis Of Moso Bamboo For High Syngas Production. *Bioresource Technology,* 256**,** 145-151.

Dong, Q. & Xiong, Y. 2014. Kinetics Study On Conventional And Microwave Pyrolysis Of Moso Bamboo. *Bioresource Technology,* 171**,** 127-131.
Duan, P., Zhang, C., Wang, F., Fu, J., Lü, X., Xu, Y. & Shi, X. 2016. Activated Carbons For The Hydrothermal Upgrading Of Crude Duckweed Bio-Oil. *Catalysis Today,* 274**,** 73-81.
Elkasabi, Y., Mullen, C. A., Pighinelli, A. L. & Boateng, A. A. 2014. Hydrodeoxygenation Of Fast-Pyrolysis Bio-Oils From Various Feedstocks Using Carbon-Supported Catalysts. *Fuel Processing Technology,* 123**,** 11-18.
Emeis, C. 1993. Determination Of Integrated Molar Extinction Coefficients For Infrared Absorption Bands Of Pyridine Adsorbed On Solid Acid Catalysts. *Journal Of Catalysis,* 141**,** 347-354.
Fahmi, R., Bridgwater, A. V., Donnison, I., Yates, N. & Jones, J. 2008. The Effect Of Lignin And Inorganic Species In Biomass On Pyrolysis Oil Yields, Quality And Stability. *Fuel,* 87**,** 1230-1240.
Febrero, L., Granada, E., Patiño, D., Eguía, P. & Regueiro, A. 2015. A Comparative Study Of Fouling And Bottom Ash From Woody Biomass Combustion In A Fixed-Bed Small-Scale Boiler And Evaluation Of The Analytical Techniques Used. *Sustainability,* 7**,** 5819-5837.
Fermoso, J., Pizarro, P., Coronado, J. M. & Serrano, D. P. 2017. Advanced Biofuels Production By Upgrading Of Pyrolysis Bio-Oil. *Wiley Interdisciplinary Reviews: Energy And Environment,* 6**,** E245.
Fernandez, E., Santamaria, L., Artetxe, M., Amutio, M., Arregi, A., Lopez, G., Bilbao, J. & Olazar, M. 2021. In Line Upgrading Of Biomass Fast Pyrolysis Products Using Low-Cost Catalysts. *Fuel,* 296**,** 120682.
Ferreira-Santos, P., Genisheva, Z., Botelho, C., Santos, J., Ramos, C., Teixeira, J. A. & Rocha, C. M. 2020. Unravelling The Biological Potential Of Pinus Pinaster Bark Extracts. *Antioxidants,* 9**,** 334.
French, R. & Czernik, S. 2010. Catalytic Pyrolysis Of Biomass For Biofuels Production. *Fuel Processing Technology,* 91**,** 25-32.
Gao, M., Wang, Y., Dong, J., Li, F. & Xie, K. 2016. Release Behavior And Formation Mechanism Of Polycyclic Aromatic Hydrocarbons During Coal Pyrolysis. *Chemosphere,* 158**,** 1-8.
Garba, M., Musa, U., Olugbenga, A., Mohammad, Y. S., Yahaya, M. & Ibrahim, A. 2018. Catalytic Upgrading Of Bio-Oil From Bagasse: Thermogravimetric Analysis And Fixed Bed Pyrolysis. *Beni-Suef University Journal Of Basic And Applied Sciences,* 7**,** 776-781.
Gaur, S. & Reed, T. B. 2020. *Thermal Data For Natural And Synthetic Fuels,* Crc Press.
Ge, X., Xu, F., Vasco-Correa, J. & Li, Y. 2016. Giant Reed: A Competitive Energy Crop In Comparison With Miscanthus. *Renewable And Sustainable Energy Reviews,* 54**,** 350-362.
Ghaffar, S. H. & Fan, M. 2013. Structural Analysis For Lignin Characteristics In Biomass Straw. *Biomass And Bioenergy,* 57**,** 264-279.
Gholizadeh, M., Gunawan, R., Hu, X., Kadarwati, S., Westerhof, R., Chaiwat, W., Hasan, M. M. & Li, C.-Z. 2016. Importance Of Hydrogen And Bio-Oil Inlet Temperature During The Hydrotreatment Of Bio-Oil. *Fuel Processing Technology,* 150**,** 132-140.
Glasser, W. G., Atalla, R. H., Blackwell, J., Malcolm Brown, R., Burchard, W., French, A. D., Klemm, D. O. & Nishiyama, Y. 2012. About The Structure Of Cellulose: Debating The Lindman Hypothesis. *Cellulose,* 19**,** 589-598.

Gollakota, A. R., Reddy, M., Subramanyam, M. D. & Kishore, N. 2016. A Review On The Upgradation Techniques Of Pyrolysis Oil. *Renewable And Sustainable Energy Reviews,* 58**,** 1543-1568.
González, J. F., Encinar, J. M., Canito, J. L., Sabio, E. & Chacón, M. 2003. Pyrolysis Of Cherry Stones: Energy Uses Of The Different Fractions And Kinetic Study. *Journal Of Analytical And Applied Pyrolysis,* 67**,** 165-190.
Grønli, M. G., Várhegyi, G. & Di Blasi, C. 2002. Thermogravimetric Analysis And Devolatilization Kinetics Of Wood. *Industrial & Engineering Chemistry Research,* 41**,** 4201-4208.
Guilhaume, N., Schuurman, Y. & Geantet, C. 2021. The Role Of Catalysis In The Valorization Of Woody Biomass Fast Pyrolysis Liquids: Overview And Contribution Of Ircelyon. *Catalysis Today,* 373**,** 5-23.
Guiotoku, M., Pangrácio, A. R., Hansel, F. A. & De Lacerda, A. E. B. 2024. Physico-Chemical Properties Of Brazilian Native Bamboo Species. *Advances In Bamboo Science,* 7**,** 100075.
Guo, X., Yang, H., Wenga, T., Zhang, R., Liu, B. & Chen, G. 2022. Catalytic Fast Pyrolysis Of Arundo Donax In A Two-Stage Fixed Bed Reactor Over Metal-Modified Hzsm-5 Catalysts. *Biomass And Bioenergy,* 156**,** 106316.
Guo, Y., Wang, S., Xu, D., Gong, Y., Ma, H. & Tang, X. 2010. Review Of Catalytic Supercritical Water Gasification For Hydrogen Production From Biomass. *Renewable And Sustainable Energy Reviews,* 14**,** 334-343.
Han, Y., Gholizadeh, M., Tran, C.-C., Kaliaguine, S., Li, C.-Z., Olarte, M. & Garcia-Perez, M. 2019. Hydrotreatment Of Pyrolysis Bio-Oil: A Review. *Fuel Processing Technology,* 195**,** 106140.
Hassan, E.-B. M., Steele, P. H. & Ingram, L. 2009. Characterization Of Fast Pyrolysis Bio-Oils Produced From Pretreated Pine Wood. *Applied Biochemistry And Biotechnology,* 154**,** 3-13.
Hoang, A. T., Ong, H. C., Fattah, I. R., Chong, C. T., Cheng, C. K., Sakthivel, R. & Ok, Y. S. 2021. Progress On The Lignocellulosic Biomass Pyrolysis For Biofuel Production Toward Environmental Sustainability. *Fuel Processing Technology,* 223**,** 106997.
Horáček, J. & Kubička, D. 2017. Bio-Oil Hydrotreating Over Conventional Como & Nimo Catalysts: The Role Of Reaction Conditions And Additives. *Fuel,* 198**,** 49-57.
Hu, Q., Jung, J., Chen, D., Leong, K., Song, S., Li, F., Mohan, B. C., Yao, Z., Prabhakar, A. K. & Lin, X. H. 2021. Biochar Industry To Circular Economy. *Science Of The Total Environment,* 757**,** 143820.
Hu, W., Yang, X., Mi, B., Liang, F., Zhang, T. & Liu, Z. 2017. Investigating Gaseous Carbon, Nitrogen, And Sulfur Compounds Of Bamboo, Wood, And Coal During Pyrolysis Process. *Wood And Fiber Science,* 49**,** 269-276.
Hu, X. & Gholizadeh, M. 2020. Progress Of The Applications Of Bio-Oil. *Renewable And Sustainable Energy Reviews,* 134**,** 110124.
Huang, L., Chen, Y., Liu, G., Li, S., Liu, Y. & Gao, X. 2015. Non-Isothermal Pyrolysis Characteristics Of Giant Reed (Arundo Donax L.) Using Thermogravimetric Analysis. *Energy,* 87**,** 31-40.
(Iea), I. E. A. 2023. Co2 Emissions In 2023. A New Record High, But Is There Light At The End Of The Tunnel?

Imran, A., Bramer, E. A., Seshan, K. & Brem, G. 2018. An Overview Of Catalysts In Biomass Pyrolysis For Production Of Biofuels.
Jahirul, M. I., Rasul, M. G., Chowdhury, A. A. & Ashwath, N. 2012. Biofuels Production Through Biomass Pyrolysis—A Technological Review. *Energies,* 5**,** 4952-5001.
Janković, B., Manić, N., Dodevski, V., Popović, J., Rusmirović, J. D. & Tošić, M. 2019. Characterization Analysis Of Poplar Fluff Pyrolysis Products. Multi-Component Kinetic Study. *Fuel,* 238**,** 111-128.
Jessop, P. G. & Leitner, W. 2008. *Chemical Synthesis Using Supercritical Fluids*, John Wiley & Sons.
Jiang, Z., Liu, Z., Fei, B., Cai, Z. & Yu, Y. 2012. The Pyrolysis Characteristics Of Moso Bamboo. *Journal Of Analytical And Applied Pyrolysis,* 94**,** 48-52.
Jung, S.-H., Kang, B.-S. & Kim, J.-S. 2008. Production Of Bio-Oil From Rice Straw And Bamboo Sawdust Under Various Reaction Conditions In A Fast Pyrolysis Plant Equipped With A Fluidized Bed And A Char Separation System. *Journal Of Analytical And Applied Pyrolysis,* 82**,** 240-247.
Kariim, I., Swai, H. & Kivevele, T. 2023. Bio-Oil Upgrading Over Zsm-5 Catalyst: A Review Of Catalyst Performance And Deactivation. *International Journal Of Energy Research,* 2023**,** 4776962.
Kato, Y., Kohnosu, T., Enomoto, R., Akazawa, M., Yoon, S.-L. & Kojima, Y. 2014. Chemical Properties Of Bio-Oils Produced By Fast Pyrolysis Of Bamboo. *Transactions Of The Materials Research Society Of Japan,* 39**,** 491-498.
Khan, M. S., Min, Y., Broumand, M., Yun, S., Hong, Z. & Thomson, M. J. 2022. Advancing The Application Of Pyrolysis Liquid (Bio-Oil) By The Improvement Of Its Fuel Properties By Thermo-Catalytic Reforming. *Energy & Fuels,* 36**,** 4381-4395.
Khuenkaeo, N. & Tippayawong, N. 2020. Production And Characterization Of Bio-Oil And Biochar From Ablative Pyrolysis Of Lignocellulosic Biomass Residues. *Chemical Engineering Communications,* 207**,** 153-160.
Kim, G., Seo, J., Choi, J.-W., Jae, J., Ha, J.-M., Suh, D. J., Lee, K.-Y., Jeon, J.-K. & Kim, J.-K. 2018. Two-Step Continuous Upgrading Of Sawdust Pyrolysis Oil To Deoxygenated Hydrocarbons Using Hydrotreating And Hydrodeoxygenating Catalysts. *Catalysis Today,* 303**,** 130-135.
Kim, J.-S. & Choi, G.-G. 2018. Pyrolysis Of Lignocellulosic Biomass For Biochemical Production. *Waste Biorefinery*. Elsevier.
Kim, T.-S., Oh, S., Kim, J.-Y., Choi, I.-G. & Choi, J. W. 2014. Study On The Hydrodeoxygenative Upgrading Of Crude Bio-Oil Produced From Woody Biomass By Fast Pyrolysis. *Energy,* 68**,** 437-443.
Kumar, A., Chakraborty, J. & Singh, R. 2017. Bio-Oil: The Future Of Hydrogen Generation. *Biofuels,* 8**,** 663-674.
Kumar, A., Singh, E., Mishra, R. & Kumar, S. 2022a. Biochar As Environmental Armour And Its Diverse Role Towards Protecting Soil, Water And Air. *Science Of The Total Environment,* 806**,** 150444.
Kumar, M., Upadhyay, S. N. & Mishra, P. 2022b. Pyrolysis Of Sugarcane (Saccharum Officinarum L.) Leaves And Characterization Of Products. *Acs Omega,* 7**,** 28052-28064.

Kurzyna-Szklarek, M., Cybulska, J. & Zdunek, A. 2022. Analysis Of The Chemical Composition Of Natural Carbohydrates–An Overview Of Methods. *Food Chemistry,* 394**,** 133466.
Lahijani, P., Mohammadi, M., Mohamed, A. R., Ismail, F., Lee, K. T. & Amini, G. 2022. Upgrading Biomass-Derived Pyrolysis Bio-Oil To Bio-Jet Fuel Through Catalytic Cracking And Hydrodeoxygenation: A Review Of Recent Progress. *Energy Conversion And Management,* 268**,** 115956.
Landrat, M., Abawalo, M. T., Pikoń, K. & Turczyn, R. 2022. Bio-Oil Derived From Teff Husk Via Slow Pyrolysis Process In Fixed Bed Reactor And Its Characterization. *Energies,* 15**,** 9605.
Le, T. T., Chawla, A. & Rimer, J. D. 2020. Impact Of Acid Site Speciation And Spatial Gradients On Zeolite Catalysis. *Journal Of Catalysis,* 391**,** 56-68.
Lee Seongbeom, L. S. & Fasina, O. 2009. Tg-Ftir Analysis Of Switchgrass Pyrolysis.
Leghari, S. J., Wahocho, N. A., Laghari, G. M., Hafeezlaghari, A., Mustafabhabhan, G., Hussaintalpur, K., Bhutto, T. A., Wahocho, S. A. & Lashari, A. A. 2016. Role Of Nitrogen For Plant Growth And Development: A Review. *Advances In Environmental Biology,* 10**,** 209-219.
Lei, J., Wang, Y., Wang, Q., Deng, S. & Fu, Y. 2024. Evaluation Of Kinetic And Thermodynamic Parameters Of Pyrolysis And Combustion Processes For Bamboo Using Thermogravimetric Analysis. *Processes,* 12**,** 2458.
Leite, S., Leite, B., Carrico, C., Isola, A. D. & Dangelo, J. 2018. Characterization Of Biomass Residues Aiming Energy And By-Products Generation. *Chemical Engineering Transactions,* 65**,** 733-738.
Li, W., Pan, C., Sheng, L., Liu, Z., Chen, P., Lou, H. & Zheng, X. 2011. Upgrading Of High-Boiling Fraction Of Bio-Oil In Supercritical Methanol. *Bioresource Technology,* 102**,** 9223-9228.
Liang, F., Wang, R., Hongzhong, X., Yang, X., Zhang, T., Hu, W., Mi, B. & Liu, Z. 2018. Investigating Pyrolysis Characteristics Of Moso Bamboo Through Tg-Ftir And Py-Gc/Ms. *Bioresource Technology,* 256**,** 53-60.
Liang, J., Shan, G. & Sun, Y. 2021. Catalytic Fast Pyrolysis Of Lignocellulosic Biomass: Critical Role Of Zeolite Catalysts. *Renewable And Sustainable Energy Reviews,* 139**,** 110707.
Lievens, C., Ci, D., Bai, Y., Ma, L., Zhang, R., Chen, J. Y., Gai, Q., Long, Y. & Guo, X. 2013. A Study Of Slow Pyrolysis Of One Low Rank Coal Via Pyrolysis–Gc/Ms. *Fuel Processing Technology,* 116**,** 85-93.
Liu, C., Wang, H., Karim, A. M., Sun, J. & Wang, Y. 2014. Catalytic Fast Pyrolysis Of Lignocellulosic Biomass. *Chemical Society Reviews,* 43**,** 7594-7623.
Liu, R., Rahman, M. M., Sarker, M., Chai, M., Li, C. & Cai, J. 2020a. A Review On The Catalytic Pyrolysis Of Biomass For The Bio-Oil Production With Zsm-5: Focus On Structure. *Fuel Processing Technology,* 199**,** 106301.
Liu, R., Sarker, M., Rahman, M. M., Li, C., Chai, M., Cotillon, R. & Scott, N. R. 2020b. Multi-Scale Complexities Of Solid Acid Catalysts In The Catalytic Fast Pyrolysis Of Biomass For Bio-Oil Production–A Review. *Progress In Energy And Combustion Science,* 80**,** 100852.
Liu, S., Ge, X., Liu, Z. & Li, Y. 2016. Effect Of Harvest Date On Arundo Donax L.(Giant Reed) Composition, Ensilage Performance, And Enzymatic Digestibility. *Bioresource Technology,* 205**,** 97-103.

Liu, S., Wang, Z., Xu, X., Ding, Y. & Guo, Z. 2017. Production Of Conjugated Linoleic Acid-Rich Cottonseed Oil By Supported Ru Catalyzed Isomerization. *Industrial Crops And Products,* 97**,** 10-20.
Liu, W.-J., Jiang, H. & Yu, H.-Q. 2015. Development Of Biochar-Based Functional Materials: Toward A Sustainable Platform Carbon Material. *Chemical Reviews,* 115**,** 12251-12285.
Liu, Z., Fei, B., Jiang, Z., Cai, Z., Yu, Y. & Liu, X. E. 2013. A Comparative Study Of Thermal Properties Of Sinocalamus Affinis And Moso Bamboo. *Journal Of Thermal Analysis And Calorimetry,* 111**,** 393-399.
Lo, S.-L., Huang, Y.-F., Chiueh, P.-T. & Kuan, W.-H. 2017. Microwave Pyrolysis Of Lignocellulosic Biomass. *Energy Procedia,* 105**,** 41-46.
Lohitharn, N. & Shanks, B. H. 2009. Upgrading Of Bio-Oil: Effect Of Light Aldehydes On Acetic Acid Removal Via Esterification. *Catalysis Communications,* 11**,** 96-99.
Lowe, S., Browne, M., Boudjelas, S. & De Poorter, M. 2000. *100 Of The World's Worst Invasive Alien Species: A Selection From The Global Invasive Species Database,* Invasive Species Specialist Group Auckland.
Lu, Q., Yang, X.-L. & Zhu, X.-F. 2008. Analysis On Chemical And Physical Properties Of Bio-Oil Pyrolyzed From Rice Husk. *Journal Of Analytical And Applied Pyrolysis,* 82**,** 191-198.
Lyu, H., Zhang, Q. & Shen, B. 2020. Application Of Biochar And Its Composites In Catalysis. *Chemosphere,* 240**,** 124842.
Ma, X., Zhou, B., Budai, A., Jeng, A., Hao, X., Wei, D., Zhang, Y. & Rasse, D. 2016. Study Of Biochar Properties By Scanning Electron Microscope–Energy Dispersive X-Ray Spectroscopy (Sem-Edx). *Communications In Soil Science And Plant Analysis,* 47**,** 593-601.
Martínez Montero, C., Rodríguez Dodero, M., Guillén Sánchez, D. & Barroso, C. 2004. Analysis Of Low Molecular Weight Carbohydrates In Food And Beverages: A Review. *Chromatographia,* 59**,** 15-30.
Martínez-Sanz, M., Erboz, E., Fontes, C. & López-Rubio, A. 2018. Valorization Of Arundo Donax For The Production Of High Performance Lignocellulosic Films. *Carbohydrate Polymers,* 199**,** 276-285.
Mettler, M. S., Mushrif, S. H., Paulsen, A. D., Javadekar, A. D., Vlachos, D. G. & Dauenhauer, P. J. 2012. Revealing Pyrolysis Chemistry For Biofuels Production: Conversion Of Cellulose To Furans And Small Oxygenates. *Energy & Environmental Science,* 5**,** 5414-5424.
Mishra, G., Kumar, J. & Bhaskar, T. 2015. Kinetic Studies On The Pyrolysis Of Pinewood. *Bioresource Technology,* 182**,** 282-288.
Monti, A., Di Virgilio, N. & Venturi, G. 2008. Mineral Composition And Ash Content Of Six Major Energy Crops. *Biomass And Bioenergy,* 32**,** 216-223.
Moon, J., Mun, T.-Y., Yang, W., Lee, U., Hwang, J., Jang, E. & Choi, C. 2015. Effects Of Hydrothermal Treatment Of Sewage Sludge On Pyrolysis And Steam Gasification. *Energy Conversion And Management,* 103**,** 401-407.
Moreira, R., Dos Reis Orsini, R., Vaz, J. M., Penteado, J. C. & Spinacé, E. V. 2017. Production Of Biochar, Bio-Oil And Synthesis Gas From Cashew Nut Shell By Slow Pyrolysis. *Waste And Biomass Valorization,* 8**,** 217-224.

Mortensen, P. M., Grunwaldt, J.-D., Jensen, P. A., Knudsen, K. & Jensen, A. D. 2011. A Review Of Catalytic Upgrading Of Bio-Oil To Engine Fuels. *Applied Catalysis A: General,* 407**,** 1-19.
Mullen, C. A. & Boateng, A. A. 2015. Production Of Aromatic Hydrocarbons Via Catalytic Pyrolysis Of Biomass Over Fe-Modified Hzsm-5 Zeolites. *Acs Sustainable Chemistry & Engineering,* 3**,** 1623-1631.
Nanda, S., Mohanty, P., Kozinski, J. A. & Dalai, A. K. 2014. Physico-Chemical Properties Of Bio-Oils From Pyrolysis Of Lignocellulosic Biomass With High And Slow Heating Rate. *Energy Environ Res,* 4**,** 21.
Neto, C. P., Seca, A., Nunes, A., Coimbra, M., Domingues, F., Evtuguin, D., Silvestre, A. & Cavaleiro, J. 1997. Variations In Chemical Composition And Structure Of Macromolecular Components In Different Morphological Regions And Maturity Stages Of Arundo Donax. *Industrial Crops And Products,* 6**,** 51-58.
Newalkar, G., Iisa, K., D'amico, A. D., Sievers, C. & Agrawal, P. 2014. Effect Of Temperature, Pressure, And Residence Time On Pyrolysis Of Pine In An Entrained Flow Reactor. *Energy & Fuels,* 28**,** 5144-5157.
Nolte, M. W. & Shanks, B. H. 2017. A Perspective On Catalytic Strategies For Deoxygenation In Biomass Pyrolysis. *Energy Technology,* 5**,** 7-18.
Nordin, A. 1994. Chemical Elemental Characteristics Of Biomass Fuels. *Biomass And Bioenergy,* 6**,** 339-347.
Northern Natal News, S. M. 2021. *Ladysmith Kzn: Chaos As Flooding Continues In Many Areas Of The Cbd* [Online]. Ladysmith: Ladysmith Gazzette. Available: Https://Northernnatalnews.Co.Za/327463/Ladysmith-Kzn-Chaos-As-Flooding-Continues-In-Many-Areas-Of-The-Cbd/ [Accessed July 1, 2021 2021].
Oasmaa, A., Kuoppala, E. & Elliott, D. C. 2012. Development Of The Basis For An Analytical Protocol For Feeds And Products Of Bio-Oil Hydrotreatment. *Energy & Fuels,* 26**,** 2454-2460.
Oh, S., Hwang, H., Choi, H. S. & Choi, J. W. 2015. The Effects Of Noble Metal Catalysts On The Bio-Oil Quality During The Hydrodeoxygenative Upgrading Process. *Fuel,* 153**,** 535-543.
Ohyama, T. 2010. Nitrogen As A Major Essential Element Of Plants. *Nitrogen Assim. Plants,* 37**,** 1-17.
Omar, S., Alsamaq, S., Yang, Y. & Wang, J. 2019. Production Of Renewable Fuels By Blending Bio-Oil With Alcohols And Upgrading Under Supercritical Conditions. *Frontiers Of Chemical Science And Engineering,* 13**,** 702-717.
Ortega, Z., Bolaji, I., Suárez, L. & Cunningham, E. 2024. A Review Of The Use Of Giant Reed (Arundo Donax L.) In The Biorefineries Context. *Reviews In Chemical Engineering,* 40**,** 305-328.
Oudenhoven, S., Lievens, C., Westerhof, R. J. M. & Kersten, S. R. 2016. Effect Of Temperature On The Fast Pyrolysis Of Organic-Acid Leached Pinewood; The Potential Of Low Temperature Pyrolysis. *Biomass And Bioenergy,* 89**,** 78-90.
Panwar, N. L. & Paul, A. S. 2021. An Overview Of Recent Development In Bio-Oil Upgrading And Separation Techniques. *Environmental Engineering Research,* 26.
Park, G., Kang, J., Park, S.-J., Kim, Y. T., Kwak, G. & Kim, S. 2022. Effect Of Acid Modification Of Zsm-5 Catalyst On Performance And Coke Formation For Methanol-To-Hydrocarbon Reaction. *Molecular Catalysis,* 531**,** 112702.

Park, L. K.-E., Ren, S., Yiacoumi, S., Ye, X. P., Borole, A. P. & Tsouris, C. 2016. Separation Of Switchgrass Bio-Oil By Water/Organic Solvent Addition And Ph Adjustment. *Energy & Fuels,* 30**,** 2164-2173.
Park, Y.-K., Yoo, M. L., Jin, S. H. & Park, S. H. 2015. Catalytic Fast Pyrolysis Of Waste Pepper Stems Over Hzsm-5. *Renewable Energy,* 79**,** 20-27.
Patel, A., Agrawal, B. & Rawal, B. 2020. Pyrolysis Of Biomass For Efficient Extraction Of Biofuel. *Energy Sources, Part A: Recovery, Utilization, And Environmental Effects,* 42**,** 1649-1661.
Patel, M. & Kumar, A. 2016. Production Of Renewable Diesel Through The Hydroprocessing Of Lignocellulosic Biomass-Derived Bio-Oil: A Review. *Renewable And Sustainable Energy Reviews,* 58**,** 1293-1307.
Pawar, A., Panwar, N. & Salvi, B. 2020. Comprehensive Review On Pyrolytic Oil Production, Upgrading And Its Utilization. *Journal Of Material Cycles And Waste Management,* 22**,** 1712-1722.
Pecha, M. B. & Garcia-Perez, M. Pyrolysis Of Lignocellulosic Biomass: Oil, Char, And Gas. Bioenergy, 2020. Elsevier, 581-619.
Pidtasang, B., Sukkasi, S. & Pattiya, A. 2016. Effect Of In-Situ Addition Of Alcohol On Yields And Properties Of Bio-Oil Derived From Fast Pyrolysis Of Eucalyptus Bark. *Journal Of Analytical And Applied Pyrolysis,* 120**,** 82-93.
Pilu, R., Bucci, A., Badone, F. C. & Landoni, M. 2012. Giant Reed (Arundo Donax L.): A Weed Plant Or A Promising Energy Crop. *Afr. J. Biotechnol,* 11**,** 9163-9174.
Prajitno, H., Insyani, R., Park, J., Ryu, C. & Kim, J. 2016. Non-Catalytic Upgrading Of Fast Pyrolysis Bio-Oil In Supercritical Ethanol And Combustion Behavior Of The Upgraded Oil. *Applied Energy,* 172**,** 12-22.
Promsampao, N., Chollacoop, N. & Pattiya, A. 2022. Regeneration Of Pristine Hzsm-5 Extrudates During The Production Of Deeply Deoxygenated Bio-Oil From Ex Situ Catalytic Fast Pyrolysis Of Biomass In A Bench-Scale Fluidised-Bed Reactor. *Reaction Chemistry & Engineering,* 7**,** 398-415.
Qian, K., Kumar, A., Zhang, H., Bellmer, D. & Huhnke, R. 2015. Recent Advances In Utilization Of Biochar. *Renewable And Sustainable Energy Reviews,* 42**,** 1055-1064.
Qin, C., Wang, H., Yuan, X., Xiong, T., Zhang, J. & Zhang, J. 2020. Understanding Structure-Performance Correlation Of Biochar Materials In Environmental Remediation And Electrochemical Devices. *Chemical Engineering Journal,* 382**,** 122977.
Qin, Y., Yan, X., Xu, W., Zhang, X., Huang, M., Peng, H. & Ma, Z. 2024. Production Of Monocyclic Aromatic Hydrocarbons By The Catalytic Pyrolysis Of Moso Bamboo At Different Ages And Parts Using Zn And Cr Modified Zeolite Catalysts. *Journal Of Analytical And Applied Pyrolysis***,** 106558.
Qiu, B., Deng, N., Zhang, Y. & Wan, H. 2018. Application Of Industrial Solid Wastes In Catalytic Pyrolysis. *Asia-Pacific Journal Of Chemical Engineering,* 13**,** E2150.
Qu, L., Jiang, X., Zhang, Z., Zhang, X.-G., Song, G.-Y., Wang, H.-L., Yuan, Y.-P. & Chang, Y.-L. 2021. A Review Of Hydrodeoxygenation Of Bio-Oil: Model Compounds, Catalysts, And Equipment. *Green Chemistry,* 23**,** 9348-9376.

Rahman, M. M., Chai, M., Sarker, M. & Liu, R. 2020. Catalytic Pyrolysis Of Pinewood Over Zsm-5 And Cao For Aromatic Hydrocarbon: Analytical Py-Gc/Ms Study. *Journal Of The Energy Institute,* 93**,** 425-435.
Rahman, M. M., Liu, R. & Cai, J. 2018. Catalytic Fast Pyrolysis Of Biomass Over Zeolites For High Quality Bio-Oil–A Review. *Fuel Processing Technology,* 180**,** 32-46.
Rajaei, H., Esmaeilzadeh, F. & Mowla, D. 2021. Elucidation Of Si/Al Ratio On Physicochemical Properties Of Hzsm-5 Zeolites. *Journal Of Thermal Analysis And Calorimetry,* 146**,** 581-586.
Rajapaksha, A. U., Chen, S. S., Tsang, D. C., Zhang, M., Vithanage, M., Mandal, S., Gao, B., Bolan, N. S. & Ok, Y. S. 2016. Engineered/Designer Biochar For Contaminant Removal/Immobilization From Soil And Water: Potential And Implication Of Biochar Modification. *Chemosphere,* 148**,** 276-291.
Ramsey, E., Qiubai, S., Zhang, Z., Zhang, C. & Wei, G. 2009. Mini-Review: Green Sustainable Processes Using Supercritical Fluid Carbon Dioxide. *Journal Of Environmental Sciences,* 21**,** 720-726.
Ramsurrun, B. R. & Surroop, D. 2019. Biofuel From Thermally Treated Giant Reed. *Sustainable Energy Technologies And Assessments,* 35**,** 230-244.
Rangel, M. D. C., Mayer, F. M., Carvalho, M. D. S., Saboia, G. & De Andrade, A. M. 2023. Selecting Catalysts For Pyrolysis Of Lignocellulosic Biomass. *Biomass,* 3**,** 31-63.
Rathore, N., Sanjay Paul, A. & Panwar, N. 2020. Experimental Investigation On The Production Of Bio-Oil From Maize Straw At A Pilot Scale. *Environmental Engineering Research,* 27**,** 200592.
Remón, J., Arauzo, J., García, L., Arcelus-Arrillaga, P., Millan, M., Suelves, I. & Pinilla, J. 2016. Bio-Oil Upgrading In Supercritical Water Using Ni-Co Catalysts Supported On Carbon Nanofibres. *Fuel Processing Technology,* 154**,** 178-187.
Rezaei, P. S., Shafaghat, H. & Daud, W. M. A. W. 2014. Production Of Green Aromatics And Olefins By Catalytic Cracking Of Oxygenate Compounds Derived From Biomass Pyrolysis: A Review. *Applied Catalysis A: General,* 469**,** 490-511.
Rosdiana, F., Falahudin, A., Wibowo, R. H. & Gustian, I. Preparation Of Silver-Incorporated Rhynchospora Corymbosa (L.) Cellulose Via In-Situ Green Reduction And Its Antibacterial Study. Iop Conference Series: Materials Science And Engineering, 2020. Iop Publishing, 012090.
Rout, T., Pradhan, D., Singh, R. & Kumari, N. 2016. Exhaustive Study Of Products Obtained From Coconut Shell Pyrolysis. *Journal Of Environmental Chemical Engineering,* 4**,** 3696-3705.
Roy, P., Jahromi, H., Rahman, T., Adhikari, S., Feyzbar-Khalkhali-Nejad, F. & Oh, T.-S. 2022. Understanding The Effects Of Feedstock Blending And Catalyst Support On Hydrotreatment Of Algae Htl Biocrude With Non-Edible Vegetable Oil. *Energy Conversion And Management,* 268**,** 115998.
Saffe, A., Fernandez, A., Echegaray, M., Mazza, G. & Rodriguez, R. 2019. Pyrolysis Kinetics Of Regional Agro-Industrial Wastes Using Isoconversional Methods. *Biofuels,* 10**,** 245-257.
Saikia, R., Chutia, R. S., Kataki, R. & Pant, K. K. 2015. Perennial Grass (Arundo Donax L.) As A Feedstock For Thermo-Chemical Conversion To Energy And Materials. *Bioresource Technology,* 188**,** 265-272.

Sakhiya, A. K., Anand, A. & Kaushal, P. 2020. Production, Activation, And Applications Of Biochar In Recent Times. *Biochar,* 2**,** 253-285.
Sánchez, J., Curt, M. D., Robert, N. & Fernández, J. 2019. Biomass Resources. *The Role Of Bioenergy In The Bioeconomy*. Elsevier.
Santos, J., Ouadi, M., Jahangiri, H. & Hornung, A. 2020. Valorisation Of Lignocellulosic Biomass Investigating Different Pyrolysis Temperatures. *Journal Of The Energy Institute,* 93**,** 1960-1969.
Santos, J., Pereira, J., Ferreira, N., Paiva, N., Ferra, J., Magalhães, F., Martins, J., Dulyanska, Y. & Carvalho, L. 2021. Valorisation Of Non-Timber By-Products From Maritime Pine (Pinus Pinaster, Ait) For Particleboard Production. *Industrial Crops And Products,* 168**,** 113581.
Satya, S., Singhal, P., Bal, L. M. & Sudhakar, P. 2012. Bamboo Shoot: A Potential Source Of Food Security. *Mediterranean Journal Of Nutrition And Metabolism,* 5**,** 1-10.
Sebestyén, Z., Barta-Rajnai, E., Bozi, J., Blazsó, M., Jakab, E., Miskolczi, N., Sója, J. & Czégény, Z. 2017. Thermo-Catalytic Pyrolysis Of Biomass And Plastic Mixtures Using Hzsm-5. *Applied Energy,* 207**,** 114-122.
Shah, M. A., Khan, N., Kumar, V. & Qurashi, A. 2021. Pyrolysis Of Walnut Shell Residues In A Fixed Bed Reactor: Effects Of Process Parameters, Chemical And Functional Properties Of Bio-Oil. *Journal Of Environmental Chemical Engineering,* 9**,** 105564.
Shao, S., Zhang, H., Xiao, R. & Shen, D. 2017. Catalytic Conversion Of Furan To Hydrocarbons Using Hzsm-5: Coking Behavior And Kinetic Modeling Including Coke Deposition. *Energy Technology,* 5**,** 111-118.
Shende, V. S., Saptal, V. B. & Bhanage, B. M. 2019. Recent Advances Utilized In The Recycling Of Homogeneous Catalysis. *The Chemical Record,* 19**,** 2022-2043.
Shezi, M., Kiambi, S. L. & Isa, Y. M. 2024. Seasonal Harvesting Impact On Biomass Fuel Properties And Pyrolysis-Derived Bio-Oil Organic Phase Composition. *Gcb Bioenergy,* 16**,** E70011.
Shumeiko, B., Auersvald, M., Straka, P., Šimáček, P., Vrtiška, D. & Kubička, D. 2020. Efficient One-Stage Bio-Oil Upgrading Over Sulfided Catalysts. *Acs Sustainable Chemistry & Engineering,* 8**,** 15149-15167.
Shun, T., Zhang, Z., Jianping, S. & Qingwen, W. 2013. Recent Progress Of Catalytic Pyrolysis Of Biomass By Hzsm-5. *Chinese Journal Of Catalysis,* 34**,** 641-650.
Si, Z., Zhang, X., Wang, C., Ma, L. & Dong, R. 2017. An Overview On Catalytic Hydrodeoxygenation Of Pyrolysis Oil And Its Model Compounds. *Catalysts,* 7**,** 169.
Silverstein, R. M., Webster, F. X., Kiemle, D. J. & Bryce, D. L. 2014. *Spectrometric Identification Of Organic Compounds,* John Wiley & Sons.
Sluiter, A., Hames, B., Ruiz, R., Scarlata, C., Sluiter, J., Templeton, D. & Crocker, D. 2008. Determination Of Structural Carbohydrates And Lignin In Biomass. *Laboratory Analytical Procedure,* 1617**,** 1-16.
Sluiter, A., Hames, B., Ruiz, R., Scarlata, C., Sluiter, J., Templeton, D. & Crocker, D. 2012. Laboratory Analytical Procedure (Lap): Determination Of Structural Carbohydrates And Lignin In Biomass, Nrel/Tp-510-42618.
Sluiter, A., Ruiz, R., Scarlata, C., Sluiter, J. & Templeton, D. 2005. Determination Of Extractives In Biomass. *Laboratory Analytical Procedure (Lap),* 1617**,** 1-16.

Smith, A. L., Klenk, N., Wood, S., Hewitt, N., Henriques, I., Yan, N. & Bazely, D. R. 2013. Second Generation Biofuels And Bioinvasions: An Evaluation Of Invasive Risks And Policy Responses In The United States And Canada. *Renewable And Sustainable Energy Reviews,* 27**,** 30-42.
Smith, R. & Slater, F. M. 2011. Mobilization Of Minerals And Moisture Loss During Senescence Of The Energy Crops Miscanthus× Giganteus, Arundo Donax And Phalaris Arundinacea In Wales, Uk. *Gcb Bioenergy,* 3**,** 148-157.
Stark, N. M., Yelle, D. J. & Agarwal, U. P. 2016. Techniques For Characterizing Lignin. *Lignin In Polymer Composites,* 2016**,** 49-66.
Suárez, L., Barczewski, M., Kosmela, P., Marrero, M. D. & Ortega, Z. 2023. Giant Reed (Arundo Donax L.) Fiber Extraction And Characterization For Its Use In Polymer Composites. *Journal Of Natural Fibers,* 20**,** 2131687.
Sun, X., Atiyeh, H. K., Li, M. & Chen, Y. 2020. Biochar Facilitated Bioprocessing And Biorefinery For Productions Of Biofuel And Chemicals: A Review. *Bioresource Technology,* 295**,** 122252.
Suttibak, S., Sriprateep, K. & Pattiya, A. 2012. Production Of Bio-Oil Via Fast Pyrolysis Of Cassava Rhizome In A Fluidised-Bed Reactor. *Energy Procedia,* 14**,** 668-673.
Taarning, E., Osmundsen, C. M., Yang, X., Voss, B., Andersen, S. I. & Christensen, C. H. 2011. Zeolite-Catalyzed Biomass Conversion To Fuels And Chemicals. *Energy & Environmental Science,* 4**,** 793-804.
Tan, K. T. & Lee, K. T. 2011. A Review On Supercritical Fluids (Scf) Technology In Sustainable Biodiesel Production: Potential And Challenges. *Renewable And Sustainable Energy Reviews,* 15**,** 2452-2456.
Tan, Y., Abdullah, A. & Hameed, B. 2017. Fast Pyrolysis Of Durian (Durio Zibethinus L) Shell In A Drop-Type Fixed Bed Reactor: Pyrolysis Behavior And Product Analyses. *Bioresource Technology,* 243**,** 85-92.
Tang, Z., Zhang, Y. & Guo, Q. 2010. Catalytic Hydrocracking Of Pyrolytic Lignin To Liquid Fuel In Supercritical Ethanol. *Industrial & Engineering Chemistry Research,* 49**,** 2040-2046.
Tawalbeh, M., Al-Othman, A., Salamah, T., Alkasrawi, M., Martis, R. & El-Rub, Z. A. 2021. A Critical Review On Metal-Based Catalysts Used In The Pyrolysis Of Lignocellulosic Biomass Materials. *Journal Of Environmental Management,* 299**,** 113597.
Temiz, A., Akbas, S., Panov, D., Terziev, N., Alma, M. H., Parlak, S. & Kose, G. 2013. Chemical Composition And Efficiency Of Bio-Oil Obtained From Giant Cane (Arundo Donax L.) As A Wood Preservative. *Bioresources,* 8**,** 2084-2098.
Tong, W., Cai, Z., Liu, Q., Ren, S. & Kong, M. 2020. Effect Of Pyrolysis Temperature On Bamboo Char Combustion: Reactivity, Kinetics And Thermodynamics. *Energy,* 211**,** 118736.
Toor, S. S., Rosendahl, L. & Rudolf, A. 2011. Hydrothermal Liquefaction Of Biomass: A Review Of Subcritical Water Technologies. *Energy,* 36**,** 2328-2342.
Tran, Q. K., Le, M. L., Ly, H. V., Woo, H. C., Kim, J. & Kim, S.-S. 2021. Fast Pyrolysis Of Pitch Pine Biomass In A Bubbling Fluidized-Bed Reactor For Bio-Oil Production. *Journal Of Industrial And Engineering Chemistry*, 98**,** 168-179.
Trubetskaya, A., Von Berg, L., Johnson, R., Moore, S., Leahy, J., Han, Y., Lange, H. & Anca-Couce, A. 2023. Production And Characterization Of Bio-Oil From Fluidized Bed Pyrolysis

Of Olive Stones, Pinewood, And Torrefied Feedstock. *Journal Of Analytical And Applied Pyrolysis,* 169**,** 105841.
Tsekos, C., Tandurella, S. & De Jong, W. 2021. Estimation Of Lignocellulosic Biomass Pyrolysis Product Yields Using Artificial Neural Networks. *Journal Of Analytical And Applied Pyrolysis,* 157**,** 105180.
Valizadeh, S., Pyo, S., Kim, Y.-M., Hakimian, H. & Park, Y.-K. 2022. Production Of Aromatics Fuel Additives From Catalytic Pyrolysis Of Cow Manure Over Hzsm-5, Hbeta, And Hy Zeolites. *Chemical Engineering Journal,* 450**,** 137971.
Valle, B., Palos, R., Bilbao, J. & Gayubo, A. G. 2022. Role Of Zeolite Properties In Bio-Oil Deoxygenation And Hydrocarbons Production By Catalytic Cracking. *Fuel Processing Technology,* 227**,** 107130.
Van Krevelen, D. W. 1993. Coal: Typology-Physics-Chemistry-Constitution.
Van Soest, P. V., Robertson, J. B. & Lewis, B. A. 1991. Methods For Dietary Fiber, Neutral Detergent Fiber, And Nonstarch Polysaccharides In Relation To Animal Nutrition. *Journal Of Dairy Science,* 74**,** 3583-3597.
Varma, A. K. & Mondal, P. 2017. Pyrolysis Of Sugarcane Bagasse In Semi Batch Reactor: Effects Of Process Parameters On Product Yields And Characterization Of Products. *Industrial Crops And Products,* 95**,** 704-717.
Varma, A. K. & Mondal, P. 2018. Pyrolysis Of Pine Needles: Effects Of Process Parameters On Products Yield And Analysis Of Products. *Journal Of Thermal Analysis And Calorimetry,* 131**,** 2057-2072.
Varma, A. K., Shankar, R. & Mondal, P. 2018. A Review On Pyrolysis Of Biomass And The Impacts Of Operating Conditions On Product Yield, Quality, And Upgradation. *Recent Advancements In Biofuels And Bioenergy Utilization.* Springer.
Van Krevelen, D. W. 1993. *Coal: Typology - Physics - Chemistry - Constitution,* Netherlands, Amsterdam (Netherlands); Elsevier Science Publishers;.
Wang, D.-L., Chen, Z.-H., Jian, Y. & Gao, S.-Q. 2021. Effect Of Si/Al Ratio Of Hzsm-5 Zeolites On Catalytic Upgrading Of Coal Pyrolysis Volatiles. *Journal Of Fuel Chemistry And Technology,* 49**,** 634-641.
Wang, G.-C. & Nakamura, J. 2010. Structure Sensitivity For Forward And Reverse Water-Gas Shift Reactions On Copper Surfaces: A Dft Study. *The Journal Of Physical Chemistry Letters,* 1**,** 3053-3057.
Wang, H., Male, J. & Wang, Y. 2013. Recent Advances In Hydrotreating Of Pyrolysis Bio-Oil And Its Oxygen-Containing Model Compounds. *Acs Catalysis,* 3**,** 1047-1070.
Wang, R.-Z., Huang, D.-L., Liu, Y.-G., Zhang, C., Lai, C., Wang, X., Zeng, G.-M., Gong, X.-M., Duan, A. & Zhang, Q. 2019. Recent Advances In Biochar-Based Catalysts: Properties, Applications And Mechanisms For Pollution Remediation. *Chemical Engineering Journal,* 371**,** 380-403.
Wang, T., Hovland, J. & Jens, K. J. 2015. Amine Reclaiming Technologies In Post-Combustion Carbon Dioxide Capture. *Journal Of Environmental Sciences,* 27**,** 276-289.
Wang, Y. & Wu, J. J. 2023. Thermochemical Conversion Of Biomass: Potential Future Prospects. *Renewable And Sustainable Energy Reviews,* 187**,** 113754.

Wang, Z., Ma, R. & Song, W. 2016. Influence Of Hsapo-34, Hzsm-5, And Nay On Pyrolysis Of Corn Straw Fermentation Residue Via Py-Gc/Ms. *Journal Of Analytical And Applied Pyrolysis,* 122**,** 183-190.
Wildschut, J., Mahfud, F. H., Venderbosch, R. H. & Heeres, H. J. 2009. Hydrotreatment Of Fast Pyrolysis Oil Using Heterogeneous Noble-Metal Catalysts. *Industrial & Engineering Chemistry Research,* 48**,** 10324-10334.
Xu, X., Zhang, C., Liu, Y., Zhai, Y. & Zhang, R. 2013. Two-Step Catalytic Hydrodeoxygenation Of Fast Pyrolysis Oil To Hydrocarbon Liquid Fuels. *Chemosphere,* 93**,** 652-660.
Xu, X., Zhang, C., Zhai, Y., Liu, Y., Zhang, R. & Tang, X. 2014. Upgrading Of Bio-Oil Using Supercritical 1-Butanol Over A Ru/C Heterogeneous Catalyst: Role Of The Solvent. *Energy & Fuels,* 28**,** 4611-4621.
Xu, Y., Duan, P. & Wang, B. 2015. Catalytic Upgrading Of Pretreated Algal Oil With A Two-Component Catalyst Mixture In Supercritical Water. *Algal Research,* 9**,** 186-193.
Yang, H., Yan, R., Chen, H., Lee, D. H. & Zheng, C. 2007. Characteristics Of Hemicellulose, Cellulose And Lignin Pyrolysis. *Fuel,* 86**,** 1781-1788.
Yao, Q., Tang, Z., Guo, J.-H., Zhang, Y. & Guo, Q.-X. 2015. Effect Of Catalyst Properties On Hydrocracking Of Pyrolytic Lignin To Liquid Fuel In Supercritical Ethanol. *Chinese Journal Of Chemical Physics,* 28**,** 209-216.
Yarulina, I., De Wispelaere, K., Bailleul, S., Goetze, J., Radersma, M., Abou-Hamad, E., Vollmer, I., Goesten, M., Mezari, B. & Hensen, E. J. 2018. Structure–Performance Descriptors And The Role Of Lewis Acidity In The Methanol-To-Propylene Process. *Nature Chemistry,* 10**,** 804-812.
Yathavan, B. K. & Agblevor, F. 2013. Catalytic Pyrolysis Of Pinyon–Juniper Using Red Mud And Hzsm-5. *Energy & Fuels,* 27**,** 6858-6865.
Yildiz, G., Ronsse, F., Venderbosch, R., Van Duren, R., Kersten, S. R. & Prins, W. 2015. Effect Of Biomass Ash In Catalytic Fast Pyrolysis Of Pine Wood. *Applied Catalysis B: Environmental,* 168**,** 203-211.
Yildiz, G. R., Lathouwers, T., Toraman, H. E., Van Geem, K. M., Marin, G. B., Ronsse, F., Van Duren, R., Kersten, S. R. & Prins, W. 2014. Catalytic Fast Pyrolysis Of Pine Wood: Effect Of Successive Catalyst Regeneration. *Energy & Fuels,* 28**,** 4560-4572.
Yu, F., Deng, S., Chen, P., Liu, Y., Wan, Y., Olson, A., Kittelson, D. & Ruan, R. Physical And Chemical Properties Of Bio-Oils From Microwave Pyrolysis Of Corn Stover. Applied Biochemistry And Biotecnology: The Twenty-Eighth Symposium Proceedings Of The Twenty-Eight Symposium On Biotechnology For Fuels And Chemicals Held April 30–May 3, 2006, In Nashville, Tennessee, 2007. Springer, 957-970.
Zacher, A. H., Olarte, M. V., Santosa, D. M., Elliott, D. C. & Jones, S. B. 2014. A Review And Perspective Of Recent Bio-Oil Hydrotreating Research. *Green Chemistry,* 16**,** 491-515.
Zhang, C., Duan, P., Xu, Y., Wang, B., Wang, F. & Zhang, L. 2014a. Catalytic Upgrading Of Duckweed Biocrude In Subcritical Water. *Bioresource Technology,* 166**,** 37-44.
Zhang, J., Luo, Z., Dang, Q., Wang, J. & Chen, W. 2012. Upgrading Of Bio-Oil Over Bifunctional Catalysts In Supercritical Monoalcohols. *Energy & Fuels,* 26**,** 2990-2995.
Zhang, J., Tang, R., Shen, Z., Liang, S. & Zhong, H. 2020. Catalytic Oligomerization Of Ethylene Over Nano-Sized Hzsm-5. *Journal Of The Energy Institute,* 93**,** 2550-2557.

Zhang, M., Hu, Y., Wang, H., Li, H., Han, X., Zeng, Y. & Xu, C. C. 2021. A Review Of Bio-Oil Upgrading By Catalytic Hydrotreatment: Advances, Challenges, And Prospects. *Molecular Catalysis,* 504**,** 111438.
Zhang, Q., Chang, J., Wang, T. & Xu, Y. 2006. Upgrading Bio-Oil Over Different Solid Catalysts. *Energy & Fuels,* 20**,** 2717-2720.
Zhang, Q., Zhang, L., Wang, T., Xu, Y., Zhang, Q., Ma, L., He, M. & Li, K. 2014b. Upgrading Of Bio-Oil By Removing Carboxylic Acids In Supercritical Ethanol. *Energy Procedia,* 61**,** 1033-1036.
Zhang, X. & Brown, R. C. 2019. Introduction To Thermochemical Processing Of Biomass Into Fuels, Chemicals, And Power. *Thermochemical Processing Of Biomass: Conversion Into Fuels, Chemicals And Power***,** 1-16.
Zhang, Y., Chen, P. & Lou, H. 2016. In Situ Catalytic Conversion Of Biomass Fast Pyrolysis Vapors On Hzsm-5. *Journal Of Energy Chemistry,* 25**,** 427-433.

9. APPENDICES

9.1 Appendix A: Acid Hydrolysis Sample Calculation

The water and ethanol extractives for pine biomass were determined as follows:

At a moisture content of 0.0676, the total solids were determined as follows,

$$\text{Total Solids} = 1 - \text{MC} = 1 - 0.0676 = 0.932$$

At a biomass sample of 10 g, the oven dry weight was determined as follows,

$$\text{ODW} = \text{m}_{\text{sample}} \times \text{Total Solids}$$

$$= 10 \times 0.932$$

$$= 9.324 \text{ g}$$

The water extractives were calculated as follows,

$$\%\text{Extractives}_{\text{water}} = \frac{\text{Dish Weight} + \text{Extractives} - \text{Dish Weight}}{\text{ODW}} \times 100$$

$$= \frac{4.722 - 4.581}{9.324} \times 100$$

$$= 1.52\%$$

The ethanol extractives were calculated as follows,

$$\%\text{Extractives}_{\text{ethanol}} = \frac{\text{Dish Weight} + \text{Extractives} - \text{Dish Weight}}{\text{ODW}} \times 100$$

$$= \frac{2.47 - 2.31}{9.324} \times 100$$

$$= 1.72\%$$

After extraction, hydrolysis was performed using ODW of 0.3 g, and the determination of total lignin in pine biomass was determined by initially determining acid insoluble residue (AIR) as follows,

$$\%\text{AIR} = \frac{\text{m}_{\text{sample+crucible}} - \text{m}_{\text{crucible}}}{\text{ODW}} \times 100$$

$$= \frac{34.640 - 34.526}{0.3} \times 100$$

$$= 37.8\%$$

Following the sequential drying and oxidation of the sample, the ash in the filter (AIF) was determined as follows,

$$\%\text{AIF} = \frac{\text{m}_{\text{AIR}} - \text{m}_{\text{ASH}}}{\text{ODW}} \times 100$$

$$= \frac{34.526 - 34.441}{0.3} \times 100$$

$$= 28.4\%$$

The acid-insoluble lignin (AIL) was determined as follows,

$$\%\text{AIL} = \%\text{AIR} - \%\text{AIF}$$
$$= 37.8 - 28.4$$
$$= 9.37\%$$

The acid-soluble lignin (ASL) was determined at an absorbance (UV_{abs}) of 0.514 absorptivity (ε) of biomass at a specific wavelength of 12 L/g.cm. The volume of filtrate ($V_{filtrate}$) of 86.73 ml was used with a dilution of 10 and a pathlength of 1.

$$\%\text{ASL} = \frac{\text{UV}_{\text{abs}} \times \text{V}_{\text{filtrate}} \times \text{Dilution}}{\varepsilon \times \text{ODW} \times \text{Pathlength}}$$

$$= \frac{0.514 \times 0.08673 \times 10}{12 \times 0.3 \times 1}$$

$$= 12.4\%$$

The total lignin was determined as follows,

$$\%\text{Lignin} = \%\text{AIL} + \%\text{ASL}$$
$$= 9.37 + 12.4$$
$$= 21.8\%$$

9.2 Appendix B: Seasonal Effect GCMS Analysis Data

Table 9. 1: GCMS analysis of BOP from Giant Reed biomass during HS-4 season.

Peak#	Ret.Time	Name	Ret. Index	Area%	Height%	SI
1	3,093	1,3-Benzenediol (CAS)	Phenolics	15,99	0,22	87
2	3,311	PHENOL, 2-METHOXY-	Phenolics	11,21	0,52	84
3	3,878	Phenol, 2,6-dimethoxy- (CAS)	Phenolics	8,49	1,17	76
4	4,011	1,2-BENZENEDIOL, 3-METHOXY-	Phenolics	8,38	1,64	94
5	4,379	4 METHYL CATECHOL	Phenolics	6	0,76	69
6	4,567	Butane, 2-methyl- (CAS)	Olefins	5,32	0,31	79
7	4,734	2-Cyclopenten-1-one, 2-hydroxy-3-methyl- (CAS)	Ketones	4,88	2,54	88
8	5,086	Phenol (CAS)	Phenolics	3,85	4,14	95
9	5,362	**(+)-s-2-Phenethanamine, 1-methyl-N-vanillyl-**	**Amines**	**3,78**	1,73	77
10	5,622	3,5-Dimethoxy-4-hydroxytoluene	Phenolics	3,77	8,25	84
11	5,798	2-Cyclopenten-1-one, 3-ethyl-2-hydroxy-	Ketones	3,51	4,77	86
12	5,948	1,2-Cyclopentanedione	Ketones	3,2	3,25	89
13	6,215	1,3-Benzenediol, 4-ethyl- (CAS)	Phenolics	2,4	0,89	84
14	6,404	Phenol, 3-methyl- (CAS)	Phenolics	1,96	2,14	90
15	6,548	1,4-Benzenediol, 2,6-dimethyl-	Phenolics	1,96	2,21	94
16	6,883	Phenol, 4-ethyl-	Phenolics	1,91	9,82	81
17	7,247	R(-)-1-Cyano-2-methylpyrrolidine	Amines	1,79	8,32	88
18	7,567	4,6-Dipropyl-nonan-5-one	Ketones	1,54	4,37	87
19	7,855	Creosol	Phenolics	1,43	16,25	91
20	7,995	Phenol, 3,5-dimethyl- (CAS)	Phenolics	1,36	2,95	72
21	8,104	Furan, 2,5-dimethyl- (CAS)	Furans	1,14	1,88	78
22	8,231	Ethanone, 1-(4-hydroxy-3-methoxyphenyl)- (CAS)	Ketones	1,1	2,55	82
23	8,376	Nordavanone	Phenolics	1,04	1,53	68
24	8,526	Idosan triacetate	Esters	0,78	6,19	87
25	8,888	2-Butanone, 3-methyl- (CAS)	Ketones	0,71	0,98	89
26	9,162	3,5-Dimethoxy-4-hydroxyphenylacetic acid	Acids	0,58	**4,47**	**78**
27	9,309	Benzaldehyde, 4-hydroxy-3,5-dimethoxy- (CAS)	Aldehydes	0,31	1,02	82
28	9,565	Ethanone, 1-(4-hydroxy-3,5-dimethoxyphenyl)- (CAS)	Ketones	0,28	0,63	88
29	9,666	(E)-2,6-Dimethoxy-4-(prop-1-en-1-yl)phenol	Phenolics	0,27	0,25	76
30	9,886	(E)-2,6-Dimethoxy-4-(prop-1-en-1-yl)phenol	Phenolics	0,27	0,44	88
31	10,014	(E)-2,6-Dimethoxy-4-(prop-1-en-1-yl)phenol	Phenolics	0,2	0,53	95
32	10,197	Pyridine, 4-methyl- (CAS)	Aromatics	0,19	0,66	94
33	10,446	Furan-2-carbonyl chloride, tetrahydro-	Furans	0,14	0,63	93
34	10,644	1,2-Cyclohexanediol, monoacetate	Esters	0,1	1,62	78
35	10,965	1,2-Benzenedicarboxylic acid, bis(2-ethylhexyl) ester (CAS)	Esters	0,09	0,15	79
36	14,696	Ethanone, 1-(4-hydroxy-3,5-dimethoxyphenyl)- (CAS)	Ketones	0,07	0,2	97
				100		

Table 9. 2: GCMS analysis of BOP from Giant Reed biomass during HS-1 season.

Peak#	Ret.Time	Name	Ret. Index	Area%	Height%	SI
1	3,236	1,2-Benzenediol (CAS)	Phenolics	12,26	0,51	93
2	3,287	D-Allose	Sugars	11,56	0,46	93
3	3,36	4 METHYL CATECHOL	Phenolics	5,58	0,91	93
4	3,416	4-Hydroxy-2-methoxybenaldehyde	Aldehydes	5,4	1,3	92
5	3,531	2-FURANCARBOXALDEHYDE, 5-(HYDROXYMETHYL)-	Furans	5,34	1,69	87
6	3,665	anhydro - sugar	Sugars	5,33	1,2	93
7	3,807	Ethanone, 1-(1-cyclohexen-1-yl)- (CAS)	Ketones	4,4	0,57	93
8	3,915	(+)-s-2-Phenethanamine, 1-methyl-N-vanillyl-	Amines	4,3	0,15	89
9	4,066	1,6-ANHYDRO-BETA-D-GLUCOPYRANOSE (LEVOGLUCOSAN)	Sugars	4,04	1,16	94
10	4,167	1,2-Benzenediol, 3-methyl- (CAS)	Phenolics	3,81	0,42	81
11	4,418	2-Vinyl-9-[3-deoxy-.beta.-d-ribofuranosyl]hypoxanthine	Nucleoside	3,07	1,06	80
12	4,66	2-Cyclopenten-1-one, 2-hydroxy-3-methyl- (CAS)	Ketones	3	0,11	93
13	4,834	2,5-Dimethoxytetrahydrofuran	Furans	2,83	0,52	77
14	4,975	Ethanone, 1-(4-hydroxy-3-methoxyphenyl)- (CAS)	Ketones	2,22	0,55	84
15	5,12	Phenol, 2,6-dimethoxy- (CAS)	Phenolics	2,13	4,18	96
16	5,342	Creosol	Phenolics	1,74	2,32	78
17	5,52	Butanoic acid, propyl ester (CAS)	Esters	1,59	1,08	81
18	5,656	Benzenepropanol, 4-hydroxy-3-methoxy-	Phenolics	1,56	3,2	78
19	5,783	2-Cyclopenten-1-one, 3-ethyl-2-hydroxy-	Ketones	1,39	4,81	92
20	5,962	UNDECANE, 6,6-DIDEUTERO-3-METHYL-	Aliphatic	1,24	1,72	89
21	6,068	2,5-Dimethoxytetrahydrofuran	Furans	1,17	1,18	78
22	6,244	.GAMMA. HEXALACTONE	Esters	1,11	0,43	76
23	6,445	4-Dimethyl(isopropyl)silyloxyoctane	Organosilicon/Aliphatic	1,09	0,66	70
24	6,558	2-Amino-6-(isopropylamino)1,3,5-triazine	Amines	1,08	2,77	95
25	6,615	Furan, tetrahydro-2,5-dimethoxy-	Furans	1,07	1,51	83
26	6,725	2-Oxiranecarboxylic acid, 3-(2,2-dimethoxyethyl)-3-methyl-, methyl ester	Esters	1,02	2,19	81
27	6,823	1,4-BENZENEDIOL, 2-METHOXY-	Phenolics	1	9,16	87
28	7,013	1,4:3,6-Dianhydro-.alpha.-d-glucopyranose	Sugars	0,94	4,4	95
29	7,23	1,2,4-Cyclopentanetriol (CAS)	Cyclopentanetriols/Polyol	0,86	1,72	78
30	7,316	Phenol (CAS)	Phenolics	0,85	2,89	84
31	7,438	2(5H)-Furanone	Ketones	0,83	1,4	71
32	7,557	Phenol, 2,4-dimethyl- (CAS)	Phenolics	0,77	3,72	90
33	7,786	3-Furanol, tetrahydro- (CAS)	Furans	0,67	1,51	79
34	7,832	4-Methoxymethylphenol	Phenolics	0,67	3,35	94
35	7,979	2,5-Dimethoxytetrahydrofuran	Furans	0,55	0,91	70
36	8,075	Ethanone, 1-(4-hydroxy-3-methoxyphenyl)- (CAS)	Ketones	0,44	0,48	71
37	8,261	4-(1-Hydroxyallyl)-2-methoxyphenol	Phenolics	0,42	5,5	84
38	8,51	Furan, tetrahydro-2,5-dimethoxy-	Furans	0,4	0,66	84
39	8,8	2-Piperidinimine	Amines	0,33	4,26	95
40	8,87	3,5-Dimethoxy-4-hydroxytoluene	Phenolics	0,31	3,26	94
41	9,048	Idosan triacetate	Esters	0,29	0,54	80
42	9,15	2,5-Dimethoxytetrahydrofuran	Furans	0,28	6,18	79
43	9,278	4-Ethyl-3,7-nonandione	Ketones	0,23	8,24	94
44	9,446	Benzene, 1,2,3-trimethoxy-5-methyl- (CAS)	Aromatics	0,18	0,98	96
45	9,526	Butanoic acid, 2-propenyl ester (CAS)	Esters	0,17	0,58	83
46	9,642	1,2-Benzenedicarboxylic acid, bis(2-ethylhexyl) ester (CAS)	Esters	0,15	0,56	81
47	9,869	Benzeneacetic acid, .alpha.,4-dihydroxy-3-methoxy-, methyl ester	Esters	0,13	0,35	88
48	9,929	.alpha.-Amino-3'-hydroxy-4'-methoxyacetophenone	Ketones	0,09	2,27	94
49	10,208	2(5H)-Furanone, 3-methyl- (CAS)	Ketones	0,07	0,15	81
50	14,699	3 - carboxy - 2 - propen - al	Aldehydes	0,06	0,28	96
				100,02		

Table 9. 3: GCMS analysis of BOP from Giant Reed biomass during HS-2 season.

Peak#	Ret.Time	Name	Ret. Index	Area%	Height%	SI
1	3,099	1,3-Benzenediol (CAS)	Phenolics	14,79	0,35	87
2	3,295	PHENOL, 2-METHOXY-	Phenolics	13,74	0,84	84
3	3,34	Phenol, 2,6-dimethoxy- (CAS)	Phenolics	10,28	0,82	80
4	3,531	1,2-Benzenediol, 3-methoxy-	Phenolics	6,95	0,16	91
5	3,865	anhydro - sugar	Sugars	6,36	0,81	73
6	3,91	2-Cyclopenten-1-one, 2-hydroxy-3-methyl- (CAS)	Ketones	5,23	1,06	95
7	4,002	4 METHYL CATECHOL	Phenolics	4,51	1,06	84
8	4,095	2-Cyclopenten-1-one, 3-ethyl-2-hydroxy-	Ketones	4,45	0,68	76
9	4,351	3,5-Dimethoxy-4-hydroxytoluene	Phenolics	3,78	1,2	68
10	4,75	(+)-s-2-Phenethanamine, 1-methyl-N-vanillyl-	Amines	3,06	1,85	82
11	5,075	PHENOL	Phenolics	2,9	3,7	94
12	5,367	3-(5-Methyl-1,3,4-oxadiazol-2-yl)propanoic acid	Acids	2,86	0,98	71
13	5,621	4-Ethylcatechol	Phenolics	1,9	8,31	88
14	5,838	Phenol, 4-ethyl- (CAS)	Phenolics	1,74	5,02	90
15	5,934	Creosol	Phenolics	1,72	2,87	88
16	6,403	3-Decanone (CAS)	Ketones	1,6	1,85	89
17	6,544	1,4-Benzenediol, 2,6-dimethyl-	Phenolics	1,53	2,55	95
18	6,888	DL-Lysine, N2,N6-bis[(phenylmethoxy)carbonyl]- (CAS)	Acids	1,49	8,91	74
19	7,252	Benzene, 1,2,3-trimethoxy-5-methyl-	Aromatics	1,26	7,92	80
20	7,596	1,2-Cyclopentanedione	Ketones	1,18	2,52	80
21	7,85	3,3-dimethylcyclohexanol	Alcohols	0,87	16,85	91
22	7,997	5-Hexen-2-one (CAS)	Ketones	0,84	2,09	71
23	8,092	9-Oxabicyclo[3.3.1]nonan-2-one, 5-hydroxy-	Ketones	0,73	1,84	75
24	8,252	4,4-DIMETHYL DIOXANE	Ethers	0,72	1,58	75
25	8,363	Idosan triacetate	Esters	0,72	1,07	67
26	8,521	(E)-2,6-Dimethoxy-4-(prop-1-en-1-yl)phenol	Phenolics	0,61	6,44	88
27	8,883	3,5-Dimethoxy-4-hydroxyphenylacetic acid	Acids	0,61	0,73	89
28	9,058	Propanenitrile, 3-(dimethylamino)- (CAS)	Nitriles	0,51	4,04	82
29	9,157	Pyridine, 2-methyl- (CAS)	Amines	0,46	4,57	78
30	9,318	Ethanone, 1-(4-hydroxy-3-methoxyphenyl)- (CAS)	Ketones	0,41	0,87	75
31	9,561	(E)-2,6-Dimethoxy-4-(prop-1-en-1-yl)phenol	Phenolics	0,4	0,91	90
32	9,668	Furan-2-carbonyl chloride, tetrahydro-	Furans	0,36	0,25	77
33	9,882	(E)-2,6-Dimethoxy-4-(prop-1-en-1-yl)phenol	Phenolics	0,36	0,61	92
34	10,011	Benzaldehyde, 4-hydroxy-3,5-dimethoxy- (CAS)	Aldehydes	0,32	0,47	95
35	10,193	Ethanone, 1-(4-hydroxy-3,5-dimethoxyphenyl)- (CAS)	Ketones	0,25	1,73	94
36	10,444	Furan, tetrahydro-2,5-dimethoxy-	Furans	0,13	0,52	94
37	10,54	2-HYDROXYCYCLOHEXYL ACETATE #	Esters	0,11	0,09	90
38	10,641	1,2-Benzenedicarboxylic acid, bis(2-ethylhexyl) ester (CAS)	Esters	0,1	1,46	78
39	10,963	Ethanone, 1-(4-hydroxy-3,5-dimethoxyphenyl)- (CAS)	Ketones	0,09	0,16	80
40	11,08	Coniferyl aldehyde	Aldehydes	0,04	0,04	57
41	14,695	Methyl 3,5-tetradecadiynoate	Esters	0,01	0,19	97
				99,98		

Table 9. 4: GCMS analysis of BOP from Giant Reed biomass during HS-3 season.

Peak#	Ret.Time	Name	Ret. Index	Area%	Height%	SI
1	3,095	PHENOL, 2-METHOXY-	Phenolics	17,56	0,33	89
2	3,275	1,3-Benzenediol (CAS)	Phenolics	11,8	0,51	80
3	3,346	Phenol, 2,6-dimethoxy- (CAS)	Phenolics	8,46	0,72	76
4	3,544	2-Cyclopenten-1-one, 2-hydroxy-3-methyl- (CAS)	Ketones	6,08	0,32	91
5	3,868	Ethanone, 1-(3-cyclohexen-1-yl)-	Ketones	3,98	0,69	74
6	3,966	Phenol, 4-ethyl-2-methoxy-	Phenolics	3,41	1,03	88
7	3,995	anhydro - sugar	Sugars	3,23	0,97	87
8	4,05	2-Cyclopenten-1-one, 3-ethyl-2-hydroxy-	Ketones	3,09	0,86	74
9	4,14	N-OCTANAL DIMETHYLACETAL	Aliphatic	3,06	0,62	94
10	4,165	3,5-Dimethoxy-4-hydroxytoluene	Phenolics	2,97	0,5	94
11	4,327	(+)-s-2-Phenethanamine, 1-methyl-N-vanillyl-	Amines	2,82	1,48	69
12	4,742	Phenol (CAS)	Phenolics	2,68	1,62	84
13	5,093	1-Methyl-1-(2-buty)oxy)-1-silacyclobutane	Alkoxysilanes	2,39	4,34	92
14	5,361	2-Furancarboxaldehyde, 5-(hydroxymethyl)- (CAS)	Furans	2,37	1,01	71
15	5,62	4-Hydroxy-2-methoxybenaldehyde	Aldehydes	1,94	7,69	88
16	5,84	Phenol, 4-ethyl-	Phenolics	1,89	4,16	88
17	5,941	Oxirane, [(dodecyloxy)methyl]-	Ether	1,83	2,87	90
18	6,053	Creosol	Phenolics	1,74	1,39	76
19	6,4	2-propenyl butanoate	Esters	1,7	1,8	90
20	6,542	2-Ethoxy-4-methylphenol	Phenolics	1,65	2,64	95
21	6,715	3,5-DIMETHYL CYCLOPENTENOLONE	Ketones	1,54	1,72	75
22	6,905	3-Decanone (CAS)	Ketones	1,48	7,2	77
23	7,084	1,4-Benzenediol, 2-methyl-	Phenolics	1,15	2,06	90
24	7,252	Benzene, 1,2,3-trimethoxy-5-methyl-	Aromatics	1,09	6,32	73
25	7,32	3,4,4-Trimethyl-1-penten-3-ol	Alcohols	0,92	2,44	77
26	7,384	Phenol, 2-methoxy-4-propyl-	Phenolics	0,92	1,73	81
27	7,635	9-Oxabicyclo[3.3.1]nonan-2-one, 5-hydroxy-	Ketones	0,82	2,55	70
28	7,852	Pyridine, 2-methyl- (CAS)	Amines	0,78	12,9	92
29	7,935	Desaspidinol	Alcohols	0,75	1,6	78
30	8	1-(N-Phenylcarbamyl)-2-morpholinocyclohexene	Olefins	0,69	1,45	75
31	8,093	2(3H)-Furanone, dihydro- (CAS)	Ketones	0,66	1,52	75
32	8,284	1,2-Cyclopentanedione	Ketones	0,56	1,82	88
33	8,367	.ALPHA.-.BETA.-D-RIBOPYRANOSE, 1,3-DI-O-ACETYL-	Sugars	0,48	0,99	69
34	8,519	1,3-Dioxolane-4-methanol, 2,2-dimethyl- (CAS)	Alcohols	0,46	5,2	87
35	8,886	Furan-2-carbonyl chloride, tetrahydro-	Furans	0,37	0,57	90
36	9,056	2,5-Dimethoxytetrahydrofuran	Furans	0,3	3,4	83
37	9,158	Ethanone, 1-(4-hydroxy-3-methoxyphenyl)- (CAS)	Ketones	0,26	4,28	79
38	9,312	Benzaldehyde, 4-hydroxy-3,5-dimethoxy- (CAS)	Aldehydes	0,26	0,63	80
39	9,559	(E)-2,6-Dimethoxy-4-(prop-1-en-1-yl)phenol	Phenolics	0,25	0,85	94
40	9,595	Ethanone, 1-(4-hydroxy-3,5-dimethoxyphenyl)- (CAS)	Ketones	0,24	0,49	81
41	9,669	(E)-2,6-Dimethoxy-4-(prop-1-en-1-yl)phenol	Phenolics	0,2	0,28	75
42	9,881	Glycine, N,N-dimethyl-, methyl ester (CAS)	Esters	0,19	0,48	94
43	9,94	PYRIDINE, 2-ETHYL-	Amines	0,19	0,21	85
44	10,009	(E)-2,6-Dimethoxy-4-(prop-1-en-1-yl)phenol	Phenolics	0,19	0,51	95
45	10,08	4 - propyl - syringol	Phenolics	0,13	0,17	88
46	10,192	2-HYDROXYCYCLOHEXYL ACETATE #	Esters	0,13	0,57	94
47	10,44	Benzenepropanol, 4-hydroxy-3-methoxy-	Alcohols	0,09	0,54	94
48	10,638	Ethanone, 1-(4-hydroxy-3,5-dimethoxyphenyl)- (CAS)	Ketones	0,08	1,71	78
49	10,959	Methyl 3-(4-hydroxy-3-methoxyphenyl)propanoate	Esters	0,07	0,17	80
50	14,687	1,2-Benzenedicarboxylic acid, mono(2-ethylhexyl) ester	Esters	0,07	0,15	97
				99,97		

Table 9. 5: GCMS Analysis of BOP from Pine biomass.

PK	RT	Area Pct	Library/ID	Area	Pct Max
1	5,1229	0,4757	Acetic acid, hydrazide	798915	2,48
2	6,1879	0,7457	Succindialdehyde	1252486	3,89
3	6,7011	0,6817	2-Furanmethanol	1144986	3,56
4	6,7864	2,3135	Furfural	3885490	12,08
5	7,0928	1,5936	2-Cyclopenten-1-one	2676522	8,32
6	7,9156	0,8686	2-Propanone, 1-(acetyloxy)-	1458822	4,54
7	8,8221	0,8257	2-Cyclopenten-1-one, 2-methyl-	1386812	4,31
8	9,4818	2,3894	1,2-Cyclopentanedione	4013107	12,48
9	10,2384	1,5682	Phenol	2633780	8,19
10	10,7357	0,4062	Butyrolactone	682164	2,12
11	10,8448	1,6834	2-Furancarboxaldehyde, 5-methyl-	2827377	8,79
12	11,2091	0,656	2-Cyclopenten-1-one, 3-methyl-	1101717	3,43
13	12,3904	0,4833	Cyclopentanecarboxaldehyde	811644	2,52
14	12,607	3,7217	Phenol, 2-methyl-	6250658	19,43
15	13,2771	2,8026	p-Cresol	4707003	14,63
16	14,2563	2,9462	Phenol, 2-methoxy-	4948109	15,38
17	15,0058	1,1081	4-Methyl-5H-furan-2-one	1861147	5,79
18	15,5093	1,5694	Phenol, 2,3-dimethyl-	2635770	8,19
19	16,0433	0,4006	Phenol, 4-ethyl-	672811	2,09
20	17,1766	8,3589	2-Methoxy-5-methylphenol	14038932	43,65
21	18,0831	0,699	Phenol, 4-ethyl-3-methyl-	1173918	3,65
22	19,0009	1,8564	Cyclopentane, ethyl-	3117872	9,69
23	19,1725	1,0268	1,2-Benzenediol, 3-methyl-	1724513	5,36
24	19,3679	0,7262	Methacrylic acid, ethyl ester	1219611	3,79
25	19,4383	2,9183	Phenol, 4-ethyl-2-methoxy-	4901393	15,24
26	19,9575	2,914	1,2-Benzenediol, 4-methyl-	4894040	15,22
27	20,0289	1,9132	1,2-Benzenediol, 4-methyl-	3213256	9,99
28	20,4297	0,8274	Hydroquinone	1389650	4,32
29	20,9063	3,2506	2-Methoxy-4-vinylphenol	5459511	16,97
30	21,5531	0,6222	Phenol, 4-(2-propenyl)-	1044949	3,25
31	21,6546	1,2401	Phenol, 2-methoxy-4-propyl-	2082809	6,48
32	21,7295	2,1174	Eugenol	3556124	11,06
33	22,4935	1,7997	4-Ethylcatechol	3022675	9,4
34	23,2476	1,8406	trans-Isoeugenol	3091397	9,61
35	23,4546	0,565	2-Allyl-4-methylphenol	948908	2,95
36	24,0386	1,8545	N,N'-(1,2-Propylene)-thiourea	3114605	9,68
37	24,4663	7,236	trans-Isoeugenol	12152947	37,78
38	24,5277	1,0592	Vanillin	1778901	5,53
39	25,8736	0,7924	Phenol, 2-methoxy-4-propyl-	1330928	4,14
40	26,1456	2,873	D-Allose	4825323	15
41	26,5923	1,6302	Ethanone, 1-(3-hydroxy-4-methoxyphenyl)-	2737907	8,51
42	27,5088	19,151	D-Allose	32164428	100
43	27,5923	1,0935	Hydroxychavicol	1836625	5,71
44	28,7001	0,6825	4-(1-Hydroxyallyl)-2-methoxyphenol	1146232	3,56
45	30,0804	1,4676	Benzenepropanol, 4-hydroxy-3-methoxy-	2464792	7,66
46	31,2429	0,7098	4-Heptanol, 2,6-dimethyl-	1192119	3,71
47	32,7659	0,9314	Coniferyl aldehyde	1564225	4,86
48	44,7236	0,6034	Dehydroabietic acid	1013495	3,15
		100,000			

Table 9. 6: GCMS analysis of BOP from Bamboo biomass.

PK	RT	Area Pct	Library/ID		Ref	CAS
1	6,7786	3,8669	Furfural	Furans	3075	000098-01
2	7,0885	2,4886	2-Cyclopenten-1-one	Ketones	1341	000930-30
3	8,8206	1,3652	2-Cyclopenten-1-one, 2-methyl-	Ketones	3178	001120-73
4	10,2325	8,4492	Phenol	Phenolics	2909	000108-95
5	10,8479	1,2891	2-Furancarboxaldehyde, 5-methyl-	Aldehydes	6533	000620-02
6	11,2117	1,8047	2-Cyclopenten-1-one, 3-methyl-	Ketones	3176	002758-18
7	12,6031	6,7286	Phenol, 2-methyl-	Phenolics	6069	000095-48
8	13,0791	1,1731	2-Cyclopenten-1-one, 2,3-dimethyl-	Ketones	6629	001121-05
9	13,2735	8,2268	p-Cresol	Phenolics	6063	000106-44
10	14,2558	1,5102	Phenol, 2-methoxy-	Phenolics	11911	000090-05
11	15,5139	1,7633	Phenol, 2,4-dimethyl-	Phenolics	11339	000105-67
12	16,0418	17,5933	Phenol, 4-ethyl-	Phenolics	11307	000123-07
13	17,174	1,1256	2-Methoxy-5-methylphenol	Phenolics	19924	001195-09
14	18,0016	18,0227	4-Vinylphenol	Phenolics	10651	002628-17
15	18,0784	2,7278	Benzenamine, 2,5-dimethyl-	Others	10944	000095-78
16	18,7794	1,6706	2-Isopropoxyphenol	Phenolics	30113	004812-20
17	19,4351	1,1224	Benzenethiol, o-isopropyl-,	Others	30299	006262-87
18	20,0329	1,6132	2-(1-Cyclopentenyl)furan	Furans	17557	115754-78
19	20,5682	1,4639	3-(1-Cyclopentenyl)furan	Furans	17556	115754-79
20	20,9043	1,7438	2-Methoxy-4-vinylphenol	Phenolics	28294	007786-61
21	21,5557	2,3614	Phenol, 4-(2-propenyl)-	Phenolics	17553	000501-92
22	22,7255	1,7414	Phenol, 2,6-dimethoxy-	Phenolics	31855	000091-10
23	24,4601	0,4874	trans-Isoeugenol	Phenolics	39176	005932-68
24	27,3753	6,98	D-Allose	Sugars	55180	002595-97
25	33,3779	2,6808	n-Hexadecanoic acid	Others	143511	000057-10
		100				

Table 9. 7: GCMS analysis of ethanol stabilized BOP.

PK	RT	Area Pct	Library/ID	Ref	CAS
1	3,8217	2,7902	Propylene Glycol	1083	000057-55-6
2	4,1825	0,5161	2-Butanol, 1,4-dimethoxy-3-(1,2,2-trimethylpropoxy)-	115777	079449-92-6
3	4,297	0,3236	Butanoic acid, ethyl ester	9243	000105-54-4
4	4,4266	0,3582	Acetic acid, hydroxy-, ethyl ester	5303	000623-50-7
5	4,8834	0,7659	Propanoic acid, 2-hydroxy-, ethyl ester	9919	000097-64-3
6	5,3879	0,558	Cyclopentanone	1586	000120-92-3
7	6,3205	0,4411	Cyclopentanone, 2-methyl-	3637	001120-72-5
8	6,8242	0,6457	1,2-Ethanediol, monoacetate	5297	000542-59-6
9	7,4828	0,4981	Propanamide, 2-methyl-2-(1-oxobutoxy)-N-(3-trifluoromethyl-4-nitrophenyl)-	271086	110990-15-3
10	8,807	2,0788	2-Cyclopenten-1-one, 2-methyl-	3178	001120-73-6
11	8,9185	0,3435	Ethanone, 1-(2-furanyl)-	6529	001192-62-7
12	10,0116	0,6249	2,5-Hexanedione	8123	000110-13-4
13	10,283	2,728	Phenol	2909	000108-95-2
14	10,733	0,8851	Butyrolactone	1855	000096-48-0
15	11,2076	0,7513	2-Cyclopenten-1-one, 3-methyl-	3176	002758-18-1
16	11,4803	0,7284	2-Cyclopenten-1-one, 2,3-dimethyl-	6629	001121-05-7
17	12,3854	0,7291	2(5H)-Furanone, 3-methyl-	3494	022122-36-7
18	12,6205	3,6173	Phenol, 2-methyl-	6069	000095-48-7
19	13,0698	0,7926	2-Cyclopenten-1-one, 2,3-dimethyl-	6629	001121-05-7
20	13,1581	0,7089	Furaneol	13907	003658-77-3
21	13,3051	3,4624	p-Cresol	6061	000106-44-5
22	13,6732	2,0466	Pentanoic acid, 4-oxo-, ethyl ester	23879	000539-88-8
23	13,8818	0,4832	2-Furanmethanol, tetrahydro-, acetate	23885	000637-64-9
24	14,1076	0,9799	2H-Pyrane, tetrahydro-2-(9-iodo-8-nonynyloxy)-	259075	098442-66-1
25	14,2479	4,2355	Phenol, 2-methoxy-	11911	000090-05-1
26	14,4422	0,5911	Phenol, 2,6-dimethyl-	11324	000576-26-1
27	15,0076	0,7167	4-Methyl-5H-furan-2-one	3491	006124-79-4
28	15,0885	0,3392	Phenol, 2-ethyl-	11304	000090-00-6
29	15,5289	2,7572	Phenol, 2,3-dimethyl-	11336	000526-75-0
30	15,6154	0,3628	5-Ethyl-2-octen-4-one	31019	1000374-14-3
31	15,741	0,5512	Maltol	12676	000118-71-8
32	16,077	1,4307	Phenol, 4-ethyl-	11307	000123-07-9
33	16,149	0,2439	Phenol, 2-ethyl-	11302	000090-00-6
34	16,5395	1,3911	Butanedioic acid, diethyl ester	49493	000123-25-1
35	16,8866	0,601	Diethyl methylsuccinate	63330	004676-51-1
36	17,1682	6,1548	2-Methoxy-5-methylphenol	19925	001195-09-1
37	17,3781	0,7818	Catechol	6510	000120-80-9
38	17,7157	0,3713	Phenol, 2-ethyl-6-methyl-	18875	001687-64-5
39	18,0968	1,055	Phenol, 4-ethyl-3-methyl-	18876	001123-94-0
40	18,6083	1,1462	Phenol, 4-propyl-	18816	000645-56-7
41	18,9937	0,6265	Geranyl nitrile	26984	101660-61-1
42	19,2383	0,4368	Pentanedioic acid, diethyl ester	63357	000818-38-2
43	19,3494	0,316	4-Hydroxy-2,4,5-trimethyl-2,5-cyclohexadien-1-one	30270	014353-72-1
44	19,4287	3,4821	Phenol, 4-ethyl-2-methoxy-	30172	002785-89-9
45	19,6111	1,4905	Propanoic acid, 2-methyl-, 2-methylpropyl ester	24295	000097-85-8
46	19,7779	1,3867	5-(Hydroxymethyl)dihydrofuran-2(3H)-one	9132	010374-51-3
47	20,0632	2,9262	1,2-Benzenediol, 4-methyl-	11929	000452-86-8
48	20,4485	0,5944	Phenol, 4-(1-methylpropyl)-	27511	000099-71-8
49	20,4962	1,2034	Hydroquinone	6520	000123-31-9
50	20,8334	0,2439	1,5-Anhydro-d-mannitol	39958	000492-93-3
51	21,6469	4,7976	Phenol, 2-methoxy-4-propyl-	41138	002785-87-7
52	21,7238	0,6029	Phenol, 2-methoxy-3-(2-propenyl)-	39350	001941-12-4
53	22,1501	0,3043	4-Methoxy-3-methylphenylacetic acid	54381	004513-73-9
54	22,2203	0,2969	1H-Cyclopenta[c]furan-1,4(3H)-dione, tetrahydro-	21142	127708-95-6
55	22,4536	0,534	Orcinol	11896	000504-15-4
56	22,6265	3,4409	Methacrylic acid, ethyl ester	8195	000097-63-2
57	22,6902	1,0903	2-(1-Methylcyclopropyl)thiophene	20070	1000100-02-7
58	22,943	0,4584	4-Acetylanisole	28254	000100-06-1
59	23,2449	0,2679	Allyl (2-methylphenyl) sulfide	39501	024309-31-7
60	24,0538	1,3589	2H-Thiopyran-3(4H)-one, dihydro-	9141	019090-03-0
61	24,4552	1,8468	trans-Isoeugenol	39178	005932-68-3
62	24,5222	0,6092	Vanillin, isopropyl ether	68670	1010395-32-3
63	26,5898	2,0777	Apocynin	42059	000498-02-2
64	27,4053	4,9932	D-Allose	55180	002595-97-3
65	27,5132	1,2355	2-Propanone, 1-(4-hydroxy-3-methoxyphenyl)-	54451	002503-46-0
66	28,1985	0,1386	2-Oxo-2-(1,2,3,4-tetrahydronaphthalen-1-ylamino)ethyl acetate	131865	1000509-65-9
67	28,6248	0,5667	1-Propanone, 1-(4-hydroxy-3-methoxyphenyl)-	54449	001835-14-9
68	29,0981	0,7877	Benzenepropanol, 4-methoxy-	41140	005406-18-8
69	29,2489	2,6841	Ethyl ,alpha,-d-glucopyranoside	85607	019467-01-7
70	29,6204	0,395	Ethyl ,alpha,-d-glucopyranoside	85607	019467-01-7
71	30,0778	2,3014	Benzenepropanol, 4-hydroxy-3-methoxy-	56452	002305-13-7
72	33,5989	0,693	Hexadecanoic acid, ethyl ester	179131	000628-97-7
73	37,0809	1,5214	Ethyl Oleate	212138	000111-62-6
74	37,2409	1,5055	Octadecanoic acid, ethyl ester	214945	000111-61-5
75	43,8742	0,3843	(E)-1,7-bis(4-Hydroxy-3-methoxyphenyl)hept-4-en-3-one	265737	128700-97-0
76	44,7304	1,4928	Dehydroabietic acid	199992	001740-19-8
77	49,5582	0,3227	(E)-3,3'-Dimethoxy-4,4'-dihydroxystilbene	163555	007329-69-3
		100,0006			

Table 9. 8: GCMS analysis of methanol stabilized BOP.

PK	RT	Area Pct	Library/ID	Ref	CAS
1	5,7201	1,2307	Cyclopentanone	1586	000120-92-3
2	6,6726	0,9301	Cyclopentanone, 2-methyl-	3637	001120-72-5
3	7,8528	1,0089	Butanoic acid, 3-methyl-2-oxo-, methyl ester	15266	003952-67-8
4	9,1936	1,967	2-Cyclopenten-1-one, 2-methyl-	3175	001120-73-6
5	9,813	0,7226	(R,R)-(-)-2,3-Dimethoxy-1,4-bis(dimethylamino)butane	79379	026549-22-4
6	10,6759	2,608	Phenol	2909	000108-95-2
7	11,1311	0,6587	Butyrolactone	1855	000096-48-0
8	11,6129	0,9473	2-Cyclopenten-1-one, 3-methyl-	3176	002758-18-1
9	11,8838	0,7973	6-Methyl-3-heptyne	6685	054050-92-9
10	12,0138	1,4154	Pentanoic acid, 4-oxo-, methyl ester	15247	000624-45-3
11	12,8043	0,92	1-Penten-3-one, 2-methyl-	3636	025044-01-3
12	13,0258	2,4214	Phenol, 2-methyl-	6073	000095-48-7
13	13,4817	0,608	2-Cyclopenten-1-one, 2,3-dimethyl-	6629	001121-05-7
14	13,5924	0,9679	Butanedioic acid, methyl-, dimethyl ester	36518	001604-11-1
15	13,7171	4,4279	p-Cresol	6061	000106-44-5
16	14,5123	0,6436	1,1'-Bicyclopentyl-1,1'-diol	45023	005181-75-9
17	14,6593	3,1463	Phenol, 2-methoxy-	11911	000090-05-1
18	14,8646	0,3637	Phenol, 2,5-dimethyl-	11319	000095-87-4
19	15,4263	1,0532	4-Methyl-5H-furan-2-one	3491	006124-79-4
20	15,9388	3,1214	Phenol, 2,4-dimethyl-	11330	000105-67-9
21	16,4861	0,8664	Phenol, 4-ethyl-	11307	000123-07-9
22	16,5508	0,3643	Phenol, 3-ethyl-	11292	000620-17-7
23	17,58	5,2827	Creosol	19866	000093-51-6
24	17,7874	1,3993	Catechol	6510	000120-80-9
25	18,4039	0,4669	Butyric acid, 4-pentadecyl ester	197329	1000280-57-
26	18,5089	1,0881	Benzene, 1-ethyl-4-methoxy-	18911	001515-95-3
27	19,0215	1,2695	Phenol, 4-propyl-	18824	000645-56-7
28	19,8434	4,391	Phenol, 4-ethyl-2-methoxy-	30172	002785-89-9
29	20,1909	1,3631	(S)-(+)-2',3'-Dideoxyribonolactone	9115	032780-06-6
30	20,4763	3,5958	1,2-Benzenediol, 4-methyl-	11921	000452-86-8
31	20,8583	1,0232	Benzene, 1-methoxy-4-propyl-	27518	000104-45-0
32	20,92	1,0327	Hydroquinone	6520	000123-31-9
33	21,9408	0,8595	2(5H)-Furanone, 4-(mercaptomethyl)-3-methoxy-	36437	010478-17-8
34	22,0605	6,0031	Phenol, 2-methoxy-4-propyl-	41138	002785-87-7
35	22,8778	0,179	Orcinol	11894	000504-15-4
36	23,0172	0,3833	4-Ethylcatechol	19867	001124-39-6
37	24,4768	2,1792	2H-Thiopyran-3(4H)-one, dihydro-	9141	019090-03-0
38	24,8739	2,796	trans-Isoeugenol	39178	005932-68-3
39	26,5793	1,5503	D-Allose	55180	002595-97-3
40	27,0148	2,0596	Ethanone, 1-(3-hydroxy-4-methoxyphenyl)-	42253	006100-74-9
41	27,871	15,8204	,beta,-D-Glucopyranose, 1,6-anhydro-	38156	000498-07-7
42	28,4046	0,8756	1,4-Dioxan-2-ol, TMS derivative	51263	100604-29-3
43	28,8918	3,989	,alpha,-D-Galactopyranoside, methyl	69619	003396-99-4
44	29,0562	3,6618	1-Propanone, 1-(4-hydroxy-3-methoxyphenyl)-	54449	001835-14-9
45	30,5065	2,7185	Benzenepropanol, 4-hydroxy-3-methoxy-	56452	002305-13-7
46	32,7838	0,7223	Hexadecanoic acid, methyl ester	161212	000112-39-0
47	36,3919	1,2728	9-Octadecenoic acid, methyl ester	194409	002462-84-2
48	36,5337	1,5015	Heptadecanoic acid, 16-methyl-, methyl ester	197352	005129-61-3
49	38,6283	0,4452	10,18-Bisnorabieta-5,7,9(10),11,13-pentaene	121373	006566-19-4
50	45,1653	0,8806	Butanoic acid, 2-(cyano)(2,4,6-trimethylphenylamino)methylene-3-oxo-, ethyl ester	199360	1000267-71-
		100,0001			

Table 9. 9: GCMS analysis of ether stabilized BOP.

PK	RT	Area Pct	Library/ID	Ref	CAS
1	5,6553	1,2895	Cyclopentanone	1586	000120-92-3
2	6,6102	0,8937	Cyclopentanone, 2-methyl-	3637	001120-72-5
3	7,1069	2,3287	1,2-Ethanediol, monoacetate	5297	000542-59-6
4	7,7098	0,7268	1,2-Propanediol, 1-acetate	9881	000627-69-0
5	7,7964	2,0689	Sulfurous acid, 2-pentyl pentyl ester	100832	1000309-15-4
6	9,144	4,6561	2-Cyclopenten-1-one, 2-methyl-	3175	001120-73-6
7	10,361	0,9348	2,5-Hexanedione	8124	000110-13-4
8	10,6355	3,9676	Phenol	2910	000108-95-2
9	11,0931	1,77	Butyrolactone	1855	000096-48-0
10	11,5782	1,3483	2-Cyclopenten-1-one, 3-methyl-	3176	002758-18-1
11	11,8524	1,8015	2-Cyclopenten-1-one, 2,3-dimethyl-	6629	001121-05-7
12	12,7655	1,1963	1-Penten-3-one, 2-methyl-	3632	025044-01-3
13	13,0013	3,6503	Phenol, 2-methyl-	6074	000095-48-7
14	13,4556	0,9936	2-Cyclopenten-1-one, 2,3-dimethyl-	6633	001121-05-7
15	13,6881	4,2091	p-Cresol	6061	000106-44-5
16	14,5022	1,992	Decane, 2,3,7-trimethyl-	59081	062238-13-5
17	14,6401	6,8928	Phenol, 2-methoxy-	11911	000090-05-1
18	15,4085	1,924	4-Methyl-5H-furan-2-one	3492	006124-79-4
19	15,9243	3,3126	Phenol, 2,3-dimethyl-	11336	000526-75-0
20	16,4734	1,3698	Phenol, 4-ethyl-	11308	000123-07-9
21	16,8985	1,7386	Methanesulfonamide, N,N-dimethyl-	11495	000918-05-8
22	17,5709	10,371	2-Methoxy-5-methylphenol	19925	001195-09-1
23	18,5025	1,6387	Benzene, 1-ethyl-4-methoxy-	18919	001515-95-3
24	19,0162	1,5007	Phenol, 4-propyl-	18824	000645-56-7
25	19,8365	6,3814	Phenol, 4-ethyl-2-methoxy-	30172	002785-89-9
26	20,1847	3,2543	5-(Hydroxymethyl)dihydrofuran-2(3H)-one	9132	010374-51-3
27	20,494	0,7259	1,2-Benzenediol, 4-methyl-	11921	000452-86-8
28	20,8534	0,1708	Benzene, 1-methoxy-4-propyl-	27518	000104-45-0
29	22,058	9,1796	Phenol, 2-methoxy-4-propyl-	41138	002785-87-7
30	24,8733	2,8273	trans-Isoeugenol	39178	005932-68-3
31	27,0123	2,5846	Ethanone, 1-(3-hydroxy-4-methoxyphenyl)-	42253	006100-74-9
32	27,7917	2,3616	,beta,-D-Glucopyranose, 1,6-anhydro-	38155	000498-07-7
33	27,9276	3,3123	Guaiacol, 4-butyl-	54635	059832-96-1
34	30,5052	4,3694	Homovanillic acid	57505	000306-08-1
35	32,7444	0,8343	Ethyl-,beta,-(4-hydroxy-3-methoxy-phenyl)-propi	103932	061292-90-8
36	45,1692	1,4232	Dehydroabietic acid	199993	001740-19-8
		100,0001			

Table 9. 10: GCMS analysis of isopropyl alcohol stabilized BOP.

PK	RT	Area Pct	Library/ID	Ref	CAS
1	3,8177	3,726	Propylene Glycol	1083	000057-55-6
2	8,7945	4,244	2-Cyclopenten-1-one, 2-methyl-	3175	001120-73-6
3	10,2706	3,708	Phenol	2909	000108-95-2
4	10,719	1,62	Butyrolactone	1851	000096-48-0
5	11,202	1,2854	2-Cyclopenten-1-one, 3-methyl-	3179	002758-18-1
6	11,4743	1,6318	2-Cyclopenten-1-one, 2,3-dimethyl-	6629	001121-05-7
7	12,6149	3,5576	Phenol, 2-methyl-	6069	000095-48-7
8	13,3088	4,7004	p-Cresol	6061	000106-44-5
9	14,2408	6,6313	Phenol, 2-methoxy-	11911	000090-05-1
10	14,3573	1,465	Pentanoic acid, 4-oxo-, 1-methylethyl ester	35153	021884-26-4
11	15,5247	2,7883	Phenol, 3,5-dimethyl-	11334	000108-68-9
12	16,0726	0,9259	Phenol, 4-ethyl-	11307	000123-07-9
13	17,1641	11,3415	2-Methoxy-5-methylphenol	19925	001195-09-1
14	18,0958	1,6559	Benzene, 1-ethyl-4-methoxy-	18911	001515-95-3
15	18,6077	1,6434	Phenol, 4-propyl-	18824	000645-56-7
16	19,427	8,0264	Phenol, 4-ethyl-2-methoxy-	30164	002785-89-9
17	19,7691	1,7871	5-(Hydroxymethyl)dihydrofuran-2(3H)-one	9132	010374-51-3
18	20,0959	3,8358	Propanoic acid, 2-methyl-, propyl ester	15557	000644-49-5
19	21,645	11,4816	Phenol, 2-methoxy-4-propyl-	41138	002785-87-7
20	22,6454	2,6458	Benzene-1,3-diol, O,O'-acetyl-2-nitro-	121768	103264-33-1
21	24,4547	4,5239	trans-Isoeugenol	39178	005932-68-3
22	26,5886	2,2843	Ethanone, 1-(3-hydroxy-4-methoxyphenyl)-	42253	006100-74-9
23	27,3831	7,1923	3,4-Altrosan	38142	1000129-76-
24	27,5108	2,4612	2-Propanone, 1-(4-hydroxy-3-methoxyphenyl)-	54451	002503-46-0
25	30,0901	4,8373	Homovanillic acid	57505	000306-08-1
		100,0002			

9.3 Appendix C: HPLC Sugar Curves and Calibration Curves

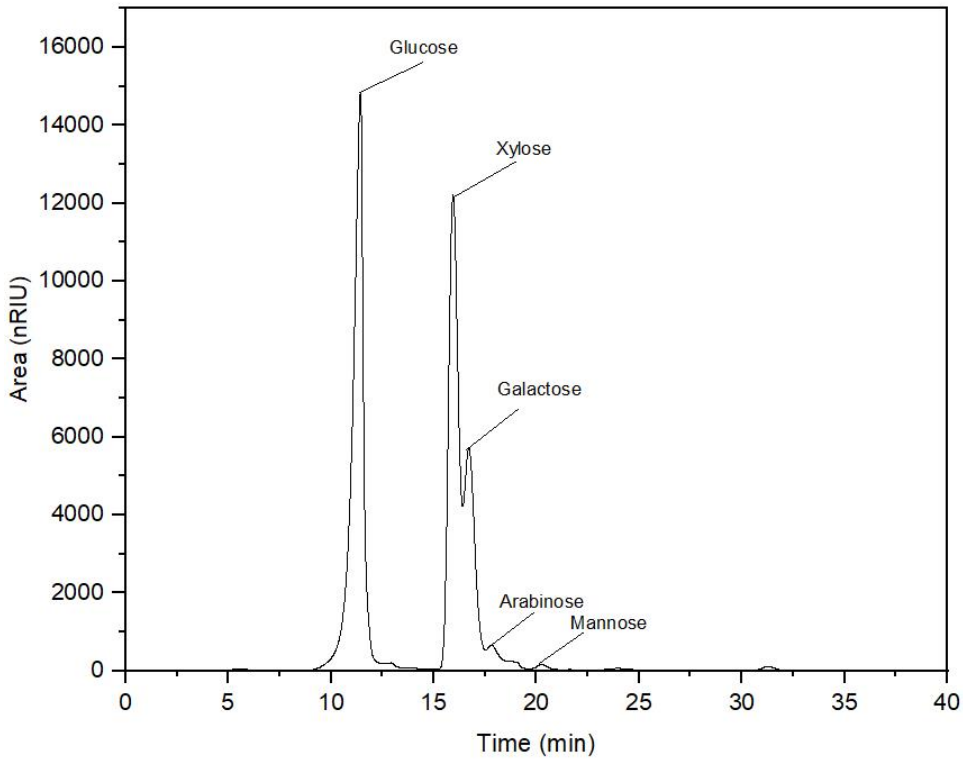

Figure 9. 1: HPLC curve of pine biomass during determination of sugars.

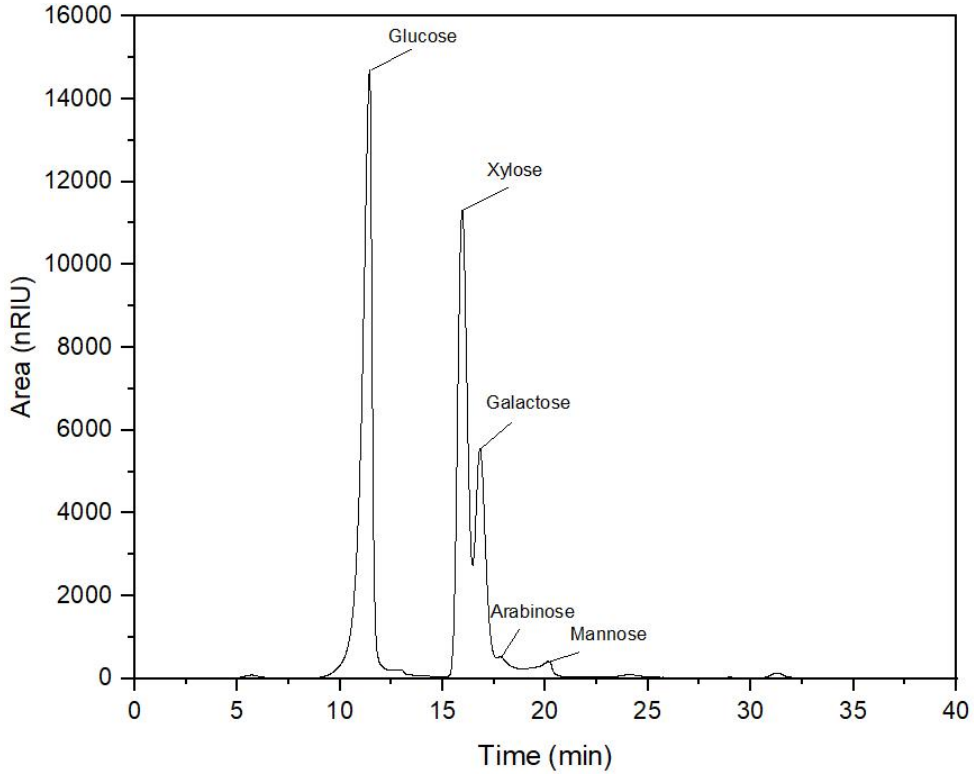

Figure 9. 2: HPLC curve of bamboo biomass during determination of sugars.

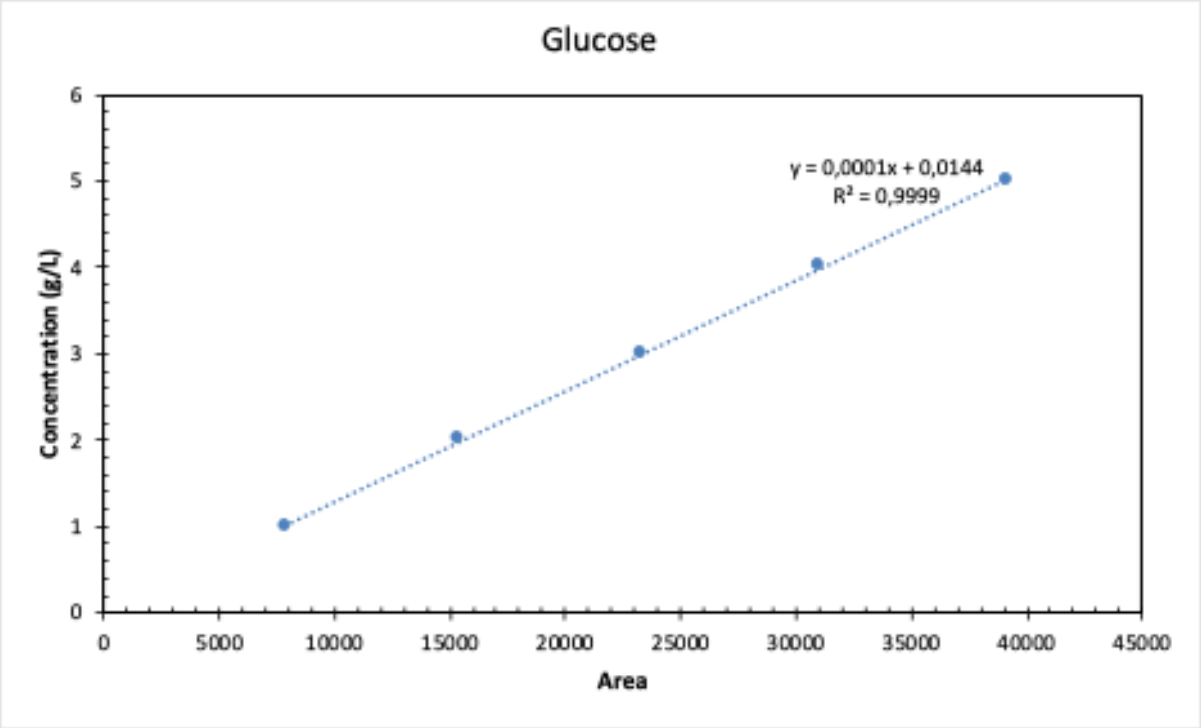

Figure 9. 3: Calibration curve of glucose sugar content.

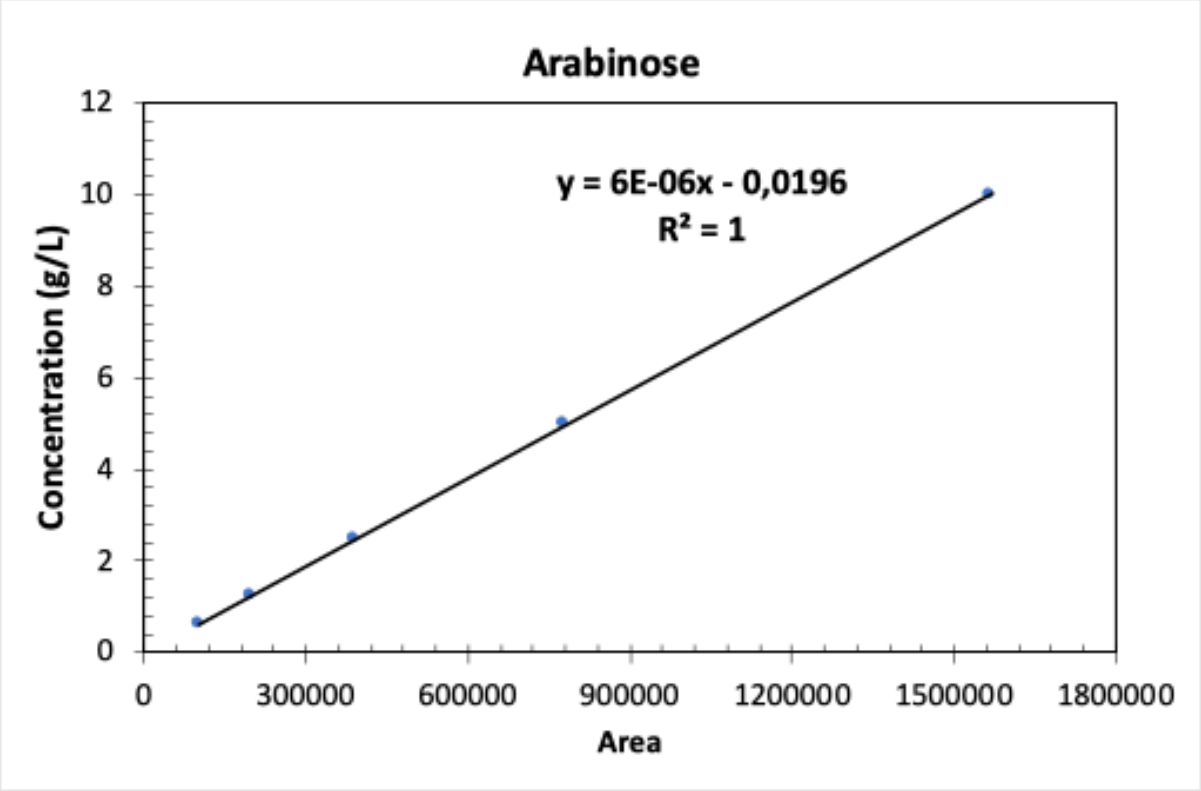

Figure 9. 4: Calibration curve of arabinose sugar content.

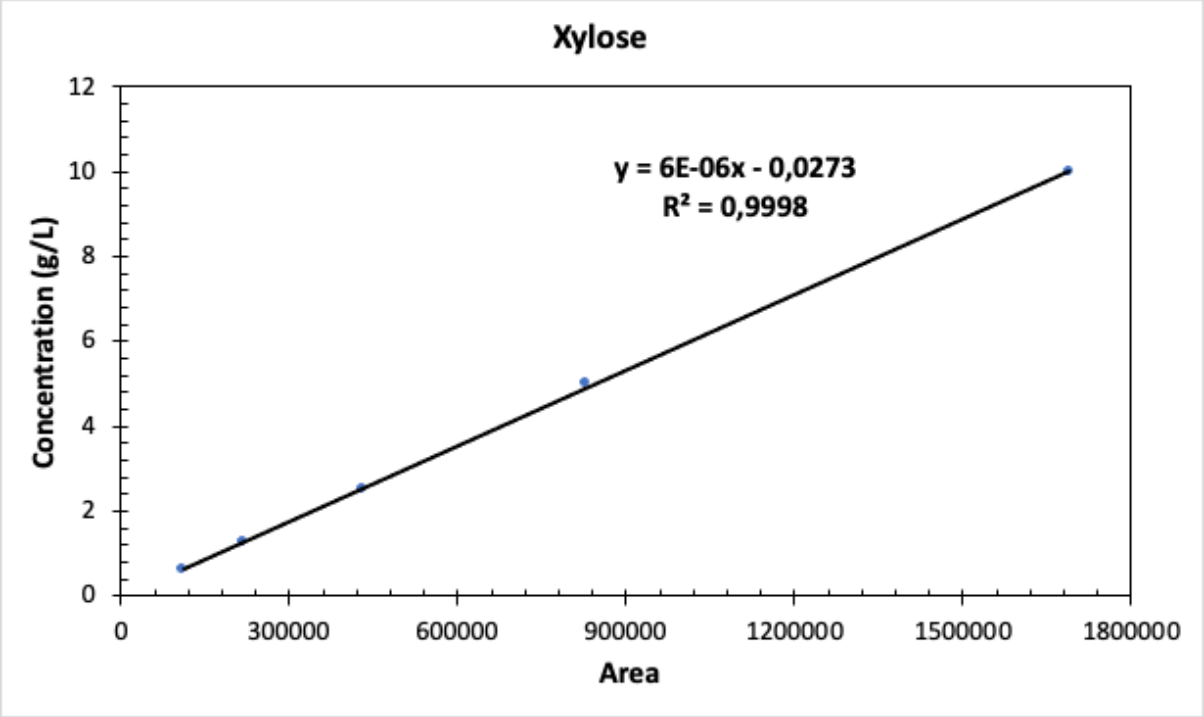

Figure 9. 5: Calibration curve of xylose sugar content.

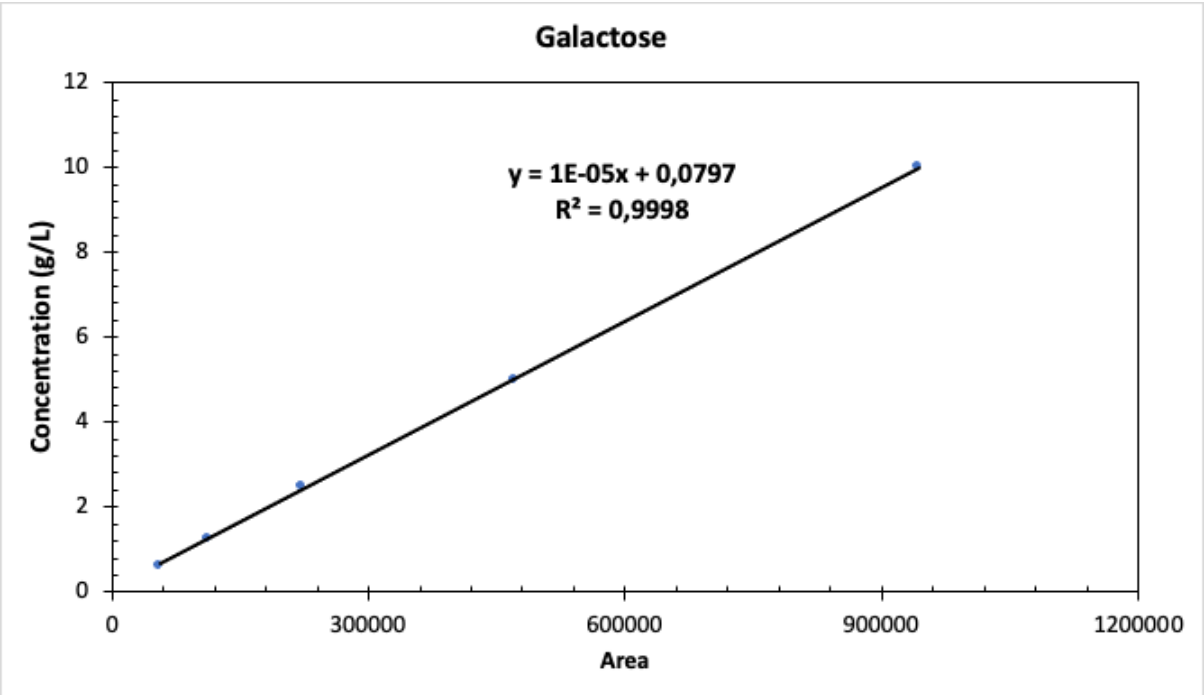

Figure 9. 6: Calibration curve of glucose sugar content.

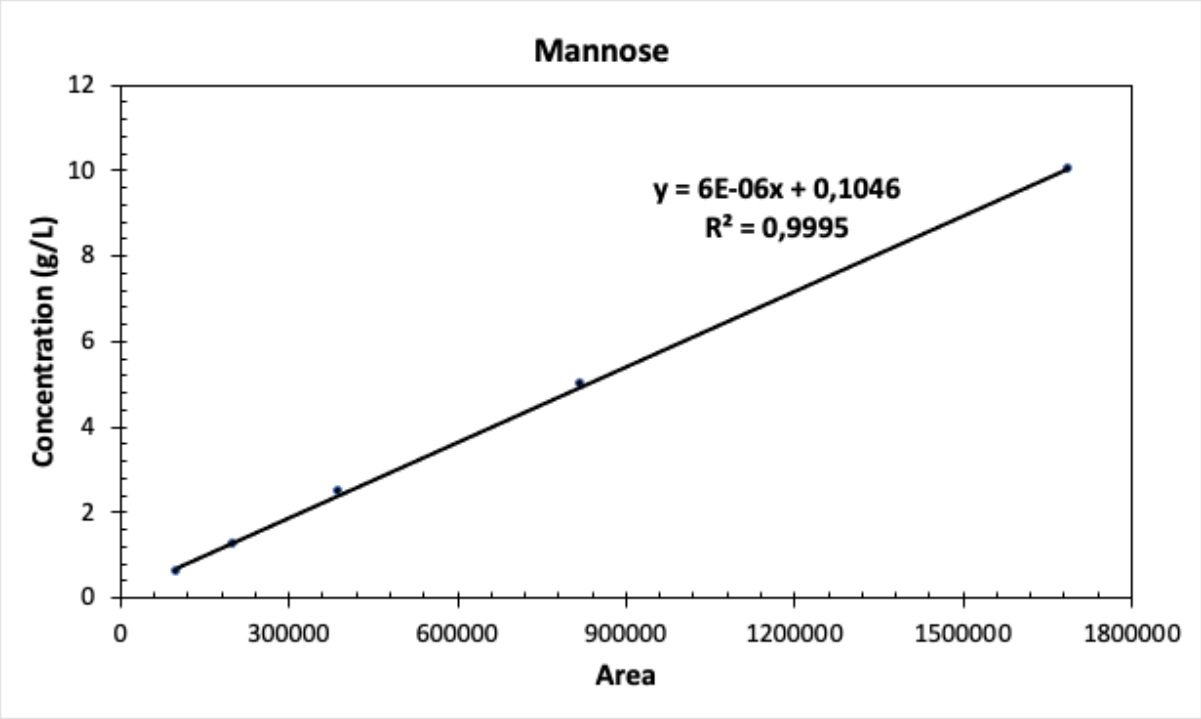

Figure 8. 1: Calibration curve of mannose sugar content.

Table 9. 11: Isothermal pyrolysis of biomass.

Description	Giant Reed						Pine					
	Run 1 (1,5)	Run 2 (2)	Wt%	Wt%	Mean	Error	Run 1	Run 2	Wt%	Wt%	Mean	Error
Loaded Biomass	6357,7	4590			5473,9	883,9	7925	7545,5			7735,3	189,75
Reacted Biomass	1887,5	2490	29,7	54,2	42,0	-12,3	3545	2654,0	44,7	35,2	40,0	4,78
Unreacted Biomass	4470,2	2100	70,3	45,8	58,0	12,3	4380	4891,5	55,3	64,8	60,0	-4,78
Bio-Oil (A+O)	691,5	946,2	36,6	38	37,3	-0,7	1473,7	1300,7	41,6	49,0	45,3	-3,72
Organic Phase (O)	166,1	234,1	8,8	9,4	9,1	-0,3	353,6	430,4	10,0	16,2	13,1	-3,12
Aqueous Phase (A)	525,4	712,1	27,8	28,6	28,2	-0,4	1120,1	870,3	31,6	32,8	32,2	-0,60
Biochar	372,0	554,4	19,7	22,3	21,0	-1,3	508	427,5	14,3	16,1	15,2	-0,89
Biogas	824,05	989,4	43,7	39,7	41,7	2,0	1563,3	925,8	44,1	34,9	39,5	4,61

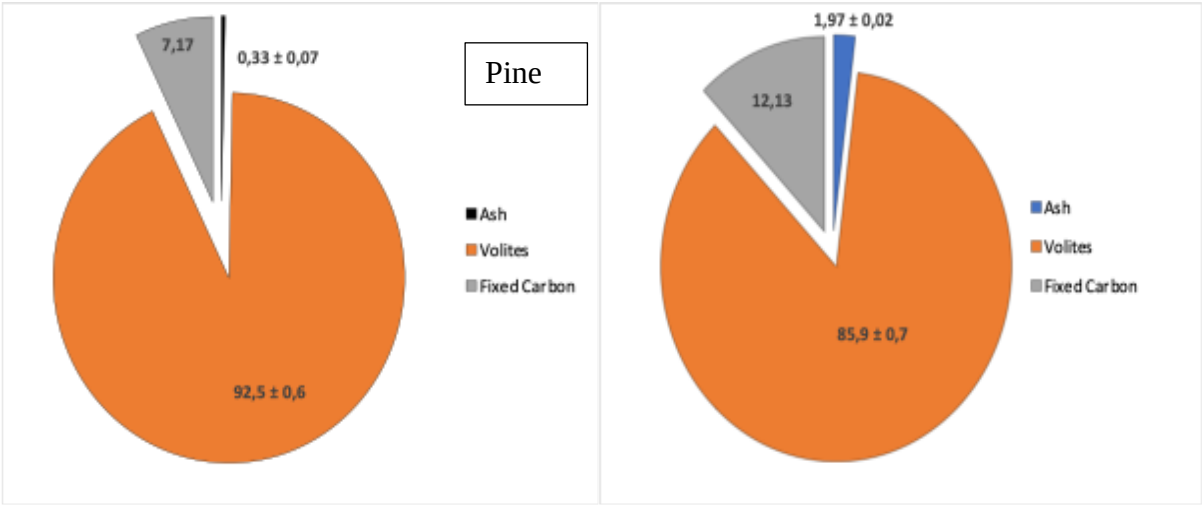

Figure 9. 7: Analysis of pine and bamboo biomass.

Table 9. 12: Moisture content data of biomass for isothermal pyrolysis.

Pine Biomass (105 C for 24 hr)				
m1 (g)	m2 (g)	Loss of drying (wt%) or MC on wet basis	Water Content (wt%)	Drying Rate (g/hr)
1,2883	1,213	5,84	6,21	0,00259
1,1077	1,0453	5,63	5,97	0,00249
1,0197	0,9639	5,47	5,79	0,00241
0,9859	0,9165	7,04	7,57	0,00316
1,049	0,9772	6,84	7,35	0,00306
1,0247	0,9583	6,48	6,93	0,00289
0,9893	0,9097	8,05	8,75	0,00365
0,9836	0,9049	8,00	8,70	0,00362
0,9915	0,9146	7,76	8,41	0,00350
Bamboo (105 C for 24 hr)				
2,2271	2,1348	4,14	4,32	0,00180
2,5369	2,436	3,98	4,14	0,00173
2,4941	2,3972	3,89	4,04	0,00168

Table 9. 13:Fixed carbon and volatiles data of biomass for isothermal pyrolysis.

Biomass	m1	m2	m3	Diff	Fixed Carbon			
B	20,8472	1,5211	21,1095	0,2623	0,172440997	17,2440997	17,9968922	
B	20,5371	1,5065	20,7934	0,2563	0,170129439	17,0129439	17,7556453	
B	19,5313	1,5247	19,8109	0,2796	0,183380337	18,3380337	19,138582	
P	20,0837	1,5035	20,3001	0,2164	0,143930828	14,3930828	15,5182509	
P	20,19	1,5067	20,4121	0,2221	0,147408243	14,7408243	15,8931768	
P	19,9395	1,5028	20,1455	0,206	0,137077455	13,7077455	14,7793379	
B	20,1942	1,5154	20,4678	0,2736	0,18054639	18,054639	19,4660464	
Biomass	m1+m2	removed mass volatiles	Volatiles (g/g)	Volatiles (%) ad	Volatiles (%) db	mean	error	
B	22,3683	1,2588	0,827559003	82,8	86,4			
B	22,0436	1,2502	0,829870561	83,0	86,6	85,9	0,7	85,9 ± 0,7
B	21,056	1,2451	0,816619663	81,7	85,2			
P	21,5872	1,2871	0,856069172	85,6	92,3			
P	21,6967	1,2846	0,852591757	85,3	91,9	92,5	0,6	92,5 ± 0,6
P	21,4423	1,2968	0,862922545	86,3	93,0			
B	21,7096	1,2418	0,81945361	81,9	85,5			

Table 9. 14: Ash content data of biomass for isothermal pyrolysis.

Biomass	mc	ms	mf	Ash	%Ash ad	%Ash db	mean	Error	
B	15,5681	1,0325	15,5878	0,0197	1,908	1,99128378			
B	15,3558	1,0314	15,3751	0,0193	1,871	1,95293223	1,97116219	0,0201216	1,97 ± 0,02
B	12,416	1,0324	12,4353	0,0193	1,869	1,95104059			
P	14,6767	1,0315	14,6805	0,0038	0,4	0,39719458			
P	14,4381	1,0325	14,4406	0,0025	0,2	0,26105913	0,32912685	0,06806772	0,33 ± 0,07
P	14,3403	1,0327	14,3441	0,0038	0,4	0,39673303			
B	15,1251	1,0315	15,1448	0,0197	1,90984004	1,99321426			
B	15,438	1,0316	15,4568	0,0188	1,82241179	1,90196932	1,94759179	0,04562247	1,95 ± 0,05

Parameter	Fresh Ru/C	METH-Used	DME-Used	ISO-Used	ETH-Used
Surface Area (m^2/g)	686.55	600.12	500.55	612.20	605.30
Pore Diameter (nm)	3.3	3.3	3.3	3.3	3.3

GCB Bioenergy

WILEY

Global Change Biology Bioenergy

RESEARCH ARTICLE OPEN ACCESS

Seasonal Harvesting Impact on Biomass Fuel Properties and Pyrolysis-Derived Bio-Oil Organic Phase Composition

Manqoba Shezi[1] | Sammy Lewis Kiambi[2] | Yusuf Makarfi Isa[3]

[1]Durban University of Technology, Durban, South Africa | [2]Chemical Engineering Department, Vaal University of Technology, Vanderbilpark, South Africa | [3]School of Chemical and Metallurgical Engineering, University of the Witwatersrand, Johannesburg, South Africa

Correspondence: Manqoba Shezi (manqoba.shezi@fulbrightmail.org)

Received: 8 September 2024 | **Revised:** 30 October 2024 | **Accepted:** 1 November 2024

Funding: This work was supported by National Research Foundation (NRF) and Durban University of Technology.

Keywords: biochar | biofuels | biomass | bio-oil | fast pyrolysis | Giant Reed | harvest seasons | invasive species

ABSTRACT

Thermochemical conversion of giant reed biomass during periodic variations has been carried out in a semi-batch tubular reactor at 550°C. This study was carried out after the incineration of giant reed along the river banks. Four periodic variations, late spring (HS-4), late summer (HS-1), late autumn (HS-2), and late winter (HS-3) were considered to investigate the effect of harvest time on biomass fuel properties, pyrolysis product distribution, non-condensable gas characterization, and bio-oil organic phase (BOP) fuel properties. The considered biomasses herein had average calorific values of 18.86 ± 0.05, 19.73 ± 0.05, 19.23 ± 0.04, and 18.44 ± 0.04 MJ/kg during HS-1, HS-2, HS-3, and HS-4, respectively. The biomass, bio-oil organic phase, biochar, and pyrolysis gas were characterized using thermogravimetric analysis (TGA), gas chromatography–mass spectroscopy (GCMS), Fourier transform infrared spectroscopy (FTIR), micro-GC, and scanning electron microscopy (SEM/EDS). The organic phase of bio-oil was isolated using a 125 mL separating funnel, allowing natural stratification of the immiscible phases. BOP yield increased from 5 to 11 wt% during HS-4 and HS-3, respectively. Higher heating values (HHV) of the BOP ranged from 19.4 ± 0.03 to 22.6 ± 0.02 MJ/kg in relation to the active growth stage and senescence-dormant phase. Physical and chemical properties (TAN, density, viscosity, water content, and CHNS) and chemical compound groups of organic phase bio-oil were analyzed. The produced BOP was rich in phenolics for all considered periods. The effect of harvest time showed that biomass and bio-oil organic phase fuel properties are improved during the senescence-dormant period. As a result, giant reed biomass should be harvested during autumn to avoid incineration that releases carbon dioxide into the atmosphere and will also reduce the occurrence of artificial flooding.

1 | Introduction

The continued use of fossil fuels poses a severe challenge because of the world's limited supply, energy insecurity, and environmental concerns over global warming due to the production of greenhouse gases (Fernandez et al. 2021; Patel, Agrawal, and Rawal 2020). Inevitably, the world will run out of oil that can be mined and burned in the long term. Sustainable energy transport and infrastructure are the endpoints. Dependence on fossil fuels is dangerous and poses a significant threat to biodiversity; thus, attaining sustainable energy transport and infrastructure is critical. Additionally, dependence on fossil fuels for energy has tampered with the natural carbon cycle. It is well known that the natural carbon cycle has existed for millions of years, and there was no urgency around it. The problem started when extra carbon was added to the natural carbon cycle through human activities, and the net result is that the carbon in the atmosphere is increasing over time. It is much more than that can be absorbed by the ecosystem. As a result, it has become evident

Manqoba Shezi
Chemical Engineering
Green Energy Research Group, Department of Chemical Engineering, Durban University of Technology
70 Steve Biko Rd. Musgrave, Berea
Durban 4000
South Africa

INVOICE

MDPI AG
Grosspeteranlage 5
4052 Basel
Switzerland
Tel.: +41 61 683 77 34
E-Mail: billing@mdpi.com
Website: www.mdpi.com
VAT nr. CHE-115.694.943

Date of Invoice:	7 December 2024
Manuscript ID:	bioengineering-3276410
Invoice Number:	3276410
Your Order:	by e-mail (manqoba.shezi@fulbrightmail.org) on 9 October 2024
Article Title:	"Isothermal Pyrolysis of Bamboo and Pinewood Biomass: Product Characterization and Comparative Study in a Fluidized Bed Reactor"
Name of co-authors:	Manqoba Shezi and Sammy Lewis Kiambi Additional Author Information
Terms of payment:	10 days
Due Date:	17 December 2024
License:	CC BY

Description	Currency	Amount
Article Processing Charges	CHF	2 700.00
Subtotal without VAT	CHF	2 700.00
VAT (0%)	CHF	0.00
Total with VAT	**CHF**	**2 700.00**

Accepted Payment Methods

1. Online Payment by Credit Card in Swiss Francs (CHF)

Please visit https://payment.mdpi.com/3210707 to pay by credit card. We accept payments in Swiss Francs (CHF) made through VISA, MasterCard, Maestro, American Express, Diners Club, Discover, China UnionPay and Alipay+.

2. Paypal in Swiss Francs (CHF)

Please visit https://payment.mdpi.com/payment/paypal and enter the payment details. Note that the fee for using Paypal is 5% of the invoiced amount.

3. Wire Transfer in Swiss Francs (CHF)

Important: **Please provide the Manuscript ID (bioengineering-3276410) when transferring the payment**

Payment in CHF must be made by wire transfer to the MDPI bank account. Banks fees must be paid by the customer for both payer and payee so that MDPI can receive the full invoiced amount.

IBAN: CH74 0023 3233 2227 2101 Y
SWIFT Code / BIC (Wire Transfer Address): UBSWCHZH80A
Beneficiary's Name: MDPI AG
Beneficiary's Address: Grosspeteranlage 5, 4052 Basel, Switzerland
Bank Account Number (CHF, Swiss Francs Account for MDPI): 0233 00222721.01Y
Bank Name: UBS Switzerland AG
Bank Address:

UBS Switzerland AG
Bahnhofstrasse 45
8001 Zürich
Switzerland

For detailed payment instruction, or for more alternative payment methods, visit the website at https://www.mdpi.com/about/payment.

Thank you for choosing MDPI.